NATIONAL AERONAUTICS AND SPACE ADMINISTRATION

The Deep Space Network
Progress Report 42-28

May and June 1975

JET PROPULSION LABORATORY
CALIFORNIA INSTITUTE OF TECHNOLOGY
PASADENA, CALIFORNIA

August 15, 1975

NATIONAL AERONAUTICS AND SPACE ADMINISTRATION

The Deep Space Network
Progress Report 42-28

May and June 1975

JET PROPULSION LABORATORY
CALIFORNIA INSTITUTE OF TECHNOLOGY
PASADENA, CALIFORNIA

August 15, 1975

Preface

Beginning with Volume XX, the Deep Space Network Progress Report changed from the Technical Report 32- series to the Progress Report 42- series. The volume number continues the sequence of the preceding issues. Thus, Progress Report 42-20 is the twentieth volume of the Deep Space Network series, and is an uninterrupted follow-on to Technical Report 32-1526, Volume XIX.

This report presents DSN progress in flight project support, tracking and data acquisition (TDA) research and technology, network engineering, hardware and software implementation, and operations. Each issue presents material in some, but not all, of the following categories in the order indicated:

Description of the DSN

Mission Support
- Ongoing Planetary/Interplanetary Flight Projects
- Advanced Flight Projects

Radio Science
- Radio Science Support
- Special Projects

Supporting Research and Technology
- Tracking and Ground-Based Navigation
- Communications—Spacecraft/Ground
- Station Control and Operations Technology
- Network Control and Data Processing

Network Engineering and Implementation
- Network Control System
- Ground Communications
- Deep Space Stations

Operations
- Network Operations
- Network Control System Operations
- Ground Communications
- Deep Space Stations

Planning and Facilities
- TDA Planning
- Facility Engineering

In each issue, the part entitled "Description of the DSN" describes the functions and facilities of the DSN and may report the current configuration of one of the five DSN systems (Tracking, Telemetry, Command, Monitor and Control, and Test and Training).

The work described in this report series is either performed or managed by the Tracking and Data Acquisition organization of JPL for NASA.

Contents

DESCRIPTION OF THE DSN

MISSION SUPPORT

Ongoing Planetary/Interplanetary Flight Projects

SPECIAL

SUPPORTING RESEARCH AND TECHNOLOGY

Tracking and Ground-Based Navigation

Communications—Spacecraft/Ground

Station Control and Operations Technology

Network Control and Data Processing

NETWORK AND FACILITY ENGINEERING AND IMPLEMENTATION

Deep Space Stations

OPERATIONS

Network Operations

Deep Space Stations

PROGRAM PLANNING

TDA Planning

Quality Assurance

DSN Functions and Facilities

N. A. Renzetti
Office of Tracking and Data Acquisition

The objectives, functions, and organization of the Deep Space Network are summarized. Deep space station, ground communication, and network operations control capabilities are described.

The Deep Space Network (DSN), established by the National Aeronautics and Space Administration (NASA) Office of Tracking and Data Acquisition (OTDA) under the system management and technical direction of the Jet Propulsion Laboratory (JPL), is designed for two-way communications with unmanned spacecraft traveling approximately 16,000 km (10,000 mi) from Earth to the farthest planets of our solar system. It has provided tracking and data acquisition support for the following NASA deep space exploration projects, for which JPL has been responsible for the project management, development of the spacecraft, and conduct of mission operations:

(1) Ranger.

(2) Surveyor.

(3) Mariner Venus 1962.

(4) Mariner Mars 1964.

(5) Mariner Venus 1967.

(6) Mariner Mars 1969.

(7) Mariner Mars 1971.

(8) Mariner Venus/Mercury 1973.

The DSN has also provided tracking and data acquisition support for the following projects:

(1) Lunar Orbiter, for which the Langley Research Center carried out the project management, spacecraft development, and mission operations functions.

(2) Pioneer, for which the Ames Research Center carried out the project management, spacecraft development, and mission operations functions.

(3) Apollo, for which the Lyndon B. Johnson Space Center was the project center and the Deep Space Network supplemented the Spaceflight Tracking and Data Network (STDN), which is managed by the Goddard Space Flight Center (GSFC).

(4) Helios, a joint United States/West Germany project.

(5) Viking, for which the Langley Research Center provides the project management and Lander spacecraft, and conducts mission operations, and for which JPL provides the Orbiter spacecraft.

The Deep Space Network is one of two NASA networks. The other, the Spaceflight Tracking and Data Network, is under the system management and technical direction of the Goddard Space Flight Center. Its function is to support manned and unmanned Earth-orbiting and lunar scientific and advanced technology satellites. Although the DSN was concerned with unmanned lunar spacecraft in its early years, its primary objective now and into the future is to continue its support of planetary and interplanetary flight projects.

A development objective has been to keep the network capability at the state of the art of telecommunications and data handling and to support as many flight projects as possible with a minimum of mission-dependent hardware and software. The DSN provides direct support to each flight project through that project's tracking and data systems. This management element is responsible for the design and operation of the hardware and software in the DSN which are required for the conduct of flight operations.

As of July 1972, NASA undertook a change in the interface between the network and the flight projects. Since January 1, 1964, the network, in addition to consisting of the Deep Space Stations and the Ground Communications Facility, had also included the Mission Control and Computing Facility and had provided the equipment in the mission support areas for the conduct of mission operations. The latter facilities were housed in a building at JPL known as the Space Flight Operations Facility (SFOF). The interface change was to accommodate a hardware interface between the network operations control functions and the mission control and computing functions. This resulted in the flight project's picking up the cognizance of the large general-purpose digital computers, which were used for network processing as well as mission data processing. It also assumed cognizance of all of the equipment in the flight operations facility for display and communications necessary for the conduct of mission operations. The network has already undertaken the development of hardware and computer software necessary to do its network operations control and monitor functions in separate computers. This activity became known as the Network Control System implementation. A characteristic of the new interface is that the network provides direct data flow to and from the stations via appropriate ground communications equipment to Mission Operations Centers, wherever they may be; namely, metric data, science and engineering telemetry, and such network monitor data as are useful to the flight project. It accepts command data from the flight project directly into the ground communications equipment for transmission to the station and thence to the spacecraft in a standardized format.

In carrying out its functions, the network activities can be divided into two general areas. The first includes those functions which are associated with the in-flight support and in tracking the spacecraft; its configuration can be characterized as follows:

(1) *DSN Tracking System.* Generates radio metric data; i.e., angles, one- and two-way doppler and range, and transmits raw data to mission control.

(2) *DSN Telemetry System.* Receives, decodes, records, and retransmits engineering and scientific data generated in the spacecraft to Mission Control.

(3) *DSN Command System.* Accepts coded signals from Mission Control via the Ground Communications Facility (GCF) and transmits them to the spacecraft in order to initiate spacecraft functions in flight.

The second category of activity supports testing, training, and network operations control functions and is configured as follows:

(1) *DSN Monitor and Control System.* Instruments, transmits, records, and displays those parameters of the DSN necessary to verify configuration and validate the network. Provides operational direction and configuration control of the network and primary interface with flight project mission control personnel.

(2) *DSN Test and Training System.* Generates and controls simulated data to support development, test, training, and fault isolation within the DSN. Participates in mission simulation with flight projects.

The capabilities needed to carry out the above functions have evolved in three technical areas:

(1) The Deep Space Stations that are distributed around Earth and which, prior to 1964, formed part of the Deep Space Instrumentation Facility. The technology involved in equipping these stations is strongly related to the state of the art of telecommunications and flight/ground design considerations and is almost completely multimission in character. Table 1 gives a description of the Deep Space Stations and the Deep Space Communications Complexes (DSCCs) they comprise.

(2) Ground communications. This technology supports the Earth-based point-to-point voice and data communications from the stations to the Network Operations Control Area at JPL, Pasadena, and to the Mission Operations Centers, wherever they may be. It is based largely on the capabilities of the common carriers throughout the world which are engineered into an integrated system by the Goddard Space Flight Center for support of all NASA programs. The term "Ground Communications Facility" is used for the sets of hardware and software needed to carry out the functions.

The Network Operations Control Center is the functional entity for centralized operational control of the network and interfaces with the users. It has two separable functional elements; namely, Network Operations Control and Network Data Processing.

The functions of the Network Operations Control Center are:

(1) Control and coordination of network support to meet commitments to network users.

(2) Utilization of the network data processing computing capability to generate all standards and limits required for network operations.

(3) Utilization of network data processing computing capability to analyze and validate the performance of all network systems.

The personnel who carry out the above functions are on the first floor of Building 230, wherein mission operations functions are carried out by certain flight projects. Network personnel are directed by an Operations Control Chief. The functions of the Network Data Processing are:

(1) Processing of data used by Network Operations Control for the control and analysis of the network.

(2) Display in Network Operations Control Area of data processed in Network Data Processing Area.

(3) Interface with communications circuits for input to and output from Network Data Processing Area.

(4) Data logging and production of the intermediate data records.

The personnel who carry out these functions are located in Building 202, which is approximately 200 m from Building 230. The equipment consists of minicomputers for real-time data system monitoring, two XDS Sigma 5's, display, magnetic tape recorders, and appropriate interface equipment with the ground data communications.

Table 1. Tracking and data acquisition stations of the DSN

DSCC	Location	DSS	DSS serial designation	Antenna		Year of initial operation
				Diameter, m (ft)	Type of mounting	
Goldstone	California	Pioneer	11	26(85)	Polar	1958
		Echo	12	26(85)	Polar	1962
		(Venus)[a]	13	26(85)	Az-El	1962
		Mars	14	64(210)	Az-El	1966
Tidbinbilla	Australia	Weemala	42	26(85)	Polar	1965
		Ballima	43	64(210)	Az-El	1973
—	Australia	Honeysuckle Creek	44	26(85)	X-Y	1973
Madrid	Spain	Robledo	61	26(85)	Polar	1965
		Cebreros	62	26(85)	Polar	1967
		Robledo	63	64(210)	Az-El	1973

[a]A maintenance facility. Besides the 26-m (85-ft) diam Az-El mounted antenna, DSS 13 has a 9-m (30-ft) diam Az-El mounted antenna that is used for interstation time correlation using lunar reflection techniques, for testing the design of new equipment, and for support of ground-based radio science.

A Viterbi Decoding Program for DSN Telemetry System Analysis

B. Benjauthrit, B. D. L. Mulhall, and J. S. Wong,
DSN Systems Engineering Section

A computer program written in Fortran V for the Univac 1108 to simulate the Viterbi decoding algorithm is described together with its capabilities and preliminary simulation results.

I. Introduction

To increase the capability of deep space telecommunication systems, convolutional coding is being implemented with Viterbi decoding. The first flight project to use this capability will be the Mariner Jupiter/Saturn 1977 mission. Subsequent interplanetary exploration missions will also employ this capability. In verifying the design and evaluating the telecommunication systems performance (particularly the DSN Telemetry System) for these missions, computer programs are a cost-effective way of achieving results. This technique can also be used for monitoring performance of the Telemetry System.

This is a progress report on the development of a computer program which implements the Viterbi decoding algorithm for analysis purposes. The program was modularized so that minor modifications or additional features can be relatively simple to incorporate into the program. Actually, there are many computer programs (Refs. 1–4) written to implement the algorithm. However, they do not possess the required capabilities for analysis of DSN Telemetry System performance.

II. Program Structure

The program is written in Fortran V and implemented on JPL's Univac 1108 system.[1] The program is conversational and is accessible through remote terminals such as Execuports and Uniscopes. Figure 1 depicts a basic flow chart of the Viterbi decoding algorithm. An enlarged version of the algorithm is block diagrammed in Fig. 2. Since most of the blocks in the diagram are self-explanatory, only brief discussions follow. Detailed explanations and terminology may be found in Refs. 1–5.

The program accepts convolutionally coded input data. The branch metrics are computed in subroutine BMTAB. The summary of decoding results can be printed out for any desirable number of decoded bits through Block 7. This is to monitor proper functioning of the program and to safeguard against total loss of decoding statistics in the event of an 1108 failure. Out-of-sync information used in

[1] The program is based on a Fortran V program written at the Johnson Space Center (Ref. 4). Capability added to the program at JPL includes the ability to read test data tapes, perform node synchronization, and compute error burst statistics.

Block 8 is flagged in Block 28. Illegal input symbols are detected in Block 8 and are outputted by Block 32. In order to determine error statistics, uncorrupted symbols and input data bits are generated internally or entered externally in Block 14. Selection of decoded bits is accomplished in Block 15, together with update statistics and print outs. The size of error-free gaps is recorded in Block 18 and is passed to Block 17 where the statistics of burst errors are analyzed. The summary of burst errors is also printed out periodically in Block 17. The out-of-sync condition determined in Block 27 on the basis of the number of decoded bits and the number of normalizations is accumulated in Blocks 19 and 26, respectively. Total decoding statistics are printed at an end-of-file, or when an error is detected in the data file.

III. Program Capabilities

The program was written for the DSN rate 1/2 and rate 1/3, constraint length 7, 8-level quantization, convolutional codes. Since the program structure is rather general, minimum modifications need be made to accommodate other short constraint length convolutional codes.

Though only two methods of selecting a decoded bit, i.e., the best metric decision and the majority vote decision, are available in the program, other alternative methods can be easily added to the program. Note that the maximum memory path length in bits (the value of $m \cdot K$ in Block 13 of Fig. 2) is 72; it can be expanded when desired. Besides providing bit error rate (BER), symbol error rate (SER), for the above two methods of selecting decoded bits, the hard input data symbols, symbol error locations, hard input data bits, and decoded data bits are also available.

The statistics of burst errors are: The number of errors per burst, the burst length in bits, and the error-free gap length in bits. These results are averaged periodically and summarized at the end of each run. The distribution of burst errors is also recorded.

IV. Preliminary Simulation Results

The program was employed to process test data obtained from CTA 21, after having been converted from a 64-level quantization into an 8-level acceptable data format. The test conditions of the data and partial input data for the program are described in Fig. 3. The statistics of raw-symbol and decoded-bit errors are tabulated in Fig. 4. Note that the result of Fig. 3a was obtained separately.[2]

Though the amount of data processed was too small to be of any significance, the results obtained appear to agree within the same order of magnitude with those provided by the LV7015 decoder of LINKABIT (Ref. 6). Comparison is made in Fig. 5.

[2]From a program written by Dr. C.A. Greenhall

References

1. Heller, J. A. and Jacobs, I. M., "Viterbi Decoding for Satellite and Space Communication," *IEEE Trans. on Comm. Tech.*, Vol. COM-19, No. 5, October 1971, pp. 835–848.

2. Gilhausen, K. S., et al., "Coding Systems Study for High Data Rate Telemetry Links," N71-27786, LINKABIT Corp., San Diego, Calif., January 1971.

3. Layland, J., "Performance of Short Constraint Length Convolutional Codes and a Heuristic Code-Construction Algorithm," in *The Deep Space Network*, Space Programs Summary 37-64, Vol. II, pp. 40–44, Jet Propulsion Laboratory, Pasadena, Calif., August 1970.

4. Batson, B., et al., "Simulation Results for the Viterbi Decoding Algorithm," NASA TR R-396, November 1972.

5. Viterbi, A. J., "Convolutional Codes and Their Performance in Communication Systems," *IEEE Trans. on Comm. Tech.*, Vol. COM-19, No. 5, pp. 751–772, October 1971.

6. *The LV7015 Reference Manual*, LINKABIT Corp., San Diego, Calif., 1972.

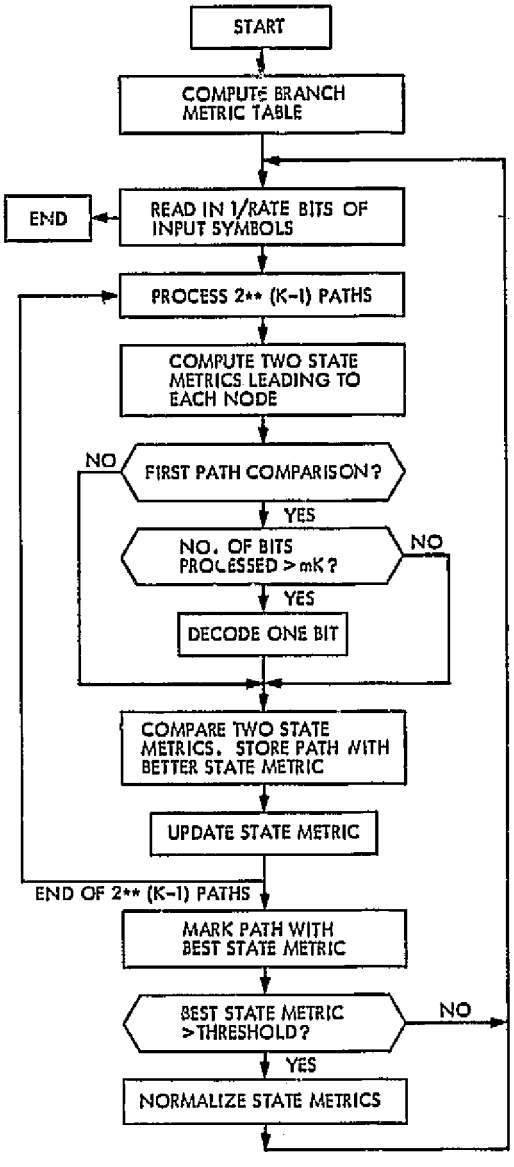

K IS THE CONSTRAINT LENGTH
K · m IS THE MEMORY PATH LENGTH
m IS USUALLY 5 OR 6

Fig. 1. Basic Viterbi decoding algorithm

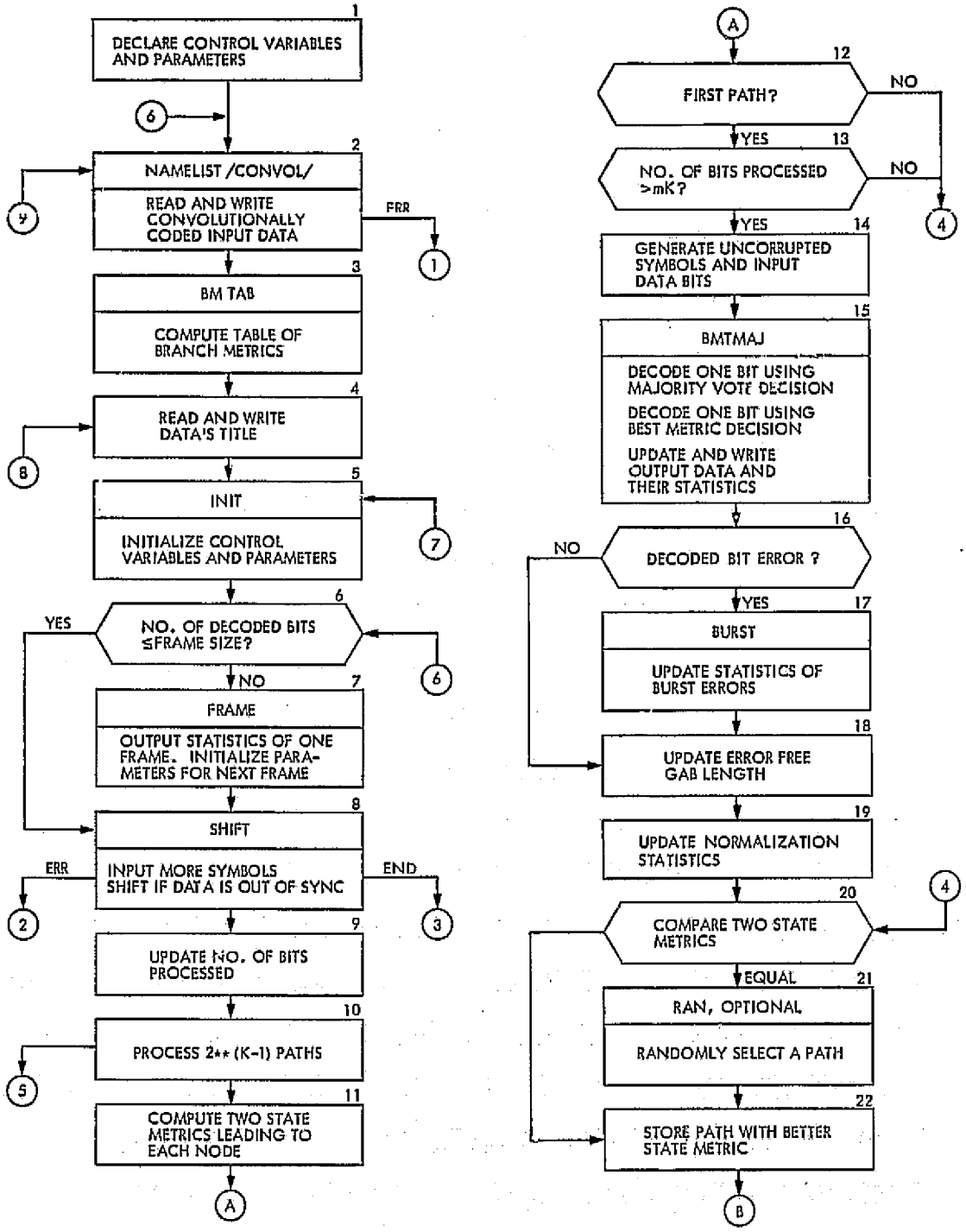

Fig. 2. Flow chart of 1108 program

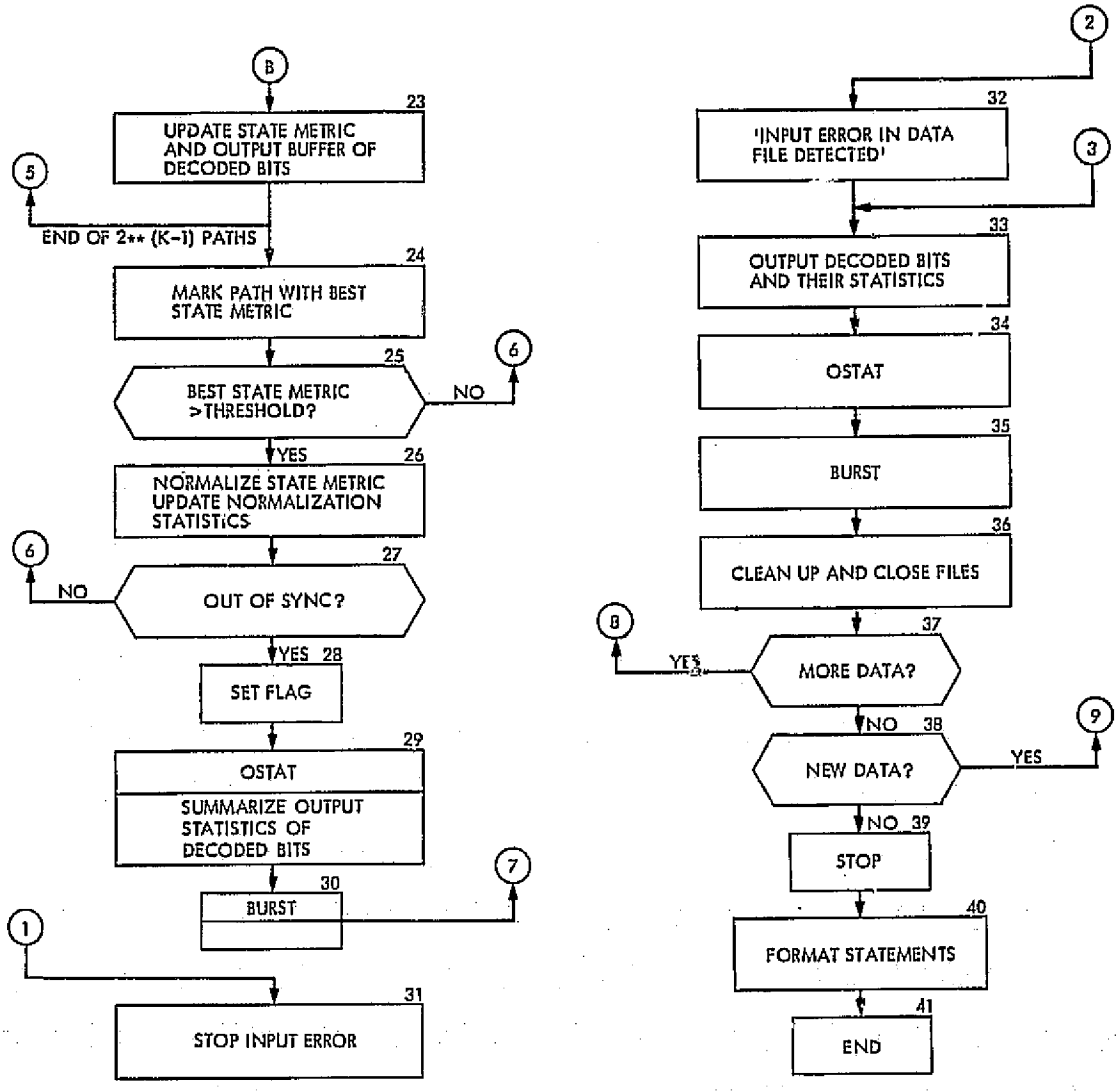
B
23
UPDATE STATE METRIC AND OUTPUT BUFFER OF DECODED BITS
5
END OF 2** (K-1) PATHS
24
MARK PATH WITH BEST STATE METRIC
25
BEST STATE METRIC >THRESHOLD?
NO
6
YES
26
NORMALIZE STATE METRIC UPDATE NORMALIZATION STATISTICS
6
NO
27
OUT OF SYNC?
YES 28
SET FLAG
29
OSTAT
SUMMARIZE OUTPUT STATISTICS OF DECODED BITS
30
BURST
7
1
31
STOP INPUT ERROR
2
32
'INPUT ERROR IN DATA FILE DETECTED'
3
33
OUTPUT DECODED BITS AND THEIR STATISTICS
34
OSTAT
35
BURST
36
CLEAN UP AND CLOSE FILES
8
37
YES
MORE DATA?
NO 38
9
NEW DATA?
YES
NO 39
STOP
40
FORMAT STATEMENTS
41
END

Fig. 2. (contd)

symbols/sec = 2048	E_b/N_0, THEORETICAL, INCLUDING LOSSES = 3.715 dB
MODULATION INDEX = 55 deg	γ FACTOR = 6.29
CARRIER SUPPRESSION = -4.828 dB	PAD = 9.14

(a) TEST CONDITIONS

RATE = 1/2	IMPULSE RESPONSE = 3133023 (QUATERNARY NOTATION)
CONSTRAINT LENGTH = 7	mK = 36

(b) PARTIAL INPUT TO 1108 PROGRAM

Fig. 3. Test conditions and program input

	NO. OF SYMBOLS	AVE. LENGTH IN BITS OF CONTINUOUS ERRORS	AVE. GAP LENGTH
1.	9072	1.0756	14.8421
2.	6482	1.0772	14.5398
3.	3564	1.0602	12.2921

(a) STATISTIC OF RAW SYMBOLS

GAP LENGTH (IN bits)	6224	543	2331	45	6405	0	1	0	2641	4164	3240	4856	1626
ERROR LOCATION	1	2	3	4	5	6	7	8	9	10	11	12	

(b) BURST STATISTIC OF DECODED BITS

Fig. 4. Statistics of symbols and decoded bit errors

	1108 PROGRAM	LV 7015*
BER	3.74×10^{-4}	1.10×10^{-4}
SER	6.83×10^{-2}	—
AVE. NO. OF ERRORS/BURST**	4	3.8
AVE. NO. OF BIT BURST LENGTH	5	6.2

* FROM REF. 6 AT 4.0 dB

** A BURST IS DEFINED HERE AS A SEQUENCE OF BIT ERRORS CONTAINING AT MOST K-2 GOOD BITS

Fig. 5. Comparison of error statistics

Viking Mission Support

D. J. Mudgway and A. I. Bryan
DSN Systems Engineering Office

D. W. Johnston
DSN Operations Office

This article continues the report on the results of RF compatibility tests between Viking Orbiter No. 1 and the Spacecraft Compatibility/Monitor Station, Merritt Island, Florida (STDN-MIL 71).

It also includes the status of the Mission Configuration Tests (MCTs) and Operational Verification Tests (OVTs). The latter tests are complete, and all crews at all stations are trained for cruise support. Initial acquisition OVTs are scheduled to be run during July 1975 with the Deep Space Stations in Canberra, Australia.

I. Background

The previous article in this series described progress in Viking compatibility testing in January and February 1975. Activity has been continuing in this area and this article assesses the test results obtained through May 29, 1975. Also included is the status of the DSN testing and training culminating in the application of Viking configuration control on July 1, 1975.

II. Viking Orbiter Radio Frequency Compatibility Tests

This assessment and status is derived from test results obtained between STDN(MIL 71) and Viking Orbiter No. 1 at Cape Canaveral, Florida, May 27–29, 1975.

Procedures for conducting these tests were prepared by the DSN with test parameters and design criteria related to Orbiter telecommunications performance. The final procedures and test plans were approved during a meeting of the DSN/Viking Orbiter Telecommunications Representatives at Cape Canaveral, Florida. The total test time was 28 hours.

All tests in Ref. 1 were completed, although specified performance criteria for auxiliary oscillator No. 2 and low-rate telemetry were not actually met. The extent of completion of tests achieved within the scheduled time period was due in large measure to the excellent support provided by the JPL/Goddard STDN(MIL 71) and spacecraft teams.

A. Test Objectives

The objective of the tests was to verify telecommunications compatibility between the DSN and Viking Orbiter No. 1. The test criteria and parameters simulated direct communications between an Orbiter flight article in Martian Orbit and a 64-m antenna station. Design

compatibility had been previously established between the DSN and Viking Orbiter No. 1 at the Compatibility Test Area in Pasadena, Calif. as reported in Ref. 2.

A selected set of standard tests were performed for verifying transponder, radio frequency (RF), command, telemetry, and radio metric compatibility. These tests were accomplished in accordance with the requirements of Ref. 1.

B. Test Conditions

Viking Orbiter No. 1 was configured for mission operations and STDN(MIL 71) was configured to simulate a DSN 64-m antenna station. Viking Orbiter No. 1 was located in the clean room of Building AO, Cape Canaveral, Florida, and STDN(MIL 71) was located at Merritt Island, Florida. An S-band two-way RF link and an X-band one-way RF downlink were utilized between the flight article and the ground station. Both links were approximately seven miles.

S-band RF link variations were 0.5 dB peak-to-peak during the test. These conditions existed during daylight and evening hours on May 28 and 29, 1975. X-band RF link variations were 1.0 dB peak-to-peak during evening hours when critical X-band testing was being performed.

The ground station software utilized in performing these tests was supplied by the DSN and was a subset of software officially released to the station for Viking Project support. The programs consisted of:

(1) Telemetry and Command Program. This program provides independent control of the commanding and telemetry handling functions. Commands may be controlled manually from the station or automatically from the Mission Control and Computing Center, in Pasadena, Calif. Telemetry may be decoded, formatted, and transmitted to the Mission Control and Computing Center for decommutation and display.

(2) Planetary Ranging Assembly Program. This program provides either continuous spectrum or discrete spectrum operation for determining very accurate range estimates of a spacecraft at planetary distances.

C. Test Results

The following radio frequency acquisition and tracking tests were performed:

(1) Downlink threshold one-way

(2) Uplink threshold

(3) Downlink threshold two-way

(4) Spacecraft receiver pull-in range and rate

(5) Carrier residual phase jitter

(6) Transponder rest frequency

(7) Auxiliary oscillator frequency

The following problems were encountered:

(1) Auxiliary oscillator No. 2 was found to be approximately 800 Hz below design center frequency. Additionally, the one-way residual carrier phase jitter on auxiliary oscillator No. 2 was greater than specified performance. Although these conditions have been identified, it is felt that neither is significant enough to impact a successful mission. No retest is necessary.

(2) Two-way carrier phase jitter measurements were performed with uplink signal levels of -110 dBm and -108 dBm, respectively. MIL 71 uplink power level during these tests was adjusted for maximum spacecraft signal level.

A test of command capability under doppler conditions was conducted. No problems were encountered.

The following radio-metric data tests were performed:

(1) Ranging channel delay threshold and polarity verification (S-band, single channel).

(2) Ranging channel delay threshold and polarity verification (X-band, single channel).

(3) Ranging channel delay threshold and polarity verification (simultaneous S/X-band)

While no problems were encountered, there was one condition which surprised the observers and the spacecraft test team: During the initial acquisition process of the ranging system, uplink modulation is removed for approximately one second. The effect is a transitory increase in spacecraft receiver automatic gain control. Initial investigation has verified that the ranging system software does, in fact, operate in this fashion. While there is no obvious harmful effect caused by this transient, it is not desirable, either. At the very least, it will be reported as a spacecraft idiosyncrasy. From the spacecraft telecommunications viewpoint, however, the software should be modified.

All objectives of these tests were met, including simultaneous S/X ranging which was accomplished for the

first time between the DSN and a flight spacecraft. Simultaneous delay measurements were within 3 ns of previously measured individual delay measurements. S-band link amplitude stability performance during this test was 1 dB peak-to-peak, and X-band was 2 dB peak-to-peak.

The following telemetry tests were performed:

(1) Modulation index and spectrum analysis

(2) Telemetry performance test

The following problems were encountered: In Test 14A (spacecraft radio mode 3[illegible]), the low-rate data (8.3 bits/s uncoded) signal-to-noise ratio performance was below specified criteria. A postcompatibility test at MIL 71 to investigate this condition revealed that the low-rate telemetry channel performance was degraded by approximately 1 dB. A realignment of the system resulted in restoring proper performance of the low rate telemetry channel. It is safe to assume that the excessive loss in the station equipment was present during the compatibility test and accounted for the measurement falling outside its predicted range. It would be desirable, but not mandatory, to repeat Test 14A with the spacecraft if time and schedules permit.

III. DSN Test and Training Preparations

A significant change from earlier planning was the decision to implement the second 26-m subnet (DSSs 12, 44, 62) prior to the first Viking launch. The majority of the Mission configuration tests for these stations have been performed, and the operational verification tests have just been completed.

Table 1 shows the current mission configuration test status of the 64-m, primary 26-m and secondary 26-m subnets, indicating actual testing status as of July 1, 1975.

The 64-m and prime 26-m subnets are considered trained to support Viking cruise operations. During the period of this report, DSSs 43 and 63 have completed cruise phase operational verification tests, DSS 14 and the prime and secondary 26-m nets have completed cruise and planetary operational verification tests. The stations have also supported Viking System Integration Tests, ground data system tests and various others of the project-related test series including flight operations personnel test and training. No problems are anticipated on future support of the latter tests. Stations 43 and 63 will be supporting planetary phase operational verification tests after launch and prior to encounter.

IV. Conclusion

The planned sequence, number and duration of the Mission configuration and operational verification tests was adhered to with only minor exceptions.

The operational verification test program is now complete and all stations and the DSN Operations Control Team have achieved the desired level of Viking mission-dependent training proficiency required for Viking cruise support. The Mission configuration test program should be complete prior to launch.

Initial Acquisition OVTs have been scheduled for DSSs 42 and 44 in July to exercise the initial acquisition strategy produced by the DSN and concurred by the Viking Project. These are the final tests to verify launch and cruise readiness.

Configuration control for Viking was applied at all stations on July 1, 1975.

References

1. *Rev. J, Master Integrated Test Plan Viking 75 Spacecraft/ Orbiter/Lander to Launch and Flight Operations System and Tracking and Data System Compatibility Test Plan*, NASA Document PL-3710005, March 29, 1972.
2. *The Deep Space Network Progress Report 42-24*, September and October 1974, pp. 9-13, Jet Propulsion Laboratory, Pasadena, Calif., Dec. 15, 1974.

Table 1. Completion status of MCTs

Stations	DSS	Systems			
		Telemetry	Command	Tracking	Monitor and control
64 m	14	C/P	4 h outstanding (dual exciter switch)	Not complete	C/P
	43	Cruise strong signal only	C	Not complete	C
	63	C	C	Not complete	C
Prime 26 m	11	C	C	Not complete	C/P
	42	C	C	Not complete	C/P
	61	C	C	Not complete	C/P
Secondary 26 m	12	C	C	RF portion only	C/P
	44	C	C	RF portion only	C/P
	62	C	C	RF portion only	C/P

C = cruise P = planetary

Pioneer Venus 1978 Mission Support

R. B. Miller
DSN System Engineering Office

Significant aspects of the Orbiter portion of the Pioneer Venus 1978 Mission are described.

I. Introduction

The Pioneer Venus 1978 Project will consist of two missions: an Orbiter Mission and a Multiprobe Mission. The Multiprobe Mission has been described in several previous *Deep Space Network Progress Report* articles; see in particular Refs. 1 and 2. This article will concentrate on the Orbiter Mission.

The Orbiter Mission will launch in late May or early June of 1978, using a Type II trajectory, while the Multiprobe Mission will be launched in August 1978, using a Type I trajectory. Both missions will arrive at Venus in early December 1978, the Orbiter arriving a few days before the Multiprobe. Both missions will utilize an Atlas SLV-IIID Centaur D-1AR launch vehicle, with approximately a 160-km altitude parking orbit. The Orbiter will be designed for a minimum lifetime of 243 Earth days in Venusian orbit which corresponds to one Venusian day. The spacecraft will be constructed by the Hughes Aircraft Company under contract to Ames Research Center, which has Project management responsibilities.

II. Orbiter Spacecraft Characteristics

The Pioneer Venus 1978 Orbiter and Multiprobe spacecraft were designed to use as much common hardware as feasible in these distinctly different missions. A commonality on the order of 70% has been claimed. The Orbiter spacecraft is shown schematically in Fig. 1. The spacecraft is spin-stabilized with a mechanically despun antenna system. The spacecraft is 254 cm (100 in.) in diameter and will use spin rates between 5 and 30 rev/min during the life of the mission. Total mass of the spacecraft is 576 kg (1270 lb) accommodating approximately 45 kg (100 lb) of scientific instruments. There are 12 on-board experiments, two of which are common to the bus spacecraft of the multiprobe mission. Located on the spin axis, below the equipment shelf, is a solid orbit insertion motor. A monopropellant hydrazine system provides propulsion for all velocity correction maneuvers, attitude, and spin control, using four radial and three axial thrusters. The outer surface of the cylindrical portion of the spacecraft is covered with a solar array to provide spacecraft power. Located on the spin axis above the

equipment shelf is a despun antenna mask accommodating a high-gain parabola used for both S- and X-band, a sleeve dipole antenna serving as the medium-gain antenna to back up the parabola, and at the top a forward omniantenna. To complete the onmiantenna pattern, an off-axis antenna is provided on the aft end of the spacecraft. The sleeve dipole antenna is linearly polarized, and all other antennas are right-hand circularly polarized. The high-gain antenna is 109 cm (43 in.) in diameter.

III. Science Payload

The Orbiter mission will carry a complement of 12 scientific instruments. The on-board instruments are listed in Table 1. In addition, there are six ground-based radio science experimenters who will utilize the telecommunications link from the spacecraft and ground-based equipment for their experiments, which are listed in Table 2.

The individual experiments listed in Tables 1 and 2 will be described in more detail in subsequent *Deep Space Network Progress Report* articles on the Pioneer Venus 1978 Mission.

IV. Mission Description

The Orbiter Mission will be launched between May 6 and June 4, 1978, using a Type II trajectory. The encounter window at Venus is between Dec. 4 and Dec. 12 1978. Preliminary mission sequence calls for separation from Centaur and initial spinup at launch plus 30 min and magnetometer boom deployment at launch plus 4 hours. Velocity corrections en route to Venus would occur at launch plus 5 days, launch plus 20 days, and at Venus Orbit Insertion (VOI) minus 20 days in the nominal mission. VOI would occur at approximately launch plus 200 days. The spin rate of the spacecraft would be 5 rev/min at Centaur separation, 15 rev/min during the cruise phase, 30 rev/min during the orbit insertion, and 5 rev/min during the orbital mission phase.

Figure 2 shows the Earth and Venus locations at the start and end of the 243 Earth-day primary mission. During that 243 days, Venus will have completed slightly more than one orbit around the Sun and one complete rotation on its axis. Although the final Venus orbit has not been selected, the following is typical for planning purposes: an orbital inclination that is 80 deg retrograde with an orbital period of 24 Earth hours. Peripasis altitude would be maintained between 150 and 260 km, and the latitude of periapsis would vary between 15 deg and 32 deg north. This trajectory will result in the prime Earth occultations (those occurring at periapsis) occurring from Day 0 to Day 75 in orbit with a maximum duration of the occultation of 25 min. There will be two periods of solar occultation (or eclipse) from Day 25 to Day 120, with a maximum eclipse of 25 min, and again from Day 183 to Day 189 in orbit with a maximum duration of 3.8 h.

Maintaining the orbit with such a low periapsis altitude will require orbital adjustment maneuvers perhaps as often as once a week, but at least as often as once a month, during the primary orbital mission.

The Orbiter spacecraft includes a 1.048×10^6-bit memory and a redundant 128-instruction command sequencer. The basic mission plan was to be able to operate on a 26-m Deep Space Station using a single pass each day centered on periapsis. During this station pass, the data from the apoapsis could be recalled from the spacecraft, the command sequence reloaded for the next 24 hours, the periapsis data taken at high rate into the spacecraft memory, and finally, the periapsis data played out of the memory to the station. As the mission design has progressed, the coverage requirements have grown considerably due to occultation requirements and expanding data rate requirements of some of the instruments. Table 1 contains a list of the currently estimated Pioneer Venus Orbiter DSN coverage requirements. The rather complex Fig. 3 (designed by J. Dyer of the Pioneer Project Office) is an attempt to portray these coverage requirements pictorially. The diagonal line in Fig. 2 extending from 16 GMT on Day 0 represents a tentative selection by the Project of a time for periapsis passage. This was selected to have the periapsis passage during the mutual Goldstone-Australia Deep Space Station view period to try and help minimize the coverage conflict between Pioneer Venus and the Mariner Jupiter-Saturn (MJS) missions which will be flying during the same time period, which includes the two Jupiter encounters. The 2-hour band extending out to Day 120, becoming 3 hours out to the end-of-mission, is the basic 26-m coverage requirement in order to perform the daily data recovery from the spacecraft memory and reloading of the command sequencer. The increase in number of hours around Day 120 is necessary due to the decreasing bit rate. Remembering Fig. 2, the range to the spacecraft while in orbit around Venus continually increases during the primary mission, which ends just before the first superior conjunction. Figure 4 translates this range increase to the bit rate as a function of days in orbit for both a DSN 26-m and a 64-m antenna, assuming the spacecraft is using the high-gain antenna and is in the high-power mode.

The prime occultations occur for the first 70 to 80 days of orbit and require 64-m coverage of approximately three hours centered on periapsis because of signal level requirements and the requirement for X-band reception. This coverage requirement is shown as the cross-hatch section in Fig. 3 along the diagonal out to Day 80. Recall that many orbit adjustment maneuvers will be required because of the low periapsis altitude, and therefore a minimum coverage requirement for radio metric data purposes for navigation has been established as a 26-m, 24-h pass at least two days out of every six, although continuous 26-m coverage is preferred. There will also be approximately 15 days of apoapsis occultations between Day 150 and Day 165, which, because of their duration, will require on the order of six hours of 64-m coverage. This is shown in Fig. 3 as the cross-hatched, irregular polygon centered on Day 160. An on-board instrument, whose data rate requirements have added to the coverage requirements, is the cloud photopolarimeter (CPP). This instrument has two modes: a polarimetry mode, requiring medium data rates; and an imaging mode requiring higher data rates. Neither of these modes can be accommodated by using the megabit memory and are therefore required to be received in real-time. The polarimetry requirement requires 18 hours per day of 26-m coverage in two approximately 10-day blocks during the mission. Table 3 lists typical days for the polarimetry observation. The imaging portion of the experiment requires two 10-day blocks of continuous 64-m coverage, which is pictured as the two vertical bands in Fig. 3 at about 100 and 120 days. In addition, 8 hours per day of 64-m coverage for apoapsis photography is required for 30 days spread between the 40th and 110th day in orbit. The most recently identified additional coverage requirement will be for 64-m coverage for a radar imaging experiment; however, the details of this requirement have not been determined.

Extensive negotiations between the Pioneer Venus Project and the MJS Project are in process in order to try to accommodate the coverage requirements of these two missions as well as Pioneer 10 and 11 during the orbital phase of the Pioneer Venus Mission. The preliminary work so far accomplished in the negotiations between these two projects indicates that, in general, the Pioneer Venus and MJS coverage requirements can probably be met, but the minimum coverage that is acceptable to Pioneer 10 and 11 will be extremely difficult to provide.

V. Telecommunications

The Pioneer Venus Orbiter spacecraft will be transmitting continuous telemetry using PCM/PSK/PM (biphase) modulation of the S-band carrier. The subcarrier frequency will be 32.768 kHz with a modulation index of either 37.2 or 67.6 deg, which is selectable by ground command independent of bit rate. The spacecraft can transmit at the following rates: 8, 16, 64, 128, 170-2/3, 256, 341-1/3, 512, 682-2/3, 1024, and 2048 bits/s. 4096 bits/s might also be possible in the early phase of the mission, although it is not yet known whether the DSN can support that data rate with sequential decoding. The normal operating mode of the spacecraft will be long-constraint-length convolutional coding to be sequentially decoded. All formats are 512 bits in length, using 64 8-bit words and incorporating a 24-bit sync word (76142511_8). Since the constraint length is 32, the encoder will be reset as the last bit of each sync word enters the encoder.

The spacecraft will have an X-band transmitter, phase-coherent to the S-band transmitter, which will be present for radio science purposes only (i.e., no X-band telemetry will be possible). The X-band transmitter will have a power of 750 mW, while the S-band will have a power selectable of either 10 or 20 W using solid-state amplifiers instead of TWTs (traveling wave tube amplifiers). The despun high-gain antenna will have a gain of 25 dBi at S-band and 29 dBi at X-band. The despun sleeve dipole antenna will have a gain of 8 dBi, and the despun forward omnidirectional antenna and aft omnidirectional antenna will have a gain of slightly more than -6 dBi. The high-gain antenna is movable up to 17 deg in elevation, measured perpendicularly to the spin axis.

There will be many different telemetry formats as a function of mission phase; however, all format changes should be transparent to the DSN.

The frequencies assigned to the Orbiter Mission are Deep Space Channel 12 for the prime transponder, Deep Space Channel 11 for the redundant transponder, and Deep Space Channel 17 for the flight spare transponder. The actual frequencies are listed in Table 1 of Ref. 2.

The Command System will be using frequency shift keying/phase modulation where the two tones will be a Data 0 of 100 Hz and a Data 1 of 225 Hz. The command rate will be 4 bits/s, and individual commands will be 59 bits long. Contiguous commands after the first 59-bit command can be 48 bits long. There will be on the order of 370 different commands, the majority of which are redundant. The on-board command storage will have a redundant capacity of 128 locations in which can be stored either a specific instruction (command) or a delta time to be counted down until executing the next instruction. The redundant command storage units can be operated either in parallel for highly critical mission events or in series to effectively double the on-board capacity.

References

1. Miller, R. B., "Pioneer Venus 1978 Mission Support," in *The Deep Space Progress Report 42-23*, pp. 37–40, Jet Propulsion Laboratory, Pasadena, Calif., Oct. 15, 1974.

2. Miller, R. B., "Pioneer Venus 1978 Mission Support," in *Deep Space Progress Report 42-27*, pp. 28–35, Jet Propulsion Laboratory, Pasadena, Calif., June 15, 1975.

Table 1. On-board experiments

Experiment	Principal investigator
Neutral particle mass spectrometer	H. B. O. Niemann Goddard Space Flight Center
Charged-particle mass spectrometer	H. A. Taylor, Jr. Goddard Space Flight Center
Electron temperature probe	L. H. Brace Goddard Space Flight Center
Retarding potential analyzer	W. C. Knudsen Lockheed Aircraft Corporation Palo Alto Research Laboratory
Ultraviolet spectrometer	A. I. Stewart University of Colorado
Infrared radiometer	F. W. Taylor Jet Propulsion Laboratory
Cloud photo-polarimeter	J. E. Hansen Goddard Institute for Space Studies
Magnetometer	C. T. Russell UCLA
Plasma analyzer	J. H. Wolfe Ames Research Center
Electric field detector	F. L. Scarf TRW
Surface radar mapper	G. H. Pettengill Massachusetts Institute of Technology
Gamma burst detector	W. D. Evans Los Alamos Scientific Laboratory

Table 2. Ground-based experiments

Earth-based radio experiments	Experimenter
Dual frequency radio occultation	A. J. Kliore/Jet Propulsion Laboratory and T. Croft/Stanford University
Atmospheric and solar corona turbulence	R. Woo/Jet Propulsion Laboratory
Drag measurements	G. N. Keating/NASA Langley Research Center
Internal density Distribution	R. J. Phillips/Jet Propulsion Laboratory
Celestial mechanics	I. I. Shapiro/Massachusetts Institute of Technology

Table 3. Pioneer Venus Orbiter—estimated DSN requirements

Network	Interval, h/day	Schedule (day number in orbit)	Purpose
26 m	4	1 to 120	Daily data and command sequence
	6	121 to 250+	Daily data and command sequence
	24	2 days out of 6[a]	Navigation, mass properties
	18	80 to 94[b] 106 to 114[b]	Cloud photopolarimeter polarimetry
64 m	3	1 to 70	Short occultations
	6	150 to 165	Long occultations
	24	95 to 105[b] 115 to 125[b]	Cloud photopolarimeter imaging
	8	80 days between 40 to 110	Cloud photopolarimeter imaging
	3	1/wk[c]	Radar imaging

[a]24 h/day every day preferred

[b]Examples, subject to adjustment

[c]Average requirement, details unknown

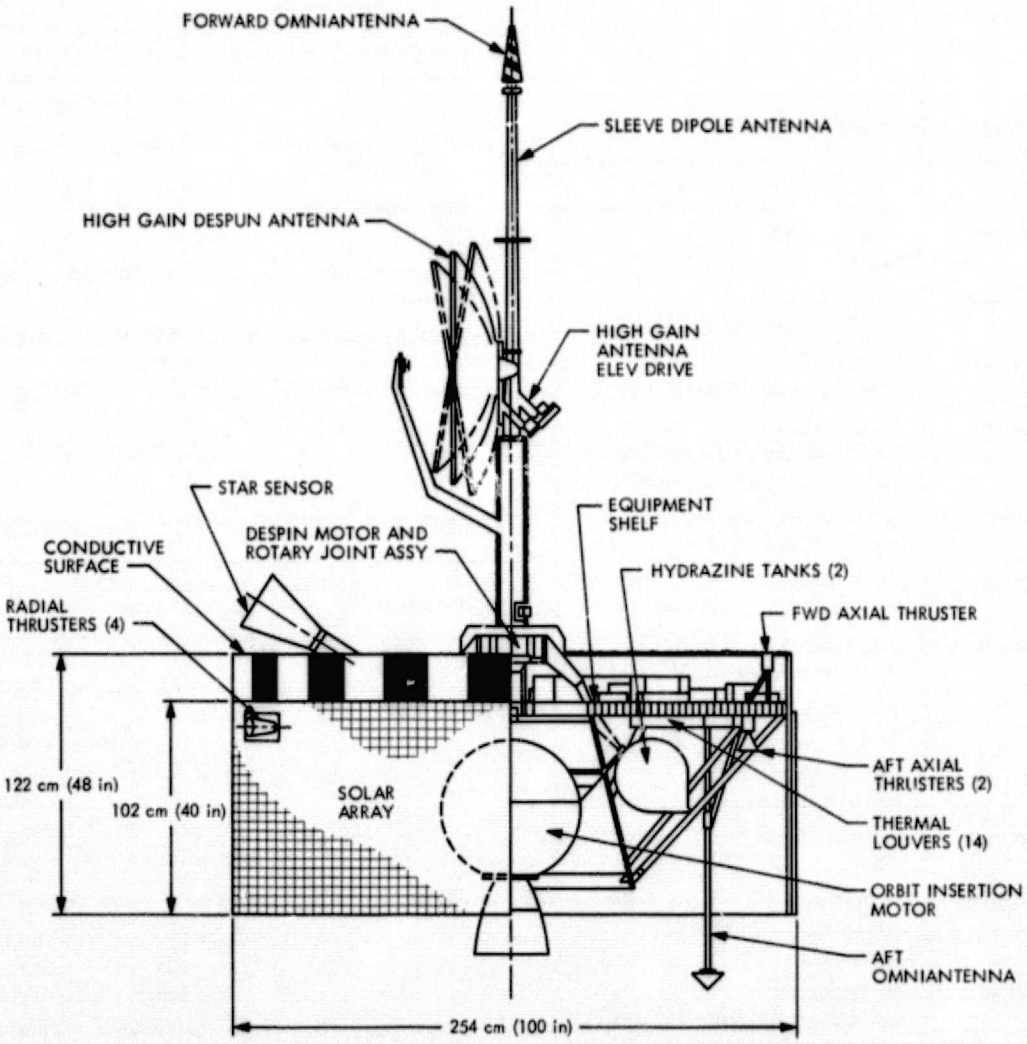

Fig. 1. Pioneer Venus 1978 Orbiter spacecraft

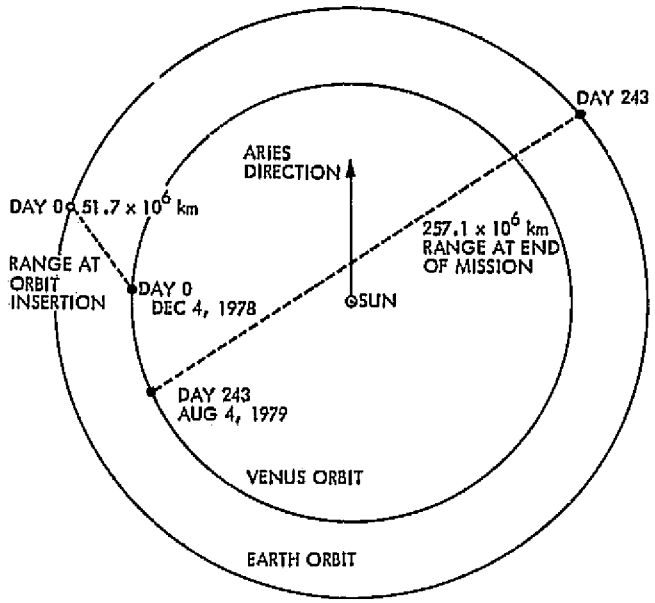

Fig. 2. Earth and Venus locations at start and end of Orbiter Mission

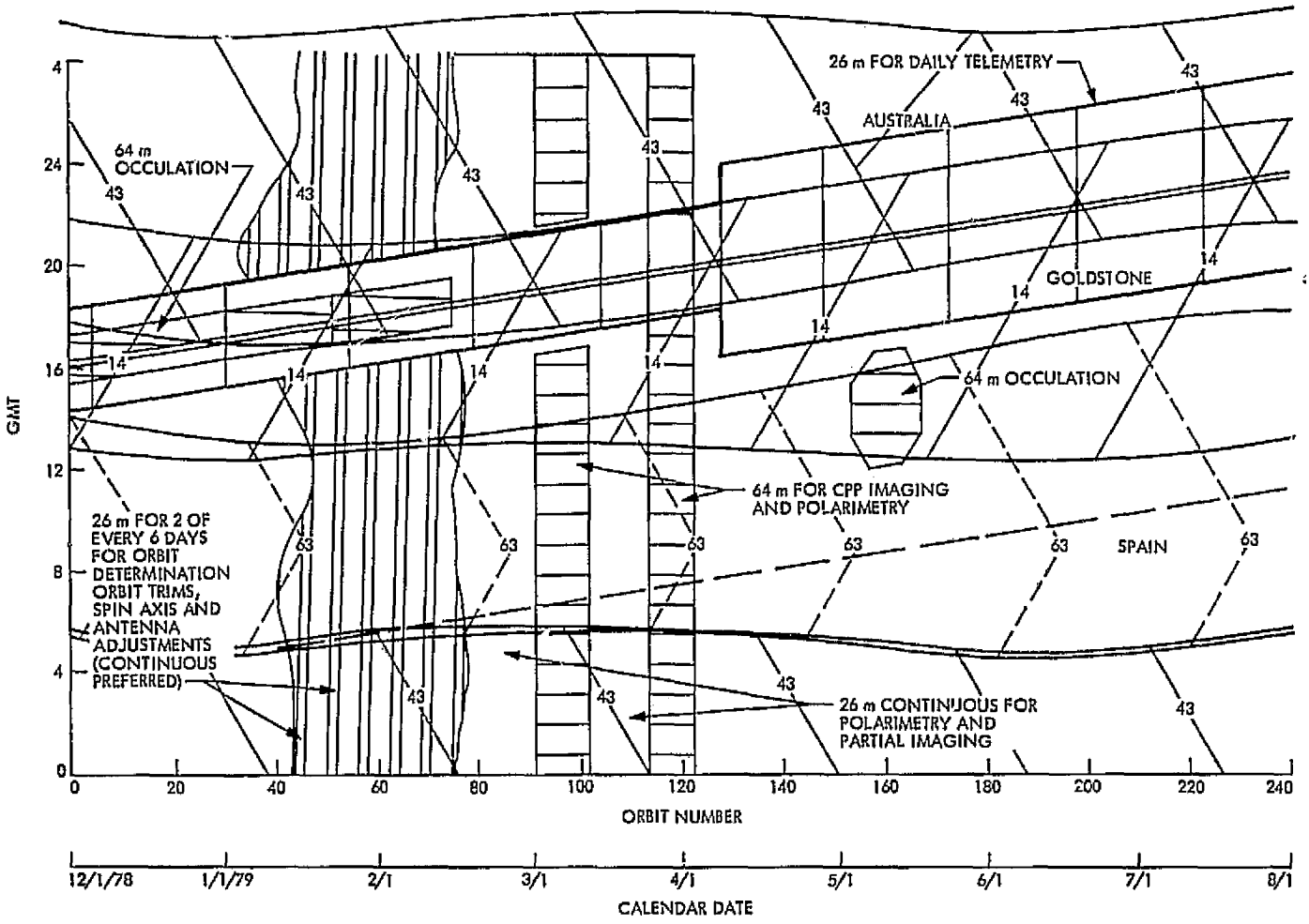

Fig. 3. DSN view periods for Pioneer Venus Orbiter and coverage requirements for suggested timing of periapsides

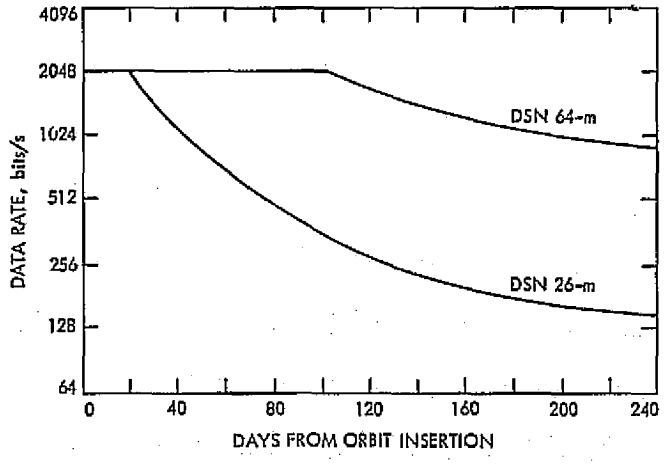

Fig. 4. Orbiter data rate capability, despun high-gain antenna high power mode

Helios Mission Support

P. S. Goodwin
DSN Systems Engineering Office
W. G. Meeks and S. E. Reed
Network Operations Office

The successful flight of the Helios-1 spacecraft continues. It has emerged from its first solar occultation and has reached aphelion at its maximum distance from Earth. Valuable scientific data were obtained during entry and exit from this solar occultation, and preparations are underway for the second solar occultation which will occur during mid-summer. Preparations are also underway for the launch of Helios-B in December 1975.

I. Introduction

This is the fourth article in a series that discusses the Helios-1 flight support provided by the DSN. The previous article (Ref. 1) reported the results of Helios-1 inferior conjunction and perihelion operations. Helios-1 superior conjunction and initial Helios-B planning were also discussed. This article covers the Helios-1 superior conjunction passage and the initial plans for a second superior conjunction in August 1975. Additionally, DSN tracking coverage and system performance are covered as well as current Helios-B DSN Operations planning. The Helios-B DSN Test and Training schedule has been submitted in preparation for launch in December 1975.

II. Mission Status and Operations

A. Helios-1 Superior Conjunction

The Helios-1 Mission Phase II ended and Phase III commenced as the spacecraft's trajectory reached a Sun–Earth–probe (SEP) angle of 3 degrees on April 13, 1975. The first Helios superior conjunction was not completed until June 8, 1975. As the SEP angle diminished to 0.43 degrees on May 6, the degradation of the telemetry data increased until a total telemetry blackout was observed. Telemetry blackout occurred at the 26-meter stations on April 25, and telemetry data were not recoverable again until May 23. Due to a greater antenna gain factor, telemetry blackout at the 64-meter stations was not as severe as at the 26-meter stations; therefore, the total 64-meter station blackout lasted only from May 2 through May 15, 1975.

The Helios superior conjunctions are highly unusual as compared to those of previous spacecraft, which were more nearly polar conjunctions. The unique Helios trajectory (Fig. 1) has an orbital eccentricity of 0.016 degrees and offers the Helios Radio Science Team their first opportunity to measure solar and corona effects upon the radio-frequency (RF) line, which is within the plane of the ecliptic during a superior conjunction.

The Faraday rotation experiment, which is one of the passive radio science experiments for Helios, exhibited an unexpected magnitude during superior conjunction. This phenomenon affected the polarization of the RF link more than had been anticipated and invalidated the DSN's polarization predicts near the station's local meridian. A special polarizer configuration and procedure were implemented at DSS 14 (64-meter station at Goldstone, California) to permit the auto-polarizer to track the received RF signal completely through 360 degrees. This procedure, along with a polarization boresite calibration procedure, removed a potential 180-degree ambiguity in the Faraday rotation data. It is understandable that stations not equipped with remotely controlled polarizers encountered more difficulty maintaining a correct polarizer setting. Fortunately, biases to correct the polarization predicts could be obtained from the stations with auto-polarizers.

The celestial mechanics experiment, the second passive radio science experiment, was supported with the Planetary Ranging Assembly at DSS 14. Additionally, the experiment was supported by the MU II Sequential Ranging equipment. This equipment was designed to support the Mariner Venus/Mercury 1973 radio science experiments (Ref. 2). The experimenter is currently attempting to correlate the planetary ranging and MU II ranging data. Continued investigation of celestial mechanics will be supported during the next Helios-1 superior conjunction.

Helios-1 will enter its second superior conjunction period on August 20, 1975. The second superior conjunction, which occurs at 1.6 AU from Earth, will result in a total occultation on August 31, 1975. The second Helios-1 superior conjunction will be supported by the DSN at a level equal to that of the first solar occultation. Telemetry data may be degraded somewhat during the interval between the first and second occultations due to the relatively small SEP angle throughout this period. The Helios-1 second superior conjunction and second perihelion phase will almost overlap each other. The second occultation period will end on September 6, and Perihelion II will start on September 9, 1975. DSN planning for the second perihelion has started, with 64-meter antenna support for the second perihelion requested from September 9 through October 4, 1975.

B. Helios-B Planning

The 11th Helios Joint Working Group Meeting was held in Munich, West Germany, from May 20 through 22, 1975. This meeting was to formally consummate the ongoing Helios-B planning. The Helios-B spacecraft will be launched from Cape Canaveral, with the window opening on December 8, 1975. The planned trajectory will place the spacecraft in a solar orbit with a perihelion distance of 0.29 AU. The Helios-B launch profile will be similar to that of Helios-1, with initial acquisition over DSS 42/44 in Australia.

The entire Helios-B scientific mission will, in fact, closely parallel that of Helios-1, and it is anticipated that Helios-B will provide the project scientists with three perihelion crossings during its planned mission. Mission operations, however, will be markedly different during launch and Phase I operations. Unlike Helios-1, Helios-B launch and Phase I operations will be controlled from the German Space and Operations Center (GSOC) and not from the Jet Propulsion Laboratory. This will be a new launch configuration and another first in the field of outer space exploration and cooperation. This launch configuration for Helios-B is only one indication of the ever-increasing ability of GSOC. In preparation for an unforeseen emergency, a backup Spacecraft Operations Team will be located at JPL during Helios-B launch and Phase I activities. All Helios-B attitude and orbit determination functions will be accomplished by teams located at JPL. The DSN will continue to provide tracking support over Australia and Goldstone while the German stations will be prime in the zero-longitude area.

Helios-B test and training will start in early August with the DSN Operational Verification Tests and terminate in early December with the Mission Operations System Operational Readiness Tests one week prior to launch. Intervening Simulation System and Ground Data System tests will be performed in September. DSN Performance Demonstration Tests and Helios-B end-to-end testing, from the spacecraft through the STDN (MIL 71) station at Merritt Island, Florida, will be performed in October 1975. In early November, DSN launch and Step II Maneuver Operational Verification Tests will be conducted. DSN Helios-B test and training will be concluded in late November with the Configuration Verification Tests.

C. Actual Tracking Coverage Versus Scheduled Coverage

This report covers Helios-1 tracking coverage which was provided by the DSN from April 15 through June 12, 1975. With Helios Phase III operations commencing at the start of superior conjunction on April 13, there were substantially fewer tracks supported by the DSN during this period than during the two previous reporting

periods. There were only 79 tracks supported by the DSN, while theoretically 177 tracks were available. This was primarily due to the telemetry data blackout caused by solar effects when the Earth-spacecraft line is near the Sun.

Prior to Helios-1 launch, 82 tracks had been forecast in the long-range schedule for this time period, but the long-range forecast had provided less coverage than desired at the entry and exit of solar conjunction, and more than was required during the telemetry blackout phase. To rectify this and to obtain a more operationally desirable superior conjunction tracking schedule, the tracks during solar blackout were negotiated away to other projects in return for tracks that would fulfill the Helios requirements. The actual coverage provided by the DSN during this period more than satisfied Project requirements.

III. DSN System Performance for Helios

A. Command System

The DSN command activity in support of Helios-1 during April and May 1975 totaled only 977 transmitted commands. The cumulative total since launch is 13,480 commands. The significant reduction in command activity during April- May is the result of entering into mission Phase III operations on April 13, 1975. Mission Phase I and II command activities had produced a level of activity which resulted in an approximate average of 100 commands per day being transmitted to the spacecraft.

Even though overall command activity was at a lower level during this period, the total number of command system anomalies did not decrease in proportion to the total activity. During the April-May time period, there was only one Command System abort and this was due to a Block IV receiver/exciter problem at DSS 14. The cause was an erroneous exciter/ transmitter off alarm, and was corrected by cycling the auto/manual strobe switches.

Lost command capability throughout the network increased from 7 hours during the previous reporting period to over 9 hours for this period. More than 50% of this lost time is directly attributed to antenna failures at Goldstone, California, and Canberra, Australia. The remaining 50% is split relatively evenly between computer software problems and transmitter/exciter hardware problems.

While there was an apparent drop in the performance of the Command System, it should be noted that the Helios spacecraft was in a relatively quiescent state as it traversed the blackout region of its first superior conjunction; therefore, little or no impact was observable as a result of the loss of command capabilities. Indeed, to date the total percentage of commands transmitted by the DSN versus the total number of commands aborted (6, which includes Project aborts) gives the DSN a Command System performance achievement rate of 99.99956%.

B. Tracking System

The DSN Tracking System performance was excellent during this period while fulfilling all of the Helios Project requirements for radio metric data during the first Helios superior conjunction. With the exception of the early launch phase, which was a very short period of time, the present superior conjunction phases of the Helios mission represent the next highest period of activity for radio metric data.

The DSN continued to provide support for both of the passive radio metric experiments, Faraday rotation and celestial mechanics, while gathering specific quantities of radio metric data for analysis. The small Sun–Earth–probe angle has caused the doppler noise to remain at a higher than normal level. Due to Helios proximity to the Sun, the doppler noise will continue at a level which is substantially higher than is normal for other operational missions. Figure 2 is a plot of the expected doppler noise from June 15 through August 10, 1975. Figures 3 and 4 are plots of Helios doppler noise versus Earth–Sun–probe and Sun–Earth–probe angles, respectively, as Helios entered its first superior conjunction. It is felt that data derived from plots versus Sun–Earth–probe angle may reveal patterns caused by station antenna structure, and plots versus Earth–Sun–probe angle may reveal patterns caused by solar plasma. A detailed study is planned, and a better model for these effects is expected to be forthcoming from this study.

There were no significant Helios Tracking System discrepancy reports during this period.

C. Telemetry System

The Helios Telemetry System Performance Analysis during superior conjunction, which was from April 13 to June 25, 1975, inclusive, will be the subject of a separate DSN Progress Report. Inasmuch as these data were not within the normal analysis range, due to solar effects during solar conjunction, a special analysis will be performed. A Helios Telemetry Report covering the Helios superior conjunction is planned.

During this reporting period, there were no significant discrepancy reports. All telemetry data analyzed prior to

superior conjunction were nominal and within the predicted DSN Telemetry System specifications.

IV. Conclusions

Phase III marked the start of Helios-1 first superior conjunction, and, within a few days after a successful superior conjunction passage, Helios-1 reached its first aphelion. The passive experiments (Faraday rotation and celestial mechanics) were the prime scientific experiments under observation during the initial portion of Phase III operations. Phase III operations also resulted in a marked reduction of flight support for Helios-1. However, flight support will increase somewhat when the second superior conjunction and perihelion occur in the late summer of 1975. Helios-B activities will increase as the DSN prepares for a launch in early December.

References

1. Goodwin, P. S., Meeks, W. G., and Reed, S. E., "Helios Mission Support," in *The Deep Space Network Progress Report 42-27*, pp. 36–40, Jet Propulsion Laboratory, Pasadena, Calif., June 15, 1975.
2. Martin, W. L., "System Performance of the Dual-Channel MU II Sequential Ranging," in *The Deep Space Network Progress Report 42-26*, pp. 54–68, Jet Propulsion Laboratory, Pasadena, Calif., Apr. 15, 1975.

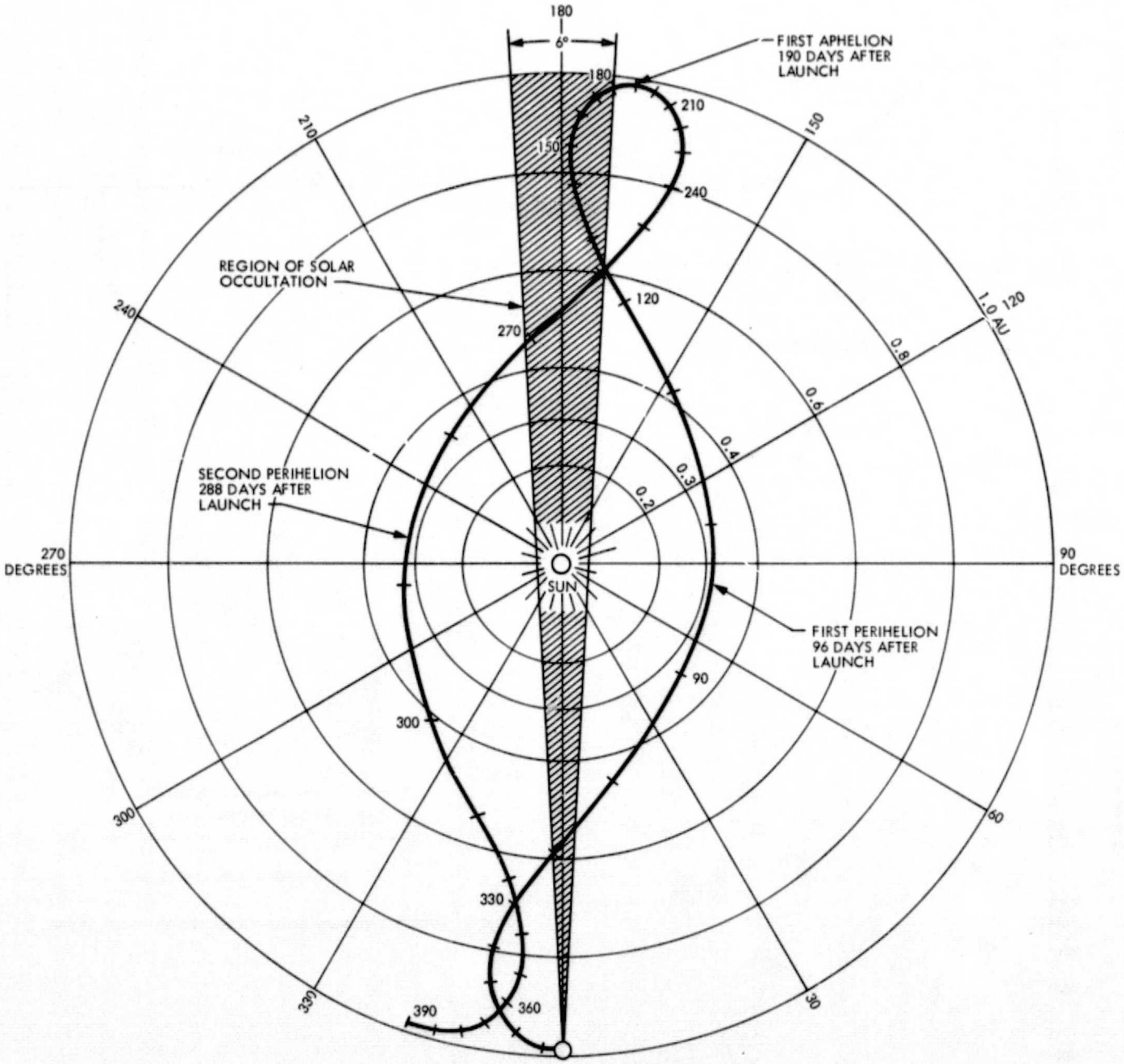

Fig. 1. Helios-1 0.31 AU perihelion trajectory

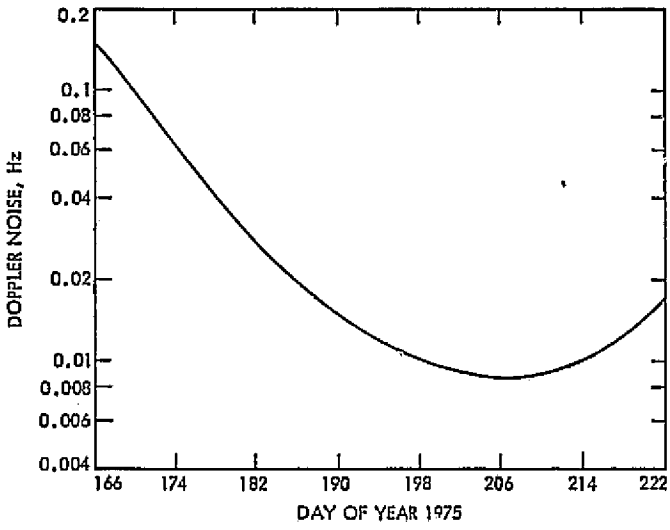

Fig. 2. Helios-1 estimated doppler noise

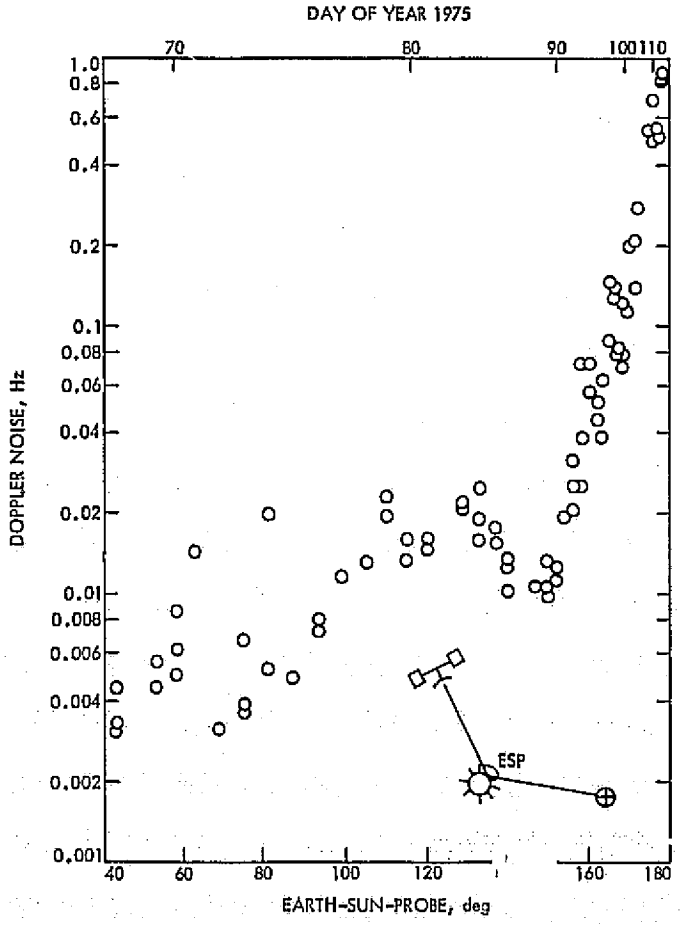

Fig. 3. Helios-1 doppler noise vs Earth-Sun-probe angle

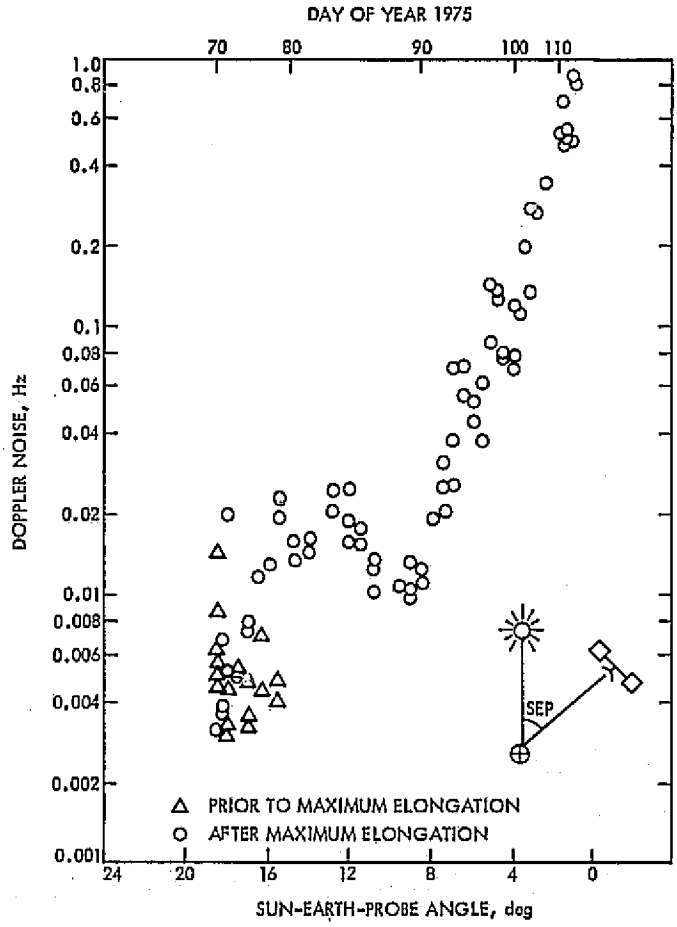

Fig. 4. Helios-1 doppler noise vs Sun-Earth-probe angle

Performance Testing of a Solar Energy Collector

W. H. Higa and E. R. Wiebe
Communications Elements Research Section

A simplified calorimetry technique was developed for evaluating the performance of a parabolic trough type of solar energy collector. In order to gain some experience with single-axis concentrating collectors, a simple parabolic collector was fabricated.

I. Introduction

There will undoubtedly be many suggestions for rapid evaluation of solar energy collectors emerging as increasing numbers of investigators turn their attention to the problem. This report describes one approach which has achieved its objectives. The main objective was to develop a simple procedure which required a minimum of laboratory apparatus. A second objective was to devise a simple technique for fabricating a parabolic trough type of solar energy collector.

II. Parabolic Collector Design

The basic approach in the fabrication of a parabolic collector was to machine parabolic ribs in a programmed milling machine; these ribs were then attached to a torque tube as shown in Fig. 1. Aluminum sheets 3.2 mm (1/8 inch) thick were then rolled to the appropriate circular radius to match the parabolic shape of the ribs. The preformed aluminum sheets were then bolted to the ribs to serve as the foundation for the parabolic collector. The mirror (not shown) was a 3.2-mm (1/8-inch)-thick sheet of acrylic aluminized on one side (Ram Products: Industrial grade mirror) and was clamped into the structure in a simple manner for easy replacement. The aluminized acrylic mirror had a reflectivity of around 85%, even though the radiation had to traverse the plastic twice. The protection of the mirror by the plastic is a desirable feature for hostile environments and well worth the small sacrifice in reflectivity.

The drive mechanism was not a matter of concern in this phase of the investigations, and a synchronous motor with a gear box was used in conjunction with a chain drive to provide adequate solar tracking. The techniques used enjoyed the experiences of the Minneapolis-Honeywell project (Ref. 1), and the authors are grateful to Dr. J. Ramsey for helpful information.

III. Solar Collector Evaluation

The performance of solar energy collectors may be determined through some simple calorimetric measurements. By supplementing experimental data with reasonable approximations, it is possible to derive a theoretical model which permits the calculation of the performance under various operating conditions.

The analyses described here are particularly adapted to cylindrical trough collectors.

As stated previously the detailed design and fabrication of solar collectors have been discussed in considerable detail in the literature (Refs. 1 and 2). The purpose here is to consider the evaluation of the performance of any given solar thermal system. A simplified calorimetric procedure is suggested as shown in Fig. 2. Instead of using the usual flowing fluid for measurements, a solid rod of metal, such as aluminum, is used for calorimetry.

The thermal balance equation for Fig. 2 is given by

$$I_n A_e \eta_n \cos\phi = MC\frac{dT}{dt} + aK_1(T^4 - T_a^4) + aK_2(T - T_a) \tag{1}$$

where

I_n = direct normal insolation

A_e = effective area of solar collector per unit length

η_n = optical efficiency

ϕ = angle of incidence of solar radiation relative to surface normal of collector

M = mass of aluminum rod

C = specific heat of aluminum rod

T = temperature of rod in kelvins

T_a = ambient temperature

a = surface area of aluminum rod per unit length

K_1 = radiation loss parameter

K_2 = convection loss parameter in linear approximation.

The motivation for the present approach is the observation that the insolation is substantially constant between 10 a.m. and 2 p.m. on a clear day. For a polar-mounted collector, the solar angle ϕ is also constant; hence, the input is an easily measured constant for any given clear day. Under these circumstances the nonlinear heat balance equation may be solved in various approximations as discussed below.

IV. The Linear Approximation

It is well known that for small variations in temperature the radiation loss term in Eq. (1) may be approximated as

$$aK_1[(T_0^2 + T_a^2)(T_0 + T_a)](T - T_a) \tag{2}$$

where T_0 is the mean operating temperature. Thus, for small variations in T about T_0, the radiation loss may be combined with the linear loss term in Eq. (1), or

$$I(t) = MC\frac{dT}{dt} + aK(T - T_a) \tag{3}$$

where K is a new constant which accounts for all losses and

$$I(t) = I_n A_e \eta_n \cos\phi \tag{4}$$

Although Eq. (3) is applicable for a relatively small temperature range, it is exactly solvable even for the case when insolation $I(t)$ is a variable (cloudy day). Some insight into the dynamics of a solar collector could thus be gained.

V. Nonlinear Approximation

An alternative approximation to Eq. (1) is to assume dominance of the radiation loss term; then

$$I(T) = MC\frac{dT}{dt} + aK_0(T^4 - T_a^4) \tag{5}$$

where K_0 is adjusted to account for all thermal losses. Equation (5) is applicable especially to high-temperature operation of a collector. Figure 3 shows a typical heating curve for constant insolation. The first deduction from Fig. 3 and Eq. (5) is that initially there are no losses because $T = T_a$. Thus,

$$MC\left(\frac{dT}{dt}\right)_0 = I_0 A_e \eta_0 \cos\phi \tag{6}$$

where $(dT/dt)_0$ indicates the initial slope at t = 0. All quantities in Eq. (6) are known except η_0, the optical efficiency, which is given by

$$\eta_0 = \rho\tau\alpha = \frac{MC\left(\frac{dT}{dt}\right)_0}{I_0 A_c \cos\phi} \tag{7}$$

where

ρ = mean reflectivity of mirror

τ = mean transmissivity of glass tube (see Fig. 2)

α = mean absorptivity of pipe

The second observation from Fig. (3) and Eq. (5) is that when thermal equilibrium is achieved, all the solar power incident on the receiver pipe is reradiated as infrared power and

$$K_0 = \frac{I_0 A_c \eta_0 \cos\phi}{a(T_s^4 - T_a^4)} \tag{8}$$

where K_0 is the hitherto unknown loss parameter, and T_s is the stagnation temperature. All quantities in Eq. (5) are now known, and for any operating temperature, T_0, the thermal power available is given by

$$P_t(T_0) = MC\left(\frac{dT}{dt}\right)_{T=T_0}$$
$$= I_0 A_c \eta_0 \cos\phi - aK_0(T_0^4 - T_a^4) \tag{9}$$

By combining Eqs. (8) and (9), it is possible to obtain a simple expression for thermal efficiency η_t:

$$\eta_t = \frac{T_s^4 - T_0^4}{T_s^4 - T_a^4} \tag{10}$$

VI. Test Results

Preliminary results indicate that stagnation temperatures up to 400°C are readily obtained with the parabolic trough collector shown in Fig. 1. An aluminum rod 3.8 cm in diameter, coated with black chrome, was mounted at the focus within a pyrex tube. The receiver rod was thus operated with or without a vacuum environment. The temperature of the rod was measured as described previously and typical results are shown in Fig. 4.

References

1. *Research Applied to Solar-Thermal Power Systems*, Report NSF/RANN/SE/G1-34871/PR/73/2, prepared by University of Minnesota and Honeywell, Minneapolis, Minn., July 1973.

2. Duffie, J. A., and Beckman, W. A., *Solar Energy Thermal Processes*, John Wiley & Sons, Inc., New York, 1974.

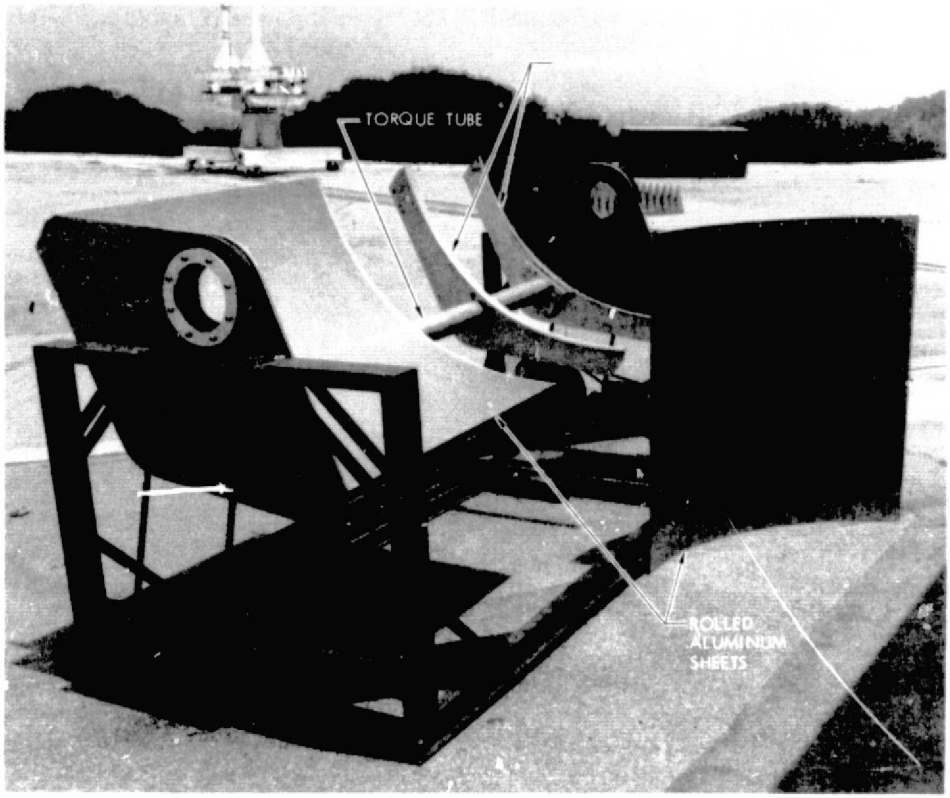

Fig. 1. Construction of parabolic solar energy collector

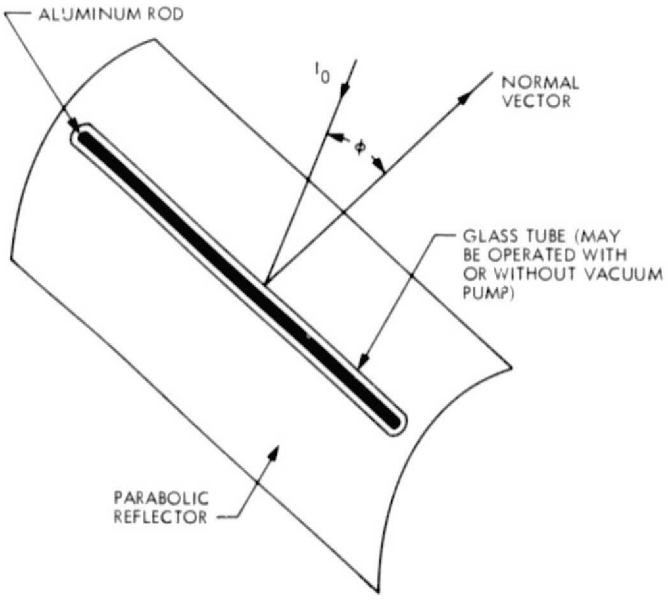

Fig. 2. Test configuration for solar collector

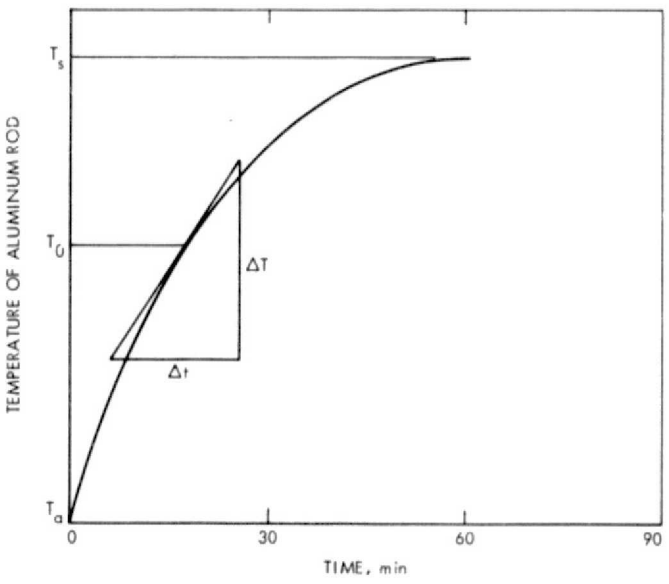

Fig. 3. Heating curve for aluminum rod

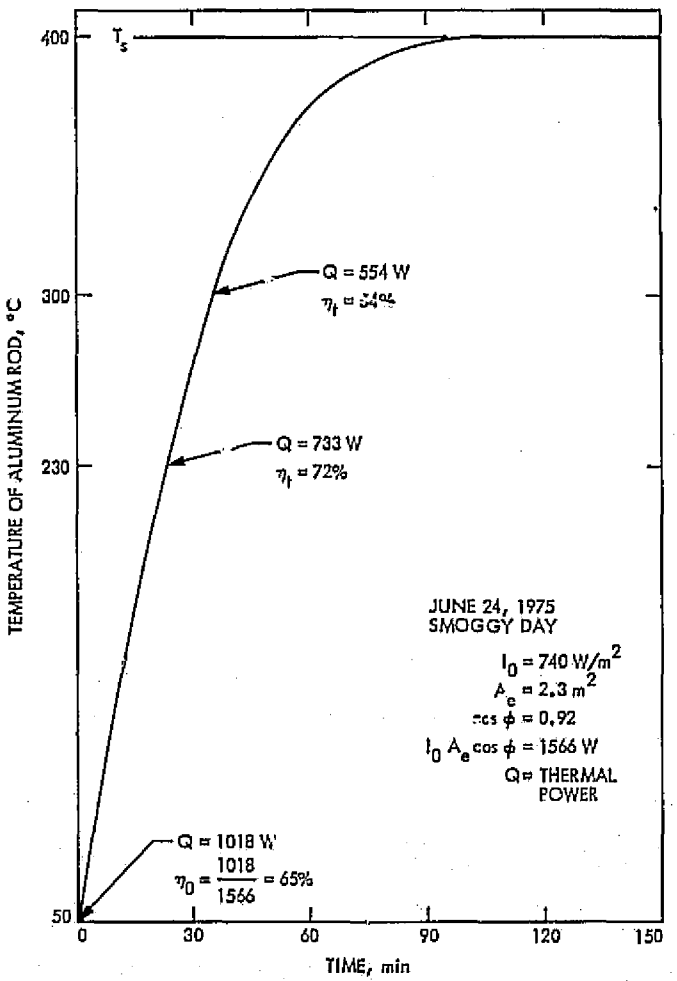

Fig. 4. Typical experimental result (with vacuum)—the values of Q are derived by measuring the slopes (dT/dt) for the specific temperature (Note: Thermocouple nonlinearity is apparent)

A Microwave Frequency Distribution Technique for Ultrastable Standard Frequencies

J. W. MacConnell and R. L. Sydnor
Communications Systems Research Section

A radio distribution system is needed which allows for distribution of stable reference frequency standards, such as those from the hydrogen maser, over long distances (inter-site) without degrading the stability of the frequency standard. The distribution systems described here are two-way radio links that compute the change in path length and correct the phase of the transmitted signal such that the phase of the signal arriving at the remote site is independent of perturbations in the path linking the two sites.

I. Introduction

Distribution of stable frequencies over one-way radio links longer than a few hundred meters is not possible without degradation of the stability of the frequency. For example, a 50-km path has a stability of about 1.7×10^{-10} (reference = NRL RPT 7140). This stability would completely mask the 10^{-14} stability of a hydrogen maser frequency standard. If radio links are to be employed for frequency distribution, some method of correction must be employed. One such method is to use a two-way link, which can automatically adjust the phase of the transmitted signal from the master station such that the phase at the remote station remains constant. The return link transmits the signal received by the remote station back to the master station, allowing the master station to determine the change in propagation time of the path and correct the transmitted phase such that no change in the phase of the signal received at the remote station is observed.

II. Basic System Concept

The basic concept of the frequency distribution system is shown in Fig. 1a. A frequency $\omega \angle \omega\tau$ is transmitted from the master site to the remote site. After encountering a delay of τ, the phase of the received signal is $\omega \angle 0$, the reference frequency to be distributed, at the reference phase angle. This signal is then returned to the master station, where the phase is $\omega \angle -\omega\tau$. By forcing the transmitted signal to lead the reference phase by the same

amount that the received signal lags the reference phase, correction for perturbations in the path can be effected. This whole system is predicated on reciprocity of the path. If τ is different for the two directions, it will be impossible to obtain proper correction. Any equipment that is common to both transmit and receive functions (coax, waveguide, antennas, etc.) will be considered part of the path and will be corrected. Any phase shifts that are not reciprocal will appear directly at the output of the remote site.

III. Practical Circuit Considerations

The circuit shown in Fig. 1a shows conceptually the operation of a self-correcting distribution system. There are, however, practical problems with the configuration shown in Fig. 1a. The most obvious problem is that the transmitter and receiver at each site are operating at the same frequency. A practical circuit would, therefore, be required to operate at different transmit and receive frequencies. The use of different operating frequencies requires additional synthesis before a phase comparison between transmitted and received phases can be made without error. Figure 1b shows the transmitted and received phases being compared. As can be seen, the transmit phase $\omega\tau$ is being forced to equal the received phase $K\omega\tau$. This will result in a phase error at the receiving end, i.e., some correction for the path will be made; however, there will be some phase error. If K is near one, this error will be small and will be able to provide corrections adequate to distribute standards with stabilities of 10^{-15} without severe degradation. Figure 1c shows a system that corrects for the different frequencies being used. This system simply multiplies the received signal by $1/K$. Beyond this point operation is identical to the system discussed in Fig. 1a. The problem with the system shown in Fig. 1c is that K is not always an integer. For example, in one system under consideration $K = 84001/84000$, a nontrivial synthesis.

An additional problem with the configuration shown in Fig. 1c is the use of separate phase comparators for the transmit and receive phase versus the master frequency standard. This system would require exactly matched phase detectors, which is a problem, although possible if they are not required to track over large regions. Over long paths, with high frequency or microwave links, many cycles of phase may change, requiring the phase detectors to track over a complete cycle—a difficult requirement to meet. Figure 1d shows an alternative system that eliminates the aforementioned difficulty. The transmit signal is mixed with twice its frequency, yielding the same frequency with opposite sign on the phase. This signal can be compared to the received signal in a single phase detector with the received signal. This phase detector will always be operating at or very near 0-deg phase error. Figure 1d is still a conceptual circuit and should not be construed to be a proposal for an actual circuit.

IV. An Exact Synthesis System

The details of the operation may be understood by referring to the block diagrams of Figs. 2a and b.

The transmitter voltage-controlled oscillator (VCO), operating at $\omega_s \angle\theta_s$ ($\approx$8400.1 MHz), is used to send a signal to the receiver at the remote site, where it is received with a time delay T; thus, the received signal is $\omega_s \angle\theta_s - \omega_s T$. The receiver local oscillator (LO) signal is phase-locked to the signal with an offset of -100 kHz, which is derived (along with all the other standard frequencies of 1, 5, 10, and 100 MHz) from the receiver VCO. This LO signal is also transmitted back to the transmitter. The signal leaves the receiver as

$$\omega_s \frac{84000}{84001} \Big/ (\theta_s - \omega_s T) \frac{84000}{84001}$$

as is seen by examining the operation of the receiver system. This signal arrives at the transmitter with an additional time delay T, so that the signal received at the transmitter is

$$\omega_s \frac{84000}{84001} \Big/ (\theta_s - 2\omega_s T) \frac{84000}{84001}$$

where it is mixed with the original transmitted signal to give an intermediate frequency (IF) of

$$\omega_s \frac{1}{84001} \Big/ (\theta_s + 2\omega_s T) \frac{84000}{84001}$$

(This is written differently in the block diagram, but $N = 84000$ on this diagram, so the two ways of writing it are equivalent.) At the transmitter, the reference frequency $\omega_0 \angle 0$ (taken as 100 MHz from the hydrogen maser) is multiplied by 84 and mixed with the transmitter VCO to give an IF reference of $\omega_s/84001 \angle\theta_s$ (100 kHz) if we use the fact that

$$\omega_s = \omega_0 \frac{84000}{84001}$$

This IF reference is then operated on by a synthesizer, which in effect multiplies it by

$$\frac{2N+1}{N+1} = \frac{168001}{84001}$$

producing a signal

$$\frac{2N+1}{(N+1)^2} \quad \omega_x \angle \theta_x \frac{2N+1}{N+1} \approx 200 \text{ kHz}$$

This is mixed with another reference frequency

$$\frac{10\omega_s}{N+1} = 1 \text{ MHz}$$

to produce

$$\frac{10\omega_s}{N+1} + \frac{2N+1}{(N+1)^2} \omega_x \angle \theta_x \frac{2N+1}{N+1} \approx 1.2 \text{ MHz}$$

which is then mixed with another signal,

$$\frac{10\omega_s}{N+1} \angle 0 + \frac{N\omega_s}{(N+1)^2} \angle 0 \approx 1.1 \text{ MHz}$$

which has been synthesized from the

$$\frac{10\omega_s}{N+1} \angle 0 = 1 \text{ MHz}$$

and

$$\frac{100\omega_x}{N+1} \angle 0 = 10 \text{ MHz}$$

reference frequencies. The result of all this synthesis and mixing is the signal which is used as the local reference for the phase detector. This signal,

$$\frac{\omega_s}{N+1} \angle \theta_s \frac{2N+1}{N+1}$$

is subtracted from the IF of

$$\frac{\omega_s}{N+1} \angle \theta_s \frac{1}{N+1} + 2\omega_s T \frac{N}{N+1}$$

giving zero frequency and phase of

$$\angle \frac{2N}{N+1} (\omega_s T - \theta_s)$$

Under the usual assumptions for phase-locked loops (δ small such that $\sin \delta \cong \delta$), the output of the phase detector is then

$$K_\eta \frac{2N}{N+1} (\omega_x T - \theta_x)$$

Since the phase gain of the loop is infinite at zero frequency, the output of the phase detector is constrained such that $\phi \equiv 0$; therefore, $\omega_x T = \theta_x$.

Under these conditions, the receiver at the remote site receives (and retransmits) a signal which has the same phase as the reference. In the proposed system for Goldstone, the total time delay will be ≈10 ms. Such perturbations of the time delay will, of course, cause variations in phase, but *only at times corresponding to this round-trip delay or shorter.* For such short times the phase-locked loop will have low gain, and the receiver VCO will give the main control over phase. In other words, for long time stability down to <0.1 s, the output phase of the receiver will be determined by the transmitter, while for short term, the phase will be determined by the receiver (crystal) VCO; this is identical to the situation in the original hydrogen maser signal.

There are, of course, innumerable ways to implement such a system. This particular one is being considered for several reasons:

(1) To ensure good spectral characteristics, no synthesis is performed on signals which are multiplied to X-band.

(2) To reduce development and implementation costs, maximum use is made of components which have already been developed for the hydrogen maser.

(3) All complicated synthesis is done at the transmitter, thus allowing a great many of the synthesized signals to be used for several transmitters, further reducing costs.

(4) The operating frequency (8.4 GHz) lies in a very low dispersion region in the spectrum and is also an unused area in the DSN microwave communications link.

V. Approximate System

As can be seen in the previous section, the exact synthesis scheme requires a relatively complex synthesizer. An alternative approach is to use an approximate system

that will allow substantial, though not complete, corrections for perturbations in the path. Figure 3 shows an approximate system under study in this section. This system will provide a path stability improvement of about 1.7×10^5. Such an improvement should allow an overall stability of about 10^{-15} over a 50-km path.

VI. Time Synchronization

By using suitable modulation/demodulation schemes, time signals may be impressed on the signals to allow time synchronization between sites to a level $\approx$10 ns. Several different methods for performing this synchronization will be reported in a future report.

VII. Conclusion

These systems allow frequency standards to be available at several sites without the high cost of separate frequency standards. One hydrogen maser could provide a frequency reference for all of Goldstone at a fraction of the cost of individual masers. An additional advantage of such a system will be for Very Long Baseline Interferometry experiments. Using this system the same LO and time tick will be available at both stations, eliminating the problem of frequency skew between standards and improving some types of tracking data (reference). In the future it may be possible to use such a system in conjunction with a communications satellite to provide the same clock at all the DSN stations throughout the world.

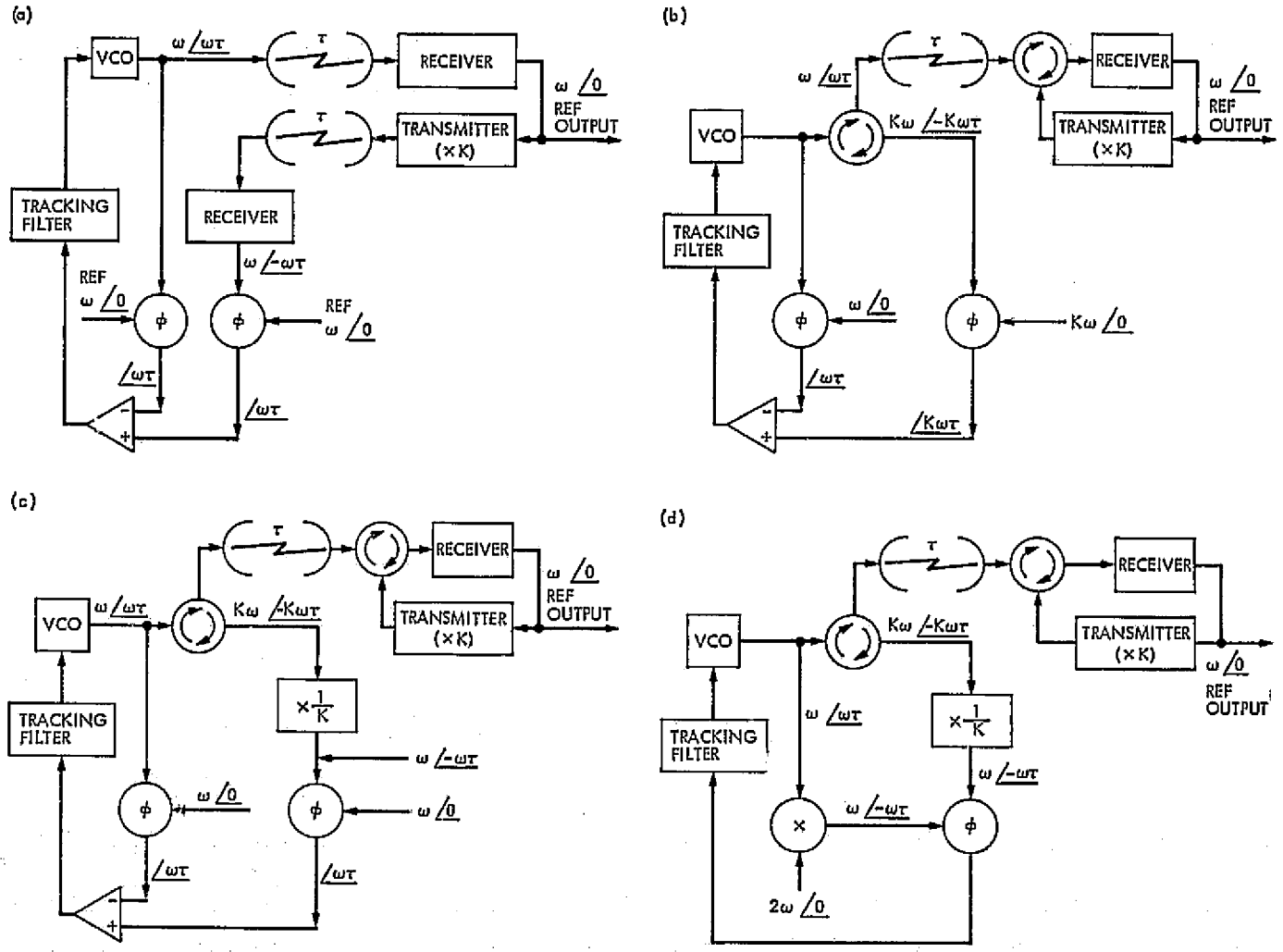

Fig. 1. Conceptual frequency distribution systems

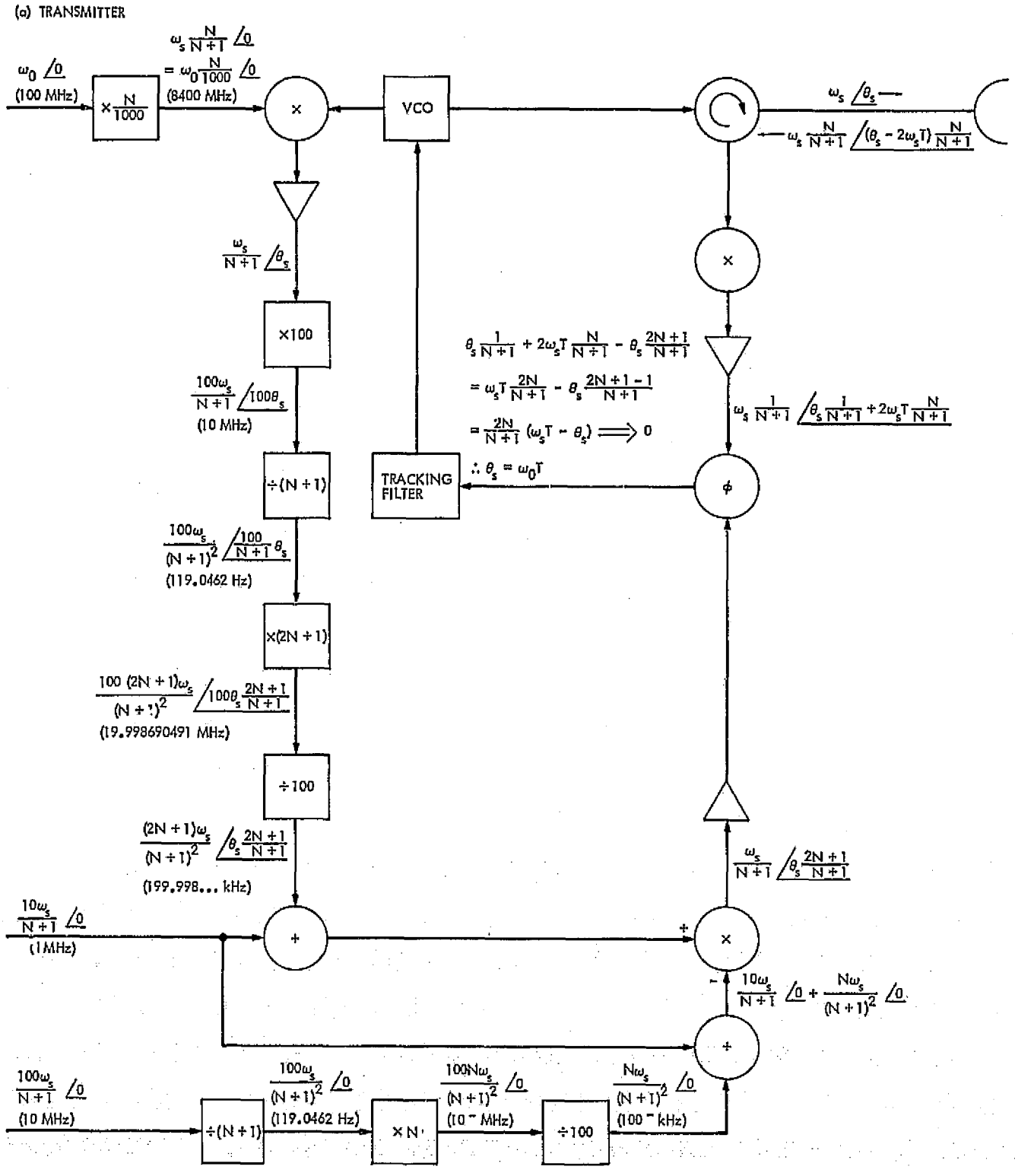

Fig. 2. Exact synthesis system

(b) RECEIVER

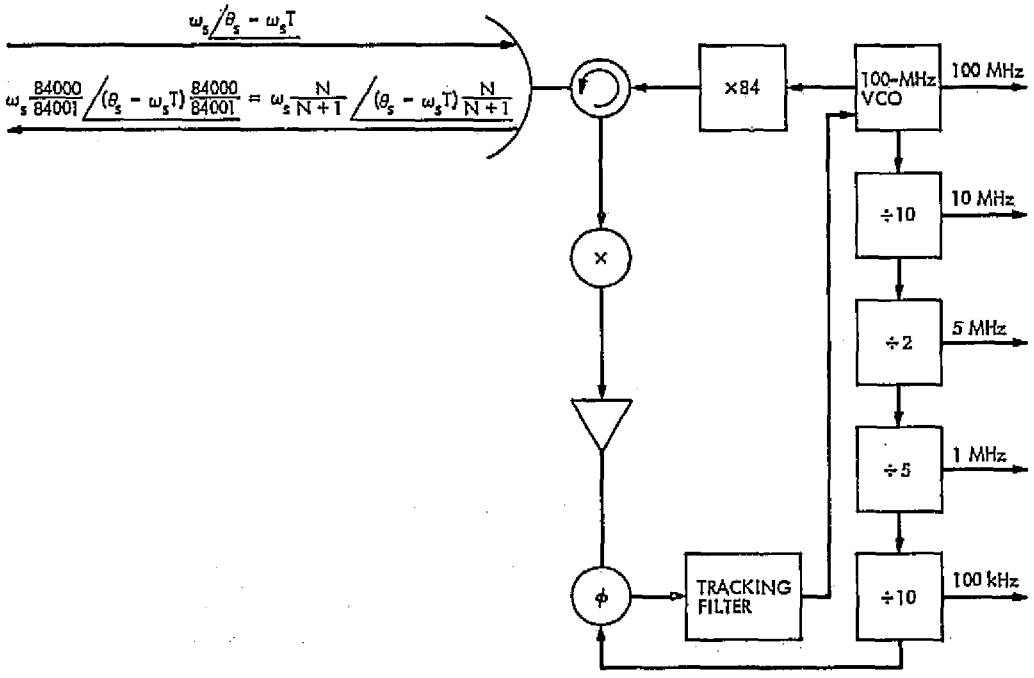

Fig. 2 (contd)

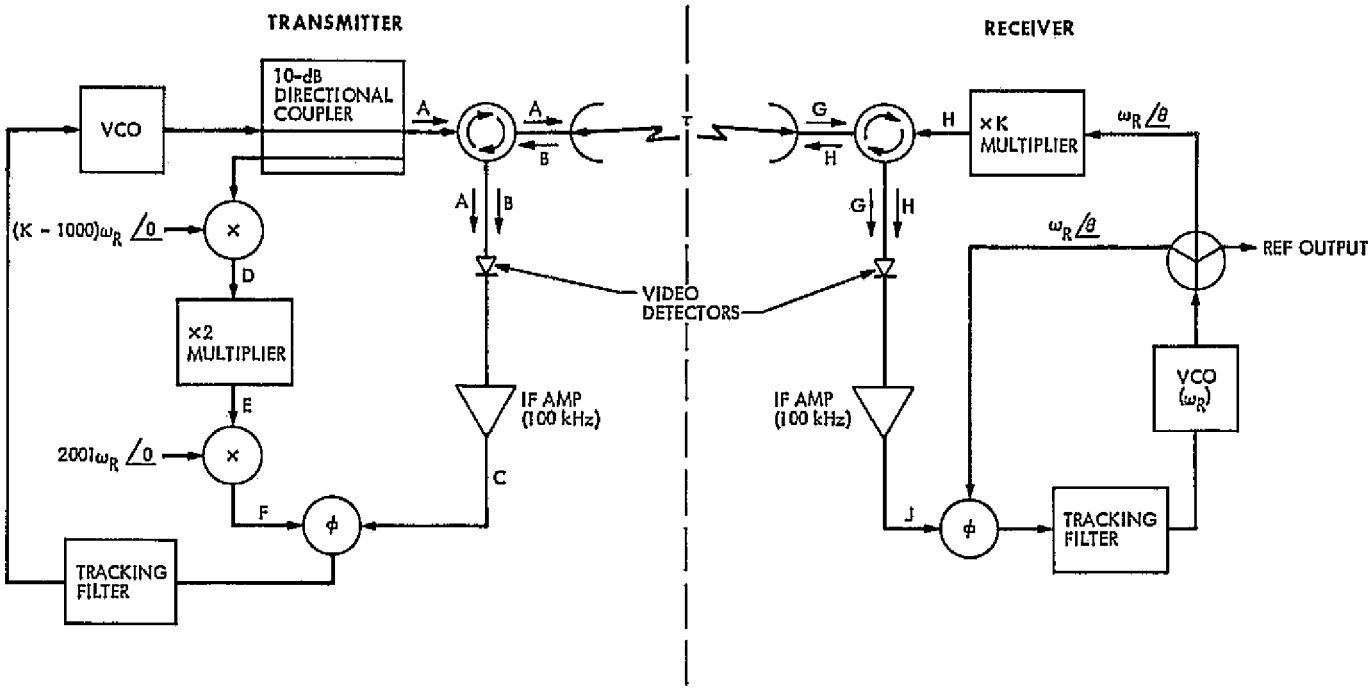

TRANSMITTER PHASES:

(A) $(K+1)\omega_R \angle\phi$

(B) $K\omega_R \angle -2K\omega_R\tau + \frac{K\phi}{K+1}$

(C) $(A) - (B) = (K+1)\omega_R \angle\phi - \left[K\omega_R \angle -2K\omega_R\tau + \frac{K\phi}{K+1}\right]$

$$= \omega_R \angle \phi - \frac{K}{K+1}\phi + 2K\omega_R\tau$$

(D) $(K+1)\omega_R \angle\phi - \left[(K-1000)\omega_R \angle 0\right] = 1001\omega_R \angle\phi$

(E) $2(D) = 2002\omega_R \angle 2\phi$

(F) $2002\omega_R \angle 2\phi - 2001\omega_R \angle 0 = \omega_R \angle 2\phi$

THE PHASE DETECTOR AND LOOP FORCES (F) AND (C) TO BE EQUAL:

$$\omega_R \angle 2\phi = \omega_R \angle \phi - \frac{K}{K+1}\phi + 2K\omega_R\tau$$

SOLVING FOR PHASE PORTION OF EXPRESSION:

$$2\phi = \phi - \frac{K}{K+1}\phi + 2K\omega_R\tau$$

$$\phi = \left(\frac{2K}{2K+1}\right)(K+1)\omega_R\tau$$

RECEIVER PHASES:

(G) $(K+1)\omega_R \angle -(K+1)\omega_R\tau + \phi$

(H) $K\omega_R \angle K\theta$

(J) $\omega_R \angle -K\theta - (K+1)\omega_R\tau + \phi$

BUT $-K\theta - (K+1)\omega_R\tau + \phi = \theta$

$$\therefore \theta = \omega_R\tau + \frac{\phi}{K+1} \qquad (1)$$

IDEALLY ϕ SHOULD EQUAL $(K+1)\omega_R\tau$ (OBTAINED BY SETTING θ IN (1) TO 0 AND SOLVING FOR ϕ). THEREFORE, ERROR = $1/(2K+1)$.

WITH THE JPL APPROXIMATE SYSTEM $K = 8.4 \times 10^4$. THE RESULTANT ERROR IS 5.95×10^{-6} YIELDING A CORRECTION OF 1.68001×10^5.

Fig. 3. Approximate synthesis system

Low-Noise Receivers: 3-Kelvin Refrigerator Development for Improved Microwave Maser Performance

E. R. Wiebe
Communications Elements Research Section

A closed-cycle helium refrigerator with a 3-kelvin station has been built and tested. A 200-mW net refrigeration capacity was demonstrated at 3.1 kelvins. The system has been operated continuously for 1200 hours with no detectable degradation of performance. Reduced refrigerator temperature (from 4.5 to 3.0 kelvins) will increase the available gain and bandwidth, and reduce the noise temperature of microwave masers.

I. Introduction

4.5-kelvin closed-cycle helium refrigerators (CCRs) are currently used in the Deep Space Network with Microwave Masers at S, X, and Ku-band frequencies (Ref. 1). These versatile and reliable refrigerators have been described in detail previously (Ref. 2). The performance of a Microwave Maser can be improved substantially by reducing its physical temperature from 4.5 to 3.0 K. A previously described X-band maser (Ref. 3) achieves 45-dB net gain and has a theoretical noise temperature of 3.5 K (defined at the maser input connection at the final stage of refrigeration) when operated at 4.5 K. A reduction of temperature from 4.5 to 3.0 K will reduce the maser noise temperature from 3.5 to 2.0 K; the net gain will increase from 45 to 72 dB. The increased gain can be traded for additional bandwidth (Ref. 3).

II. Description of 3-K Closed-Cycle Helium Refrigerator

A 3-K refrigerator was built by adding counterflow heat exchangers, a 3-K expansion valve, a 3-K station, and a vacuum pump to a 4.5-K refrigerator. A simplified block diagram of the combined 4.5- and 3-K system is shown in Fig. 1. Compressed helium gas is supplied by, and returned to, a compressor identical to those used throughout the network. A pressure regulator is used to reduce the supply pressure to 3.04×10^5 N/m^2 (3 atm) for use in the 3-K portion of the system. The helium gas is cooled by the 70-, 15-, and 4.5-K stations, liquefying at about 5 K. The liquid experiences a partial vacuum in the 3-K station after passing through the expansion valve. The temperature of the boiling liquid in the 3-K station is determined by the absolute pressure in the 3-K station.

Efficient counterflow heat exchangers (same design as used in 4.5-K refrigerators) permit cooling of helium for the 3-K system with a minimum of heat being delivered to the 4.5-, 15-, and 70-K stations. Helium gas flow through the 3-K heat exchanger system is approximately 8 standard liters per minute.

A model 8815 DIRECTORR Sargent-Welch vacuum pump (free air displacement of 150 liters per minute) is used to maintain a partial vacuum in the 3-K station. Helium at 1.22×10^5 N/m^2 (1.2 atm) is sent from the vacuum pump to the compressor. The vacuum pump is shown in Fig. 2; its mounting versatility permits antenna-mounted operation with proximity to the 3-K refrigerator. Ucon-type lubricant is used in the vacuum pump and the compressor. Initial helium and lubricant purification is accomplished with a liquid nitrogen-cooled charcoal trap.

III. Performance

The 3-K CCR system produces 200-mW net refrigeration capacity at 3.1 K. 600-mW net refrigeration is available at 4.5 K in addition to the 3-K station capacity. Continuous operation for 1200 hours in the laboratory has demonstrated the feasibility of the 3-K closed-cycle helium refrigerator.

Additional work is needed to increase refrigeration capacity to 250 mW at 3.0 K. Further tests are required to assure adequate temperature stability and long-term reliability.

It is intended to use the 4.5-K station to intercept all heat loads except the pump energy dissipated within the maser at 3 K.

References

1. Reid, M. S., et al., "Low-Noise Microwave Receiving Systems in a Worldwide Network of Large Antennas," *Proc. IEEE*, Vol. 61, No. 9, pp. 1330–1335, Sept. 1973.
2. Higa, W. H., and Wiebe, E., "A Simplified Approach to Heat Exchanger Construction for Cryogenic Refrigerators," *Cryogenic Technol.*, Vol. 3, pp. 47–51, Mar./Apr. 1967.
3. Clauss, R., Wiebe, E., and Quinn, R., "Low Noise Receivers: Microwave Maser Development," in *The Deep Space Network Progress Report*, Technical Report 32-1526, Vol. XI, pp. 71–80, Jet Propulsion Laboratory, Pasadena, Calif., Oct. 15, 1972.

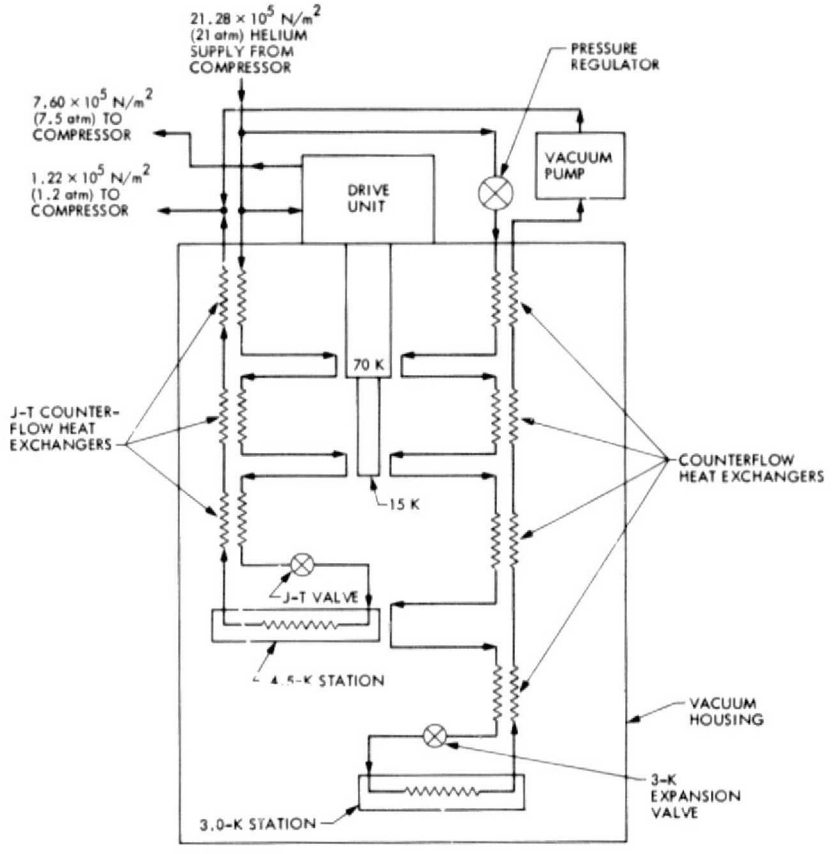

Fig. 1. 3-K closed-cycle helium refrigerator block diagram

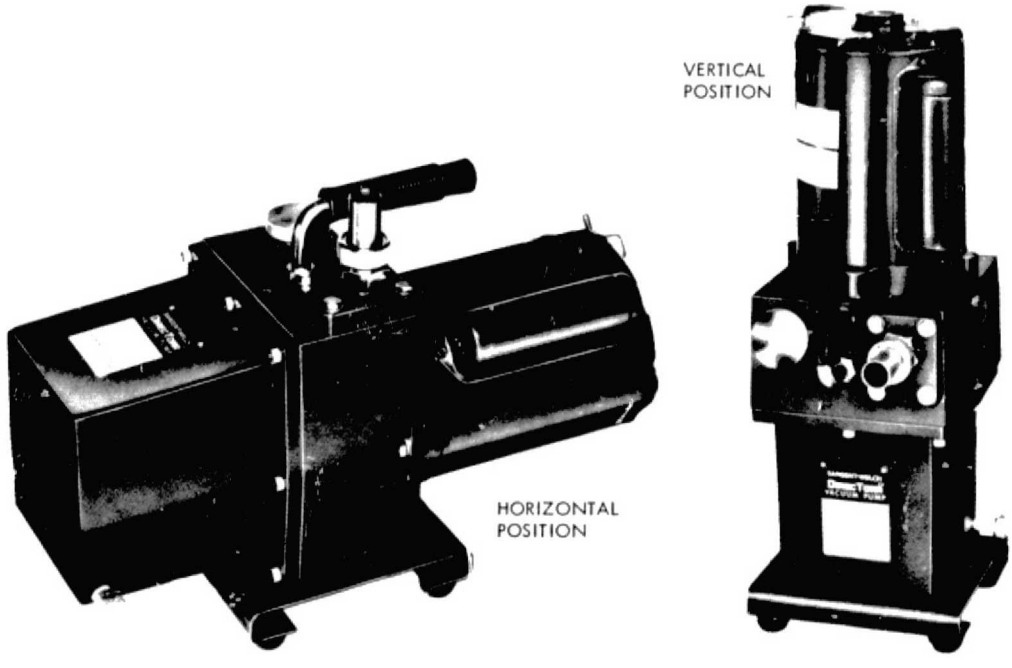

Fig. 2. Antenna-mountable vacuum pump for 3-K CCR

Cost-Effectiveness of Pooled Spares in the Deep Space Network

I. Eisenberger
Communications Systems Research Section

G. Lorden
California Institute of Technology

Providing a common pool of spares for types of equipment that are in operation in more than one station of a complex can result in a cost which is substantially less than the total cost of sparing each station separately. This report presents a cost-effective method of determining such spares complements, which is an extension of a previously proposed method. The generalized algorithm of the present method can also be used for unpooled sparing whenever appropriate. Several practical examples are given which illustrate the cost savings that can be achieved by pooling spares. For these examples, savings range from 45 to 75%.

I. Introduction

A cost-effective method of spares provisioning for repairable equipment (modules) at Deep Space Stations (DSSs) is described in Ref. 1. That report considered the determination of spares packages for a system consisting of k types of modules. For the system to be operational, at least m_j modules of type j must be unfailed for $j = 1, \cdots, k$, and there are $n_j \geq m_j$ modules of type j in the system, not counting spares. The time required to replace a failed module by a spare is assumed to be negligible in this analysis. The uptime ratio (UTR) for the jth type of module is defined as the fraction of time in the long run that at least m_j modules of type j are unfailed, which depends on the number of spares, N_j, of type j. It is assumed that failures and repairs of different module types are independent, so that the system UTR is the product of the UTRs of the k types. These k UTRs are computed using the Markovian model for failures and repairs described in Ref. 2. The algorithm of Ref. 1 is then used to determine spares packages $(N_1, \cdots, N_k)$ which are cost-effective in that they yield system UTRs which cannot be improved upon without increasing the total cost.

The present report describes the extension of this method, which was developed to deal with actual sparing problems in the DSN involving an additional feature: the possibility of pooling spares for three stations at the same complex, with different system configurations. Examples of the cost-effective spares packages developed for these problems are presented in Section III. Comparisons with the cost of unpooled spares packages for the individual stations are given. It is shown that to achieve the same station UTRs, the cost of pooled spares is substantially smaller.

II. Extension of the Sparing Algorithm

Whenever a module fails at the ith station ($i = 1,\cdots,s$), it is replaced by a spare of the same type, unless there are none in the pool, in which case a "back order" is recorded. In the latter case, it is assumed that when the repaired modules of that type become available, the back orders are filled in the same order as they were recorded. One could do better sometimes by filling back orders judiciously; for example, by rescuing a station from a down condition whenever possible. But this would require monitoring the numbers of operating modules at the stations and would not result in significant improvements.

Under these assumptions, the stationary (long-term) probabilities of $0,\cdots,n_j$ modules of type j operating at, say, station 1 can be obtained as follows. First, use the algorithm of Ref. 2 to find the stationary probabilities $p_0,p_1,\cdots,p_{N_j+r_j}$ of $0,\cdots,N_j+r_j$ modules being failed in the entire complex, where N_j = total number of spares of type j, and r_j = total number operating in all the stations. If the number failed is V, say, and V is N_j or less, then all n_j modules will be operating at station 1. If $V > N_j$, however, then $V-N_j$ modules among the r_j are down. The probability that exactly i of these are at station 1 is

$$\frac{\binom{n_j}{i}\binom{r_j-n_j}{V-N_j-i}}{\binom{r_j}{V-N_j}}$$

where $\max(0,V-N_j+n_j-r_j) \leq i \leq \min(n_j,V-N_j)$. Hence, the stationary probability that exactly i ($i > 0$) of the type j modules are down at station 1 is

$$\sum_{V=i+N_j}^{i+N_j+r_j-n_j} P_V \frac{\binom{n_j}{i}\binom{r_j-n_j}{V-N_j-i}}{\binom{r_j}{V-N_j}}$$

Summing over $i > n_j-m_j$ gives the stationary probability of the jth module type being down at station 1. Subtracting this sum from one gives the UTR of the jth module type at station 1. Multiplying the results over $j = 1,\cdots,k$ yields the station UTR for station 1. The cost-effective spares provisioning algorithm can then be applied with the "value" (see Ref. 1) of a spares package defined to be the sum of the log UTRs of the individual stations (thus weighting all stations equally).

III. Examples of Cost Savings Through Spares Pooling

The first example is concerned with terminet sparing at Goldstone. A spares complement was to be provided for a total of 552 operating modules, 24 modules of each of 23 types. Three cases were considered. For the first case it was assumed that all the modules were contained in one system and that for each type of module $m_j=n_j = 24$. In effect, this means that if any of the 552 operating modules fails and there is no spare available to replace it, the system is down. For the remaining cases it was assumed that there are three identical systems, one at each station and operating independently, and that for each system $m_j=n_j = 8$ for each of the types. However, for the second case a common pool of spares was to be provided for these three systems, while in the third case each system was to have its own spares complement. In all cases, spares packages were generated using the extended algorithm as given in Section II, which can also be used for the unpooled case when the proper parameter values are inserted. Repair time was assumed to be two weeks. Table 1 gives the pertinent results for spares packages with UTRs of about 0.90, 0.95 and 0.99. The UTRs shown for the first case are the fractions of time that the total system is operational, while the UTRs shown for the second and third cases are those for each station. The contents of the spares packages are omitted. It can be seen from the costs shown in Table 1 that pooled sparing in this example results in a cost savings of about 55% for comparable UTRs.

The next example is concerned with magnetic tape sparing at Goldstone. There are three independent, identical systems, one at each station. Each system is made up of 2 modules each of 5 types and 4 modules of a sixth type, a total of 42 operating modules. Four cases are considered. For cases 1 and 2, we assume for each system that $m_j=n_j = 2$ for $j = 1,\cdots,5$ and $m_6=n_6 = 4$. For cases 3 and 4, we assume that the n_j's are the same as in cases 1 and 2 but that for each system $m_j = 1, j = 1,\cdots,5$

and $m_n = 2$. For cases 1 and 3, we assume pooled sparing, and for cases 2 and 4 separate spares complements for the three systems. Repair time was assumed to be 6 weeks. Table 2 gives some of the results obtained. A cost savings of about 45% is achieved by pooling spares. This example also illustrates the importance of the m_j's, since their values relative to those of the respective n_j's reflect the amount of redundancy in the system. This explains the high UTR achieved for cases 3 and 4 when no spares are provided.

The final example concerns megadata terminal sparing at JPL and involves an unusual situation. There are seven independent systems. System 1 consists of 2 each of 9 types of modules, while systems 2 through 7 each consist of 1 each of the same 9 types. Thus, any spares pool for the seven systems will result in a UTR_1 for system 1 and a UTR_2 for each of the remaining systems, where $UTR_1 \neq UTR_2$. We consider four cases. For cases 1 and 2, we assume that for each system $m_j = n_j$ for all j. For cases 3 and 4, we assume that for system 1, $m_j = 1$ for all j. For cases 1 and 3, we assume pooled sparing, while for cases 2 and 4 separate sparing. Table 3 lists some of these results obtained. A comparison between the pooled and separate sparing shows an average cost savings of about 75%. This example illustrates the fact that, in general, as the number of systems containing the same types of modules increases, the cost savings for pooled sparing, rather than separate sparing, also increase.

IV. Conclusions

The cost of pooling spares for several systems containing the same types of modules will always be less than the total cost of sparing each system separately. The extended algorithm, designed for pooled sparing, can be applied to systems containing redundant as well as nonredundant elements. Thus, this algorithm provides a flexible method for achieving substantial reductions in sparing costs.

References

1. Eisenberger, I., Lorden, G., and Maiocco, F., "Cost Effective Spares Provisioning for the Deep Space Network," in *The Deep Space Network Progress Report 42-20*, pp. 128–134, Jet Propulsion Laboratory, Pasadena, Calif., Apr. 15, 1974.
2. Eisenberger, I., Lorden, G., and Maiocco, F., "A Preliminary Study of Spares Provisioning for the Deep Space Network," in *The Deep Space Network Progress Report*, Technical Report 32-1526, Vol. XVIII, pp. 102–110, Jet Propulsion Laboratory, Pasadena, Calif., Dec. 15, 1973.

Table 1. Terminet sparing at Goldstone (23 types of modules, 24 modules of each type)

One system			Three systems, pooled sparing			Three systems, separate sparing		
Number of spares	System UTR	Spares cost, $	Number of spares	System UTR	Spares cost, $	Number of spares	System UTR	Spares cost, $
0	0.038	0	0	0.335	0	0	0.335	0
31	0.905	3499	23	0.915	2608	57	0.901	5808
38	0.952	4155	27	0.952	3190	66	0.951	7086
48	0.980	5337	40	0.990	4576	93	0.990	10497

Table 2. Magnetic tape sparing at Goldstone (6 types of modules; 6 modules each of 5 types; 12 modules of sixth type)

Pooled sparing $m_j = n_j$			Separate sparing $m_j = n_j$			Pooled sparing $m_j < n_j$			Separate sparing $m_j < n_j$		
Number of spares	System UTR	Spares cost, $	Number of spares	System UTR	Spares cost, $	Number of spares	System UTR	Spares cost, $	Number of spares	System UTR	Spares cost, $
0	0.363	0	0	0.363	0	0	0.9792	0	0	0.9792	0
10	0.944	30480	21	0.946	53820	4	0.9924	8770	8	0.9925	17310
13	0.981	38250	24	0.982	71130	5	0.9967	14540	12	0.9964	26310
14	0.991	44020	33	0.990	80130	9	0.9993	28080	15	0.9990	43620

Table 3. Megadata terminal sparing at JPL (9 types of modules; one system of 2 modules of each type; 6 systems each containing 1 module of each type)

Case 1 Pooled sparing				Case 2 Separate sparing				Case 3 Pooled sparing				Case 4 Separate sparing			
Number of spares	System UTR_1	System UTR_2	Spares cost, $	Number of spares	System UTR_1	System UTR_2	Spares cost, $	Number of spares	System UTR_1	System UTR_2	Spares cost, $	Number of spares	System UTR_1	System UTR_2	Spares cost, $
0	0.585	0.765	0	0	0.585	0.765	0	0	0.9807	0.765	0	0	0.9807	0.765	0
8	0.902	0.949	4588	36	0.907	0.951	20098	4	0.9974	0.904	2888	14	0.9969	0.902	9660
12	0.979	0.989	8245	64	0.976	0.989	39275	8	0.9983	0.949	4588	33	0.9984	0.951	19470
15	0.992	0.996	10453	71	0.994	0.998	48285	12	0.9996	0.989	9445	62	0.9996	0.989	38098

A New Feedback Protocol for the Ground Communications Facility

O. H. Adeyemi
Communications Systems Research Section

This report summarizes a simulation study of a feedback scheme that can reduce the Ground Communications Facility error rate by more than two orders of magnitude in real time even in the highest error mode. The after-pass retransmission time is eliminated or reduced drastically in the case of long time outages. The new scheme also provides storage for outage data, thus eliminating the search time for data to be retransmitted after-the-pass for the Clean Tape Log. No new hardware is required.

I. Introduction

Until now, our efforts to reduce the Ground Communications Facility (GCF) error rate from the present bit error rate (BER) of 10^{-4} (or block rate of about 10^{-3} to 10^{-2}) to an acceptable value of less than 10^{-6} (or block rate of less than 10^{-5}) have been hampered, first, by the discovery in 1974 that forward error correction was not effective (Ref. 1) and then, later, by objections to the long time required for necessary internal processing implicit in the two feedback retransmission schemes proposed at that time (Refs. 2 and 3). The feedback protocol proposed in Ref. 4 was designed mainly to eliminate these objections by letting our USER dictate what time he can give us for this internal processing and then finding the reduction in error rate that can be achieved as a function of this *waiting* time. It also has the important feature of providing a storage for bad data, including outage data that cannot be delivered in real time, to hold such data for retransmission during the filler block times (when the data line is clean) or after the pass in the case of long outages (a rare event, but still a problem), thus eliminating the search time for outage data. Equally important, no new hardware is required.

Real-time error reduction is not the only feature desirable in the GCF. It must be possible to log error-free data with minimum after-pass retransmission. There are, therefore, two main parameters by which to evaluate the performance of this scheme (and indeed any feedback scheme on the GCF). Given the acceptable USER waiting time, we need to know the error rate of the data delivered to him in real time and the reduction in the time for

retransmission of bad data after the pass. As to the second requirement, we show that this scheme cleans up all the *normal* errors on the GCF *during* the pass, including all short outages; part of the long outage data (several thousand blocks long) may have to wait until after the pass for retransmission for the Clean Tape Record. This report is addressed principally to the first question: the real-time error rate to the USER.

In a simulation study of about 10½ hours of real-time data in the *noisiest* mode of the high-speed 4.8-kbps data line, 2000 block errors were reduced to 128 block errors to the USER at a maximum waiting time of only 3 seconds and to only 40 block errors if the maximum waiting time is increased to 6 seconds. This is a reduction in error rate from a BER of 10^{-4} to 10^{-6} at a waiting time of 3 seconds, and it is the highest USER error in all the simulations. In several cases, all the errors were corrected within the allowable waiting time. The highest errors delivered for different USER waiting times were:

Waiting time t, seconds	Error to USER
0	2000
3	128
6	40
9	31

The time $t = 0$ corresponds to no processing (no feedback retransmission).

The wideband data line is known to be better than the high-speed line, which explains the better performance of this scheme in the wideband mode at a waiting time of 3 seconds. The error rate to the USER in this case is 10^{-7}. The wideband data line performance at the noisiest mode was:

Waiting time t, seconds	Error to USER
0	2000
3	69
6	52
9	49

In both the high-speed and the wideband data line modes, 10 hours of line use provide literally thousands of filler block times at 90% (or 95%) data rate during which the 128 blocks (high speed) or the 69 blocks (wideband) for the Clean Tape Record can be retransmitted. Thus, as mentioned above, this scheme requires no after-the pass retransmission time during 99.9% of the total GCF operation comprising the normal error and short outage (up to several hundred blocks) modes.

II. The Retransmission Scheme

A schematic diagram (Fig. 1) is given to aid in understanding the feedback protocol.

The operating procedure is as follows: Each new data block transmitted is stored in the Priority Buffer (PB) until an acknowledgment signal has been received at transmitter T as to whether it has been received correctly. Thus, by the time word is received about the error status of the first block transmitted, as many new data blocks as can be transmitted within a loop time (LD blocks) will have been sent. All these LD blocks will be stored in the Priority Buffer. As soon as an acknowledgment signal indicates that a block has been received error-free, that block is dropped from the Priority Buffer. Thus, at any time not more than LD blocks are stored in this buffer, and the current feedback error status signal applies to the oldest block in it.

Now suppose an error message is received and the USER allows only t seconds for any internal processing that can be done to correct this error block and the burst that may follow. Since data must be delivered in sequence to the USER, delivery of all subsequent blocks is held up in the Receive Buffer (RB) until the error block is corrected or until t seconds are up, whichever comes first. Think of this USER waiting time in terms of the $tR_T/1200$ blocks that can be transmitted in the allowable t seconds. Better still, let us think of it in terms of the $NT = [(tR_T/1200) - LD]$ blocks that can be transmitted from T to the receiver R starting from when the error status message is received at the transmitter until the time required for a new block transmitted to reach the receiver just before the t seconds are up. The NT block times are all we can use for any possible retransmissions we must do.

When the error message reaches the transmitter T indicating the beginning of a burst:

(a) The transmitter time is set at TIME = NT, counting down one every block time.

(b) The incoming new data stream is diverted into the New Data (ND) Buffer.

(c) The error block is taken from the first position in the Priority Buffer, transmitted, and re-inserted in the PB but now as the newest entry. Thus, the Priority Buffer still contains the *LD* blocks on which error status reports have not been received.

Steps (b) and (c) are continued in the case of consecutive errors. However, if within the execution of these two steps there is a good block, then:

(i) Drop the acknowledged block off the Priority Buffer.

(ii) Transmit the oldest block of the new data stream in *ND* Buffer.

(iii) Insert the new block into the newest block position in the Priority Buffer.

STEPS (b) AND (c) ARE OPERATIVE ONLY IF $NT > 0$.

As soon as the retransmission time is up (when $NT = 0$):

(1) Start transmitting new data from the queue in the ND Buffer.

(2) Empty all the *LD* blocks in the Priority Buffer into the Old Data Buffer (ODB). These are the blocks on which error status reports have not been received and which may contain errors. When the acknowledgments, if any, are received, only the bad data are retained in the ODB. The ODB contents are transmitted within the filler block times during 99% of the time when the GCF is in the normal error-free mode. These blocks are then merged with stored error-free real-time blocks to form the Clean Tape Log.

(3) Deliver all the blocks in the Receive Buffer (though some are in error) to the USER *and* write a copy of these blocks on the Clean Tape Log. Since up to 40% of the bad blocks contain 50-bit errors or more (almost 50% in the wideband data line), not many of the error blocks delivered to USER would be useful.

In summary, we need four buffers and a storage for clean data.

(1) The Receive Buffer stores all blocks correctly received during retransmission time until all prior blocks have been successfully retransmitted or until the retransmission time is up, whichever comes first.

(2) The New Data Buffer stores the new data stream during the retransmissions.

(3) The Priority Buffer retains each new block until its error status report is received and each retransmitted block until the retransmission time is over, then all the contents are emptied into the ODB.

(4) The Old Data Buffer holds all the data that cannot be delivered in real time. During periods of long line outages, this buffer becomes increasingly long as undelivered data continue to pour into it from the Priority Buffer. The Priority Buffer and the Old Data Buffer can be part of the same physical device with two pointers: one to the data that can still be corrected before they are delivered to the USER, and the other to those data that must wait until filler block times or after-the-pass.

(5) The Clean Tape Log is a record of only correct data. It acquires error-free data by merging real-time good blocks with those retransmitted later from the ODB.

The following is an example of how the scheme works:

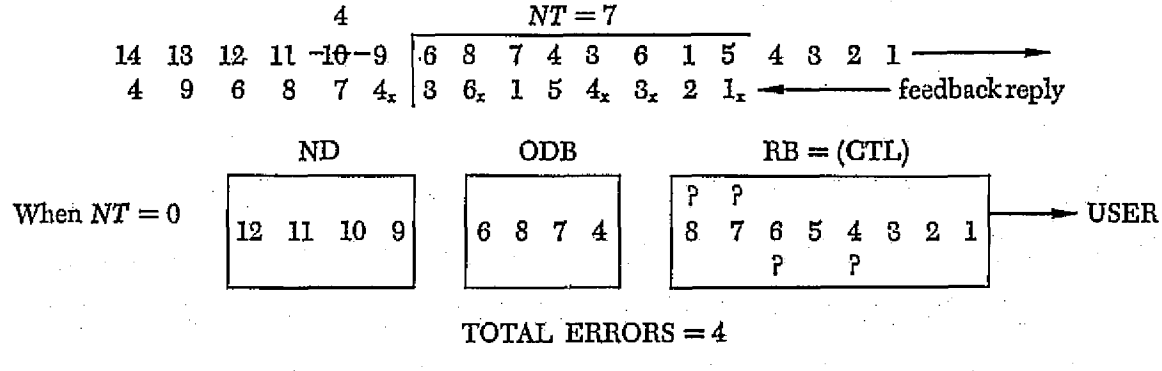

This is an example of high-speed 4.8-kbps data line performance for which the USER allows up to 8 seconds for retransmissions. The 8 seconds is a total of 12 block times. Suppose the loop time is equivalent to 5 block times; then we have 7 block times for all the retransmissions we may need to do. When block 5 is being transmitted, the feedback reply on block 1 says error, so block 1 is retransmitted next. Meanwhile, block 2 got through, so transmit block 6, etc. The error blocks in feedback replies are x-ed. Just after the second retransmission of block 6, retransmission time $NT = 0$. So

(i) Deliver blocks 8 7 6 5 4 3 2 1 to USER *and* write a copy on CTL.

(ii) Old Data Buffer gets blocks 6 8 7 4; block 4 being the oldest block while 6 is the newest; block 3 having just been confirmed error-free.

Meanwhile, blocks 9, 10, 11, and 12 are being stored in the New Data Buffer. Here we assume the data rate to be 90%, which makes every tenth block a filler. The next block to be transmitted is block 9 and, the 10th being a filler, we use the space to retransmit block 4 for the Clean Tape Log. When block 14 is being transmitted, the status as known to the transmitter is:

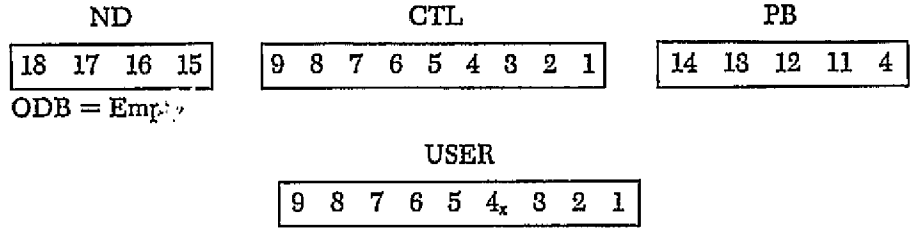

Instead of retransmitting block 4 during filler time 10, we may elect to send the new block 11, which is already waiting in ND, since priority is not on retransmissions to the Clean Tape Log. Indeed, this is what should be done to clear the new data buildup in ND and catch up with normal new data flow at the buffer. The subsequent filler block times before the next burst can then be used for retransmissions from the ODB.

III. Simulation

The functional diagram of the simulation program is presented in Fig. 2. The important parameters are NT (the number of retransmissions that can be done within the waiting time), LD (the loop delay or the number of block storage locations in the Priority Buffer), and NR, an integer describing the input data rate R_D: for every NR transmitted block times, $NR - 1$ data blocks enter the system at times $N \not\equiv 0 \bmod NR$ (see Ref. 3). In other words, every NR^{th} transmitted block is a filler for line synchronization. For example, data rates 0.9 and 0.95 data blocks per channel block correspond to NR = 10 and 20, respectively.

The channel errors were generated according to the GCF model developed earlier (Ref. 5) driven with pseudo-random inputs. Block errors were generated directly in the following way: In the model p_i, c_i, $i = 1, \cdots, 4$, are, respectively, the proportion of times spent in the good (error-free) states and the probabilities of entering these states. Then it can be shown that the conditional probability, starting from an error block, of getting a good block *after not more than n error blocks* is given by

$$1 - \left\{ \frac{\sum ci \dfrac{(1-p_i^s)^2}{p_i(1-p_i)}}{\sum ci \dfrac{(1-p_i^s)}{p_i(1-p_i)}} \right\}^{n+1} \tag{1}$$

Similarly, the conditional probability, starting from a good block, of getting an error block *after not more than n good blocks* is given by

$$\frac{\sum c_i p_i^{\dagger} \dfrac{(1-p_i^{s(n+1)})}{p_i(1-p_i)}}{\sum \dfrac{c_i p_i^{s}}{p_i(1-p_i)}} \tag{2}$$

It may be noted that (1) and (2) are just the cumulative probabilities of the time, or the number of blocks, until a change of state (error or error-free); the block length is NASA-standard $s = 1200$ bits. Uniformly distributed random numbers between 0 and 1 were generated and used to find the values of n until the first error occurs

in (2). By using (2) and (1) alternately in this way with the random numbers, error sequences for the different error phases of the GCF were generated. Each run was continued until 2000 block errors occurred. The experiment consists of counting the number of the 2000 block errors left uncorrected (unretransmitted) within the allowable waiting time t seconds and different loop delay times LD corresponding to the two different loops now being employed on the GCF. The total block lengths of each of the runs varied from 152×10^3 to 190×10^5 in both the high-speed and the wideband data lines. This variation is equivalent to from 8 hours to a few hundred hours of real-time GCF channel use.

IV. Results

A general conclusion from this simulation study is that this scheme can reduce the real-time USER error by at least two orders of magnitude. This error reduction can be achieved if the allowable waiting time is at least $2 \times LD$. This means, for example, that if the longer two-hop link is used between stations, at 4800 bps ($LD = 8$), the user must allow up to 4 seconds for possible retransmissions. If, on the other hand, the shorter one-hop link is used ($LD = 5$), a maximum waiting time of 3 seconds is enough.

The USER error rate decreases with LD. This is so because for short loop delay the transmitter is told earlier about the beginning of a burst and starts retransmitting those blocks already affected, thus preventing further new data from being garbled. Of the 2000 errors in each of the over 300 runs, the maximum USER error was 128 at a waiting time of 3 seconds; more than 50% of the runs delivered less than 10 block errors each to the USER. The error rates for the red, amber, and green error phases of the high-speed data line and the overall average performance in both the high-speed and the wideband modes are shown in Tables 1 and 2 for maximum waiting times varying from 3 to 10 seconds.

The real-time USER error rate is independent of data rate. However, straightforward analysis shows that both the New Data and Old Data Buffer buildups depend strongly on the channel statistics and data rate. A 90% (or 95%) data rate provided enough filler block times to clean up both buffers but the question of how large ND ever gets before it is cleaned up during the long error-free periods is still under investigation. The Receiver Buffer can never be as large as $LD + NT$ but can be as small as LD during repeated retransmissions of consecutive errors.

References

1. Adeyemi, O. H., and McEliece, R. J., "Forward Error Correction for the Ground Communications Facility?" in *The Deep Space Network Progress Report 42-22*, pp. 114–117, Jet Propulsion Laboratory, Pasadena, Calif., Aug. 15, 1974.
2. McClure, J. P., "Basic Algorithm for Retransmission Error Correction," Interoffice Memorandum, Oct. 1972 (JPL internal document).
3. Welch, L. R., "Simulation Study of a GCF Retransmission Scheme," in *The Deep Space Network Progress Report 42-22*, pp. 125–128, Jet Propulsion Laboratory, Pasadena, Calif., Aug. 15, 1974.
4. Adeyemi, O. H., "A Simple GCF Feedback Protocol," IOM 331-75-12, Feb. 1975 (JPL internal document).
5. Adeyemi, O., *Error Control in the GCF: An Information-Theoretic Model for Error Analysis and Coding*, Technical Memorandum 33-699, Jet Propulsion Laboratory, Pasadena, Calif., Oct. 15, 1974.

Table 1. Performance on high-speed data line

Raw block rate (BER)	Maximum USER waiting time, seconds (blocks)	Real-time run duration, hours	USER block rate (BER)
		$LD = 5$	
Red 6.50×10^{-3} (2.45×10^{-4})	3 (12)	29	1.26×10^{-4} ($\times 10^{-6}$)
	5 (20)	28.50	5.36×10^{-5} ($\times 10^{-6}$)
	6 (24)	28	3.92×10^{-5}
	9 (36)	29	3.45×10^{-5}
	10 (40)	29	3.38×10^{-5}
Amber 2.12×10^{-3} (2.93×10^{-4})	3	82	2.36×10^{-5} ($< \times 10^{-6}$)
	5	82.6	1.78×10^{-5}
	6	81	1.38×10^{-5}
	9	84	1.23×10^{-5}
	10	82.5	1.18×10^{-5}
Green 1.18×10^{-3} (3.32×10^{-4})	3	118	4.12×10^{-6}
	5	119.30	3.66×10^{-6}
	6	119.56	2.90×10^{-6}
	9	118	2.35×10^{-6}
	10	116	2.29×10^{-6}
		$LD = 8$	
Red 6.50×10^{-3} (2.45×10^{-4})	3 (12)	27	7.15×10^{-4}
	5 (20)	26.80	6.86×10^{-5}
	6 (24)	25	3.92×10^{-5}
	9 (36)	28	3.81×10^{-5}
	10 (40)	29	3.61×10^{-5}
Amber 2.12×10^{-3} (2.93×10^{-4})	3	82.5	2.95×10^{-5}
	5	82.8	1.93×10^{-5}
	6	79.4	1.66×10^{-5}
	9	82.5	1.32×10^{-5}
	10	82.5	1.21×10^{-5}
Green 1.18×10^{-3} (3.32×10^{-4})	3	116	5.38×10^{-6}
	5	119.4	4.73×10^{-6}
	6	119.5	4.31×10^{-6}
	9	118	3.29×10^{-6}
	10	118	3.06×10^{-6}

Table 2. Overall average performance

Raw block rate (BER)	Maximum USER waiting time, seconds (blocks)	Real-time run duration, hours	USER block rate (BER)
	HSP data line		
$LD = 5$ 2.19×10^{-3} (4.38×10^{-5})	3 (12)	69	2.31×10^{-5} ($\times 10^{-7}$)
	5 (20)	64.4	2.05×10^{-5}
	6 (24)	67.7	1.76×10^{-5}
	9 (36)	68	1.25×10^{-5}
	10 (40)	65	1.19×10^{-5}
$LD = 8$	3	65.25	6.28×10^{-5}
	5	67.4	3.81×10^{-5}
	6	67.50	2.26×10^{-5}
	9	69	1.76×10^{-5}
	10	69	1.4×10^{-7}
	50-kbps wideband data line		
$LD = 31$ 1.63×10^{-3} (3.54×10^{-5})	3 (125)	8.6	4.35×10^{-5} ($\sim \times 10^{-7}$)
	5 (209)	8.2	3.00×10^{-5}
	6 (250)	8	1.39×10^{-5}
	9 (375)	7.8	1.12×10^{-5}
	10 (417)	8	1.07×10^{-6}
$LD = 51$	3	8.5	5.33×10^{-5}
	5	8.1	4.47×10^{-5}
	6	8.7	3.52×10^{-5}
	9	8.5	2.32×10^{-5}
	10	8	1.71×10^{-5}

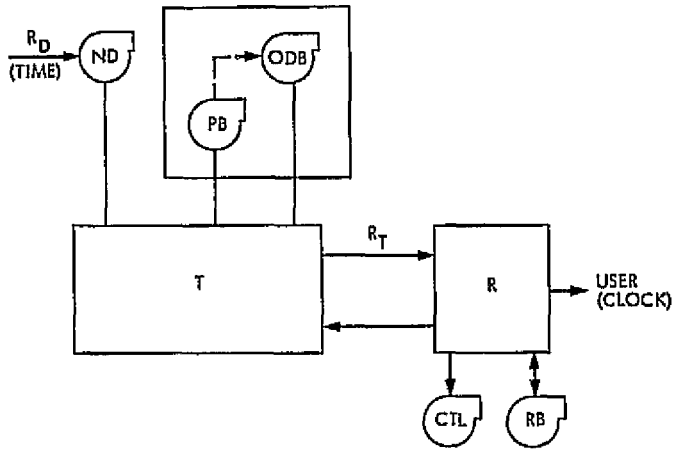

R_D DATA RATE

R_T TRANSMISSION RATE IN BITS PER SECOND; USUALLY $R_D < R_T$, i.e., $R_D = \gamma R_T$, WHERE $0 < \gamma < 1$ MAY BE 90 OR 95%

ND NEW DATA BUFFER. ND HOLDS THE INCOMING NEW DATA STREAM UNTIL IT IS CALLED FOR TRANSMISSION

PB PRIORITY BUFFER

ODB OLD DATA BUFFER

T TRANSMITTER

CTL CLEAN TAPE LOG ON WHICH THE CLEAN DATA ARE WRITTEN AFTER ERROR CORRECTION

RB RECEIVE BUFFER

R RECEIVER

Fig. 1. Retransmission scheme

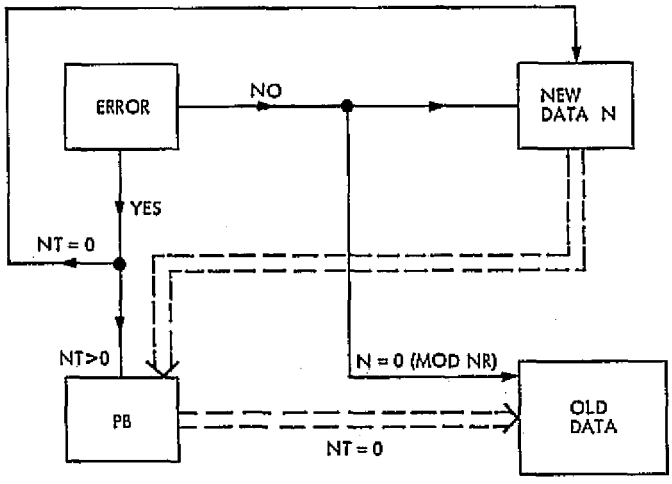

Fig. 2. Simulation functional diagram

Development of Real-Time Hardware/ Software Systems

J. W. Layland
Communications Systems Research Section

This report presents a concentrated overview of the critical issues and tools for the development of real-time systems. Real-time systems are defined to be those which perform their actions in response to stimuli from outside themselves, and which must respond to these stimuli within fixed, predetermined time limits. A real-time system with many independent external stimuli almost certainly contains a large number of interacting asynchronous processes. From the viewpoint of the equipment surrounding this real-time system, these processes operate in parallel, and their operations are only partially ordered. A single process can be well represented by a flow chart which relates step-by-step exactly which action follows the last one. Multiple interacting asynchronous processes cannot be conveniently described by a flow chart of their combined operations, even though when taken individually each process can be depicted on a flow chart. However, each of the multiple asynchronous processes can be readily understood as a finite state machine, and the interaction between machines can be graphically represented by a state-transition net, or "Petri-net." This report develops the use of such nets for software and hardware design through description and example.

I. Introduction

The purpose of this report is to present a concentrated overview of the critical issues and tools for the development of real-time systems. Real-time systems are defined to be those which perform their actions in response to stimuli from outside of themselves, and which must respond to these stimuli within fixed, predetermined time limits. Typically there are many independent stimuli which require a response. Each stimulus causes the activation of, or creation of, at least one process within the system, which in turn will develop the responses required by the source of the stimulation. In software terminology, a process is a sequence of operations which is fully ordered, and has a well-defined start and end. A real-time system with many independent external stimuli

almost certainly contains a large number of interacting asynchronous processes. From the viewpoint of the equipment surrounding this real-time system, these processes operate in parallel, and their operations are only partially ordered.

A single process can be well represented by a flow chart which relates step-by-step exactly which action follows the last one. Multiple interacting asynchronous processes cannot be conveniently described by a flow chart of their combined operations, even though when taken individually each process can be depicted on a flow chart. The early conceptual developments (Ref. 1) which engendered the current raging fad of structured programming were aimed primarily at the taming of the complexities of software containing asynchronous processes. The more recent, more formalized development of structured programming (Refs. 2, 3) has emphasized the decomposition of single-process flow charts over the less tractable real-time problems. This report is one step of an attempt to bridge the gap between the underlying principles of structured programming and the problems of developing a working real-time system.

The act of solving a complex problem, or designing a complex system can be characterized as a hiding of locally irrelevant details, so that those details which are relevant to the locale of interest can be properly studied and interpreted. A significant fraction of such improvements as have been observed with structured programming may well be attributable to such hiding of detail as is induced, instead of to the rigorous application of the restricted control structures themselves.

In Part II we present some views on the process of solving complex problems or designing complex systems. Part III considers the problem of choosing a language for the description and/or implementation of real-time software. Part IV presents assorted advice on the implementation of real-time systems. Some large portion of Part IV consists of quasi-obvious common sense, yet it is this collection of obvious things that taken together represents the bulk of the increment in difficulty between nonreal-time and real-time systems.

Part V is an introduction to the syntax of the Petri net (Ref. 4), or state-transition net. Such nets describe the partial ordering of events within a finite-state machine, and as such can be well used to represent the interactions of the asynchronous processes in a real-time system. Part VI makes use of the transition nets to describe the behavior of a suitably substantial synthetic example system. This description includes both processes which are totally software and processes which operate both in hardware and software. Part VII and subsequent discussions contain additional examples of processes which are represented by transition nets, and also contain examples of the mechanization of transition nets as both software and hardware. They will be written in the future as additional experience is gained through the use of this system description tool.

II. On Problem Solving and System Design

Design problems, whether they are destined to be executed as computer software, logical hardware, or as some entirely unrelated material come in two varieties. They are either small enough that their entire character fits inside the problem-solver's head as a single chunk, or they are not. An example of a thing which is single-chunk could be "a transparent green glass marble." An example of a thing which is not single chunk could be "a thousand marbles rolling down a giant slide." The features which make this second example not a single chunk for most of us are that it contains a large number of identifiable things and that these things move in a quasi-independent way.

Differentiation between those things which are comprehensible as a single chunk, and those things which are not is subjective, and varies from person to person on the basis of training, experience, desire, mental capacity, etc. Single-chunk problems can be solved or implemented in an almost random fashion without undue difficulties. Larger problems must be either laboriously studied until they resemble single chunk problems (if this is possible), or dissected into smaller problems which are single chunk in nature, and which taken together solve the original problem. In order to make the subproblems single chunk when the original one was not, some information or design detail that is present in the problem as a whole must be hidden from the subproblem. Contrarily, each of the subproblems should contain detail that is hidden from the others. It is this systematic selective hiding of design details which makes solution of the larger problems possible. This problem-solving philosophy is similar to one which has been voiced by Parnas (Refs. 5, 6).

The design rules and restricted control structures of structured programming are intended to guide the dissection of a problem into subproblems which are single-chunk in nature, not only for the designer, but also for his managers, and for any future casual readers. The oft-quoted structure theorems (Ref. 2) tell us that we can reorganize any flow chart using only three control structures, no matter how complex it may appear. Flow charts, however, are single-process in nature and cannot

completely and/or conveniently represent all features of a multiprocess operation. Small details, like timing constraints or conflicts, don't fit and are left for prose commentary, or worse, are left to clutter the designer's head while he works on each of the pieces, because these details are not hidden from any of them. Because these most troublesome details of real-time software do not fit a flow-chart representation, the ritual of structured programming as it is conventionally preached cannot solve the real-time software designer's biggest problems, although it can assist him in handling those pieces of his problem which can be isolated as single processes.

We should remember, however, that some of the earliest work in the realm of structured programming was aimed directly at the methodical design of a system containing multiple asynchronous processes (Ref. 1). That these early efforts were successful is evidence that the principles which underly structured programming can be used to great advantage in real-time systems, even if some large part of the recently formalized superstructure cannot.

III. Programming Languages for Design and Implementation

We can segment the design of a system into two primary tasks. The first is to fully describe the actions of the system in its response to the external stimuli, be they human or electromechanical in origin. The second is to implement those actions within the available hardware/software resources. Again, we are hiding details, by considering first what is to be done, and then, separately, how it is to be accomplished. Actual development almost always requires an iteration between these two phases, because some of the actions which appear to be needed may be impossible to implement, or simply expensive, whereas some actions which are close in some sense to the needed action might be very much simpler to implement. The alternate actions could not be known to be acceptable without considering the overall response demands of the world outside the system being designed.

With some problems, and an appropriate programming language, a complete description of that problem can also be the implementation of its solution. The ease with which any task can be performed via a specific programming language actually seems to depend upon the extent to which that language is able to describe the problem to be solved, as opposed to implementing the solution to that problem. A near-classical example here is any numerical formula calculation, and one of the popular FORmula TRANslation languages. Such languages intrinsically hide a great quantity of implementation detail from the problem solver; and therein lies the power of the higher level languages (HLL) with respect to their proper domain. Outside of that domain, however, any specific higher level language may be no better than a machine assembly language (MAL), and may, in fact, be much poorer if the operations required to implement the required problem solution cannot easily be synthesized from the repertoire of that higher level language.

The power of a language with respect to a particular problem may be measured by the number of statements within that language which are required to implement the solution to that problem. For largely algebraic problems, a single FORTRAN statement may contain the equivalent of many tens of machine-assembly language instructions. On the other hand, to complement a bit in a data-structure may require ten FORTRAN statements and only two or three MAL statements. Both language classes would implement the operation, rather than describe it, and both would be machine-dependent in nature. Some other types of operations would require a comparable number of statements in either the MAL, or an HLL; some of these would be machine-dependent by the nature of the data structures involved, and in none of these would the implementation details be hidden from the designer. Thus, only in very special circumstances does any programming language hide enough details to be appropriate for describing the system design.

For most problems there is no uniformly most powerful language, and the choice of an implementation language (or languages) must be made on other considerations. Standardization upon a major HLL is one apparently reasonable way. However, using an HLL to implement operations for which it is poorly suited may require the implementer to know details of the implementation of the HLL itself, thereby greatly increasing the difficulty of his task. In these situations, the HLL has hidden the wrong machine details from the designer; the HLL is nontransparent to some specifically important elements of the machine's hardware capability.

A mixed arsenal of an algebraic HLL, used where appropriate, and the target computer's MAL can combine the best features of both. The MACRO capability that is present with many MALs, or a machine-independent MACRO preprocessor (Refs. 7, 8) can be used to locally extend the power of the MAL with respect to the problem at hand. It may, in fact, be quite desirable to use

MACROs to implement the restricted control structures of structured programming within the MAL and HLL, and maintain commonality between control statements of both.

Although most specific major HLLs seem presently to be a poor choice for the sole implementation language of a real-time system, the HLLs as a class are not yet ruled out. Several attempts have been made, usually in a university environment, to define an HLL specifically for the implementation of real-time, or systems software. None of these have as yet achieved widespread acceptance outside of their native centers, yet the achievements that are claimed are positive enough to warrant their serious consideration. BLISS (Ref. 9) is one such language, which was designed originally for the PDP-10, and has since been adapted for the PDP-11 minicomputer. BLISS is ALGOL-like in structure, yet was designed to require negligible software support at execution time and to allow the program designer great flexibility in the accessing of data. Because the method for accessing various data elements is specified as the data is declared, BLISS programs are not machine-independent, but can apparently be readily modified to transport them between machines. Two other relevant efforts are BCPL (Ref. 10), and the Graphical Automatic Programming system (Ref. 11), which is almost a language.

Graphical representations have been used for many years in the design of software systems. Simple flow charts are widely accepted as software documentation and software design documentation. The syntax of a programming language and the operations required to interpret it have been graphically represented in the form of a finite state machine (FSM) (Ref. 12). Similar FSM representations have been used to describe the interactions between a user and a computer operating system, and to design communications-handling software for a time-sharing operating system (Refs. 13, 14). The multiple asynchronous processes of a real-time system can each be understood as an FSM which interacts with the periphery equipment and with the other FSMs as it acts to produce the required responses. These interactions, and the partial ordering of actions of the FSMs, can be well represented graphically, even though not by the conventional flow chart.

One particular graphical FSM representation known as the Petri net (Refs. 4, 15), or state-transition net was developed to deal with asynchronous interactions between FSMs, and contains the operations necessary to describe the partial ordering of events, and the timing interactions of asynchronous software processes, as well as within hardware realizations of an FSM, or at the hardware/software interface. The syntax of the transition net representation is defined in Section V.

IV. Implementation of Real-Time Software

Three characteristics are desired for real-time software, that it: is consistent, is reasonably efficient, and meets appointed deadlines of execution. One of the last things a designer wishes to have is for the results of computation to vary from time to time, with no apparent change in input parameters and conditions. For a nonreal-time single-process computation, this can be assured by ensuring that all parameters and variables that are used by that process are preset to their proper initial condition at the start of the process. This requirement is obvious, yet it is one source of occasional errors. It is also obvious that all data used as input to a process must be valid when that process starts executing and not changed by another process until the using process has terminated. However, failure to satisfy this requirement is probably the most common error encountered in real-time systems. The problem is basically one of communication between, and synchronization of, intrinsically asynchronous processes. It appears as a race between events in logical hardware, as well as intermittent software errors.

Stimuli from the world surrounding our computer almost always appear as a logic signal at the interrupt portion of the computer's hardware at some particular point in time. In due course, the computer will respond to this interrupt signal by saving a small amount of information (the current instruction address, and perhaps some additional status) in a predetermined location in memory, and obtaining a new current instruction address for the interrupt subroutine associated with this signal. The computer interrupt hardware will also prevent a recurrence of this interrupt response until commanded otherwise. The next instruction executed will be the first instruction of the interrupt subroutine. The first opportunity for inconsistency is here. If all resources within the computer which are needed to service the equipment which initiated the stimulus have been saved by the computer's automatic response, we are free to service that equipment. If a resource is needed which has not been saved automatically, its current status must be temporarily saved before the resource is used within the interrupt subroutine, and then restored to its original condition after use and before returning to the process which was interrupted; the penalty for not doing so is lack of consistency in the interrupted process. Examples of resources whose state must be saved if they are to be used include hardware registers, arithmetic status bits, and

software registers which contain intermediate temporary results for subroutines called.

In the interest of efficiency, however, it is unwise to save and restore any resources which are not needed to service the requesting equipment, since these operations, while necessary for consistency on the resources used, represent a nonproductive overhead with respect to actual tasks. A strong case can be made for using a minimal MAL subroutine for at least the most frequent interrupts. By doing so, the resources needed can be made visible and controlled, thus restraining unnecessary overhead. Services requested by equipment with an interrupt signal can often be categorized with respect to the time available to perform them. Some must be performed immediately—otherwise there is no real excuse for generating the interrupt at all. Others could be deferred to another slower software process by buffering several requests together. Deferrable services for which no additional overhead is generated to allow them to be performed within the interrupt subroutine may as well be performed there. Deferrable services which would require additional overhead should be deferred if by doing so the overhead dictated by consistency requirements would be lessened.

Some simplification of process interfaces and concomitant reduction of overhead can often be achieved by anticipating the more complex parts of the required responses, and precomputing these when it is convenient to do so. These precomputed results can then be delivered via a "'mailbox"' to the using process when needed, or via a much-simplified interrupt-driven process to the external system hardware. In the implementation of software, results which are precomputed for the interrupt routines can vary greatly in character and extent. Their single common feature, and the feature which they share in common with deferred computations, is that they have been removed from the most time-critical of their possible points of action to a domain of (hopefully) lessened time criticality.

The second major category of consistency failures occurs at the interface between our interrupt subroutine and the software processes that perform those services that were deferred. This is the interface between cooperating sequential processes to which the synchronizing primitives of Dijkstra (Ref. 16) and the considerable following literature apply. The essential element for consistency here is that during no interval of time should more than one process be empowered to change the same location of memory. Areas into which a given process may store data should be privately owned by that process while it is empowered to store that data, and then deliver intact to whatever process will use that data. Semaphores are used for communication between processes, just as the interrupt signals were used for communication from the hardware to the software processes. Whether the manipulation of these semaphores is performed by synchronization primitives (Refs. 16, 17) or is implemented directly via increment/decrement and test instructions, they must, for the moment of their change, be made private to the process which is changing them.

The avoidance of deadlock dominates much of the literature on multiple process computation. A deadlock is said to exist between two or more quasi-independent processes whenever all of them possess at least a part of the resources they need for completion, none of them possess all of the resources they need for completion, and none of them are willing and/or able to release those resources to allow another process to complete. In a committed real-time system, deadlocks should not only be avoided, but they should be designed out. Any process should possess all of the resources it needs to allow it to complete its activity before it becomes active—with NO exceptions.

Determining whether the appointed execution deadlines are all satisfied can only be done with certainty after implementation is complete. This is accomplished by means of a Ganttchart (Ref. 18) or time-occupancy diagram for all of the processes with deadlines through their critical time interval (Ref. 19). If reasonably large margins are included, a high confidence in meeting deadlines can be achieved by using estimates of process execution time once enough of the overall design is completed. If deadlines are not to be met, some revision is needed, which could be as simple as increasing efficiency by reorganization of processes to reduce overhead, or as involved as renegotiating system requirements, or acquiring a new computer. For a real-time system, the side effects from deadline problems can be minimized by designing and implementing first the processes that service the highest frequency and most time-critical interrupts, and then proceeding into the more mundane parts of the system.

V. The Petri-Net Representations

As observed earlier, it is convenient for the designer of a real-time system to conceptualize his system as an ensemble of finite state machines (FSMs) which operate on command and work together to produce the intended system responses, much as the musicians of an orchestra follow their own score yet interact time-wise to reproduce the effects intended. Each of the designer's FSMs needs

only to be concerned with what it is required to do to service the needs of the periphery equipment. Each of the FSMs assumes certain states as a result of interactions with the periphery equipment or with certain others of the FSMs; the future action of each FSM is governed by its current state and future inputs. The system designer needs a representation for the FSMs that can fully describe what they do in an unambiguous, concise way. This designer's representation must also be lucid enough to permit a system implementer to add such additional interactions as may be needed to integrate the FSMs together into one computer, to allocate the FSMs between several computers and supporting hardware, or to inform the designer that his dream can't be realized within the budget.

The FSM representation known currently as the Petri-net was introduced by Dr. C. A. Petri in 1962 to deal with the communication between automata (Ref. 4). It bears a significant generic relationship to earlier graphical network representations for FSMs; for example the Neural Networks of McCulloch and Pitts (Ref. 20). Petri nets currently form the core of a slowly growing literature concerning the analysis and exploitation of parallelism in computing hardware or software (Refs. 15, 21–30). The components of the original Petri net have the same basic appeal for representation of FSMs that the basic three structures of structured programming do for single-process computations: their syntax is exceedingly simple, yet is capable of concisely describing the interaction between cooperating sequential processes.

Formally, a Petri net is a directed graph with two types of nodes. Nodes represented as open circles are called locations. Nodes represented as solid bars are called transitions. Figure 1 is an example of a trivial transition net. A location is denoted to be occupied by placing a token, a solid dot, within that location, as in location B of Fig. 1. If the entire net is to be considered as one finite state machine, that machine's state is fully defined by a list of the occupied locations. Tokens move about the net under control of the transitions. A transition is enabled to fire whenever all locations which are on lines of the graph directed into that transition are occupied, and all of the locations which are on lines of the graph directed from that transition are empty. When a transition fires, the tokens are removed from all locations which lead into that transition, and tokens are placed in all locations which are fed from that transition. The firing of a transition is instantaneous. In Fig. 1, transition a is a source of tokens, and will supply a token to location A whenever A is empty. Transition d is a drain for tokens and will remove a token from location D whenever D is occupied.

In the current state of Fig. 1, only transition a is enabled. After a has fired, location A is occupied, and a is no longer enabled, but b is. After b has fired, C is occupied and c is enabled. Since A is now empty, a is also again enabled. After c and a have fired, locations B, D, and A are occupied, and transitions b and d are enabled. An oscillatory activity now ensues with transitions d and b firing to cause locations A, B, and D to empty and location C to be occupied; followed instantly by the firing of transitions c and a. The net result is a steady migration of tokens from a to d in synchronism with the oscillation between B and C.

In representing a software activity, it is convenient to consider the tokens within a net as independent asynchronous processes. The location which each process (token) occupies then represents the state of that process. The transitions through which the processes must pass represent points of interaction between processes which ensure proper synchronism between the processes. In parallel process terminology, transition c of Fig. 1 is a FORK operation from a single process in location C to two (now independent) processes in locations B and D. Transition b of Fig. 1 is a JOIN operation wherein two independent processes at locations A and B are merged into a single process at location C. Although time does not exist explicitly within a transition net, many of the processes which we wish to represent are time-consuming in their data operations, exclusive of the interprocess interactions. This form of time consumption can be embedded within the transition net representation by stretching the change from a location being empty to that location being occupied to include that time. We should view a location as being half occupied, or perhaps, undefined, during this time interval, as no further interactions with other processes appearing explicitly in the net are possible until this time-consuming activity is completed. Upon closer examination, this time-consuming activity which we represent as being within a specific location (process state) may itself be further decomposed as multiple asynchronous processes, or may be a single process which is representable by a conventional flowchart.

The example of Fig. 1 contains nodes with only 0, 1, or 2 inputs and 0, 1, or 2 outputs. The actual number of inputs and outputs is immaterial and can be arbitrarily increased as long as operation of the transitions follows the conventions previously described. However, since clarity of representation is a principal goal, it is wise to restrict the number of inputs and outputs of any node to as small a number as can completely represent the machine operation, preferably 4 or less.

Figure 2 shows two transitions with inputs from locations that do not fit within the basic operation of transitions as previously described. The open circle input is called an enabling input, and the solid circle is called an inhibiting input. A transition with an enabling input behaves identically to a transition with only normal inputs except that when that transition fires, the token which occupied the location which provided the enabling input is not removed, but remains to enable further firing of the transition. An inhibiting input is the converse of the enabling input, in that a transition which has an inhibiting input may not fire as long as that location which provides the inhibiting input is occupied. Both enabling and inhibiting input connections will be used in the examples which follow.

VI. An Example

Previous sections have described the syntax of transition nets in a simple manner which may make the nets appear to be at best an interesting toy with which to describe concurrency which is already under control. The more substantive examples of this section are intended to show that the nets are not only interesting, but are a useful tool as well. We have used transition nets to date in the design of several segments of intercomputer communication software (Ref. 31), producing nets of varying complexity, from some almost as simple as the example Fig. 1, to some which became unpleasantly cumbersome when all necessary detail was forced into view. As a graphical display of concurrent activity, the transition net provides a skeleton within which relevant questions are easily viewed. Answering these questions remains the designer's problem, as a good representation scheme does not automatically design a system, but induces a careful consideration of all pertinent aspects of the design. It should become evident in the following discussion that some amount of prose commentary is also needed by the designers to relate the featureless tokens of the transition net to the physical resources and processes of the system being designed.

Suppose we wish to design a system to perform real-time Fourier Analysis on a continuous analog waveform. Waveform parameters specify for us the rate at which the input data arrives, and the number of input data elements which must be collected together to allow calculations to begin. Because the input data arrives nonstop, a second collection of data will be being received while the first collection is being analyzed. Likewise, the results of the analysis of the first collection of data may be being output to some recipient device while the second collection is being analyzed, and while a third collection is being input. We have a feasibility constraint in that the analysis of the first collection of data must be complete when or before the input of the second collection is complete, and that output of the first collection of data must be complete when or before the input of the third collection is completed. If one or the other of these feasibility constraints is not satisfied, the processing of data will lag behind the influx of new data to be processed and cause eventual loss of that data, no matter what other actions are taken to avoid such loss.

Figure 3 is a transition net description of the processes which operate within this system. Within this net, tokens represent both processes, as before, and resources (buffer spaces) which initially occupy locations Q_1, Q_2, and Q_3. At the level of detail presented in Fig. 3, the processes each have two states, idle (In) and active (An). These three processes correspond to the three major actions required of our system: input (data), transform (data to results), and publish (results); all three are initially idle. Operation of the net begins when a token is placed in the enabling location E, and ceases gracefully when this token is removed, presumably by some higher level process, human operator, or other. It may be worthy of note that at the level of detail shown in Fig. 3, we no longer need to know that the data transformation is a Fourier analysis; it could be any buffered data transformation.

The three active-state location for the three processes are each time-consuming, and hence can be further decomposed, either by single-process flow chart, or by expansion as transition nets with greater detail. The three idle-state locations are each simple and not time-consuming. In presenting Fig. 3 we have assumed that this transition net both restates the physical realizability constraints stated above and describes the actions of a system which conforms to these constraints. The skeptical or confused reader may find it desirable to sequence through the operation of the net in Fig. 3, using the transition behavior rules given earlier, and verify that it performs as advertised.

We can view Fig. 3 either from its manipulation of the resources (buffers), or from the actions of the processes. The buffers enter active location A_1 where they are filled with raw data. They travel briefly through queuing cell Q_4 into location A_2 where the data they carry is transformed. They travel briefly through queuing cell Q_5 into location A_3 where they are emptied of data, and are then returned to the queuing cells Q_3-Q_2-Q_1 for reuse. The three processes represent an assembly line which works upon a three-bucket conveyor system. Process 1, the input process, takes empty buffers from Q_1, fills them, and places the filled buffer in Q_4. Process 2, the transform

process, takes filled buffers from Q_4, operates on them, and places them in Q_5 after transforming. Process 3 takes filled buffers from Q_5, empties them, and returns the emptied buffer to $Q_3 \rightarrow Q_2 \rightarrow Q_1$. Interface between the processes is along near-minimum lines.

Active-state location A_3 contains within it the interaction with an asynchronous external device—the device upon which the transformed data is to be written—and should be instructive to decompose further. One feasible decomposition appears as Fig. 4. The initial state of this process is as shown. Upon activation, since we are doing output from the computer, the buffer is segmented into primitive units of accessibility (words) and saved in the queuing locations $WQ_1 \ldots WQ_n$. The process itself appears in location BSY which enables the setting of interface location (logic signal) STC. This transfers process initiative to the device which should respond by setting interface signal RSP. Since BQ_3 is nonoccupied while WQ_n is occupied, the word in WQ_n is transferred into the byte storage locations BQ_1, BQ_2, and BQ_3. The byte in BQ_3 is then transferred along with process initiative to the device via interface signal RDY. The device is expected at this point to return process initiative via $\overline{\text{RSP}}$, and will have the process initiative returned to it via $\overline{\text{RDY}}$. The signal STC has remained throughout this activity, so the four-phase cycle at the interface can begin again. The bytes remaining in BQ_2, and BQ_3 are transferred to the device with process initiative via signal RDY each time initiative is returned via signal RSP. If BQ_3 is unoccupied when the process initiative returns, a word is fetched from WQ_n into BQ_1, BQ_2, and BQ_3. If both BQ_3 and WQ_n are unoccupied when process initiative returns, the entire buffer has been written and the process activity ceases.

The active process described in the paragraph above still has a large number of open options for implementation. The interface to the device has been fixed by design, but the interface between hardware and software has not. Those readers who are familiar with the Deep Space Network standard 14-line interface (Ref. 32) will probably recognize from the signal names that Fig. 4 represents the data output mode of the 14-line standard interface adapter (SIA). A full SIA description is possible and will be generated in the future. There are at least three feasible places, which have been used in various SIA implementation, for the hardware/software interface to appear in Fig. 4: (A) at the device interface, (B) on the word-transfer path between WQ_n and the BQs, and (C) on the buffer-transfer path into the WQ_n's.

The main point of this discussion is that the active process description in Fig. 4 is complete from a functional design standpoint and works equally well in the description of hardware machine actions as in describing software actions that are best represented as finite state machines.

VII. Concluding Remarks

We have aired in this article a design concept for real-time hardware/software systems and a representation with which to describe the timing interactions of a real-time system. The design viewpoint is one of interacting finite-state machines, each performing its particular functions when resources and other enabling conditions permit. The representation is the Petri net, or state transition net. The article opens with a general discussion of real-time system design, and design rationale; then proceeds to define the transition nets and use them in an example to describe both hardware and software actions.

Although very simple, the transition net representation described herein is complete enough to aid in the development of real-time software, and it appears also to be adequate for performing resource allocation analyses for systems of asynchronous processes. As described here, the representation is not stand-alone but requires the addition of prose commentary to relate features of the real system to their manifestation in the transition net. The references contain some generalizations of transition nets which attempt to be stand-alone representations. We should, in the future, evaluate how successful these attempts have been. There is also a strong temptation to enrich the syntax of the representation. Such enrichment is at least in part self-defeating, since a syntactically rich representation scheme adds its own complexity to that of any system being represented.

References

1. Dijkstra, E.W., "The Structure of THE Multiprogramming System," *Comm. of the ACM*, May 1968, pp. 341–356.

2. Mills, H.D., "Mathematical Foundations for Structured Programming," IBM Document FSC72-6012, Federal Systems Div., IBM, Gaithersburg, Md., February 1972.

3. Tausworthe, R.C., "Standardized Development of Computer Software," to be published.

4. Petri, C.A., "Kommunikation mit Automaten," Bonn, Germany, 1962. English translation available as Supplement 1 to Rome Air Development Center, TR-65-377, January 1966 (AD630125).

5. Parnas, D.L., "On the Criteria to Be Used in Decomposing Programs Into Modules," *Comm. of the ACM*, December 1972, pp. 1053–1058.

6. Parnas, D.L., "A Technique for the Specification of Software Modules, With Examples," *Comm. ACM*, May 1972.

7. Waite, W.M., "A Language Independent Macro Processor," *Comm. ACM*, July 1967, pp. 433–440.

8. Waite, W.M., "The Mobile Programming System: STAGE2," *Comm. ACM*, July 1970, pp. 415–421.

9. Wulf, W.A., et al., "BLISS, A Language for Systems Programming," *Comm. ACM*, December 1971, pp. 780–790.

10. Richards, M., "BCPL, A Tool for Compiler Writing and Systems Programming," in *AFIPS Conference Proceedings*, Spring Joint Computer Conference 1969.

11. Kossiakoff, A., and Sleight, T.P., "A Programming Language for Real Time Systems," *AFIPS Conference Proceedings*, Fall Joint Computer Conference 1972, pp. 923–942.

12. Resnick, M., and Sable, J., "INSCAN, A Syntax Directed Language Processor," *Proceedings of ACM 23rd National Conference 1968*, pp. 423–432.

13. Birke, D.M., "State Transition Programming Techniques and Their Use in Producing Teleprocessing Device Control Programs," Second Symposium on Problems in the Optimization of Data Communication Systems, October 1971, pp. 21–31.

14. Bjorner, D., "Finite State Automaton — Definition of Data Communication Line Control Procedures," *AFIPS Conference Proceedings*, Fall Joint Computer Conference 1970, pp. 477–491.

15. Holt, Anatol, et al., *Final Report on the Information Systems Theory Project*, RADC-TR-68-305, Rome Air Development Center, New York, 1968.

16. Dijkstra, E.W., "Cooperating Sequential Processes," *Study Notes From Techniche Hogschule Eindhoven*, 1965. Reprinted in *Programming Languages*, F. Genuys (Ed.) Academic Press, New York, 1968.

17. Hansen, P.B., *Operating Systems Principles*, Prentice-Hall, Inc., New York, 1973.

18. Manacher, G.K., "Production and Stabilization of Real-Time Task Schedules," *Journal ACM*, July 1967, pp. 439–465.

19. Liu, C.L., and Layland, J.W., "Scheduling Algorithms for Multiprogramming in a Hard Real-Time Environment," *Journal ACM*, January 1973, pp. 46–61.

20. McCulloch, W.A., and Pitts, W., "A Logical Calculus of the Ideas Immanent in Nervous Activity," *Bulletin of Mathematical Biophysics* 5 (1943), pp. 115–133; also Minsky, M., *Computation: Finite and Infinite Machines*, Chapter 3, Prentice Hall, Inc., New York, 1967.

21. Baer, J.L., "Models for the Design, Simulation, and Performance of Distributed-Function Architecture, *Computer* (March 1974), pp. 25–30.

22. Rose, C.W., "LOGOS and the Software Engineer," *AFIPS Conference Proceedings*, Fall Joint Computer Conference 1972, pp. 311–323.

23. Glaser, E.L., "Introduction and Overview of the LOGOS Project," *COMPCON 72 Digest*, pp. 175–178, 191–192.

24. Heath, F.G., and Rose, C.W., "The Case for Integrated Hardware/Software Design," *COMPCON 72 Digest*, pp. 179–182.

25. Bradshaw, F.T., "Some Structural Ideas for Computer Systems," *COMPCON 72 Digest*, pp. 183–186.

26. Rose, C.W., Bradshaw, F.T., and Katzke, S.W., "The LOGOS Representation System," *COMPCON 72 Digest*, pp. 187–190.

27. Patil, S., and Dennis, J.B., "The Description and Realization of Digital Systems," *COMPCON 72 Digest*, pp. 223–227.

28. Nutt, G.J., "Evaluation Nets for Computer Systems Performance Analysis," *AFIPS Conference Proceedings of the Fall Joint Computer Conference 1972*, pp. 279–286.

29. Noe, J.D., and Nutt, G.J., "Macro E-Nets for Representation of Parallel Systems," *IEEE Transactions on Computers*, August 1973, pp. 718–727.

30. Misunas, D., "Petri Nets and Speed Independent Design," *Comm. ACM*, August 1973, pp. 474–481.

31. Layland, J.W., "Software for Multicomputer Communications," in *The Deep Space Network Progress Report 42-26*, pp. 145–154.

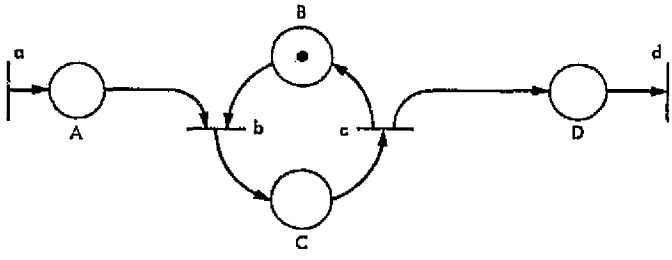

Fig. 1. Trivial transition net example

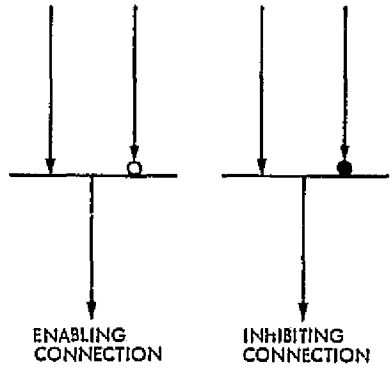

Fig. 2. Special transition—connections

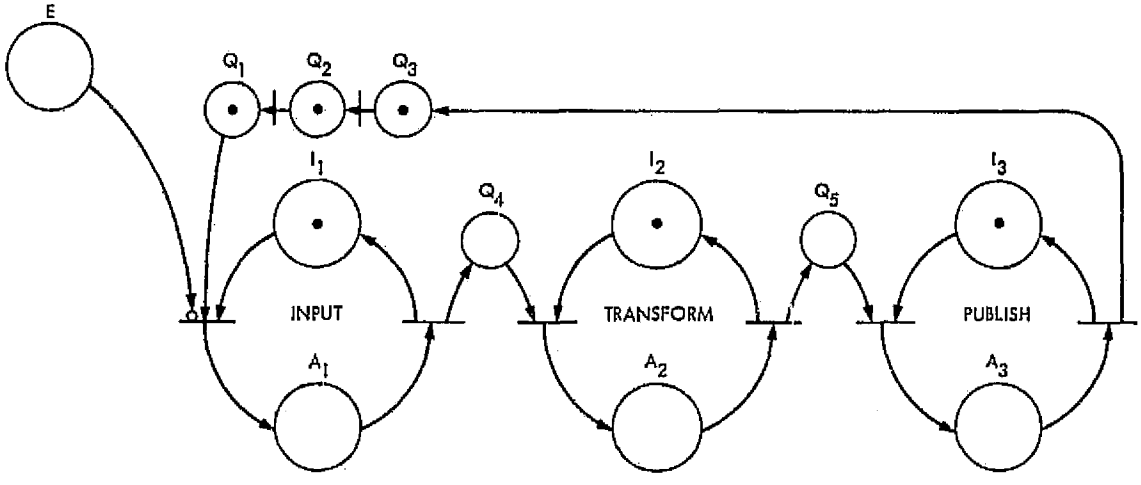

Fig. 3. Example system

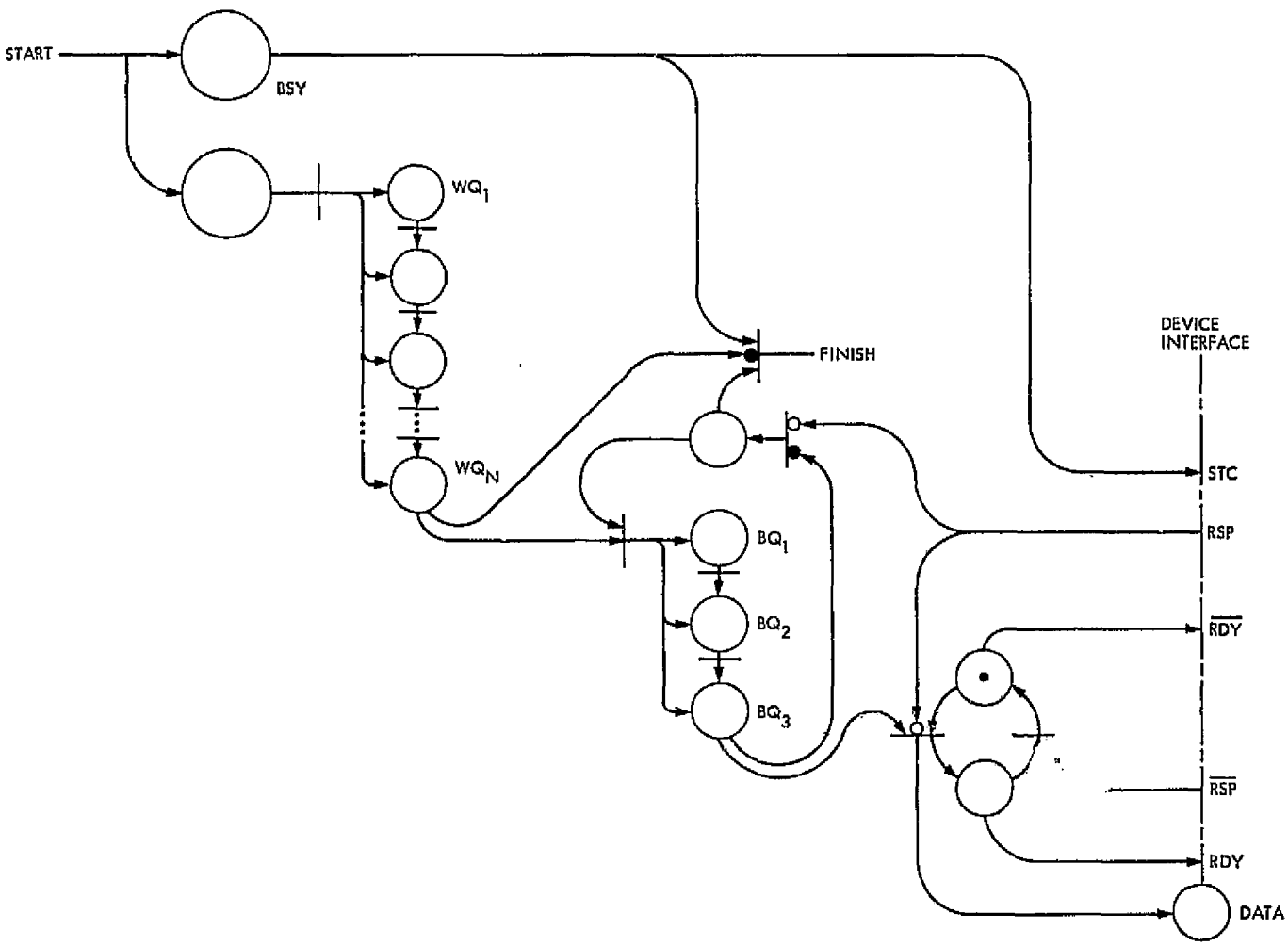

Fig. 4. Expanded net for active output process (A3)

X-Band Traveling Wave Maser Amplifier

D. L. Trowbridge
R. F. Systems Development Section

Laboratory tests on three X-band maser amplifiers have been completed. Gain, phase and group delay measurement data indicate that the maser stability performance will meet the design goals. A new method of remote gain adjustment has been achieved with the X-band maser amplifiers. The maser amplifiers have 45-dB gain over a minimum of 50-MHz 1-dB bandwidth and a noise temperature of 8 kelvins from 8400 to 8440 MHz.

I. Introduction

Three X-band traveling wave maser amplifiers (masers) have received final laboratory test and have been installed in the 64-meter antenna deep space stations of the Deep Space Network. Preliminary design parameters and testing of the maser and associated system were presented in earlier reports (Refs. 1 and 2). This report describes maser design refinements, performance, noise temperature, gain, phase, and group delay stability.

II. Maser Performance Improvements

The new X-band masers described here achieve a flat bandwidth (within 1 dB) of more than 50 MHz at 45-dB gain; this is more than 5 times the 1-dB bandwidth of previously reported tunable X-band masers (Ref. 3) at 45-dB net gain. The instantaneous bandwidth of a maser is determined by the maser material linewidth, the shape (or uniformity) of the magnetic field required for maser operation, and the electronic gain at which the maser operates. A thorough discussion of methods for increasing the bandwidth of a maser can be found in *Microwave Solid State Masers* by S. E. Siegman (Ref. 4). Siegman shows that operation of a maser using ruby (linewidth $\simeq$ 50 MHz) in a uniform magnetic field at high gain (more than 40 dB) results in a 3-dB bandwidth of less than 20 MHz. Attempts to increase bandwidth always result in substantial gain reductions. Considerable effort has been given to the task of optimizing the gain versus bandwidth trade-off. Bandwidth and gain value adjustment of previous masers (Ref. 5) was achieved by a combination of iron shim and field staggering coils. The previous methods are time consuming and require different shims or field staggering coil placement for each maser structure. A dual set of field spreading figure-eight coils was designed for gain and bandwidth adjustment; one full-sized set of coils covers the full length of the maser comb

structure (for bandwidth adjustment), and the second half-sized set of coils is used for gain level adjustment. The dual coils are shown in Fig. 1. The dual figure-eight coil arrangement provides remote and independent adjustment of bandwidth and gain to desired specifications. Figure 2 shows gain versus frequency at five gain/current control setting. The gain can be adjusted within reasonable limits (±3 dB at 45-dB gain) without changing the bandwidth. This results in minimal change in the phase and group delay characteristics of the maser as the maser gain is adjusted. This field staggering method improves the noise performance across the maser bandpass by minimizing slow-wave circuit losses prior to signal amplification. All signal frequencies are given some amplification as early as possible in the traveling wave maser structure (as shown in Fig. 2) by providing several repeated cycles of field stagger tuning along the maser's total length. The new X-band maser has a relatively flat equivalent noise temperature versus frequency performance as shown in Fig. 3. A previously used pump frequency modulator circuit (for S, X, and Ku-band uniform field masers, Ref. 6) was modified for use in the X-band maser with wide bandwidth and dual-frequency klystrons. The modulator (shown in Fig. 4) provides a 100-kHz sinewave with 26-V peak-to-peak output. The sinewave is applied to the reflector of both the 24- and 19-GHz pump klystron tubes through individual modulation level control potentiometers. Modulation of the pump frequency was previously used to improve maser gain stability in uniform field masers (Ref. 7). The new X-band field staggered maser requires pump frequency modulation to achieve the required gain over the extra wide bandwidth. The improvement in gain bandwidth with modulation of the pump frequency was previously reported (Ref. 1).

III. Maser Phase and Gain Measurements

Gain, signal phase, and group delay stability measurements were made using a Hewlett-Packard network analyzer. Figure 5 shows the gain and total signal phase shift versus frequency; the reference and test channel paths were balanced to produce the same delay and phase shift with the maser bypassed. A test signal was then swept through the maser to produce the recording of maser gain and phase shift versus frequency. The maser group delay (t_d) is calculated from the phase change versus frequency change at any point within the bandpass. Reference 8 defines transit time of signals through a device as group delay in the following manner:

$$t_d = \frac{|d\phi|}{360\,|df|} \simeq \frac{1}{360}\,\frac{|\Delta\phi|}{|\Delta f|} \qquad (1)$$

where

t_d = group delay or signal transit time in seconds

$\Delta\phi$ = incremental phase shift in degrees

Δf = incremental frequency change which produces $\Delta\phi$

The group delay time through the maser, with 45-dB net gain, varies from 50×10^{-9} s at 8422 MHz to 55×10^{-9} s at 8402 and 8442 MHz. To obtain these group delay measurements accurately, the reference path delay time was increased, with additional cable length, to equal the time delay in the test signal path at the center of the maser bandwidth. This condition enables expansion of the phase scale and improves phase shift resolution. It was used to produce the recording (Fig. 6) of gain and signal phase shift versus frequency. Data from Fig. 6 were used to plot the group delay time change versus frequency shown in Fig. 7. This represents the group delay time difference between the maser and a nondispersive network with $t_d = 50 \times 10^{-9}$ s.

IV. Stability Measurements

Changes in maser gain, group delay, and signal phase are caused by changes in magnetic field, refrigerator operating temperature, and pump frequency and power. Twelve-hour predicted parameter changes for the pump klystron power supplies, field shaping power supplies, and refrigeration temperature (variable parameters) were determined from known voltage output stability versus time and temperature and refrigerator temperature stability.

The maser change in phase shift and gain versus frequency was recorded for each of the known variable parameters. The group delay change introduced by each variable parameter versus frequency is plotted in Figs. 8 and 9 based on the recorded data. This represents the predicted ± group delay time instability versus frequency for each of the separate variable parameters over any 12-h period in an environment temperature of 25 ± 10°C. The measured maser phase and gain changes, at three frequency points across the maser gain bandwidth 8402, 8422, and 8442 MHz, are listed in Table 1 for each of the separate variable parameters. The various instabilities are expected to add in a random manner. The total rms gain, phase change, and group delay time instabilities versus frequency are listed in Table 1 and

shown in Fig. 10. The predicted total rms maximum changes for a 12-h period are as follows:

Gain	±0.5 dB
Group delay time change	$\pm 0.27 \times 10^{-9}$ s
Phase change	±5 deg

V. Conclusions

Laboratory test data show that the X-band maser system meets, and in most cases exceeds, the present design goals. The maser wide bandwidths and resulting additional pump frequency width requirements have resulted in the pump detuning factor being the major contributor to maser gain and group delay instability. The X-band maser requires a wider pump frequency range with flat power output characteristics in order to produce the wide-gain bandwidths with the desired stability. Future planned implementation of solid-state pump sources with appropriate modulation circuits should further improve the maser gain and phase stabilities. Effects of antenna movement on maser performance and solid-state pump investigation will be reported in future progress reports.

References

1. Trowbridge, D. L., "X-Band Traveling Wave Maser Amplifier," in *The Deep Space Network Progress Report*, Technical Report 32-1526, Vol. XVII, pp. 123–130, Jet Propulsion Laboratory, Pasadena, Calif. Oct. 15, 1973.
2. Buchanan, H. R., Hartop, R. W., Leflang, J. G., Loreman, J. R., and Trowbridge, D. L., "Operational X-Band Maser System," in *The Deep Space Network Progress Report 42-26*, pp. 175–182, Jet Propulsion Laboratory, Pasadena, Calif., Apr. 15, 1975.
3. Clauss, R., Wiebe, W., and Quinn, R., "Low Noise Receivers: Microwave Development," in *The Deep Space Network Progress Report*, Technical Report 32-1526, Vol. XI, pp. 71–80, Jet Propulsion Laboratory, Pasadena, Calif., Oct. 15, 1972.
4. Siegman, A. E., *Microwave Solid State Masers*, pp. 326–331, 395, McGraw-Hill Book Co., Inc., New York, 1964.
5. Trowbridge, D. L., "Block III Maser Implementation Program," in *The Deep Space Network Progress Report*, Technical Report 32-1526, Vol. XVIII, pp. 130–135, Jet Propulsion Laboratory, Pasadena, Calif., Dec. 15, 1973.
6. Clauss, R. C., and Quinn, R. B., "Low Noise Receivers: Microwave Maser Development," in *The Deep Space Network Progress Report*, Technical Report 32-1526, Vol. IX, pp. 128–136, Jet Propulsion Laboratory, Pasadena, Calif., June 15, 1972.
7. Clauss, R. C., Reilly, H. F., Jr., and Reid, M. S., "Low Noise Receivers: Microwave Maser Development," in *The Deep Space Network*, Space Programs Summary 37-62, Vol. II, pp. 74–78, Jet Propulsion Laboratory, Pasadena, Calif., Mar. 31, 1970.
8. "Network Analysis with the H.P. 8470A 0.1–110 MHz," Hewlett-Packard Application Note 121-1, Hewlett-Packard Co., Palo Alto, Calif., Feb. 1970.

Table 1. Predicted maser gain and phase stability for 12-h period and environment temperature of 25 ± 10°C (based on measured data)

Variable parameter	Parameter change	Gain change, dB			Signal phase change, deg		
		8402 MHz	8422 MHz	8442 MHz	8402 MHz	8422 MHz	8442 MHz
Beam V 24 GHz	±1 V	±0.01	±0.02	±0.07	±0.4	±0.6	+0.8 −0.6
Beam V 19 GHz	±1 V	+0.01 −0.08	+0 −0.55	+0.1 −0.2	+0.3 −0.7	+0.3 −1.0	+0.3 −1.2
Reflector V 24 GHz	±1 V	±0	±0.1	±0.3	+3.1 −2	+3.7 −2.5	+4.4 −2.9
Reflector V 19 GHz	±1 V	+0.05 −0.15	+0 −0.25	+0.03 −0.04	+1.3 −2.5	+0.9 −3.2	+1.2 −3.6
Bandwidth control supply current	±0.2 mA	∓0.02	∓0.06	−0.04 +0.03	±0.4	±0.2	+0.3 −0.4
Gain control supply current	±0.2 mA	−0.04 +0.02	−0.02 +0.01	−0.02 +0.01	+0.04 −0.08	±0	±0
Refrigerator temperature	±0.005 K	∓0.05	−0.06 +0.05	−0.05 +0.04	∓0.1	−0.06 +0.08	−0.06 +0.05
Total rms	As above	+0.07 −0.19	+0.12 −0.64	+0.33 −0.62	+3.4 −3.3	+3.9 −4.7	+4.7 −4.8

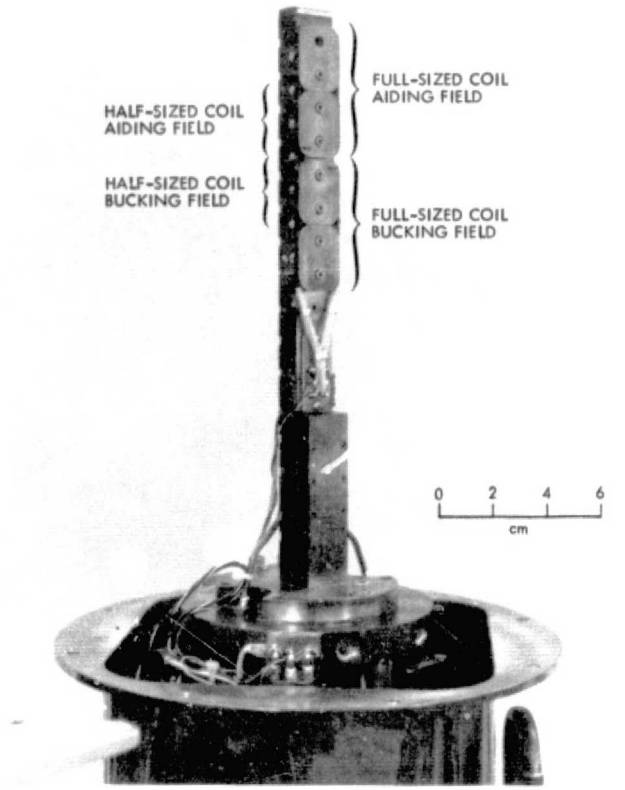

Fig. 1. Maser amplifier with field-shaping coils mounted on refrigerator

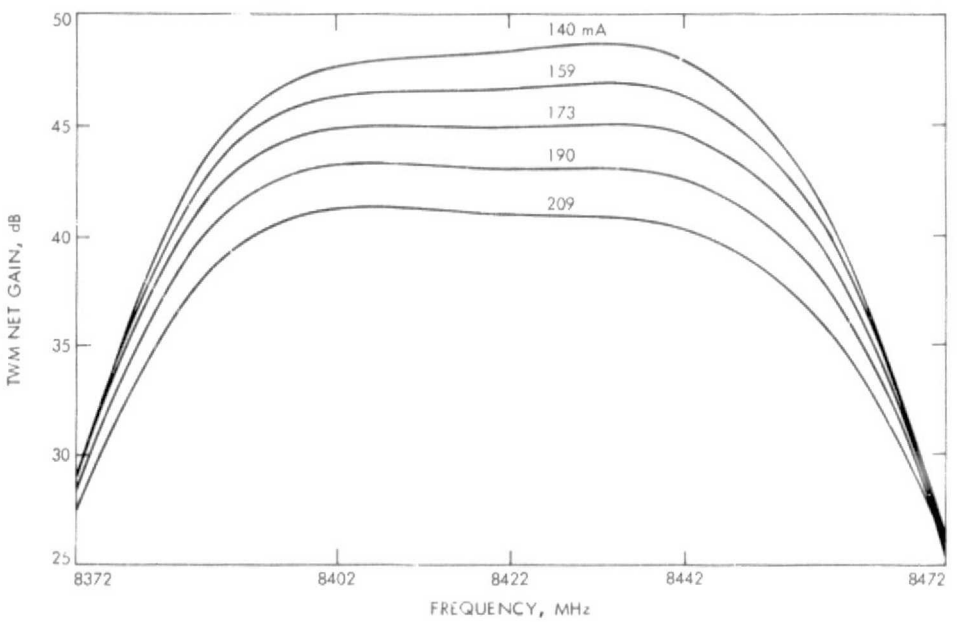

Fig. 2. Gain vs frequency at five gain control field-shaping coil current settings

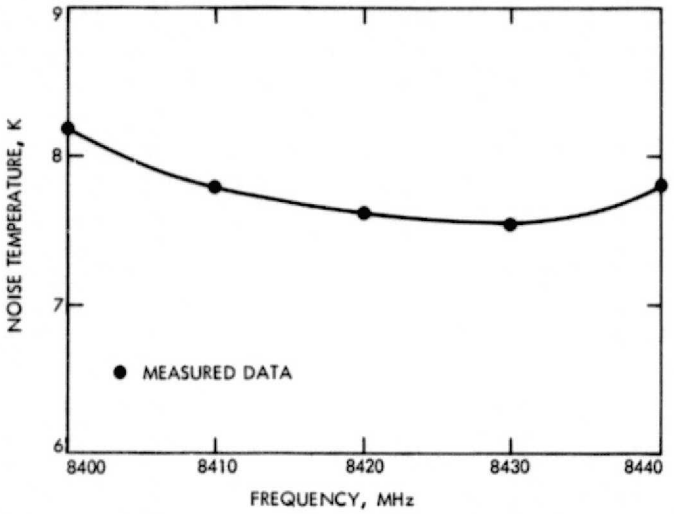

Fig. 3. Equivalent maser noise temperature vs frequency

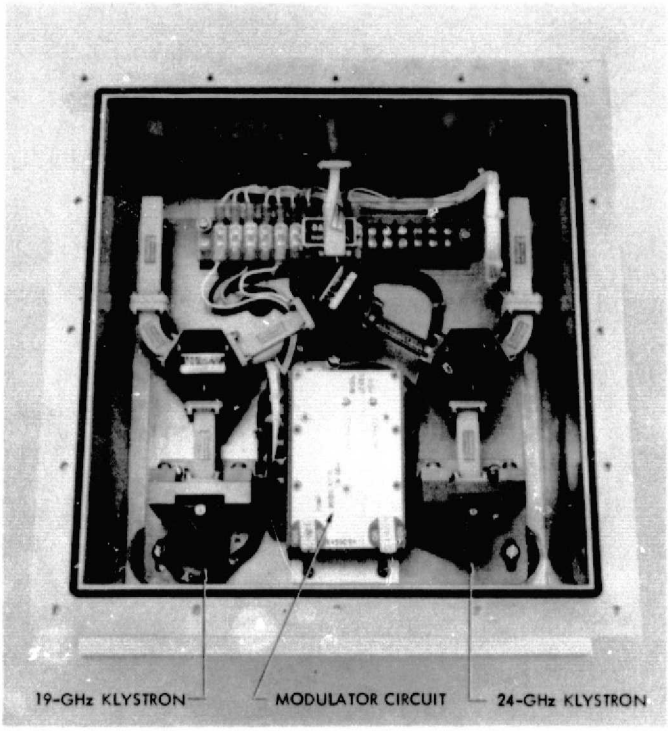

Fig. 4. Pump klystron assembly with modulator

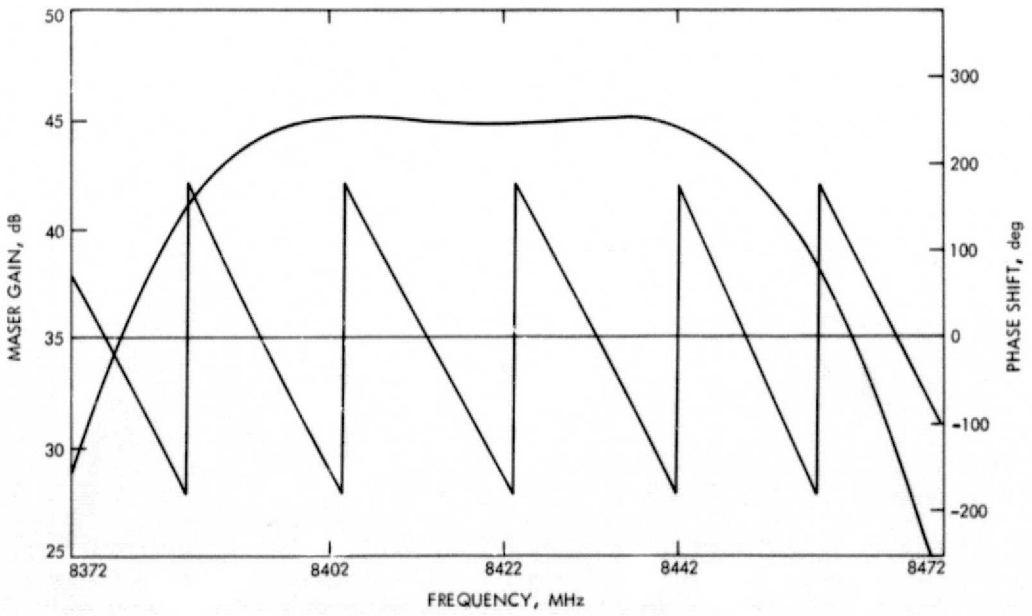

Fig. 5. Maser gain and total phase shift vs frequency

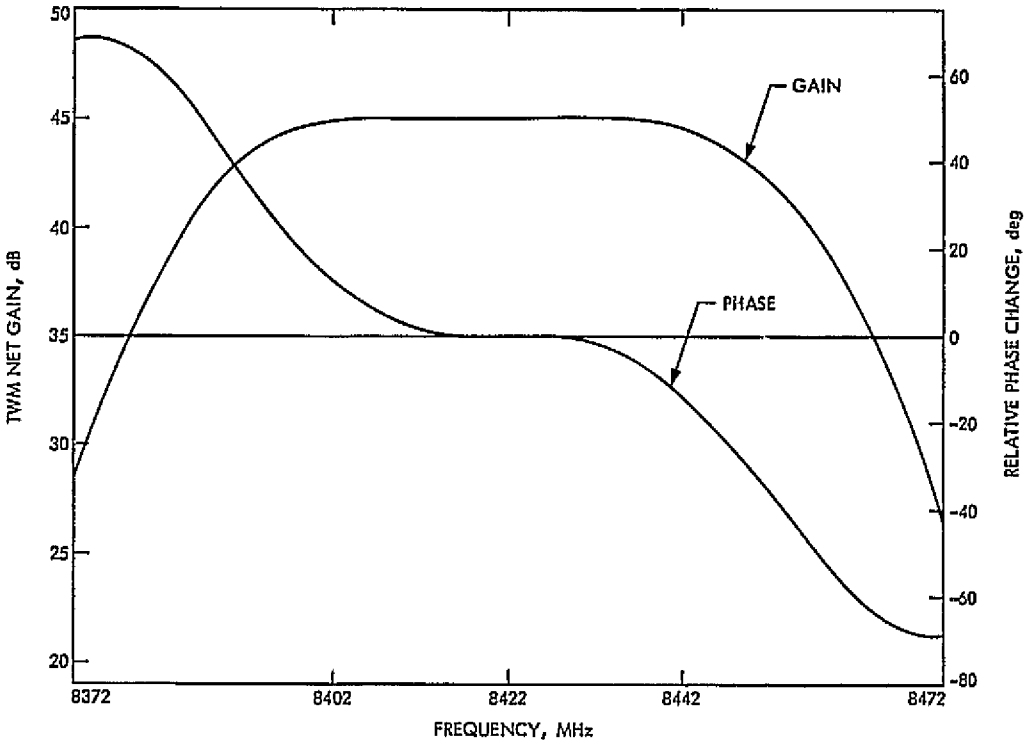

Fig. 6. Maser gain and relative phase change vs frequency

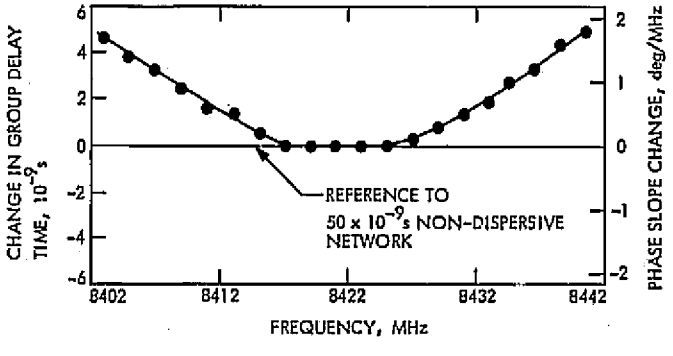

Fig. 7. Maser group delay characteristic vs frequency

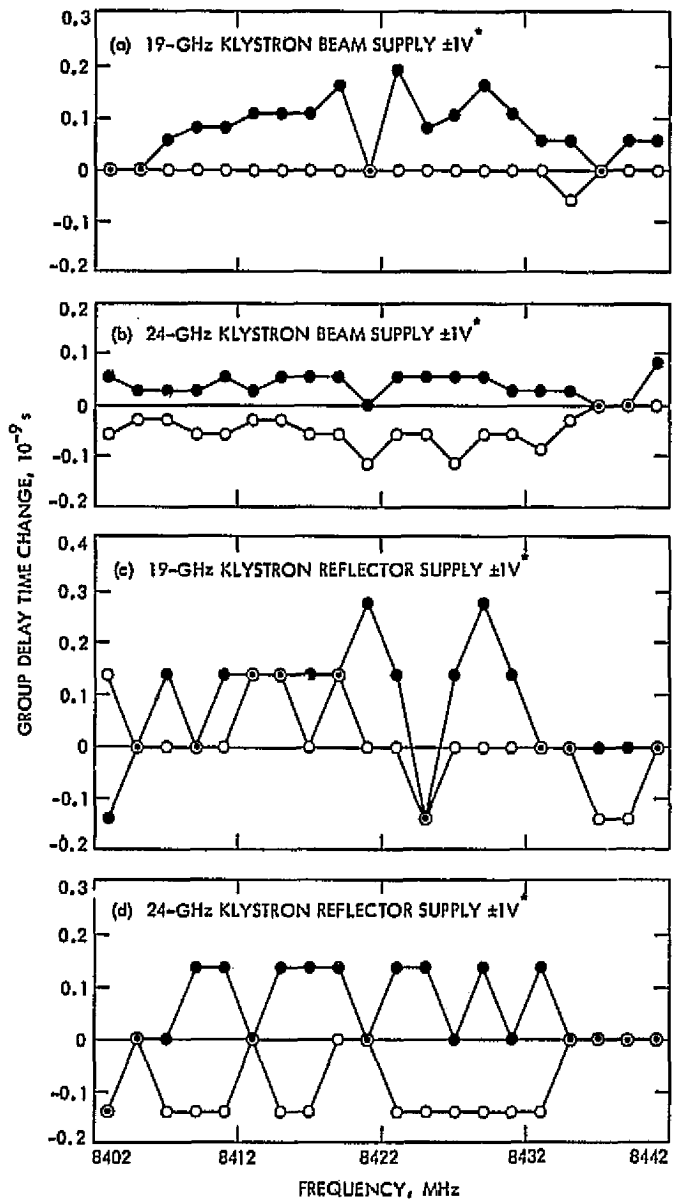

Fig. 8. Pump system effects on maser group delay stability

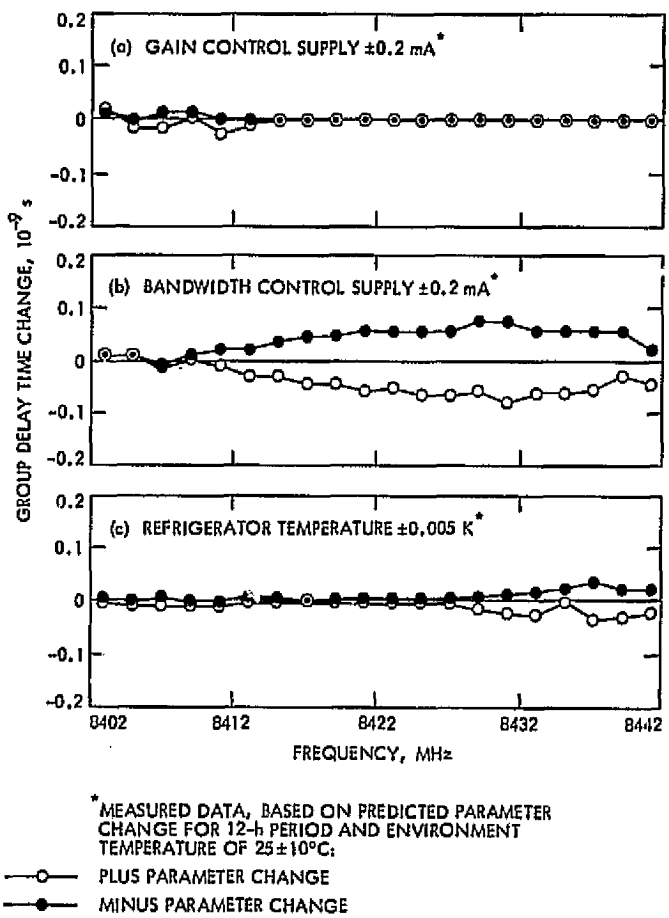

Fig. 9. Refrigerator temperature, gain, and bandwidth control supplies effect on maser group delay stability

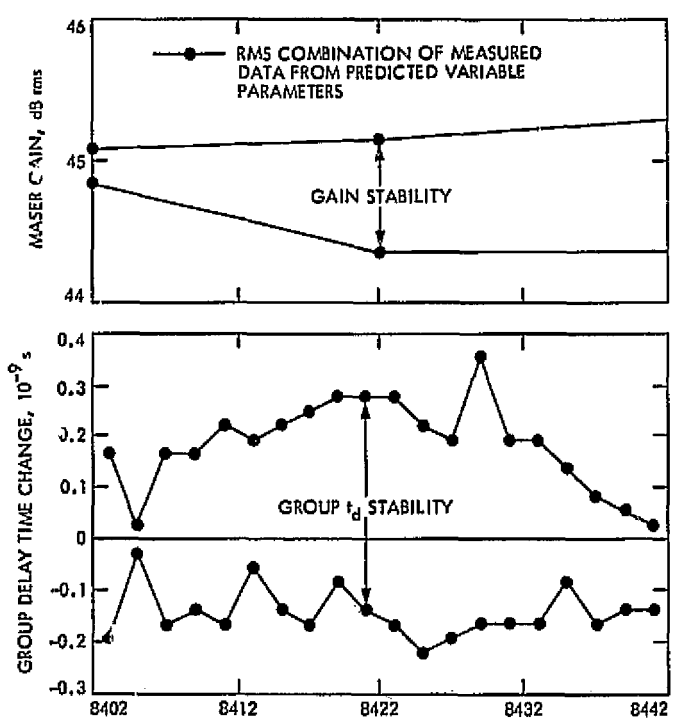

Fig. 10. Predicted maser system group delay and gain stability for 12-h period and environment temperature of 25 ± 10°C

Data Decoder Assembly Reliability and Status of Test Equipment

R. A. Mancini
DSN Data Systems Development Section

The reliability of the Data Decoder Assembly (DDA), although improved by a series of engineering change orders, continues to exhibit a failure rate higher than desired. During the past year, the major source of intermittent problems has shifted to the interface assembly which includes the couplers that provide the interfacing between the Interdata 4 and other station equipment. A mechanical stabilizer design was implemented in the DSN to inhibit physical movement in the interface assembly. Interdata power supply problems had been involved in an increasing number of failures reported on DDAs. Several modifications have been and will be implemented to correct these problems. The lack of test software has complicated troubleshooting because either operational software had to be used or individual test software programs had to be developed at the stations. To rectify the dearth of test software available, the original test software was revised and updated to help station personnel troubleshoot an assembly in its operational configuration. Several corrective actions are in the process of being developed to prevent loosening of integrated circuits and platforms on couplers, to modify and/or replace computer power supplies, and to improve noise immunity in some coupler circuits. The DDA "halt" problem has been irritating to operations. Although a low level of investigation has been going on for over a year, insufficient information has been provided to identify this "halt" problem. The plan for improving the reliability for Viking support includes the addition of personnel to devote full time to the DDA problems, closer interfacing between operations and engineering to identify and define problem areas, and development of a tester to allow off-line testing of DDAs to isolate hard faults to replaceable modules in the minimum time possible consistent with required Viking support.

I. Introduction

The Data Decoder Assembly (DDA) is part of the Telemetry and Command Subsystem of the Deep Space Station (DSS). In operation, the assembly is capable of performing three mutually exclusive functions: sequential decoding of convolutionally encoded data, block decoding of 32/6 or 16/5 biorthogonal block coded data, or high-rate data formatting of encoded or uncoded data for transmission on the wideband data line with simultaneous recording of the data on magnetic tape.

An Interdata Model 4 (ID4) minicomputer is one of nine assemblies mounted in a standard 205.74-cm (81-in.) equipment cabinet which makes up the DDA.

II. Background

Reference 1 gives a description and history of the reliability problems experienced in the assembly up to that time, the corrective actions that were taken and those which were in process, and additional problem areas which were being investigated.

III. Corrective Action Implemented

Since the last report (Ref. 1), a number of engineering change orders have been implemented in the DSN to correct identifiable problems as described below.

A. Data Decoder Assembly Interface Assembly Stabilizer

A stabilizing framework was designed to stiffen the backplane of the Interface Panel Assembly and to support and stabilize the couplers mounted on that assembly. The Interface Panel Assembly contains the interface backplane, which provides power and ground planes for the couplers, and connector wire wrap terminals for the electrical interconnection of the couplers and the intrarack cabling; the mounting for and the couplers to interface the Interdata Model 4 with the Telemetry and Command Processor, the Symbol Synchronizer Assembly, the Block Decoder Assembly, the Frequency and Timing Subsystem, and the Simulation Conversion Assembly; and the connectors for mating with the couplers and the intrarack wiring. The mechanical design of the Interface Panel Assembly was such that the backplane flexed when the coupler was removed or inserted. In addition, the coupler's connectors could not mate reliably with those connectors mounted on the backplane because of flexing of the backplane. The hold-down hardware for the couplers (guide bars and guide pins) was not capable of solidly holding the couplers so that the mating connectors were immobile. This was due to the flexing of the large backplane and the weight of the couplers on the cantilevered hold-down hardware. Correction was effected by designing a stabilizing bar to clamp the backplane to the Interface Panel Assembly side walls and anchoring the plane to the bar with hardware used to assemble the coupler guide bars, and designing a framework to support the couplers at their upper and lower extremities and clamping these points to the Interface Panel Assembly through the framework. With this bar and framework, the Interface Panel Assembly backplane is rigid and the couplers are immobile. Implementation of this interface assembly stabilizer is in process in the network.

B. Computer Power Supply Fuse Relocation

After the Data Decoder Assembly was operating in the network, it was noticed that in some cases the 30-A fuse in the 5-V portion of the power supply blew periodically. This fuse was located on the heat sinks also mounting the series regulator transistors for the 5-V supply. Upon investigation, it was apparent that the heat generated by these regulator transistors was sufficient to cause the solder to melt in the fuse and cause deterioration of the fuse resulting in failure. Electrically, the fuse is designed to protect the raw dc power supplied to the 5-V regulator circuitry.

The solution was to relocate the three fuses mounted internal to the power supply (including the 5-V 30-A fuse). The new location is external to the power supply envelope well away from any heat source and readily accessible should replacement become necessary. In the original design, replacement of this fuse was inconvenient because of its location internal to the supply on the heat sink with no available access hole. Modification kits have been distributed to the DSN and the installation of the relocating hardware is in process.

C. ID4 Power Supply Over-Stressed Component

For the second buy of 15 Interdata computers, the manufacturer changed power supply vendors. Acme power supplies were provided with the nine latest DDAs and the six new Planetary Ranging Assemblies (PRAs) for the Viking update. After part of a regulator circuit of one of these power supplies was damaged by fire, investigation showed that the four series resistors (part of the 5-V regulator circuit) were being continuously over-stressed in all but the PRA application. These 5-W resistors were being subjected to approximately 6.5 W each in the DDA Configuration II at the 64-m stations. Higher wattage replacement resistors for all of the Acme supplies have now been installed in the equipment.

D. High Error Rate Under Strong Signal Conditions

It was found that cross-coupling of signal information from the clock line to the data inputs into the Symbol Synchronizer Assembly (SSA)/DDA Coupler for both the inputs from the SSA and Block Decoder Assembly (BDA) was causing unrealisticly high error rates in many DDAs. To correct this problem, small capacitors were connected across the difference amplifier inputs to the data line receivers and the clock signal receivers in the SSA/DDA Coupler. The capacitor on each mentioned input was sufficient to preclude the previously noted marginal operating condition. Filtering was necessary to slow down the speed response of the receiving amplifiers and eliminate spurious signals cross-coupled in the cables. This problem has been corrected.

E. DDA Test Software

A test software package was developed and delivered with the initial implementation of the DDA in the DSN, but this software was not updated with each engineering change implemented in the assembly. Because of the need for more effective testing of the assembly in the operational configuration, the test software was updated and distributed throughout the network.

IV. Corrective Actions in Process

A. Questionable Retention of a Few Integrated-Circuit Sockets

A number of complaints have been received concerning integrated circuits becoming loose in their sockets or falling out of their sockets. On close inspection, it was found that a few of the older coupler boards contain some white sockets with a lighter-than-standard-gauge bronze material in the individual pin receptacles. It was also noted that, because of the positioning of the receptacles in relationship to the socket, some integrated circuits cannot be pushed into the socket until the package bottoms on the plastic body of the receptacle. This condition is caused by the shoulder of the integrated-circuit pins spreading the receptacle clip before the package body bottoms, and when the clip spreading is limited by the walls of the socket, it prevents a stable bottomed insertion of the integrated circuit. This characteristic of itself does not appear to cause electrical problems nor a permanent offset in the bronze receptacle clip. Further study indicated inserting a probe, as might be done in conjunction with scope troubleshooting, does cause permanent spreading in these and the standard bronze clips. After having been given a permanent offset, the clips can be bent back individually to give their original aperture and tension characteristics.

A coupler with the suspect type receptacles was filled with typical integrated circuits and platforms and taken for a shake test in the Environmental Testing Laboratory. The coupler was given a shake test along several axes, including the direction of insertion and removal. A detailed report is not yet available, but the coupler was given a shake of several g's over a frequency range including that expected at a DSN station. No integrated circuit or platform came out of its socket, and none was loosened during these tests.

A pull test was performed on integrated circuits inserted in all types of receptacles used in DDA coupler boards. The retention strength of the questionable white receptacles (on Interdyne boards) was measured to be from 4.45 to 8.90 N (1 to 2 lb) of pull to remove integrated circuit, while those in the standard Interdyne-manufactured board and Viking-manufactured boards required from 8.90 to 22.24 N (2 to 5 lb) of pull for removal (Viking 8.90 to 17.79 N (2 to 4 lb); Interdyne 13.34 to 22.24 N (3 to 5 lb)).

Based on the investigation so far, t would appear that the loosening of integrated circuits . , not due to vibration but probably or more likely due to handling, especially while removing or installing a coupler. It is easy to hit the coupler against other couplers or cables while installing or removing it. Therefore, at least a protective plate should he mounted on each coupler to prevent accidental knocking against integrated circuits or platforms causing loosening of one of these components. In the event some hold-down mechanism is needed to insure the seating of integrated circuits, etc., one method of holding down these chips and platforms is being tested. This design can possibly cause heating for the itegrated circuit, and so some testing in both CTA 21 equipment and the prototype DDA is in progress to study the heat rise involved to determine if it would be a problem. An engineering change will be implemented to at least provide a protective plate for the integrated circuits and platforms.

B. Additional Computer Power Supply Problems

The power supply originally provided with the Interdata Model 4 computer was manufactured by North Electric. During the original phase for support of Pioneers 10 and 11, the power supplies appeared adequate even though the specification sheet indicated a lower than required capacity (Interdata wrote a letter assuring JPL that the power supply was more than adequate for the

application). With the installation of new selector channels throughout the network, and new memories in the 64-m subnet, the logic voltage drain was increased. This condition was intensified in the new Interdata 4 computers for Data Decoder Assemblies because of additional new configuration of some of the motherboards. Problems began occurring in the network, especially with the new ID4's since, in addition to the above-mentioned changes, the computers were delivered with a power supply designed and built by a different manufacturer (Acme). These supplies were designed to supply only 20 A although Interdata performed some modifications ostensibly to increase the power output capability. Investigating the problem in depth showed this new supply marginally adequate for the DDA application and just adequate for the Planetary Ranging Assembly application. Therefore, Interdata is in the process of replacing all of the Acme power supplies with North Electric Supplies. Additionally, they are supplying to JPL modification kits to increase the power capability of the currently used North Electric Supplies (also including this modification in the replacement supplies mentioned above). Along with the equipment that will soon be delivered, Interdata is updating the power supply specification sheet to describe the new power supply capability. The ID4 power supply problem will be solved with installation of the modification kits and replacement supplies during the summer of 1975.

C. Modifications to Improve Noise Immunity in Two Couplers

The input noise immunity in the Interrupt coupler is being improved by substituting the currently used receiver network with that used in the Telemetry and Command Processor (TCP) emulator and also adding a small capacitor across the input to the receiver amplifier to further reduce noise susceptibility. This change is in the modification kit building phase.

Input noise immunity is being improved in the TCP/DDA coupler by adding capacitors to the receiver amplifiers on the command signal lines from the TCP. This change is being implemented in the DSN to make the transfer between TCP and DDA more reliable.

V. Undefined Problems

For some time and for reasons yet unknown, the DDA will stop processing data while tracking a spacecraft. These occurrences are fairly infrequent, with a period of no shorter than once in several days. The problem has been called the DDA "halt" problem although the DDA does not halt but merely stops processing data with the program jumping to a wrong area in core and trying to execute data. A low-level investigation as to what causes the program to get out of step has been in progress for over a year with no real insight as to the origin of this problem. To this end, core dumps have been requested from the station after the computer enters this "halt" condition. A procedure has been given to the stations as to how to perform this dump to avoid loss of the desired information. Analysis of the received core dumps from the network has not provided any suggestion of the source of the problem. A DDA Halt Study was conducted by Dunn (Ref. 2) in 1974. The results of analyses of the core dumps have been described in several memos written to this author.

VI. Plan for Improving DDA Reliability

A. Reliability Survey

Based on an agreement between DSN Operations and DSN Engineering, additional manpower has been acquired for the study and improvement of the reliability of the DDA hardware and software. A survey of the DSN was made in January 1975 to determine the current problems and to receive recommendations for ways of improving DDA reliability. A summary of this survey was completed and published in April. Many of the problems defined will be solved by implementation of engineering change orders already in process.

B. DDA Tester

A tester is being designed for implementation into the network. The design concepts for this tester are to disconnect the DDA from other station equipment for stand-alone testing; to isolate faults to a replaceable module (i.e., Motherboard in the ID4 or coupler in DDA Interface Assembly); to provide simple procedures allowing station operating personnel to perform the tests; and to provide a tester easily understood and usable to complete fault isolation, leading to fault correction in minimum time consistent with Viking requirements.

A study of the unit tester designed and built by Motorola is in process. That tester was used as a debugging and acceptance test unit during the building of the DDAs. The unit is being used as the basis for the design of the current tester.

To better understand the Data Decoder Assembly, the Tester Hardware Design Engineer has drawn a complete set of block diagrams of the DDA which were not provided in the original publication of the DDA Operation and Maintenance Manual. The top sheet of the block

diagrams is an overall diagram with reference to ID4 documentation in Technical Memoranda and to JPL drawings of logic diagrams to better tie together the various areas of DDA documentation.

In order to preclude the need for disconnecting subsystem and system cables to connect the tester, a design has been undertaken to incorporate a multiplex switch in the DDA to require one cable connection from the tester and allow switching of the DDA applicable interfaces from the operational configuration to the test configuration. As it is being designed, this 2 to 1 multiplex switch would be capable of being installed in all assemblies by electrically inserting this multiplexer between the intrarack cable connectors and the interface connector panel bulkhead connector and make available the tester connection at the front of the assembly.

The design has been completed for the special test equipment which will be used in the tester to simulate other station equipment that interfaces normally with the Data Decoder Assembly and also to connect with the ID4 in the assembly to provide wrap-around paths for testing of the complete assembly. The prototype special test equipment is in the process of being built and should be checked out by mid-September. The design was done in such a way as to be compatible with the existing unit test programs written by Motorola. This course was taken so that those programs can be used as the basis of the new test software needed to accomplish the design concepts.

A Functional Requirements Document for the tester is in the process of being generated.

The present schedule will provide a tester for each of the nine stations by early 1976.

References

1. Mancini, R. A., "Data Decoder Assembly Reliability Modifications," in *The Deep Space Network Progress Report 42-21*, pp. 92–94, Jet Propulsion Laboratory, Pasadena, Calif., June 15, 1974.
2. Dunn, G. L., *DDA Halt Study—Report for Period August 1 through November 18, 1974*, IOM 421E-74-354, Nov. 25, 1974 (JPL internal document).

Tracking Operations During the Helios 1 Launch Phase

A. L. Berman and L. E. Bright
Network Operations Office

Tracking operations during the Helios 1 launch phase proceeded quite smoothly and contributed to a very successful launch. Key features considered in the Helios 1 pre-launch planning were the possible "silent spacecraft" mode and the spacecraft low-gain antenna "interference zone," although in the actual launch the former did not occur and the impact of the latter was negligible. This report details the pre-launch planning and post-launch analysis of tracking operations during the Helios 1 launch phase.

I. Introduction

The Helios 1 spacecraft was launched from Cape Canaveral on December 10, 1974, at 07:11:01.537 Greenwich Mean Time (GMT), at a Launch Azimuth of 98.9 deg. The purpose of the Helios 1 mission, a joint undertaking of the Federal Republic of West Germany and the United States of America, is to study the properties of the Sun from a close range. To accomplish this goal, the Helios 1 spacecraft was lofted into an elliptical heliocentric orbit by a combination Titan III-D, Centaur, TE-364-4 launch vehicle in the parking orbit ascent mode. Heliocentric orbit injection occurred over the southern tip of Africa, and the resulting near-Earth trajectory was such that within the Deep Space Network (DSN), the Australian complex was first to view the spacecraft post-injection. The Deep Space Station (DSS) selected to perform the initial acquisition was Weemala (DSS 42), with Honeysuckle Creek (DSS 44) as a backup. Two features of the Helios 1 spacecraft sharply distinguished the preparations for and the execution of this initial acquisition from previous but otherwise similar initial acquisitions at DSS 42—the possible "Silent spacecraft" or "radio frequency safe" mode and the spacecraft low-gain antenna orientation "interference zone." These are briefly described below.

A. Helios 1 "Silent Spacecraft" Mode

If the Helios 1 spacecraft experiences a power drop, the spacecraft transmitter is automatically turned off. To reactivate the transmitter, it is necessary to acquire the

uplink (in the "blind") and subsequently command the transmitter back on. Obviously, this adds a whole new dimension of uncertainty to the initial acquisition process, viz:

> If a signal is not detected, is it because the ground antenna is correctly pointed but the spacecraft is in the silent mode, or is the ground antenna not properly pointed at the spacecraft in the normal transmitting mode? The same question exists in regard to the proper ground receiver settings, etc.

B. Helios 1 Low-Gain Antenna "Interference Zone"

During the time period shortly after DSS 42 rise, the spacecraft low-gain antenna orientation would be such as to produce very deep nulls, with the resultant effect that for an approximate 4-min period the spacecraft/ground communications might become either marginal or totally impossible. Obviously, this event would inject a great deal of uncertainty and disruption into the more normal, orderly progression of events at a DSS during an initial acquisition, typically: acquire one-way downlink, antenna to auto-track, antenna to aided track, transmitter on, sweep to acquire uplink, reacquire two-way downlink, antenna return to auto-track, etc.

In the following sections, the pre-launch tracking operations planning, which was heavily impacted by the two Helios-peculiar features described above, and the subsequent analysis of the launch tracking operations at DSS 42, will be detailed.

II. Helios 1 Trajectory Considerations

The nominal open window Helios 1 launch trajectory for December 10 resulted in only moderate angular and frequency rates, which were very typical of previous mission parking orbit ascent-type launch trajectories over Australian stations. Maximum angular and frequency rates were as follows:

$$\frac{d}{dt}\{D2\} \approx 320 \text{ Hz/s (S-band level)}$$

$$\frac{d}{dt}\{XA\} \approx 1.5 \text{ Hz/s (voltage-controlled oscillator (VCO) level)}$$

$$\frac{d}{dt}\{HA\} \approx 0.1 \text{ deg/s}$$

where

$D2$ = two-way doppler frequency

XA = spacecraft receiver best lock, with doppler accounted for

HA = local (station) hour angle

Figure 1 stereographically illustrates the Helios 1 launch pass over DSS 42, while Fig. 2 details the elevation angle versus time and Fig. 3 the XA frequency versus time. The duration of the pass was approximately 5 h and 50 min, with the retrograde point, defined by:

$$\frac{d}{dt}\{HA\} = 0$$

occurring at 08:45:00 GMT.

A necessary facet of information to the determination of the initial acquisition strategy for the Helios 1 launch was the expected uncertainties in tracking observables as translated from the expected uncertainties in the launch vehicle performance. M. Traxler (at the Air Force Eastern Test Range (AFETR)) indicated that 3σ trajectory dispersions for the Helios 1 launch could be approximated by perturbing the nominal trajectory injection conditions with the following quantities:

$$\Delta X_i = 30 \text{ km}, \qquad i = 1, 3$$

$$\Delta\left\{\frac{dX_i}{dt}\right\} = 0.1 \text{ km/s}, \qquad i = 1, 3$$

Tracking prediction observables could then be generated on the nominal and the perturbed trajectories, and the resultant approximate 3σ tracking observable uncertainties obtained by differencing the two. This procedure was performed on three different launch trajectories, and the maximum approximate 3σ uncertainties in tracking observables were determined to be:

$$\Delta HA \approx 1.15 \text{ deg}$$

$$\Delta dec \approx 0.80 \text{ deg}$$

$$\Delta uplink\,(XA) \approx 17 \text{ Hz (at VCO level)}$$

Additionally, the following approximate 3σ frequency uncertainties for the Helios 1 spacecraft receiver were assumed:

$$\Delta uplink \text{ (best lock)} \approx 12 \text{ Hz (at VCO level)}$$

$$\Delta uplink \text{ (temperature)} = \Delta T\left\{\frac{\partial}{\partial T}[uplink]\right\} \approx 10 \text{ Hz (at VCO level)}$$

Combining the trajectory, best lock, and temperature effects, above, one obtains a total approximate 3σ uncertainty in the uplink frequency of:

$$\Delta uplink \approx 23 \text{ Hz (at VCO level)}$$

These angle and frequency 3σ uncertainties were relatively small, and tended to counterbalance the difficulties posed by the possible silent spacecraft mode and the antenna interference zone in formulating the Helios 1 initial acquisition plan. In the following two sections, the angle drive strategy and frequency acquisition strategy are described.

III. Angle Drive Strategy at DSS 42

In a more typical and less complicated launch phase, the overriding emphasis insofar as the angle drive mode is concerned is to achieve auto-track as soon as possible, as the near-Earth phase is the only phase wherein angular tracking data are a powerful radio metric data type for high-precision orbital determination processing. However, the Helios 1 launch case was strongly impacted by both the silent spacecraft mode and the antenna interference zone for the following reasons:

(1) In the silent spacecraft mode, one would have to drive the antenna to the spacecraft in the blind for a long enough period to acquire, establish uplink, and subsequently command the spacecraft on.

(2) If one were able to achieve auto-track fairly soon after spacecraft rise, there would exist a strong possibility of losing it (auto-track) shortly thereafter, because of low-signal strength and signal-to-noise ratio (SNR) during the interference zone. Additionally, in the process of losing auto-track and driving the ground antenna off the spacecraft, one might easily lose downlink lock.

Therefore, the basic angle drive strategy would be to (computer) drive the ground antenna with the best predicts available until at least after the nominal end of the defined interference zone. Fortunately, because the angular 3σ uncertainties (discussed in Section II) were so small, no angular "search" schemes were deemed necessary to achieve a very high probability of a successful early acquisition. The hierarchy of decision for the angle drive mode, which was most heavily dependent on the availability of differing sets of tracking predictions, was as follows:

(1) **Phase I—Local horizon to the end of the interference zone** (prior to rise, the antenna to be positioned at the rise point)

(a) *Applicable condition:* Launch occurs within several seconds of the daily open window launch time.

Antenna drive mode: A preflight nominal Antenna Pointing Subsystem (APS) drive tape in GMT.

(b) *Applicable condition:* Launch does not occur at the open window launch time, but a verified APS drive tape generated from the actual launch time is available at DSS 42 prior to rise.

Antenna drive mode: Actual launch time APS drive tape in GMT.

(c) *Applicable condition:* Launch does not occur at the open window launch time, and a verified drive tape based on the actual time is not available at DSS 42 before rise, but actual launch time page print predictions are available.

Antenna drive mode: Preflight nominal APS drive tape in time from launch (TFL) in conjunction with a manually entered Δt offset equal to the actual launch time in GMT. Angle offsets to be manually entered to correct antenna position to actual launch time page print predictions.

(d) *Applicable condition:* Launch does not occur at the open window launch time and no actual launch time based predictions are available at DSS 42 prior to rise.

Antenna drive mode: Preflight nominal APS drive tape in TFL with a manually entered Δt offset equal to the actual launch time in GMT. Angle offsets to be provided to DSS 42 by the Tracking Network Operations Analyst, via voice.

(2) **Phase II—End of interference zone to verified uplink acquisition**

(a) *Applicable condition:* The spacecraft known to be in the silent mode (as determined by AFETR and transmitted to the Mission Control and Computing Facility (MCCF)).

Antenna drive mode: Continue as in Phase I.

(b) *Applicable condition:* The spacecraft not known to be in the silent mode but downlink has not been acquired by DSS 42.

Antenna drive mode: Continue as in Phase I.

(c) *Applicable Condition:* DSS 42 has obtained good downlink lock.

Antenna drive mode: Proceed as follows:

(i) Antenna to auto-track on the Acquisition Aid Antenna, (S-Band Acquisition Antenna (SAA), Receiver 2).

(ii) Acquire and confirm receiver lock on the main antenna (S-Band Cassegrain Monopulse (SCM) feed cone, Receiver 1).

(iii) Antenna to auto-track on SCM.

(3) **Phase III—Post verified uplink acquisition**

(a) *Applicable condition:* The downlink was previously not acquired.

Antenna drive mode: Proceed as in 2.c.

(b) *Applicable condition:* The downlink had previously been acquired and auto-track established.

Antenna drive mode: Proceed as is.

IV. Uplink Acquisition Strategy at DSS 42

The only (and minor at that) impact of the possible silent spacecraft mode and the antenna interference zone on the uplink acquisition strategy was the necessity of waiting until the end of the interference zone before attempting the uplink acquisition. Otherwise, the uplink acquisition was expected to be quite routine, particularly when considering the small 3σ uncertainties presented in Section II. The basic characteristics of the uplink acquisition strategy are as follows:

(1) The uplink acquisition to consist of a single uplink frequency sweep in the direction of *XA* change, advantageously placing the ending Track Synthesizer Frequency (TSF) near the *XA* frequency, and thus satisfying a command capability requirement that the difference between TSF and *XA* be no greater than 110 Hz at VCO level. The end point of the sweep becomes TSF for the remainder of the pass, with no additional tuning required.

(2) The uplink sweep range to be approximately *XA* ±100 Hz (at VCO level).

(3) The uplink sweep rate to be +180 Hz/min (at VCO level), resulting in an effective rate as seen by the spacecraft receiver of approximately +150 Hz/min (spacecraft receiver rate = uplink sweep rate − spacecraft (*XA*) rate).

(4) The duration of the sweep as defined above to be approximately 80 s.

(5) On each given launch date, a sweep start time to be fixed (in TFL) at a time shortly after the end of the interference zone. This sweep start time (in TFL) to remain unchanged throughout the daily launch window for each particular launch date.

For the actual launch on December 10, 1974, the uplink acquisition sweep selected according to the above guidelines was as follows:

Ramp start time = 08:05:00 GMT

Starting frequency = 22.039080 MHz (VCO)

Frequency rate = 3 Hz/s (VCO)

Ramp end time = 08:06:30 GMT

Ending frequency = 22.039350 MHz (VCO)

This uplink sweep pattern can be seen in Fig. 4.

V. Post-Flight Analysis of the Helios 1 Launch Phase

A. The Helios 1 Silent Spacecraft Mode

No information was received from the down range AFETR stations that the Helios 1 Spacecraft was in the silent mode, and, in fact, this was apparent moments after the expected rise at DSS 42, when a one-way downlink was routinely acquired. Obviously, this condition vastly reduced the uncertainties heretofore inherent to the initial acquisition procedure at DSS 42.

B. Interference Zone Results

The maximum effects of the interference zone were predicted to occur between:

08:01:00 and 08:05:00 GMT

Figure 5 shows the downlink signal strength at Receiver 2, on the SAA, while Fig. 6 shows the signal strength at Receiver 1, on the SCM, both figures encompassing the above time period. As can be seen in these data, the maximum interference zone signal strength

degradation on Receiver 2 (SAA) was approximately 6 dB, while on Receiver 1 (SCM) it was approximately 8 dB, both of these losses being considerably less than was generally anticipated. Further, this degradation in signal strength was such that neither receiver lost lock during the entire interference zone period, although there was also a very substantial degradation in SNR during this period. An interesting feature which can be seen in Fig. 6 (SCM) is the sudden increase in signal strength at 08:05:20 GMT, whereas no such increase occurs at this time in Fig. 5 (SAA). At this time, the antennna went to auto-track, previously having been computer-driven according to nominal predictions. The nominal predictions being used were in error by approximately:

$$\Delta HA \approx 0.11 \text{ deg}$$

$$\Delta dec \approx 0.08 \text{ deg}$$

$$\Delta \text{total angle error} \approx 0.14 \text{ deg}$$

Since the half-power offset for the SCM is 0.18 deg, one would expect a loss of roughly 1.8 dB for 0.14-deg error, and that is almost exactly the effect seen in Fig. 6. On the other hand, the SAA has a half-power offset of 8 deg, so the elimination of the 0.14-deg pointing error at 08:05:20 GMT would have no perceptible effect—hence, no effect is seen in Fig. 5 at the time of onset of auto-track.

The net effect of the antenna interference zone was far less traumatic than had (conservatively) been expected, and, since the worst case had been completely planned for in any event, the initial acquisition at DSS 42 was not in any substantial way adversely impacted by the effects of the antenna interference zone.

C. Preflight Prediction Accuracy

In the early portion of the pass at DSS 42, the actual radio metric data, when differenced with the preflight nominal predictions (generated from the actual liftoff time), yielded the following residuals (as obtained from the near-realtime pseudo-residual program):

$$\Delta HA \approx 0.11 \text{ deg}$$

$$\Delta dec \approx 0.08 \text{ deg}$$

$$\Delta XA \approx 1.0 \text{ Hz (VCO)}$$

These can be compared to the estimated 3σ uncertainties presented in Section II as:

$$\Delta HA \approx 1.15 \text{ deg}$$

$$\Delta dec \approx 0.80 \text{ deg}$$

$$\Delta XA \approx 17 \text{ Hz (VCO)}$$

As can be seen, the actual errors which occurred were approximately 10% of the estimated 3σ uncertainties, which would seem to (probabilistically) indicate that the estimation of the uncertainties was on the conservative side, a not wholly undesirable condition.

D. One-Way Downlink Acquisition at DSS 42

The one-way acquisition of the Helios 1 downlink by DSS 42 was executed rapidly and with no complications. Rise occurred at:

07:57:14 GMT

and DSS 42 had good, one-way lock at:

07:57:24 GMT

or ten seconds later. This acquisition can be seen in Fig. 7. The station apparently set its receivers slightly below the expected frequency (the receiver frequency being inversely related to doppler frequency) and allowed the downlink to "walk" down into the receivers—quite successfully!

E. Uplink Acquisition at DSS 42

The instructed uplink acquisition sweep was defined as:

Ramp start time	= 08:05:00 GMT
Starting frequency	= 22.039080 MHz (VCO)
Frequency rate	= 3 Hz/s (VCO)
Ramp end time	= 08:06:30 GMT
Ending frequency	= 22.039350 MHz (VCO)
Sweep duration	= 90 s

The instructed sweep and the sweep actually executed by DSS 42 can be seen in Fig. 4. As can be seen, the station tuned (manually) at about 90% of the instructed rate, a quite creditable performance, particularly when compared to the DSS 42 performance during the Mariner Venus/Mercury 1973 (MVM '73) launch, when the station was able to achieve a sweep rate of only approximately 60% of that instructed. Since the spacecraft was in the noncoherent mode, it was not immediately possible to tell exactly when or even if the uplink had been acquired—however, the fact that the uplink

sweep had been routinely successful became known via telemetry some minutes later. At 08:26:31 GMT, the downlink was reacquired as good, coherent two-way, in response to a prior command to that effect.

F. Angle Tracking

In accordance with the angle drive strategy detailed in Section III, the antenna at DSS 42 was initially computer-driven to the preflight predictions generated from the actual launch time. At 08:06:20 GMT, or approximately one minute after the earliest possible (instructed) time, the antenna was successfully switched to auto-track on the SCM.

VI. Summary of Tracking Operations During the Helios 1 Launch Phase

Key spacecraft features considered in the pre-launch planning for the Helios 1 launch phase were:

(1) The silent spacecraft mode.

(2) The low-gain antenna orientation interference zone.

In the actual launch the silent spacecraft mode did not occur, and the interference zone was considerably less difficult than expected; nonetheless, tracking operations at DSS 42 during the launch phase proceeded exactly as planned, and were highly successful.

Acknowledgment

The authors wish to acknowledge R. Allis, the Telemetry Network Operations Analyst, for providing the downlink signal strength data during the interference zone.

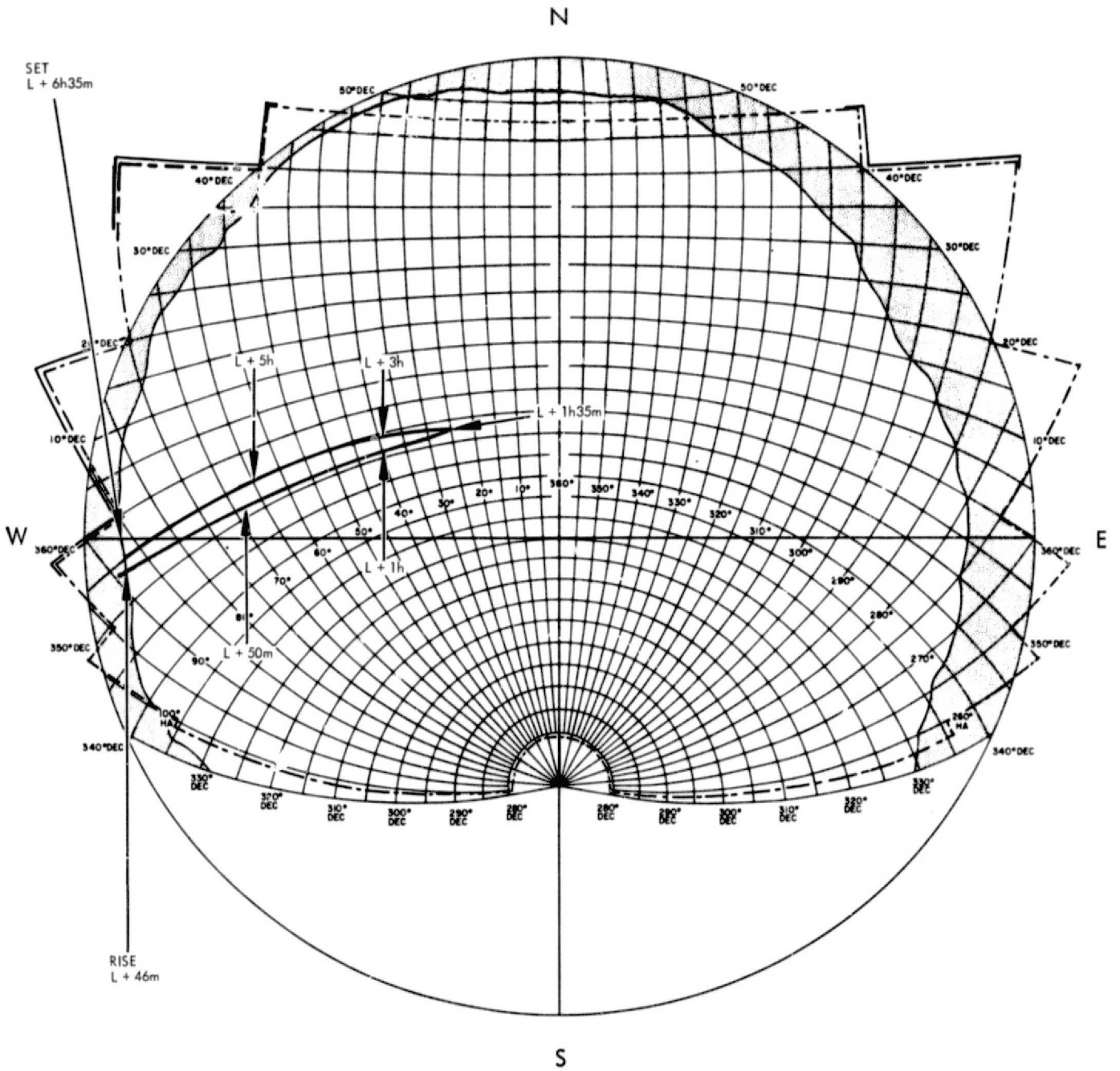

Fig. 1. DSS 42 Helios launch, December 10, 1974

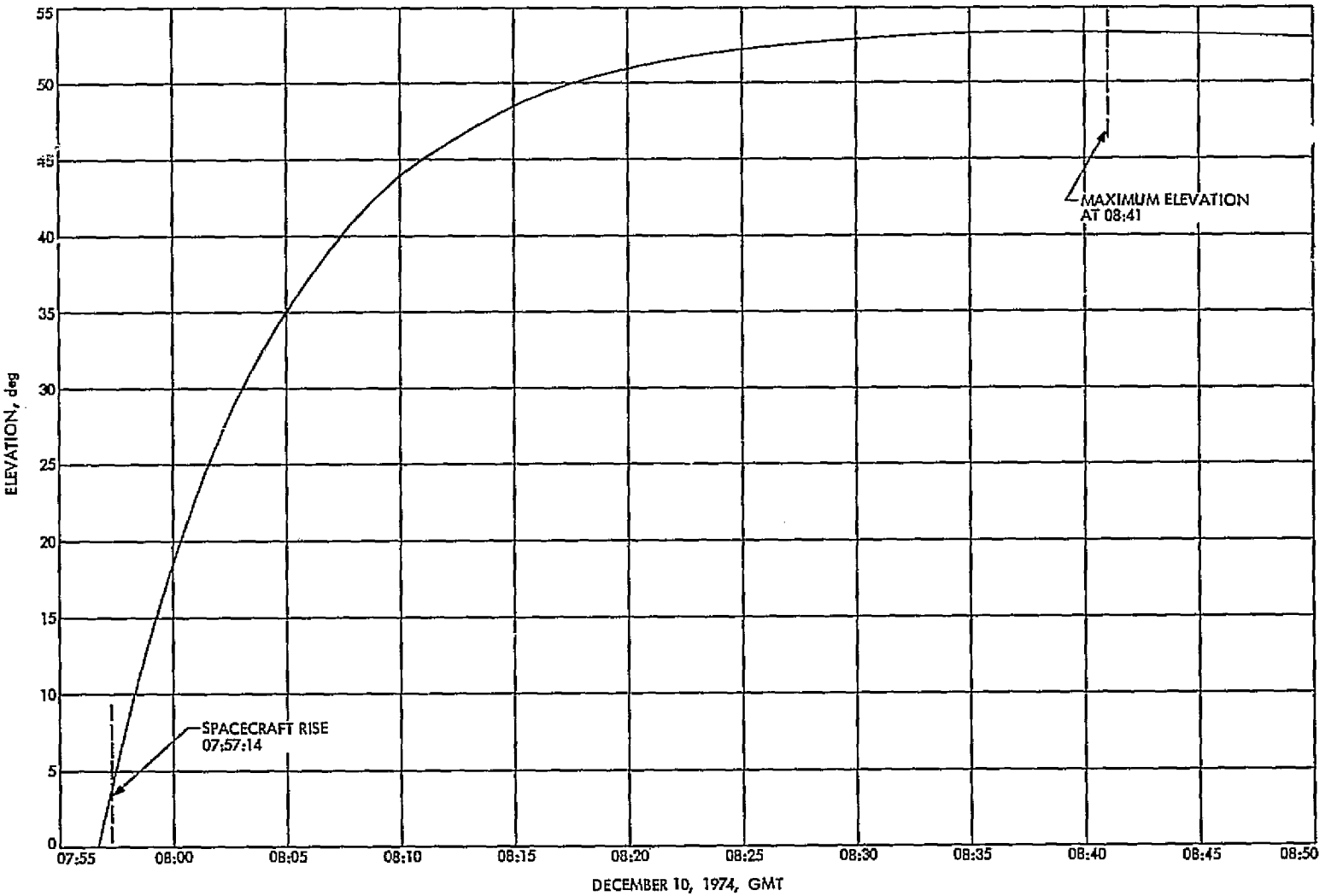

Fig. 2. Spacecraft elevation at DSS 42 Helios launch

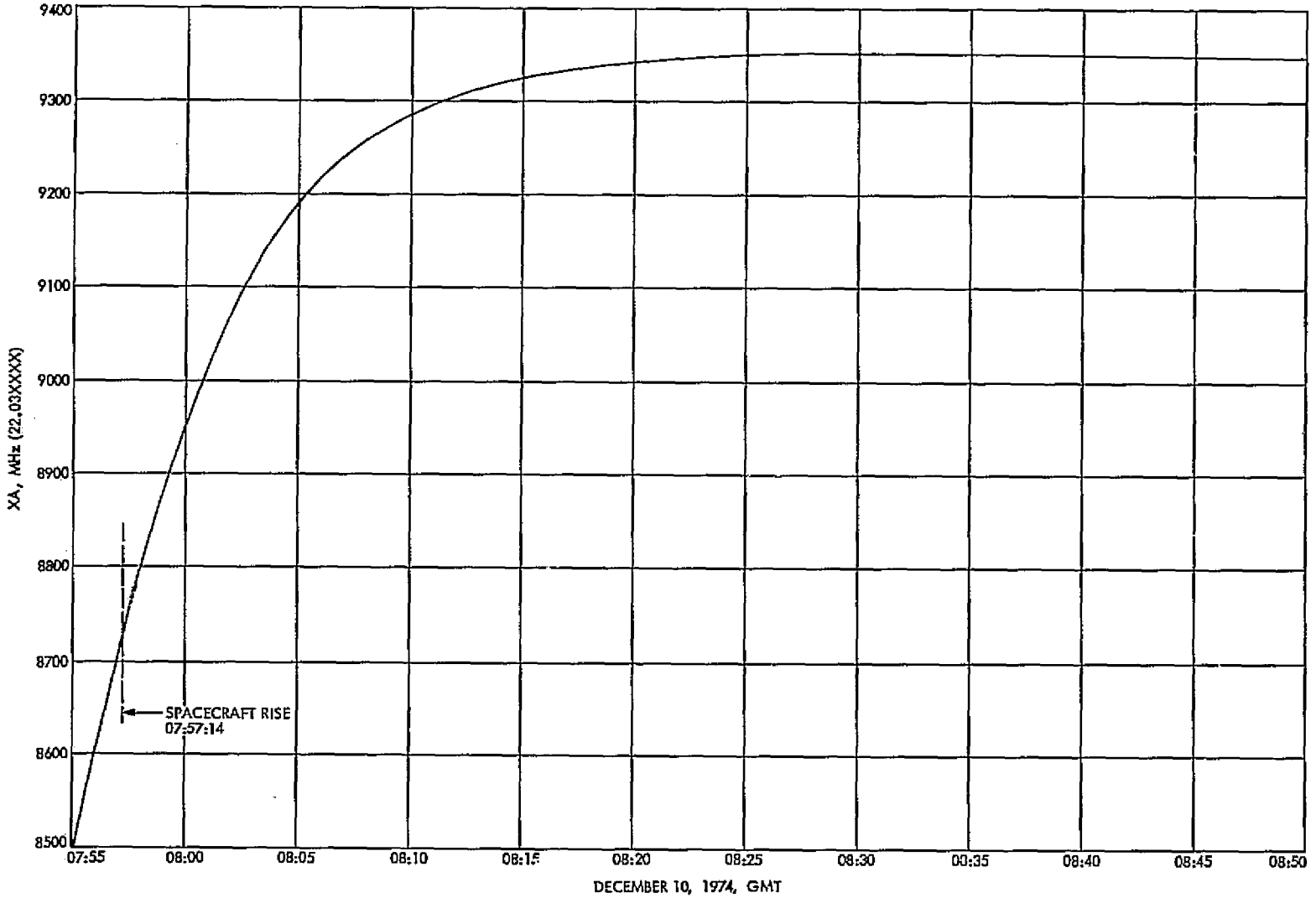

Fig. 3. Best-lock frequency at DSS 42 Helios launch

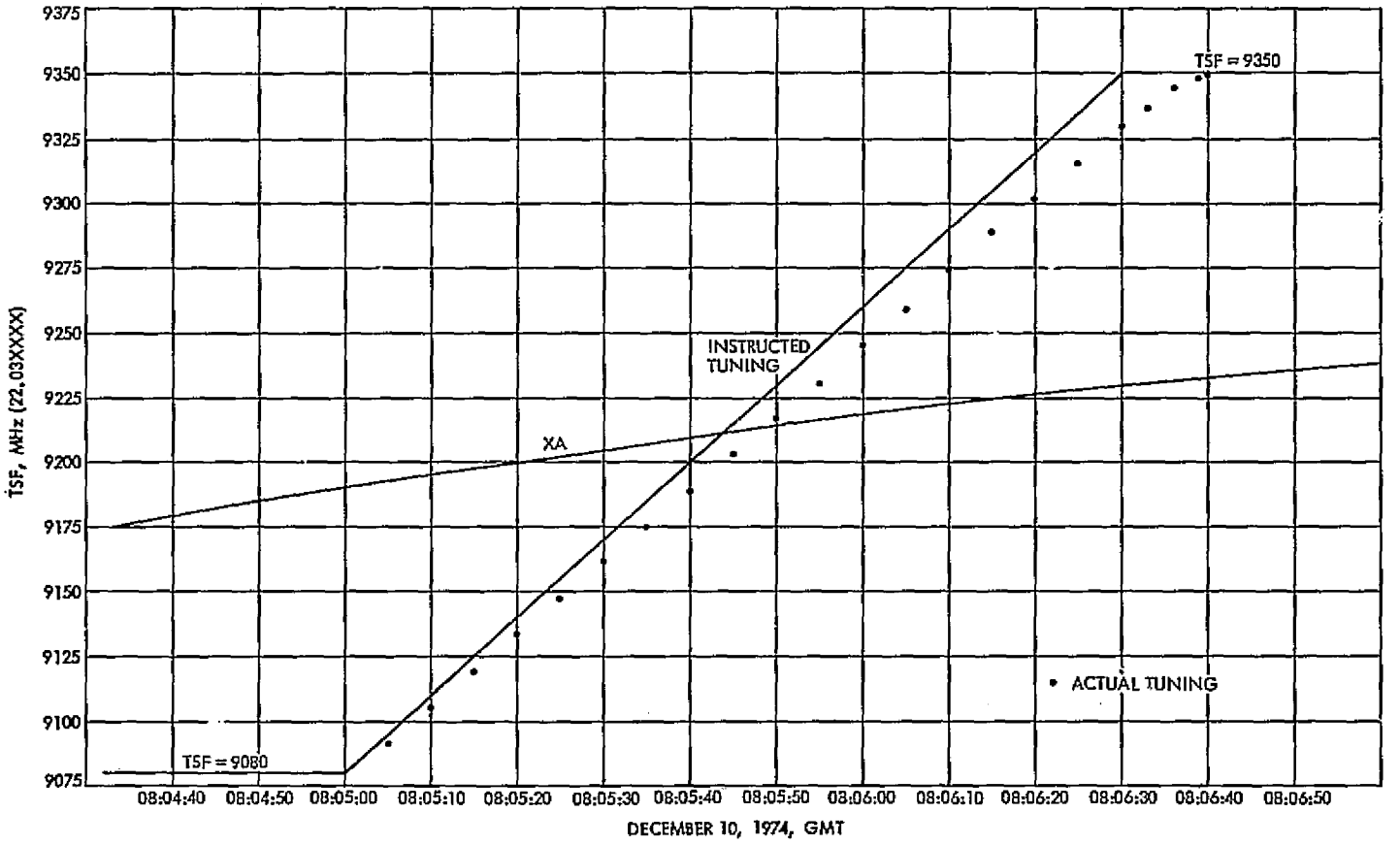

Fig. 4. Comparison of actual tuning to instructed tuning for DSS 42 Helios launch

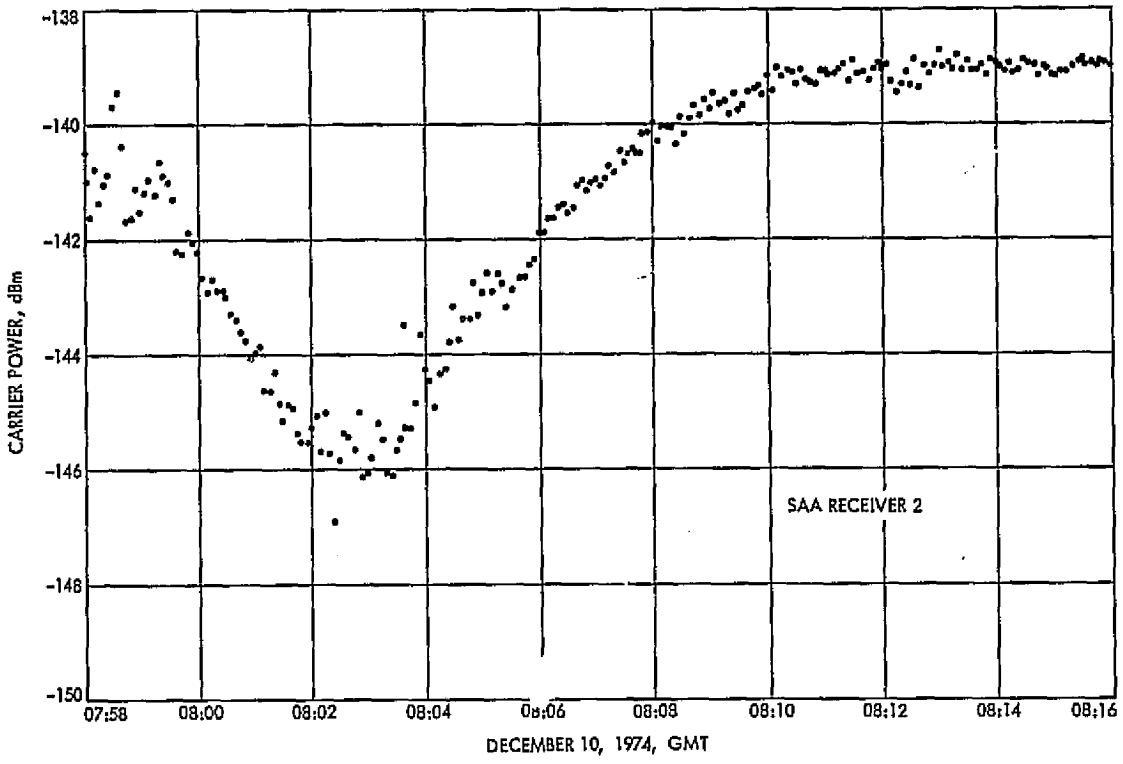

Fig. 5. Interference zone signal strength (SAA) at DSS 42 Helios 1 launch pass

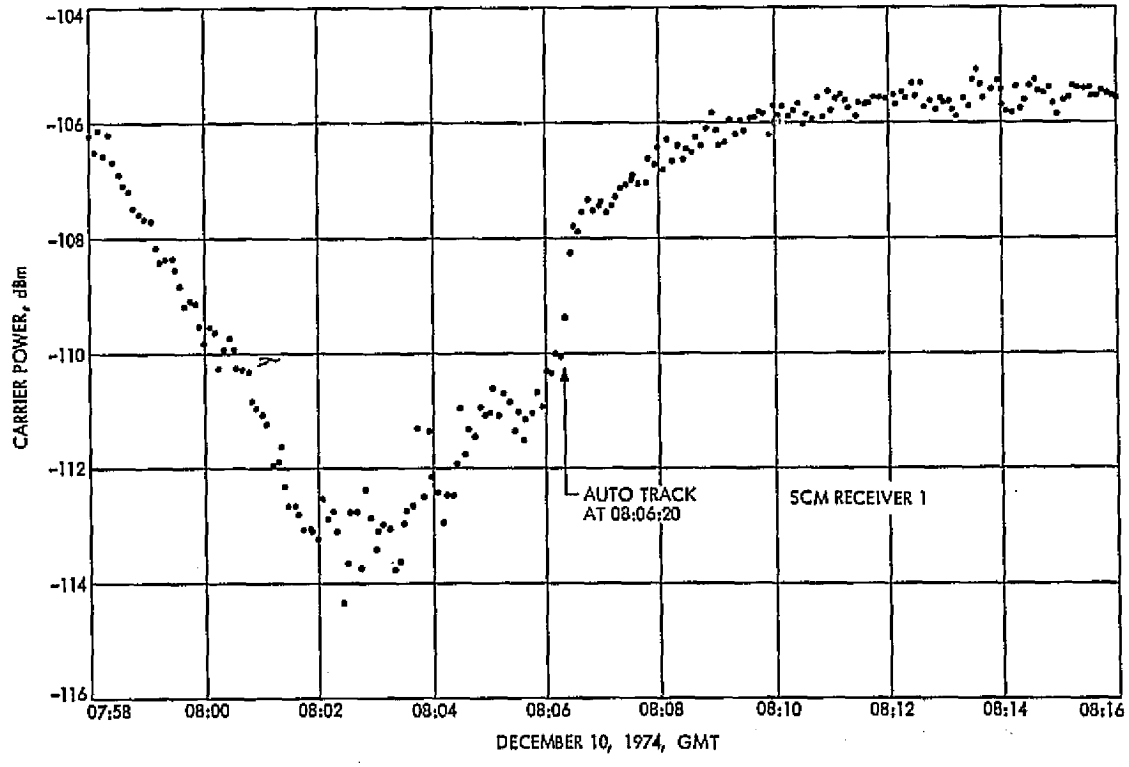

Fig. 6. Interference zone signal strength (SCM) at DSS 42 Helios 1 launch pass

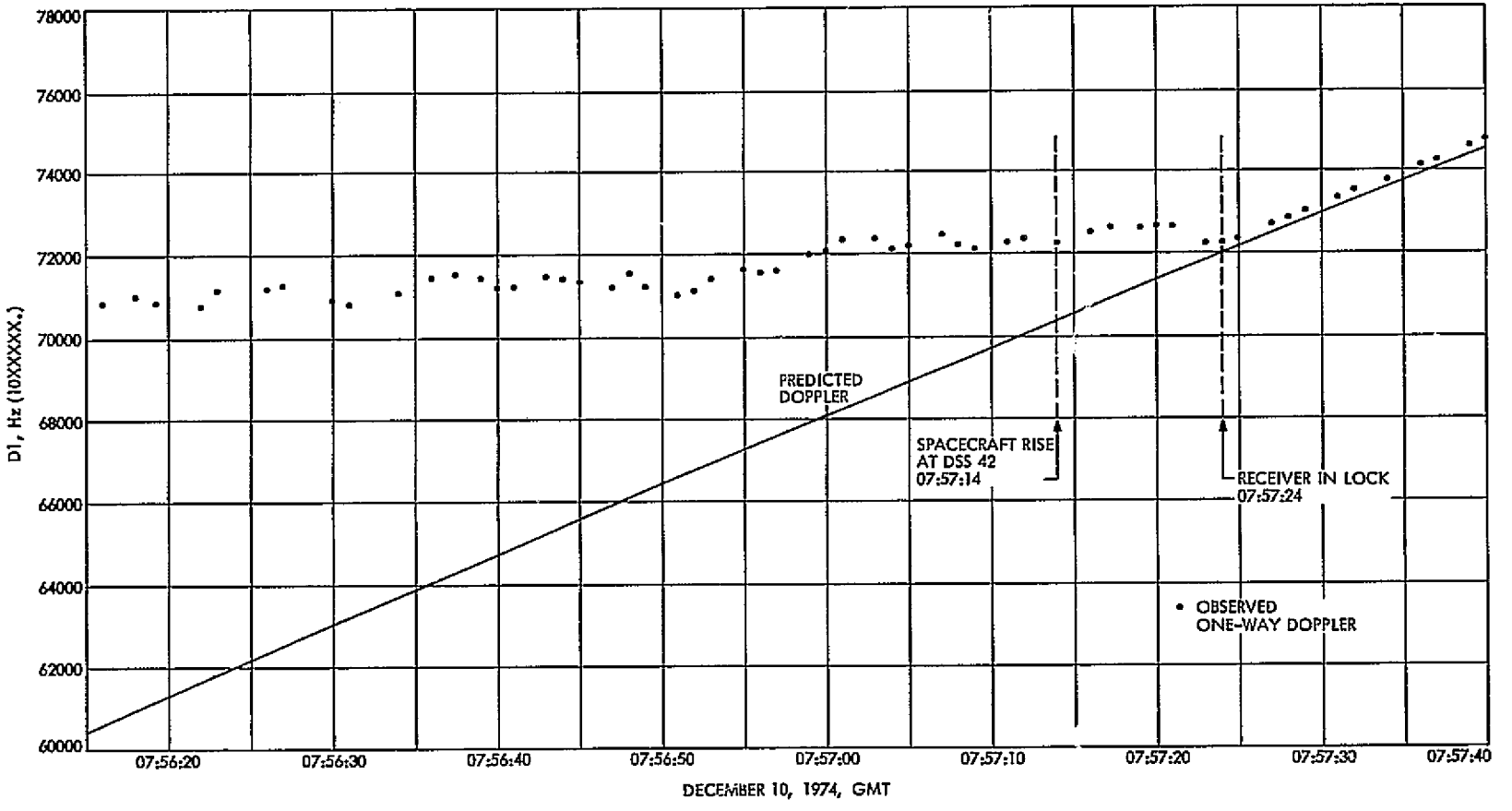

Fig. 7. Initial downlink acquisition during DSS 42 Helios launch

Symbol Synchronizer Assembly Instability Study

R. C. Bunce
Network Operations Office

This first part of a two-part analysis describes the unstable operation of the Symbol Synchronizer Assembly (SSA) in the narrow-narrow configuration at 8⅓ bits/s. Reduction of a data set signal-to-noise (dB) vs. time indicates that the SSA is cycling between unstable lock conditions and entirely out-of-lock or ramp conditions. The ramp condition is so called because a strong second-order frequency term or linear drift becomes obvious. The drift magnitude is far beyond loop tracking capability and even marginal when a data rate of 33⅓ bits/s is used. The data indicates a possible third-order term, noted casually in other unprocessed sets. Based on the ramp magnitude, it is finally recommended that bandwidths less than 0.01 Hz (design point) be avoided. Also, an outline is given of Part II, which extends the study to analyze the third-order possibility and will upgrade early results through sophisticated machine programming of statistical and iterative manipulations.

I. Introduction

The DSN Station symbol synchronizor assembly (SSA) performs according to design under all normally recommended operating conditions. However, the equipment contains operationally programmable configurations, outside of the recommended states, that result in unstable behavior.

Specifically, the predominant configuration leading to instability occurs when the narrowest bandwidth instruction (narrow-narrow) is combined with the lowest normally operational symbol rate (8⅓ bits/s). An increase in either the bandwidth instruction (to narrow-medium) or use of a higher symbol rate (nominal 33⅓ bits/s) usually relieves the instability.

Causes of the instability are not well understood. The stable operational threshold with respect to both bandwidth configuration and the product with input symbol rate is presently undefined.

The purpose of this analysis is to determine the magnitude of the instability parameters (by data reduction, particularly, raw points of signal-to-noise vs time), and, based on this analysis, state quantitative expressions that define the minimum stable SSA operating conditions, finally translated to a stable range of input instructions.

The analysis is in two parts. Part One develops elementary models of the unstable conditions and uses these to reduce a single data set to arrive at a preliminary second-order estimate of one of the parameters causing the unstable behavior and its effect on stable operational minimums. Approximate expressions are used to form the preliminary model.

Part Two, now being performed will generalize the reduction of a number of data sets, exhibiting various modes of instability to third order (prelock and lock, periodic, divergent) to bound the extent of the casual parameters and their source. More sophisticated expressions (particularly the relation between signal-to-noise in decibels and integrated phase processes) will be used, and best-estimate minimal stable operational conditions, statistically bounded, will be recommended.

II. SSA Data and Modes

This discussion will be limited to a single data set taken at CTA 21 in February, using the "narrow-narrow" 8⅓ bps condition, within which the instability is most pronounced. This unstable behavior is apparently not directly related to input signal-to-noise ratio, measured in decibels (S/N), but rather due to independent internal effects. When S/N is large, the instability effect remains unchanged.[1] The SSA acts nominally as a normal second-order phase-lock-loop.

Initial thoughts were that the instability was simple oscillator low-frequency $1/f$ noise, and could be treated as such; this noise form is common with very narrow phase-lock-loops, independent of input S/N, and in narrow-narrow, 8⅓ condition, the SSA design loop bandwidth is only 0.00125 Hz.

Data Set No. 1, S/N vs time, plotted in Fig. 1, is typical. Data was taken with straight square-wave input signals at S/N of about 17 dB. It is immediately apparent that the data is not random, but *deterministic*, except for obvious minor first-order noise effects. It can be fit (piecewise) to some kind of deterministic model or curve set, except possibly around the null points. This does not mean that the data is not statistical in the long run; whatever is causing the variations (probably temperature effects on local oscillators) may change state, or otherwise vary randomly at large intervals. The question is philosophical; the given data set, observed over a relatively short time period (with respect to bandwidth reciprocal) shows a deterministic trend or pattern. Low-frequency noise statistics must be abandoned; we are observing effects from a single, causal, and directly determinable time-dependent source.

The most informative feature in Fig. 1 is the presence of nulls. The SSA S/N measurement set is obtained by integrating across sequential symbol periods and summing results; a null could happen only if transitions occurred near the half-way point through a symbol period, a phase error of ¼ cycle, or 90 deg. This is well outside the SSA loop control range. The instability is an "in-loop-control"—"out-of-loop-control" phenomenon.[2] The control range (the phase-detector integral) is only $\pm$ 1/16 cycle, or $\pm$ 22.5 deg.

The 22.5 deg range leads immediately to another conclusion: if the actual input S/N is stable and has a peak value at 0 deg, and if the S/N (average) drops by 2.48 dB, loop control is lost. This is somewhat distorted by S/N summation effects; but, in general, the loop is not fully active if the S/N is less than 2.48 dB below peak. The figure is simply the loop S/N mean integrator output at $\pm$ 22.5 deg or 1/16 cycle, from zero phase error.

It is, therefore, obvious that the disturbing force under the stated conditions is sufficient that the loop cannot hold control; i.e., maintain lock. The most causal parameter to do this in a second-order-loop is a *frequency ramp* with magnitude beyond the tracking range. Although various spotty but observed data sets, including Set No. 1, have shown possible higher-order components, Data Set No. 1 (even intuitively) shows a strong second-order parabolic curvature. Higher-order components of significance cause multiple nulls, or, at least, successive inflections. These are minor in Data Set No. 1. See Appendix for additional discussion.

The predominant question of Fig. 1 is whether or not the signal reentered loop control at the central peak. If it did not, then the frequency turned over, due to the frequency ramp, and reentered negatively following the next null. If it did reenter, then the S/N must have been variable, with a peak of only 14 dB in the central region, or data points at the peak were missed. Consider

[1] S/N data amplitude follows the signal level, but the time-dependent form of the instability process does not change appreciably with this amplitude.

[2] Some would say "in-lock"—"out-of-lock". However, if lock is defined as a zero or steady-state phase error, the loop simply "has control" or "is out of control." When it can't "handle" the signal, it is never "in lock".

the first hypothesis above to be Mode I and the second Mode II. The S/N data cannot resolve this, for SSA S/N reduction is based on absolute values, and the sign of the error phase is indeterminate. This leads to the discussion of S/N as an indicator of phase.

III. SSA Signal-to-Noise (dB) to Phase Conversion

The SSA S/N readout results from processing of the summation of the absolute values (and their squares) of a set of measures obtained by integration over the symbol period. The result is simply the square of the mean measure (signal estimate, watts) over its variance (noise estimate, watts). It would be accurate, except that absoluting the measures causes a dc offset by noise, an inescapable error. The error becomes significant if the integrated signal component approaches the noise component. The measure then becomes nearly indeterminate; all outputs approximate 0 dB with little quantitative information possible. In general, when the SSA S/N readout is below 3 dB the number is indefinite and becomes nearly meaningless at about 1.0 dB. Detailed mathematics are omitted at this time, as the algorithm problems in the area are well known. It is handled here simply by disregarding one point of low S/N data; the point, at 0.4 dB, was obviously inaccurate. Under high S/N conditions, the S/N integral is directly proportional to the phase error across a single quadrant. The true signal level is measured at zero phase error, while the null occurs at ¼ cycle of phase error, or 90 deg, when the transition is at the integral mid-point and the two halves cancel. Thus, the elementary reduction of S/N to phase is

$$\hat{\phi}(t) = n \cdot \frac{1}{2} \pm \frac{1}{4}\left\{1 - 10\exp\left[-\left(\frac{DBX - DB(t)}{20}\right)\right]\right\} \tag{1}$$

where

$\hat{\phi}(t)$ = phase estimate with time-tag t.

DBX = system S/N, dB; the peak observed value.

$DB(t)$ = S/N readout at time t.

$n, \pm$ = index and sign choice to fix $\hat{\phi}$ according to selected mode estimate.

For data set No. 1, n, sign, and DBX were chosen as follows; see Figure 1 for null and peak position ($t = T$).

A plot of data set Number 1, both modes, and reduced to phase equivalents by Eq. (1) and Table 1, is shown in Fig. 2. This was the basic working data model for Part 1. Note uncertainty regions near nulls, and also the very narrow loop periods; the signal is out of loop control for the majority of the time. The most significant and unambiguous region is the long-ramp section between 400 and 600 s. Except for sign, this section is independent of mode, and was finally the prime data field used for analysis.

Since actual S/N readout is the result of summation over an S/N interval (80 s), Expression (1) can only be approximate. The actual phase representing a given readout is some median value within the summation, and occurs at some variable time in this period. However, without parameter estimates for the data model, corrections are impossible; in turn, parameter estimates depend on phase points. An iteration process is indicated, and a program for this is under way for use in Part II. Also, pure phase jitter, insignificant during loop periods, is not negligible in ramp periods, when loop feed-back does not control it. The program covering these effects is quite complicated, and its initial form was lost through computer malfunction before meaningful additional data sets could be obtained. However, Expression (1), with suitable initial correction near nulls for both the S/N algorithm and inherent phase jitter, was the first program step and is probably accurate within a few degrees, except near nulls.

Data Set No. 1, as reduced, showed, regardless of mode, an apparently fairly constant frequency during the out-of-loop-control, or ramp periods. However, an investigation of the data derivative, particularly in the indicated ramp period between 400 and 600 s, revealed an undeniable and relatively large second-order frequency term, or $\dot{F}$, and, (although the data was insufficient) even gave indications of a mild third-order process (to be disregarded at this time). Based on the strong ramp term, the hypothesis was established that the SSA voltage-controlled oscillator (VCO) (synthesizer sweep oscillator) was drifting. The Part I models for this internal ramp drift follow.

IV. SSA Phase-Lock Loop With Frequency Drift Models

The SSA is finally an ordinary second-order optimized loop with very narrow-band capability, and perfect integrator.

Under strong-signal input conditions (the only conditions of this study), the phase detector function (a combination of digital logic and analog-to-digital conversion of an integral) is linear over the range ±1/16 cycle, or ±22.5 deg; a cycle period being two symbol periods.

When the phase error exceeds the above limits, the phase detector output becomes a nominal constant until the phase error has increased to a point very close to null, ±¼ cycle (see Appendix for variations). The output is then indeterminate for a few degrees, emerging again as constant, but with reverse polarity; the loop turns over while passing through a null. Beyond 22.5 deg, the loop exercises no phase jitter control.[3]

Ordinarily, the detector null flip-flop condition would be a strong restoring force for loop lock. The VCO frequency differential reverses, and the ramp maximum component polarity reverses, driving the loop toward subsequent lock. Such $\dot{F}$ changes were not, however, discernible in the data, and it was concluded that they must be masked by the large internal source. However, for theoretical purposes, we include both in the models; under certain central conditions, the frequency-shift is significant and time-dependent.

A second-order phase-lock loop with internal drift has well known solutions; we assume the input signal to be a stable square-wave at phase zero.

The loop model with constant internal frequency drift, applying when the phase error is in control range, has the S-plane form:

$$\phi(s) = \frac{s\phi_0 - \dot{F}_0 - F_0/s}{(s+a)^2 + b^2} \tag{2}$$

ϕ_0 = initial phase error, cycles (±1/16)

F_0 = initial frequency offset from center, Hz

$\dot{F}_0$ = (constant) drift rate, Hz/s

a, b = loop constants at operating point

Time solutions of Eq. (2) contain linear, exponential, and trigonometric terms, and vary with gain (a function of operating point). To simplify this initial part one study, data were taken in the region where parameter b is zero (unity damping); "a" is then ω_n or just "ω," nominally 4/3 ω_L • ω_L is the design bandwidth. The time solution for Eq. (2) is then free of trigonometric terms:

$$\phi(t)\big|_{b=0} = [(1-\omega t)e^{(-\omega t)}]\,\phi_0 - \frac{1}{\omega}[(\omega t)e^{(-\omega t)}]\,F_0 - \frac{1}{\omega^2}[1-(1-\omega t)e^{(-\omega t)}]\,\dot{F}_0 \tag{3a}$$

The ramp model is elementary; expressed as step functions:

$$\phi(t) = \phi_0' + (F_0 \pm \Delta F)\cdot t + (\dot{F}_0 \pm \Delta\dot{F})\cdot\frac{t^2}{2} \tag{3b}$$

$t = (T - T(\phi_0'))$: time "in the run"

$\Delta F = 2\omega\phi_L = \frac{\omega}{8}$

$\Delta\dot{F} = \phi_L \cdot \omega^2 = \omega^2/16$

$\pm$ = sign, as required for restoring lock.

Eq. (3b) was applied to the long-ramp data in Fig. 2, by least squares fit, and the frequency and rate constants were found to be in excess of F and $\dot{F}$ maximums, as expected. The loop model, Eq. (3a), was also applied, using the ramp results, to the few data points available. The errors were less than two degrees, but these loop results can obviously not be termed conclusive, for loop error variance was not within any kind of normal limits for the three points (25 deg). The ramp results are, however, significant, particularly when the indicated indefinite null point was omitted. Results follow.

V. Concluding Expressions

It is obvious why the SSA cannot hold lock—the internal drift is excessive in the narrowest bandwidth condition. In this condition, least squares fit under two conditions (using or omitting the final ramp point) were:

$$|\dot{F}| = [4 \cdot 132 \pm 0.68] \times 10^{-6}\ \text{Hz/s}$$

Phase error rms of the fits was only 0.69 deg, making the ±0.68 approximately a one-sigma figure.

To track this requires:

$$\omega_{MIN} = [16 \times \dot{F}_{observed}]^{1/2} = 0.0081\ \text{Hz minimum} \tag{4}$$

At the 8⅓ bit/s rate, the bandwidth is 0.00167, well out of range. However, at a bit rate of 33⅓ bit/s, the equiva-

[3]Transitions, the time expression of phase, occur outside the phase detector gate, so their position cannot be included in loop feedback.

lent design bandwidth is 0.007, and tracking of the observed ramp is marginal at the higher-gain operating points. For a safety factor in the presence of the above ramp, it is recommended that, for stable operation, SSA conditions be chosen such that, at design point (at least for Compatibility Test Area (CTA 21) equipment):

$$\omega_L > 0.01\,\text{Hz} \tag{5}$$

To speculate on the source of the observed ramp is probably not valid; the ramp is there, its effects are part of each SSA installation, and it limits operating conditions. The probable third-order term, should it prove sizable, leaves the SSA with lock-drop potential under all conditions, except that time periods could be very long.

It is interesting to note that the synthesizer manufacturer's specification for the internal sweep calculator is:

$$\text{Frequency drift in 10 min} = \pm 50\ \text{Hz, maximum} \tag{6}$$

If this is divided by 10^4, as apparently occurs in the narrow-narrow SSA configuration, the result is a ramp of:

$$\frac{50}{600} \times 10^{-4} = 8.33 \times 10^{-6}\ \text{Hz/sec maximum}$$

This is roughly twice the observed value.

VI. Part Two Outline

The ramp figures above are quite preliminary. To gain confidence in this parameter and its extensions, such as third and/or possibly higher-order terms, work under way on a much more sophisticated approach will be continued. This includes:

(1) Gathering of additional data sets exhibiting all modes.

(2) Coordinating parameter data through a series of loop-ramp cycles, using a generalized rms minimization program, to obtain ramp, rate, and higher-order data results with low variance, particularly during loop runs.

(3) In conjunction with (2), iterate phase vs S/N data through the S/N algorithm model to minimize the phase and time reduction errors.

(4) Determine the variation of the disturbing parameters between data sets, and their possible effect on data degradation under full in-lock conditions.

The expressions for the above steps are summarized in the Appendix.

VII. Summary

The SSA loop exhibits internal frequency instabilities; it has been estimated by ramp-period analysis at 25 times the maximum tracking rate in "narrow-narrow 8⅓" configuration, and only marginally in range if the bit rate is 33⅓. A third-order component may also be present.

Recommended minimum tracking bandwidth is 0.01 Hz, design point.

Part Two will extend these results and generalize operational limitations due to simple drift.

Table 1. Data set no. 1 phase conversion constants

Region	Mode	Sign	n	DBX	$\hat{\phi}$, deg
$T <$ First null	I	+	0	17.3	$0 < \hat{\phi} < 90$
	II	+	0	17.3	$0 < \hat{\phi} < 90$
First peak $> T >$ first null	I	−	1	17.3	$90 < \hat{\phi} < 157$
	II	−	1	14.8	$90 < \hat{\phi} < 180$
Second null $> T >$ first peak	I	+	0	17.3	$157 < \hat{\phi} < 90$
	II	+	1	14.8	$180 < \hat{\phi} < 270$
Second peak $> T >$ second null	I	+	0	17.3	$90 < \hat{\phi} < 0$
	II	−	2	16.0	$270 < \hat{\phi} < 360$
$T >$ second peak	I	−	0	17.3	$\hat{\phi} < 0$
	II	+	2	16.0	$\hat{\phi} > 360$

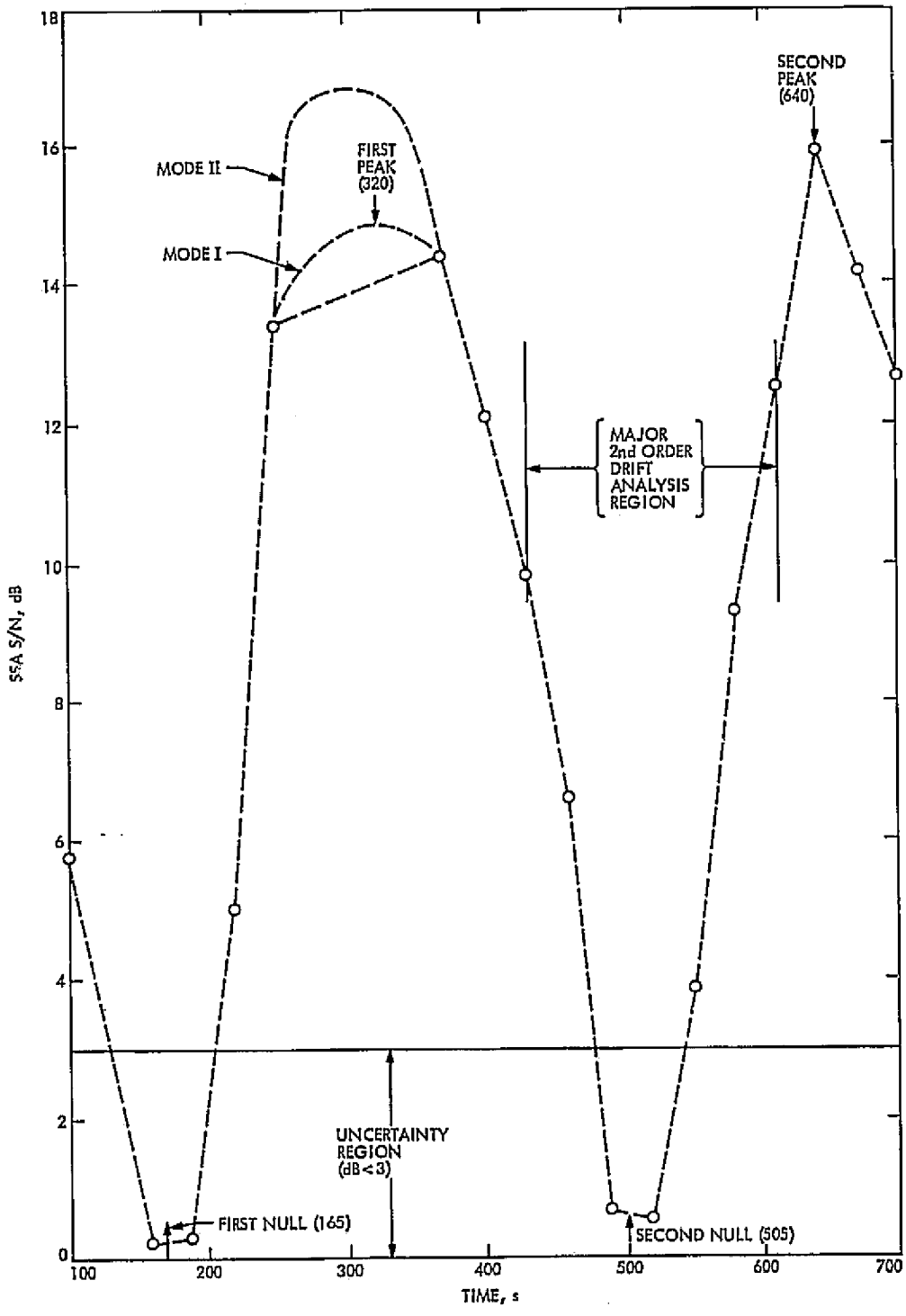

Fig. 1. SSA data set No. 1, CTA-21, March 1975. N-M bits/s raw data

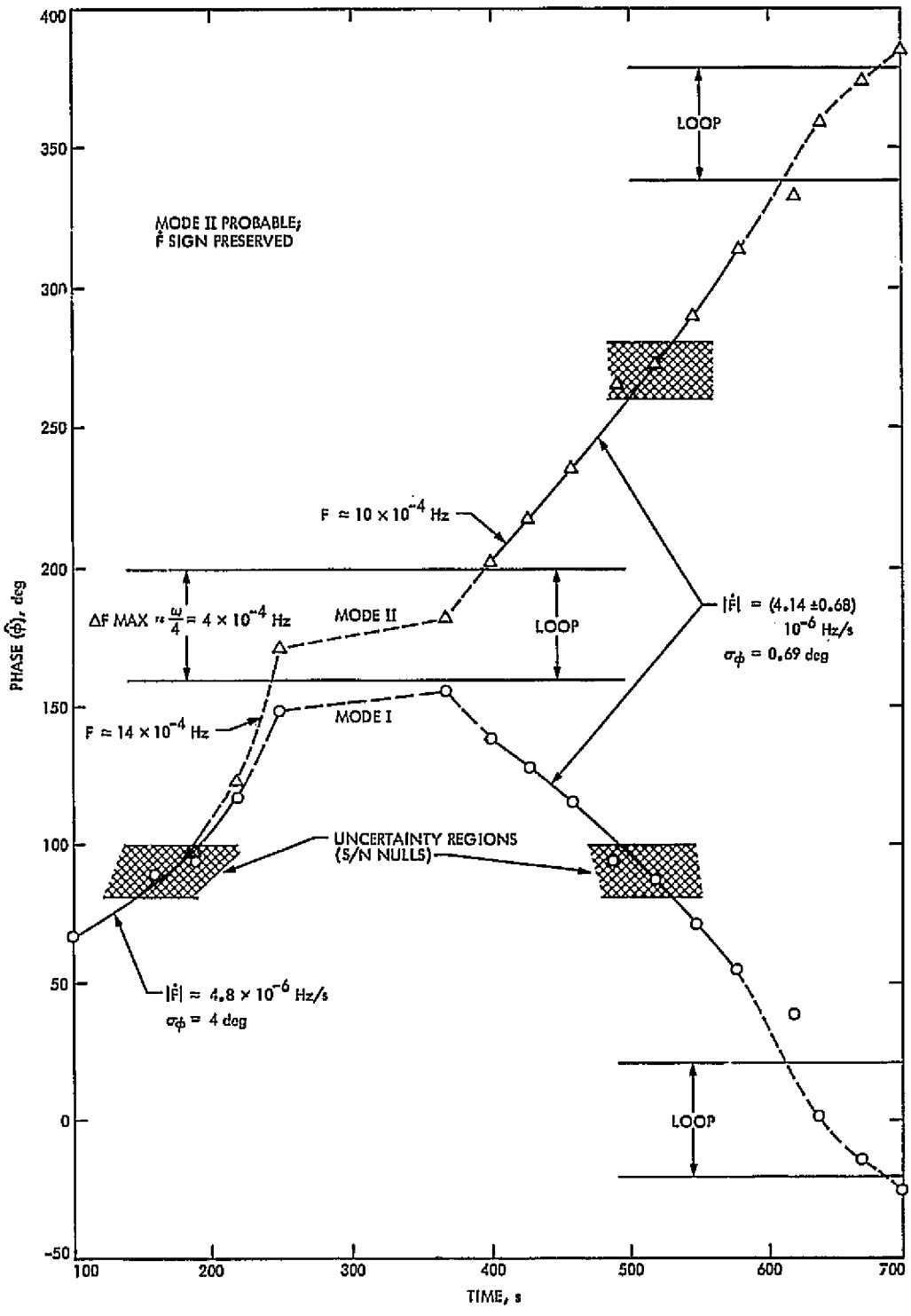

Fig. 2. SSA data set No. 1 phase estimate vs time. Two possible modes

Appendix

Program Models

Discussion begins at Part II of Fig. A-1. Let:

$$\phi'(t) = \begin{cases} F_1(t) \text{ loop} & \text{(exponential/trigonometric)} \\ F_2(t) \text{ ramp} & \text{(polynomial)} \end{cases}$$

Assume initial parameter estimates are available from ramp polynomial analysis. A "set" is one ramp-loop cycle. If phase noise is significant (ramp):

$$\phi''(t) = \sqrt{\frac{2}{\pi}}\,\sigma_\phi \exp\left[-\frac{1}{2}(\phi'(t)/\sigma_\phi)^2\right] + \phi'(t) \cdot \operatorname{erf}(\phi(t)/\sqrt{2}\,\sigma_\phi)$$

$$\sigma_\phi \approx \frac{1}{4} \cdot \sqrt{\frac{1}{R \cdot \operatorname{erf}(R)}}$$

R = system (max) S/N power ratio

If phase noise is insignificant:

$$\phi''(t) = \phi'(t)$$

For use in S/N reduction:

$$\phi(t) = |1 - 4 \cdot |\phi''(t) + \phi_m 1| 0 < \phi(t) < 1$$

ϕ_m effects covered above to obtain the phase noise mean. The S/N detector integral can be stated as (square-wave input):

$$y_i = \left| \int_{T_{0_i} - \Delta\tau}^{T_{0_i} - \Delta\tau + 2\phi(TC_i)\cdot\Delta\tau} [\,|V_i(t)| + n(t)]\,dt - \int_{T_{0_i} - \Delta\tau + 2\phi(TC_i)\cdot\Delta\tau}^{T_{0_i}} [\,|V_i(t)| - n(t)]\,dt \right|$$

TC_i = zero-crossing time; $\phi(TC_i)$ and TC_i require closure in $\phi'(t)$ and $\phi''(t)$.

T_{0_i} = completion time of the integral

= T_j at completion of sample set (final value)

$T_{0_i} = T_j - (N - i)\,\Delta\tau$

V_i = signal voltage @ $T_{0_i} - \Delta\tau$, reversing polarity @ TC_i, where phase value causes a step-function (assuming uncoded square-wave input)

$\Delta\tau$ = symbol period

N = number of symbols/samples: $\dfrac{(T_{j+1}) - T_j}{\Delta\tau}$

When $\phi(t)$ is variable, the moment solutions must necessarily carry a summation. The first two moments, taken over the S/N summation period, become extensions of well-known absolute value integrals:

$$X(T_j) = \epsilon\left\{\frac{1}{N}\sum_{i=1}^{N} Y_i\right\} = \frac{K}{N}\sum_{i=1}^{N}\left\{\sqrt{\frac{2}{\pi}} \cdot \exp - R[\phi(TC_i)]^2 + 2\sqrt{R}\,\phi(TC_i)\operatorname{erf}[\sqrt{R}\,\phi(TC_i)]\right\}$$

$$Y(T_j) = \epsilon\left\{\frac{1}{N}\sum_{i=1}(Y_i)^2\right\} = \frac{K^2}{N}\sum_{i=1}(2R \cdot \phi(TC_i) + 1)$$

$N\Delta\tau = TC$ = summation period (30 s)

$K = \sqrt{\dfrac{N_0 \cdot \Delta\tau}{2}}$, N_0 the noise spectral density

T_j = time of the readout time for the jth S/N measure

When S/N is high, as in this study (except for uncertainty around nulls), the two moments are sufficient. They combine to yield the S/N estimate:

$$(\widehat{S/N})_j = \frac{[X(T_j)]^2}{2\{Y(T_j) - \dfrac{n}{n-1} \cdot [X(T_j)]^2} = \frac{\overline{y}^2}{(\sigma^2 y)}$$

A given phase cannot be associated with this S/N. It represents summation over functions of the $\phi(TC_i)$, an entire section of the model curves:

$$\phi(T_j - \tau G) < \phi(S/N) < \phi(T_j)$$

For program use, three values were selected:

$$(\widehat{S/N})\,(T_j) \text{ represents} \begin{cases} \phi'(T_j - \tau G) \\ \phi'(T_j - \tau G/2) \\ \phi'(T_j) \end{cases}$$

Since S/N is predominantly an amplitude function, the difference between model results and data allowed original data estimates to be modified linearly:

$$\phi'_{\text{DATA}}(t) = \left[\frac{(S/N)_{\text{DATA}}}{(S/N)(T_j)}\right]^{1/2} \cdot \phi'(t)\, T_j - TG < t < T_j$$

ϕ'_{DATA}, three values, the replacement for former ϕ'. This provided data for phase iteration. The S/N to phase conversion above was the second and higher generation process; the original is covered in Part One.

To determine result quality, the S/N difference between data and model, scaled to the system S/N maximum ratio, was reduced to an rms value:

$$RMS^2 = \frac{1}{N}\sum_{i=1}^{N}\left[\frac{\sqrt{(S/N)_{i,\,\text{DATA}}} - \sqrt{(S/N)_{i,\,\text{MODEL}}}}{\sqrt{(S/N)_{\text{SYSTEM}}}}\right]^2$$

At each iteration, the "ramp" data was first subjected to a third-order fit and then, for each associated ramp-loop sequence, the entire parameter set was adjusted for the minimum mean-square condition by machine (small $\partial\Delta V$'s measured for each small "J parameter" at each point)

$$\Delta V_i = \frac{\sqrt{(S/N)_{i,\,\text{DATA}}} - \sqrt{(S/N)_{i,\,\text{MODEL}}}}{\sqrt{(S/N)_{\text{SYSTEM}}}}$$

$$E_i^2 = \left[\frac{\partial\Delta V_i}{\partial\phi_0}\cdot\Delta\phi_0 + \frac{\partial\Delta V_i}{\partial F_0}\cdot\Delta F_0 + \frac{\partial\Delta V_i}{\partial \dot{F}_0}\cdot\Delta\dot{F} + \frac{\partial\Delta V_i}{\partial \ddot{F}_0}\cdot\Delta\ddot{F}_0 + \frac{\partial\Delta V_i}{\partial\omega}\cdot\Delta\omega - \Delta V_i\right]^2$$

This leads to a system of simultaneous minimization equations from which parameter adjustments can be made. At completion, phases are readjusted and the process continued until no further reduction in RMS could be obtained.

Except on an exploratory basis, the above process has not yet been used. Additional data is required.

It remains to consolidate the program, set error measures, and bound applicability of results. This will be done in Part Two. Also, the following effect may be incorporated:

Phase Detector: Output Variation

In Part One, the effect of phase detector "flip-flop" at nulls was neglected, since the observed ramp magnitude far exceeded the maximum VCO ramp. However, the *frequency* changes are not as insignificant: the full "turnover" has the maximum final value:

$$|\Delta F_{\text{MAX}}| = 2\cdot\zeta\cdot\omega\cdot|\Delta\phi| = 4\cdot 10^{-4}\ \text{Hz}$$

This is a peak value at loop entry/exit; the actual value is noise dependent and nonlinear, being zero mean at the null.

Since actual observed frequencies fell between 10×10^{-4} and 18×10^{-4} Hz, this effect is significant in certain regions. The pending third-order model may "absorb" it, or, if it proves necessary, full phase detector noise theory in ramp regions may be applied.

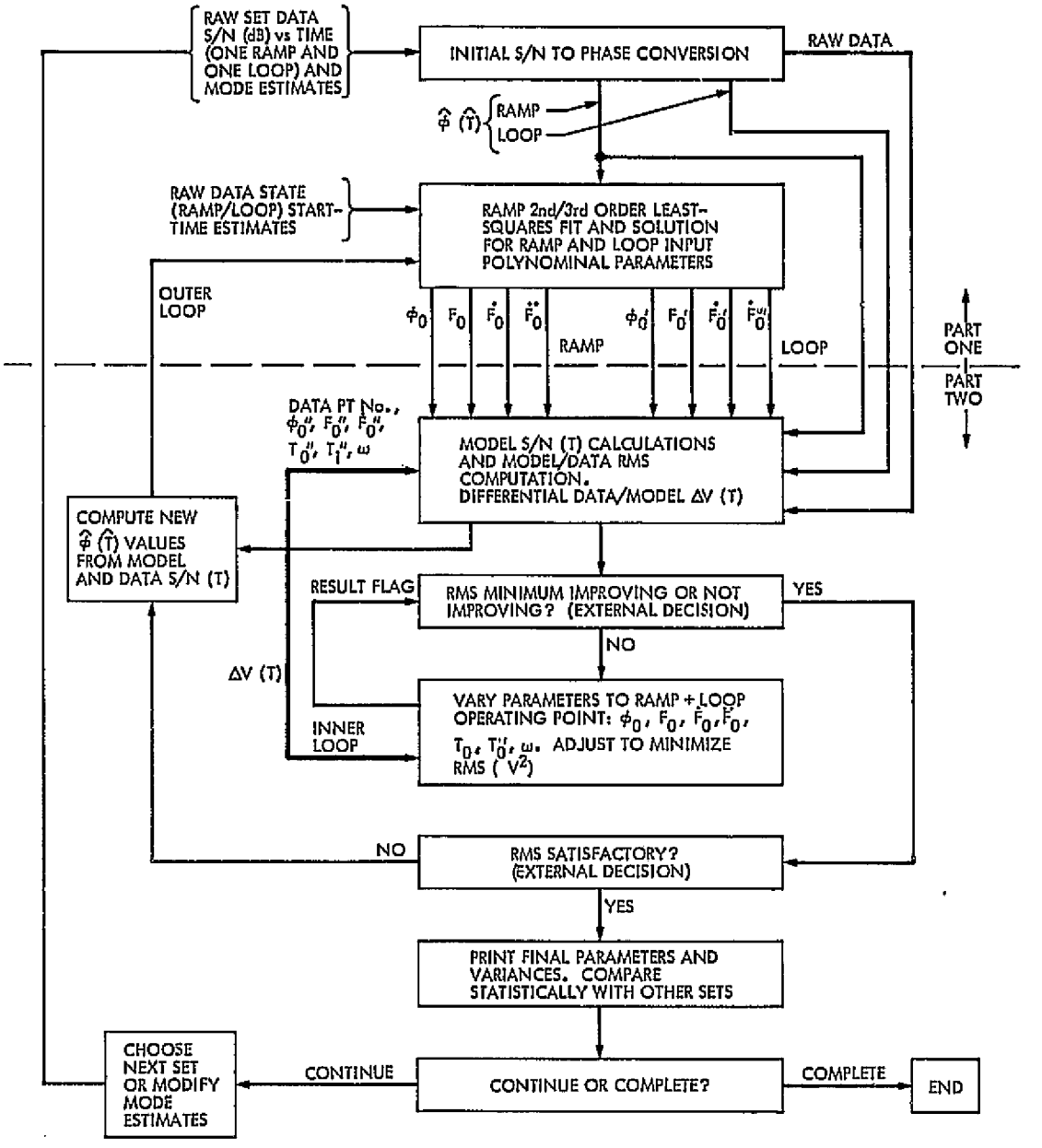

Fig. A-1. Machine data reduction plan, Part II SSA instability study

The Occultation Digital Tape Validation Program

J. Thomson and M. J. Galitzen
DSN Data Systems Development Section

The Occultation Recording Assembly (ORA) located in the JPL Compatibility Test Area is used to produce 9-track computer-compatible digital magnetic tapes from analog occultation tapes recorded at one of three Deep Space Stations. In the past, the software has been used only to static check the ORA hardware configuration. This program allows the operator to validate the contents of the completed digital tapes before they are sent on for costly processing and analysis.

I. Introduction

During a spacecraft flyby of a planet, the spacecraft undergoes an occultation as it passes behind the planet. When this occurs, the signal transmitted by the spacecraft is affected as it passes through the planet's atmosphere. An analog recording of the signal can be made at selected Deep Space Stations. The recording is then taken to the JPL Compatibility Test Area (CTA 21) for conversion to a computer-compatible digital 9-track tape representation of the signal. The digital magnetic tapes are then taken to the Network Operations Control Center (NOCC) for analysis.

The Occultation Recording Assembly (ORA) in CTA 21 is used to produce the 9-track digital tapes from the analog recordings. In the past, the operator has been able only to static check the ORA hardware configuration. The Occultation Tape Validation Program allows the operator to do a more thorough verification of the contents of the completed digital tapes before costly and time consuming computer analysis is done.

II. Hardware

The program, along with the current occultation software, uses an Interdata-4 computer contained in the Occultation Recording Assembly. The Occultation Tape Validation Program makes use of two magnetic tape units for reading in the contents of the digital records and a teleprinter for communication with the operator. The recording process makes use of the analog-to-digital (A-D) channel. The program is controlled by a clock input of 40 kHz. Each clock impulse causes the input of one 6-bit sample from the analog-to-digital channel. A 42-bit time code generator is used to input time tags placed at the head of each digital record.

III. Current Software

The current occultation software consists of a test program and an operational program. The test program allows the user to check the magnetic tape setup, the time code input, and the analog-to-digital input. Thus, it verifies the ORA to computer link. The operational program writes the data onto a series of tapes in the form of 4106-byte records. The recording process is controlled by a clock input of 40 kHz. One record is created for each 4096 clock impulses, thus the records occur every 0.1024 seconds. Each record as shown in Fig. 1 consists of the following:

(1) Station ID code: 1 byte

(2) 42-Bit NASA time code: 9 bytes

(3) Digital data: 4096 bytes

IV. Program Description

The Occultation Tape Validation Program was created to validate the tapes produced by the operational program before being considered ready for data analysis. The program is divided into two separate test operations. They are:

(1) Tape file validation and search.

(2) Tape file dump.

The file validation is used to check the information written on a completed digital tape. This can be divided into four sub-operations:

(1) The program checks the time difference (Δ) between records for any pair or series of pairs by comparing it with an inputted Δ time value. The expected Δ time can be determined from the clock rate and the analog tape speed. Any errors result in a message giving the actual Δ time between records.

(2) The program checks the size of any or all records (this should be 4106 bytes). Any size errors cause the program to type out a message indicating the error and record number.

(3) The program checks the station ID code of any or all records. The ID is compared with the value used in the operational program.

(4) The program counts the total number of occurrences of given 8-bit patterns within each record. This can be used to check for 4096 occurrences per record of a pattern in a test tape. Since up to six 8-bit patterns can be counted at a time, this operation can be used to tally the distribution of sample points in a given record. This can be compared with the expected distribution within the records to provide a statistical verification of the data.

The tape file dump operation allows the operator to dump the partial contents of any specified record onto the teleprinter. The program continuously types 32 bytes/line until a control on the computer display panel is actuated.

V. Conclusions

This program has already proven valuable in discovering and fixing hardware failures. In one case a time code error produced by a failed time code bit was discovered and corrected. In another case, a periodic data error was located and corrected with the help of this program. Without this program these problems would have been detected during the costly 9-track data reduction and analysis procedure conducted by project experimenters.

CODE	MEANING
P'	LONGITUDINAL EVEN PARITY BIT
W	DATA SAMPLE BIT
S	STATION CODE 10 - DSS 14 01 - DSS 4X 11 - DSS 6X
DS	DATA SOURCE 0 - ANALOG 1 - DIGITAL
$D_1 - D_{10}$	BCD DAY BITS
$H_1 - H_6$	BCD HOUR BITS
$M_1 - M_7$	BCD MINUTE BITS
$S_1 - S_7$	BCD SECOND BITS
$M_1 - M_{12}$	BCD MILLISECOND BITS
P	ODD PARITY BIT

START OF RECORD									
P	0	0	0	0	S	S	1	DS	HEADER
P	0	0	D_1	D_2	D_3	D_4	D_5	D_6	TIME OF DAY FOR FIRST DATA WORD IN RECORD
P	0	0	D_7	D_8	D_9	D_{10}	H_1	H_2	
P	0	0	H_3	H_4	H_5	H_6	M_1	M_2	
P	0	0	M_3	M_4	M_5	M_6	M_7	S_1	
P	0	0	S_2	S_3	S_4	S_5	S_6	S_7	
P	0	0	M_1	M_2	M_3	M_4	M_5	M_6	
P	0	0	M_7	M_8	M_9	M_{10}	M_{11}	M_{12}	
P	0	0	0	0	0	0	0	0	
P	0	0	0	0	0	0	0	0	
P	0	0	W_5	W_4	W_3	W_2	W_1	W_0	1ST DATA WORD
P	0	0	W_5	W_4	W_3	W_2	W_1	W_0	2ND DATA WORD
P	0	0	W_5	W_4	W_3	W_2	W_1	W_0	
P	0	0	W_5	W_4	W_3	W_2	W_1	W_0	4095TH DATA WORD
P	0	0	W_5	W_4	W_3	W_2	W_1	W_0	4096TH DATA WORD
P'	P'	P'	P'	P'	P'	P'	P'	P'	
									INTERRECORD GAP

Fig. 1. Tape record format

A Reexamination of the Subcarrier Demodulator Assembly Data Limiter Suppression Factor

L. Kuo and L. Webster
Network Operations Office

The data limiter suppression factor is an important parameter in determining Subcarrier Demodulator Assembly (SDA) performance in the presence of subcarrier phase jitter. A new mathematical model for this suppression factor is presented which, unlike previous models, allows for variable data symbol transitional probabilities and data filter time constant. Each of these quantities is examined for its effect on the data suppression factor. Finally, an example is presented which shows effects on SDA performance for data symbol transitional densities other than 50%.

I. Introduction

The Subcarrier Demodulator Assembly (SDA) models for use in the DSN were designed on the assumption that data have a transition probability of 50% and that $\tau_D/T_{SY} = \frac{1}{3}$, where τ_D is the data filter time constant (see Fig. 1), and T_{SY} is the data symbol period. This assumption, however, is limited in data analysis since it occurs quite frequently that the symbol transition density is other than 50% and τ_D/T_{SY} ranges from approximately $\frac{1}{8}$ to $\frac{1}{2}$.

The suppression factor (α') is a very important parameter in determining demodulation performance. Since (α') varies as a function of data transitional densities, τ_D/T_{SY}, and ST_{SY}/N_0 (signal energy to noise spectral density ratio into the data filter), a study was made to determine the data suppression factor (α') as a function of these variables. This article also presents the effects on SDA degradation (symbol energy to noise spectral density out of SDA/symbol energy to noise spectral energy into SDA) as τ_D/T_{SY} and symbol transition density change.

Figure 1 is a functional block diagram (BLK III only) for the Subcarrier Demodulator Assembly. The input signal is an RF signal at the IF frequency of the receiver. The receiver phase tracks the received carrier and heterodynes it to the IF frequency at a fixed phase. The

received signal contains telemetry data in the form of a binary waveform which biphase modulates a square-wave subcarrier. The modulated subcarrier, which is also a binary waveform, in turn modulates the carrier. The purpose of the Subcarrier Demodulator Assembly is to recover the original binary telemetry waveform by synchronously demodulating both the carrier and subcarrier. The receiver provides a reference signal at 10 MHz to demodulate the carrier. The reference signal, to demodulate the subcarrier, is provided by the demodulator itself, a portion of which acts as a phase-locked loop to track the subcarrier. Both demodulation processes take place in the upper channel of Fig. 1. The output of the upper channel is the recovered binary waveform which is sent to another part of the overall system for detection. The output waveform $m(t)$ is also filtered and limited to provide an estimate $\hat{m}(t)$ of the binary waveform (the recovered waveform is typically contaminated with noise and not strictly binary).

The term $m(t) \cdot \hat{m}(t)$ represents the data symbol stream $m(t)$ multiplied by an estimate $\hat{m}(t)$ of the symbol stream. $\hat{m}(t)$, the voltage at the output of the data hard limiter, represents the data symbol stream $m(t)$ with serrations due to Gaussian receiver noise plus a time delay at data transition due to the data filter time constant τ_D (see Fig. 2). The average value of $m(t) \cdot \hat{m}(t)$ over many digit periods is designated as (α'), the data suppression factor (Ref. 1):

$$\alpha' = \overline{m(t) \cdot \hat{m}(t)} = \text{(fraction of time } \hat{m}(t) \text{ agrees with } m(t) - \text{fraction of time } \hat{m}(t) \text{ disagrees with } m(t))$$

II. Mathematical Model

In formulating the model (see Fig. 3), consider a binary input signal $x(t)$ of the form

$$x(t) = \cdots + X_{-3}D^{-3} + X_{-2}D^{-2} + X_{-1}D^{-1} + X_0 + X_1D + X_2D^2 + X_3D^3 + \cdots$$

where X_n ($n = \cdots, -2, -1, 0, 1, 2, \cdots$) are independent binary random variables assuming the value of V with probability P and the value of $-V$ with probability $(1 - P)$, and D is the delay operator of time T_{SY}. Let this signal be immersed in white Gaussian noise $n(t)$, which is zero mean and has a two-sided noise spectral density of $N_0/2$. The composite signal $z(t) = x(t) + n(t)$ is passed through a first order linear filter with transfer function $F(s) = 1/(1 + \tau_D S)$.

The output $y(t)$ is then hard limited to produce the signal $u(t)$ (called data estimate), i.e.,

$$u(t) = +1, \quad \text{if } y(t) \geq 0$$
$$u(t) = -1, \quad \text{if } y(t) < 0$$

The problem to be examined then is to find the average value of the product of the data and data estimate, namely,

$$\alpha' = E\{u(t) \cdot x(t)\} = E\{\hat{m}(t) \cdot m(t)\}$$

as a function of $R = V^2T/N_0 = ST_{SY}/N_0$, P, and T_{SY}/τ_D.

Since the filter has the greatest effect on most recent symbols of the incoming signal, the problem could be simplified by assuming that the symbol stream is all zero except the last two symbols and then adding small effects asserted by all previous symbols. In detail, initially assume that $x(t)$ takes on value V with probability P, and value $-V$ with probability $(1 - P)$ at time from 0 to t ($t < T$), $-T$ to 0, and has value 0 all the previous time ($-\infty$ to $-T$). Examine the filter output. The same process should be repeated by tracing back one more symbol period, namely, it takes on V, $-V$ with probability P, $1 - P$ at period $-2T$ to $-T$, 0 at period ($-\infty$ to $-2T$). Using the linear property of the filter, this result could be obtained from that of the initial case by adding small changes affected by this extra symbol period. Repeating this process by adding more symbols to be analyzed, the $\alpha' = E\{u(t) \cdot x(t)\}$ should finally converge to a limit, since less effects are being produced by the filter with each previous symbol added. The iteration process could be stopped when α' converges to a limit.

In obtaining the expected value of $u(t)\ x(t)$, it would be easier to assume a particular incoming waveform, find $E\{u_i(t)\ x_i(t)\}$ given that particular waveform (called conditional expected value given a particular case), then average the expected values over all the possible cases of incoming signals according to their probabilities of occurrences.

III. Mathematical Analysis

A. Analysis of Two-Symbol Periods (One Traced Back)

First, consider the case when one symbol period is being traced back (two symbols are being analyzed), namely, the incoming signal is assumed to have voltage zero from time $-\infty$ to $-T$, have voltage V with probability P, $-V$ with probability $(1 - P)$ at time $-T$ to 0,

and have voltage V or $-V$ with probability P or $(1-P)$ from 0 to t ($t < T$). In other words, one of the following four cases might occur:

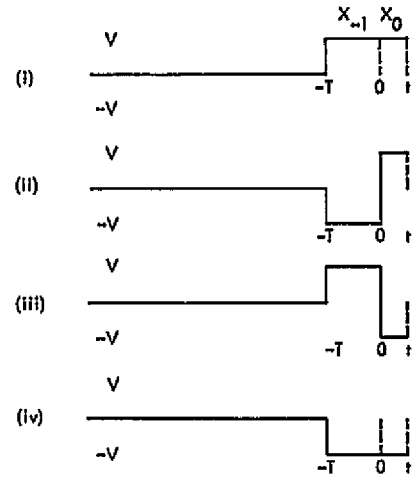

q_i denotes the probability for each case to occur; then $q_1 = P^2$, $q_2 = (1-P)P$, $q_3 = P(1-P)$, $q_4 = (1-P)^2$, since X_n's are independent binary variables. Now, assuming one of the above four cases does occur, called i, then $\zeta_i(t) = E\{u_i(t)x_i(t)/i\}$. Since $u_i(t) = 1$ or -1, $\zeta_i(t)$ could be analyzed as in discrete cases with two sample points; thus,

$$\begin{aligned}\zeta_i(t) &= E\{x_i(t)\cdot 1 \mid u_i(t)=1\}\cdot P(u_i(t)=1) \\ &\quad + E\{x_i(t)(-1)\mid u_i(t)=-1\}\cdot P(u_i(t)=-1) \\ &= X_{0_i}\cdot P(u_i(t)=1) - X_{0_i}\cdot P(u_i(t)=-1) \\ &= X_{0_i}\cdot P(u_i(t)=1) - X_{0_i}(1-P(u_i(t)=1)) \\ &= X_{0_i}(2P(u_i(t)=1)-1)\end{aligned}$$

where X_{0i} indicates the magnitude of signal from time 0 to t at event i.

Now, analyze $P(u_i(t)=1)$:

$$\begin{aligned}P(u_i(t)=1) &= P(y_i(t)\geq 0) \\ &= P\left(\int_0^\infty \frac{1}{\tau_D} e^{-\lambda/\tau_D} z(t-\lambda)\,d\lambda \geq 0/i\right) \\ &= P\left(\int_0^\infty e^{-\lambda/\tau_D}(x(t-\lambda)+n(t-\lambda))d\lambda \geq 0/i\right), \\ &\quad \text{since } \tau_D > 0 \\ &= P\left(\int_0^\infty n(t-\lambda)\,e^{-\lambda/\tau_D}\,d\lambda \geq \right. \\ &\quad \left. -\int_0^\infty e^{-\lambda/\tau_D} x_i(t-\lambda)\,d\lambda/i\right)\end{aligned}$$

Now let

$$\begin{aligned}f_i(t) &= \int_0^\infty e^{-\lambda/\tau_D} x_i(t-\lambda)d\lambda \\ &= \int_0^t e^{-\lambda/\tau_D} x_{0_i}\,d\lambda \\ &\quad + \int_t^{t+T} e^{-\lambda/\tau_D} x_{-1_i}\,d\lambda + 0\end{aligned}$$

where x_{-1_i} indicates the magnitude of the signal from $-T$ to 0 at event i. Then solving for specific values of $f_i(t)$ yields:

$$\begin{aligned}f_1(t) &= V\tau_D(1-e^{-t/\tau_D}) + V\tau_D(e^{-t/\tau_D} - e^{-(t+T)/\tau_D}) \\ f_2(t) &= V\tau_D(1-e^{-t/\tau_D}) - V\tau_D(e^{-t/\tau_D} - e^{-(t+T)/\tau_D}) \\ f_3(t) &= -V\tau_D(1-e^{-t/\tau_D}) + V\tau_D(e^{-t/\tau_D} - e^{-(t+T)/\tau_D}) \\ f_4(t) &= -V\tau_D(1-e^{-t/\tau_D}) - V\tau_D(e^{-t/\tau_D} - e^{-(t+T)/\tau_D})\end{aligned}$$

Since

$$\int_0^\infty n(t-\lambda)\,e^{-\lambda/\tau_D}\,d\lambda$$

has Gaussian distribution with zero mean and $N_0\tau_D/4$ variance, then

$$P\left(\int_0^\infty n(t-\lambda)\,e^{-\lambda/\tau_D}\,d\lambda \geq -f_i(t)\right) = \frac{1}{2}\operatorname{erf}\left[f_i(t)\left(\frac{2}{N_0\tau_D}\right)^{1/2}\right] + \frac{1}{2}$$

This claim will be proved rigorously in Subsection C. At this point, it is observed that no closed-form expression could be obtained in evaluating $\operatorname{erf}[f_i(t)(2/N_0\tau_D)^{1/2}]$ as function of $R = V^2T/N_0$, P, and T_{SV}/τ_D. A computer program will be necessary to evaluate these functions. Now, average over all the conditional expected values to obtain $E[u(t)x(t)]$.

Conditional expected value for case i:

$$\zeta_i(t) = X_{0_i}[2P(u_i(t)=1)-1] = X_{0_i}\operatorname{erf}\left[f_i(t)\left(\frac{2}{N_0\tau_D}\right)^{1/2}\right]$$

$$h(t) = \Sigma_i\, q_i\, \zeta_i(t)$$

$$\begin{aligned}\alpha' = E[u(t)x(t)] &= \frac{1}{T}\int_0^T h(t)\,dt \\ &= \Sigma_i\, q_i \frac{x_{0_i}}{T}\int_0^T \operatorname{erf}\left[f_i(t)\left(\frac{2}{N_0\tau_D}\right)^{1/2} dt\right]\end{aligned} \quad (1)$$

We will now reformulate Eq. (1) in a more convenient form for computer solution:

$$\zeta_1 = \frac{V}{T}\int_0^T \operatorname{erf}\left[f_1(t)\left(\frac{2}{N_0\tau_D}\right)^{1/2}\right]dt$$

$$= \frac{V}{T}\int_0^T \operatorname{erf}\left\{\left[V\tau_D(1-e^{-t/\tau_D}) + V\tau_D(e^{-t/\tau_D} - e^{-(t+T)/\tau_D})\right]\frac{\sqrt{2}}{\sqrt{N_0\tau_D}}\right\}$$

Let

$$R = \frac{V^2T}{N_0}, \qquad \lambda = \frac{T}{\tau_D}$$

$$\zeta_1 = \frac{V}{T}\int_0^T \operatorname{erf}\left[\sqrt{\frac{V^2T}{N_0}}\cdot\frac{\sqrt{\tau_D}\sqrt{2}}{\sqrt{T}} \cdot (1 - e^{-t/\tau_D} + e^{-t/\tau_D} - e^{-(t+T)/\tau_D})\right]dt$$

$$\zeta_1 = \frac{V}{T}\int_0^T \operatorname{erf}\{\sqrt{2R\lambda^{-1}}\,[1 + e^{-t/\tau_D}(-1 + 1 - e^{-\lambda})]\}\,dt$$

Now let

$$\alpha_1 = \sqrt{2R\lambda^{-1}}$$

$$\beta_1 = -1 + 1 - e^{-\lambda}$$

$$u = e^{-t/\tau_D}$$

Then

$$\zeta_1 = \frac{V}{T}\int_0^T \operatorname{erf}(\alpha_1 + \alpha_1\beta_1 e^{-t/\tau_D})\,dt$$

$$= \frac{V}{T}\int_1^{e^{-\lambda}} \operatorname{erf}(\alpha_1 + \alpha_1\beta_1 u)\frac{du}{u}(-\tau_D)$$

$$= \frac{V}{\lambda}\int_{e^{-\lambda}}^1 \frac{\operatorname{erf}(\alpha_1 + \alpha_1\beta_1 u)}{u}\,du$$

The same procedures are used to obtain ζ_2, ζ_3, ζ_4 such that:

$$\alpha = \sum_{i=1,4} q_i\zeta_i \tag{2}$$

where

$$\zeta_i = \frac{V}{\lambda}\int_{e^{-\lambda}}^1 \frac{\operatorname{erf}(\alpha_i + \alpha_i\beta_i u)}{u}\,du, \qquad i = 2,3,4 \tag{3}$$

$$\alpha_2 = \sqrt{2R\lambda^{-1}}$$

$$\alpha_3 = \alpha_4 = -\sqrt{2R\lambda^{-1}}$$

$$\beta_2 = -1 - 1 + e^{-\lambda}$$

$$\beta_3 = 1 + 1 - e^{-\lambda}$$

$$\beta_4 = 1 - 1 + e^{-\lambda}$$

B. Analysis of Three-Symbol Periods (Two Traced Back)

After analyzing the initial condition as in Subsection A, the next step is to add one more symbol to be traced back. It is necessary to average the following eight cases whose probabilities of occurrences are P^3, $(1-P)P^2$, $P(1-P)P$, $(1-P)^2P$, $P^2(1-P)$, $(1-P)P(1-P)$, $P(1-P)^2$, and $(1-P)^3$:

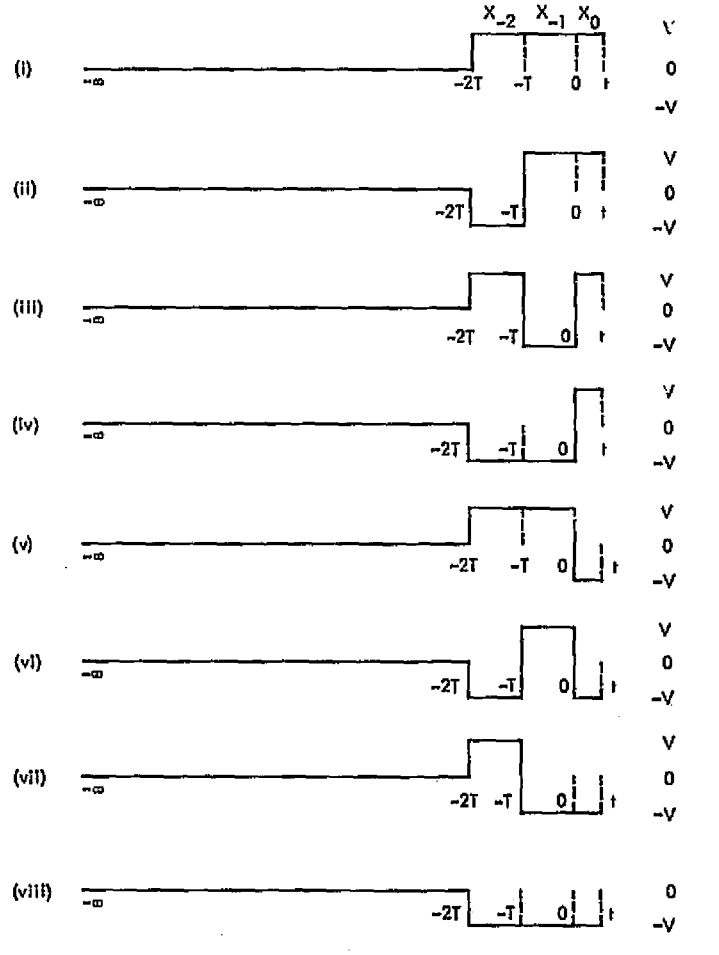

$$\zeta_1 = \frac{V}{T}\int_0^T \operatorname{erf}\left(f_1(t)\left(\frac{2}{N_0\tau_D}\right)^{1/2}\right) dt$$

$$f_1 = V\tau_D(1 - e^{-t/\tau_D}) + V\tau_D(e^{-t/\tau_D} - e^{-(t+T)/\tau_D}) + V\tau_D(e^{-(t+T)/\tau_D} - e^{-(t+2T)/\tau_D})$$

$$\zeta_1 = \frac{V}{T}\int_0^T \operatorname{erf}\sqrt{\frac{V^2T}{N_0}}\frac{\sqrt{\tau_D}\sqrt{2}}{\sqrt{T}} \cdot (1 - e^{-t/\tau_D} + e^{-t/\tau_D} - e^{-(t+T)/\tau_D} + e^{-(t+T)/\tau_D} - e^{-(t+2T)/\tau_D})\, dt$$

Letting $T/\tau_D = \lambda$,

$$\zeta_1 = \frac{V}{T}\int_0^T \operatorname{erf}\{\sqrt{2R\lambda^{-1}}\,[1 + e^{-t/\tau_D} \cdot (-1 + 1 - e^{-\lambda} + e^{-\lambda} - e^{-2\lambda})]\}\, dt$$

Let

$$\alpha_1 = \sqrt{2R\lambda^{-1}}$$

$$\beta_1 = -1 + 1 - e^{-\lambda} + e^{-\lambda} - e^{-2\lambda}$$

$$u = e^{-t/\tau_D}$$

Then,

$$\zeta_1 = \frac{V}{T}\int_0^T \operatorname{erf}(\alpha_1 + \alpha_1\beta_1 e^{-t/\tau_D})\, dt$$

$$= \frac{V}{T}\int_1^{e^{-\lambda}} \operatorname{erf}(\alpha_1 + \alpha_1\beta_1 u)\frac{du}{u}(-\tau_D)$$

$$= \frac{V}{\lambda}\int_{e^{-\lambda}}^1 \frac{\operatorname{erf}(\alpha_1 + \alpha_1\beta_1 u)}{u}\, du$$

The same procedures are applicable to obtain

$$\zeta_i = \frac{V}{\lambda}\int_{e^{-\lambda}}^1 \frac{\operatorname{erf}(\alpha_i + \alpha_i\beta_i u)}{u}\, du, \qquad i = 2,3,\cdots,8 \tag{4}$$

$$\alpha_1 = \alpha_2 = \alpha_3 = \alpha_4 = \sqrt{2R\lambda^{-1}}$$

$$\alpha_5 = \alpha_6 = \alpha_7 = \alpha_8 = -\sqrt{2R\lambda^{-1}}$$

$$\beta_2 = -1 + (1 - e^{-\lambda}) - (e^{-\lambda} - e^{-2\lambda})$$

$$\beta_3 = -1 - (1 - e^{-\lambda}) + (e^{-\lambda} - e^{-2\lambda})$$

$$\beta_4 = -1 - (1 - e^{-\lambda}) - (e^{-\lambda} - e^{-2\lambda})$$

$$\beta_5 = 1 + (1 - e^{-\lambda}) + (e^{-\lambda} - e^{-2\lambda})$$

$$\beta_6 = 1 + (1 - e^{-\lambda}) - (e^{-\lambda} - e^{-2\lambda})$$

$$\beta_7 = 1 - (1 - e^{-\lambda}) + (e^{-\lambda} - e^{-2\lambda})$$

$$\beta_8 = 1 - (1 - e^{-\lambda}) - (e^{-\lambda} - e^{-2\lambda})$$

Continue this iteration process by adding more symbols to be analyzed. A computer program was written which shows $E[u(t)\,x(t)]$ converges very rapidly. Thus, an accurate solution could be obtained with the two or three symbols traced back.

C. Proof of the Claim

Statement of the claim:

$$\int_0^\infty n(t-\lambda)\, e^{-\lambda/t_D}\, d\lambda$$

has Gaussian distribution with zero mean and $N_0\tau_D/4$ variance knowing that $E\{n(t)\} = 0$ and autocorrelation function of $n(t) = (N_0/2)\delta(\tau)$.

Proof:

$$E\left[\int_0^\infty n(t-\lambda)\, e^{-\lambda/\tau_D}\, d\lambda\right] = \int_0^\infty E[e^{-\lambda/\tau_D}\, n(t-\lambda)]\, d\lambda = \int_0^\infty e^{-\lambda/\tau_D}\, E[n(t-\lambda)]\, d\lambda = \int_0^\infty e^{-\lambda/\tau_D} \cdot 0\, d\lambda = 0$$

Variance of

$$\left[\int_0^\infty n(t-\lambda)\, e^{-\lambda/\tau_D}\, d\lambda\right] = E\left[\int_0^\infty e^{-\lambda/\tau_D}\, n(t-\lambda)\, d\lambda \int_0^\infty e^{-\beta/\tau_D}\, n(t-\beta)\, d\beta\right] = \int_0^\infty \int_0^\infty e^{-\lambda/\tau_D}\, e^{-\beta/\tau_D}\, E[n(t-\lambda)\, n(t-\beta)]\, d\lambda d\beta$$

$$= \int_0^\infty \int_0^\infty e^{-\lambda/\tau_D} e^{-\beta/\tau_D} \cdot \frac{N_0}{2} \delta(\beta - \lambda)\, d\lambda d\beta$$

$$= \int_0^\infty e^{-\beta/\tau_D} \left[\int_0^\infty e^{-\lambda/\tau_D} \frac{N_0}{2} \delta(\beta - \lambda)\, d\lambda \right] d\beta$$

$$= \int_0^\infty e^{-\beta/\tau_D} \left(\frac{N_0}{2} e^{-\beta/\tau_D} \right) d\beta$$

$$= \frac{N_0}{2} \frac{\tau_D}{2} e^{-2\beta/\tau_D} \Big|_0^\infty = \frac{N_0 \tau_D}{4}$$

so

$$n(t) = \int_0^\infty e^{-\lambda/\tau_D} n(t - \lambda)\, d\lambda \qquad \epsilon n\left(0, \frac{N_0 \tau_D}{4}\right)$$

D. Find Probability That $n(t) \geq -f_i(t)$

$$P(n(t) \geq -f_i(t)) = \int_{-f_i(t)}^\infty \frac{e^{-x^2} \Big/ \left(2 \cdot \frac{N_0 \tau_D}{4}\right)}{\sqrt{2\pi \frac{N_0 \tau_D}{4}}}\, dx$$

$$= \int_{-f_i(t)}^\infty \frac{e^{-x^2} \Big/ \left(\frac{N_0 \tau_D}{2}\right)}{\sqrt{\frac{\pi N_0 \tau_D}{2}}}\, dx - (A)$$

Let

$$y^2 = \frac{X^2}{\frac{N_0 \tau_D}{2}}$$

$$y = \sqrt{\frac{2}{N_0 \tau_D}}\, x$$

$$dy = \sqrt{\frac{2}{N_0 \tau_D}}\, dx$$

$$(A) = \int_{-f_i(t)\,(2/N_0\tau_D)^{1/2}}^\infty e^{-y^2} \cdot \sqrt{\frac{2}{N_0 \tau_D}} \cdot \sqrt{\frac{\pi N_0 \tau_D}{2}}\, dy$$

$$= \frac{1}{\sqrt{\pi}} \int_{-f_i(t)\,(2/N_0\tau_D)^{1/2}}^\infty e^{-y^2} dy$$

$$= \frac{1}{\sqrt{\pi}} \int_{-f_i(t)\,(2/N_0\tau_D)^{1/2}}^0 e^{-y^2}\, dy + \frac{1}{\sqrt{\pi}} \int_0^\infty e^{-y^2}\, dy$$

$$= \frac{1}{2} \operatorname{erf}\left\{ [f_i(t)] \left(\frac{2}{N_0 \tau_D}\right)^{1/2} \right\} + \frac{1}{2}$$

IV. Results/Discussion

Using the iteration process discussed in Subsections III-A and III-B, we obtain the data limiter suppression factor averaging over three symbols as follows:

$$\alpha' = E\{u(t) \cdot x(t)\} = \sum_{i=1}^{16} q_i \xi_i \tag{5}$$

where

q_i = probability of the ith event

$$\xi_i(t) = \frac{V}{\lambda} \int_{-\lambda}^{1} \frac{\operatorname{erf}(\alpha_i + \alpha_i \beta_i u)}{u}\, du \tag{6}$$

$\lambda = T_{SY}/\tau_D$

$V = 1$

U = variable of integration

$q_1 = P^3$; $q_2 = P^2(1 - P)$; $q_3 = q_2$; $q_4 = P^2(1 - P)^2$;

$q_5 = q_2$; $q_6 = q_4$; $q_7 = q_4$; $q_8 = (1 - P)^3 P$; $q_9 = -q_2$;

$q_{10} = -q_4$; $q_{11} = -q_4$; $q_{12} = -q_8$; $q_{13} = -q_4$;

$q_{14} = -q_8$; $q_{15} = -q_8$; $q_{16} = (1 - P)^4$

where

P = data transition probability

α_1 thru $\alpha_8 = \sqrt{2R\lambda^{-1}}$

α_9 thru $\alpha_{16} = -\sqrt{2R\lambda^{-1}}$

$\beta_1 = [-1 + D1 + D2 + D3] \cdot A$

$\beta_2 = [-1 + D1 + D2 - D3] \cdot A$

$\beta_3 = [-1 + D1 - D2 + D3] \cdot A$

$\beta_4 = [-1 + D1 - D2 - D3] \cdot A$

$\beta_5 = [-1 - D1 + D2 + D3] \cdot A$

$\beta_6 = [-1 - D1 + D2 - D3] \cdot A$

$\beta_7 = [-1 - D1 - D2 + D3] \cdot A$

$\beta_8 = [-1 - D1 - D2 - D3] \cdot A$

$\beta_9 = [1 + D1 + D2 + D3] \cdot A$

$\beta_{10} = [1 + D1 + D2 - D3] \cdot A$

$\beta_{11} = [1 + D1 - D2 + D3] \cdot A$

$\beta_{12} = [1 + D1 - D2 - D3] \cdot A$

$\beta_{13} = [1 - D1 + D2 + D3] \cdot A$

$\beta_{14} = [1 - D1 + D2 - D3] \cdot A$

$$\beta_{16} = [1 - D1 - D2 + D3] \cdot A$$

$$\beta_{16} = [1 - D1 - D2 - D3] \cdot A$$

where

$$A = \sqrt{2R\lambda^{-1}}$$

$$D1 = 1 - \mathrm{EXP}(-\lambda)$$

$$D2 = \mathrm{EXP}(-\lambda) - \mathrm{EXP}(-2\lambda)$$

$$D3 = \mathrm{EXP}(-2\lambda) - \mathrm{EXP}(-3\lambda)$$

The validity of averaging over only three symbols to calculate the data suppression was investigated with a computer program which calculated the α' averaging over one symbol, two, or three successive symbols. As can be seen from Table 1a, the result converges rapidly for averaging over three symbols when T_{SY}/τ_D is 3. Although not presented, a similar test was made for T_{SY}/τ_D in the range 3 through 12 and probability of transitions over the entire range possible. Over these values, the data suppression factor as expressed in Eqs. (5) and (6) quickly converges, thus averaging over three symbols is sufficient. It should be noted that the results of Eqs. (5) and (6) become less accurate for T_{SY}/τ_D values of less than 3 due to greater filter "memory."

The effect of varying the T_{SY}/τ_D ratio for a 50% probability of data transition is shown in Table 1b and plotted on Fig. 4 for varying values of the data filter input symbol energy to noise spectral density (ST_{SY}/N_0). The data limiter suppression factor as plotted in Fig. 4 compares quite well with results published in Ref. 1.

Variations in α' as a function of transitional probabilities (P) are shown in Fig. 5. We see that pronounced changes in the data suppression factor for a constant T_{SY}/τ_D ratio and signal-to-noise ratio occur at very low (20%) or very high (80%) values of the transition probability. Since the Mariner Jupiter/Saturn (MJS) mission will be using data rates with transitional probabilities of 30 to 80%, this result is clearly important.

Finally, Subcarrier Demodulator Assembly (SDA) degradation for various T_{SY}/τ_D ratios occurring with BLK III/IV SDA designs (see Tables 2 and 3), transitional probabilities, and a fixed ST_{SY}/N_0 of 10 dB is examined using an SDA degradation model developed by Lesh (Ref. 2). These results are shown in Fig. 6. A symbol rate of 8.33 was used with a wide (BLK IV) SDA bandwidth. SDA degradation changes of greater than 0.1 dB can result for varying probabilities of transition.

Acknowledgment

The approach used was suggested by James Lesh.

References

1. Brockman, M. H., "An Efficient and Versatile Telemetry Subcarrier Demodulation Technique for Deep Space Telecommunication," presented at the 4th Hawaii International Conference on System Science, Jan. 1971.

2. Lesh, J., "A Re-Examination of Subcarrier Demodulation Performance," in *The Deep Space Network Progress Report*, Technical Report 32-1526, Vol. XVII, pp. 137–144, Jet Propulsion Laboratory, Pasadena, Calif., Oct. 15, 1973.

Table 1. Table of suppression factor $E(u(t)x(t))$

Number of symbols being traced back	P	ST_{SY}/N_0, dB			
		−5	0	5	10
(a) $\lambda = T_{SY}/\tau_D = 3$					
1	0 or 1	0.47723	0.74420	0.95665	0.99967
2	0 or 1	0.48355	0.75142	0.95981	0.99974
3	0 or 1	0.48386	0.75177	0.95956	0.99974
1	0.5	0.33380	0.52830	0.70280	0.76276
2	0.5	0.33379	0.52827	0.70279	0.76285
3	0.5	0.33379	0.52827	0.70279	0.76285
1	0.2	0.38543	0.60603	0.79419	0.84804
2	0.2	0.38770	0.60860	0.79531	0.84813
3	0.2	0.38782	0.60873	0.79537	0.84813
(b) $\lambda = 6$					
3	0 or 1	0.35387	0.58578	0.85349	0.99018
3	0.5	0.29572	0.49181	0.72559	0.86038
3	0.2	0.31665	0.52564	0.77163	0.90711
(c) $\lambda = 12$					
3	0 or 1	0.25457	0.43630	0.69543	0.93211
3	0.5	0.23348	0.40060	0.64061	0.86539
3	0.2	0.24107	0.41345	0.66035	0.88941

Table 2. Data symbol rate selection (BLK III)

	$1/T_{SY}$, symbols/s	B_{IF}(data), Hz	G_{IF}(dist), dB	G_{IF}(WB), dB	T_{dot}, ms	T_{out}, ms
1	Future	Blank	7	44	Blank	Blank
2	5.6–12	500	14	37	39	1800
3	12–27	500	14	37	18	820
4	27–56	500	14	37	8.1	390
5	56–120	5000	20	31	3.9	180
6	120–270	5000	20	31	1.8	82
7	270–560	5000	20	31	0.81	39
8	560–1200	50K	27	24	0.39	18
9	1200–2700	50K	27	24	0.18	8.2
10	2700–5600	50K	27	24	0.081	3.9
11	5600–12K	500K	35	16	0.039	
12	12K–27K	500K	35	16	0.018	
13	27K–56K	500K	35	16	0.0081	
14	56K–120K	3M	45	6	0.0039	
15	120K–270K	3M	45	6	0.0018	

Table 3. Data symbol rate selection (BLK IV)

	$1/T_{SY}$, symbols/s	Quad gen gain, dB	Select BW filter		τ_{det}, ms	τ_{out}, ms
			Gain, dB	BW_{IF}, kHz		
1	5.6–11.9	11	36	1.03	47.5	1800
2	12–26.9	11	36	1.03	22.1	820
3	27–55.9	11	36	1.03	10.0	390
4	56–99.9	11	36	1.03	4.75	180
5	100–219	22	25	11.9	2.21	180
6	220–479	22	25	11.9	1.00	180
7	480–999	22	25	11.9	0.475	180
8	1.00K–2.19K	29	18	49.5	0.221	180
9	2.20K–4.79K	29	18	49.5	0.100	180
10	4.80K–9.99K	36	11	209	0.0475	180
11	10.0K–21.9K	36	11	209	0.0221	180
12	22.0K–47.9K	42	5	1020	0.0100	180
13	48.0K–99.9K	42	5	1020	0.00475	180
14	100.0K–219.K	47	0	5000	0.00221	180
15	220.K–500.K	47	0	5000	0.00100	180

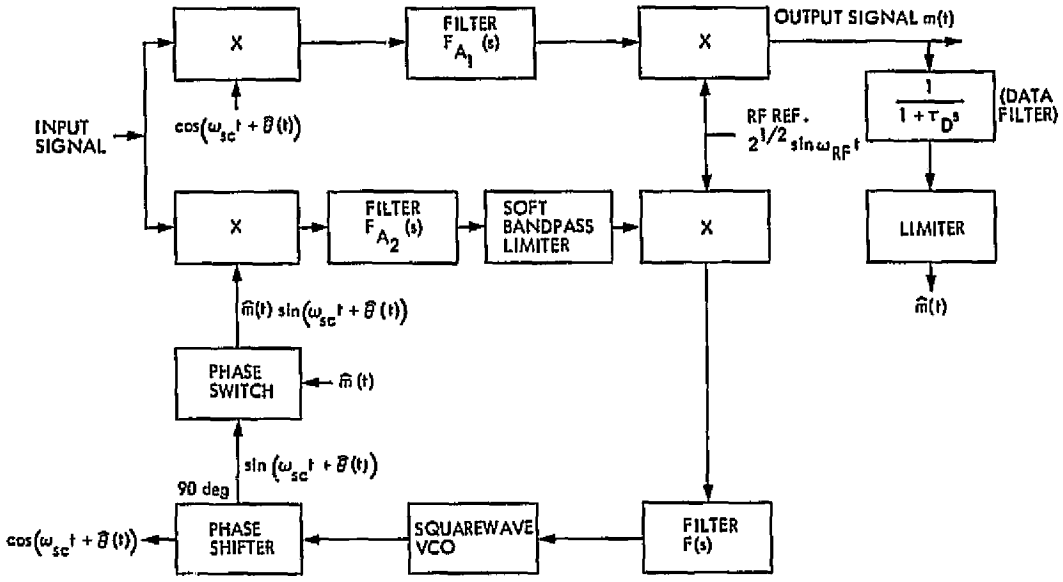

Fig. 1. Functional block diagram of telemetry subcarrier demodulator (BLK III)

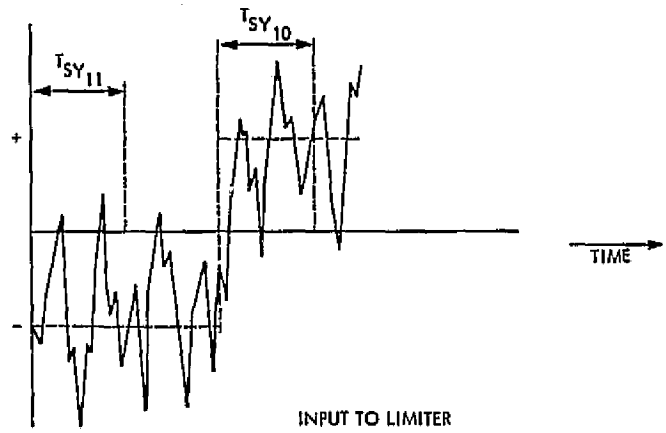

Fig. 2. Limiter input and output waveforms

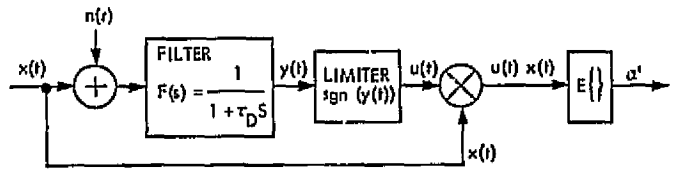

Fig. 3. Model of problem being examined

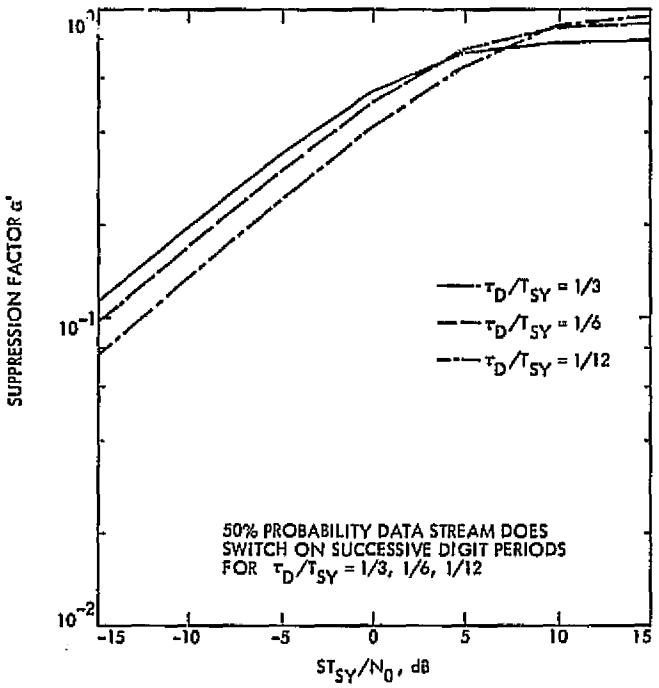

Fig. 4. MMTS subcarrier demodulator suppression factor vs ratio of signal energy per symbol to noise spectral density

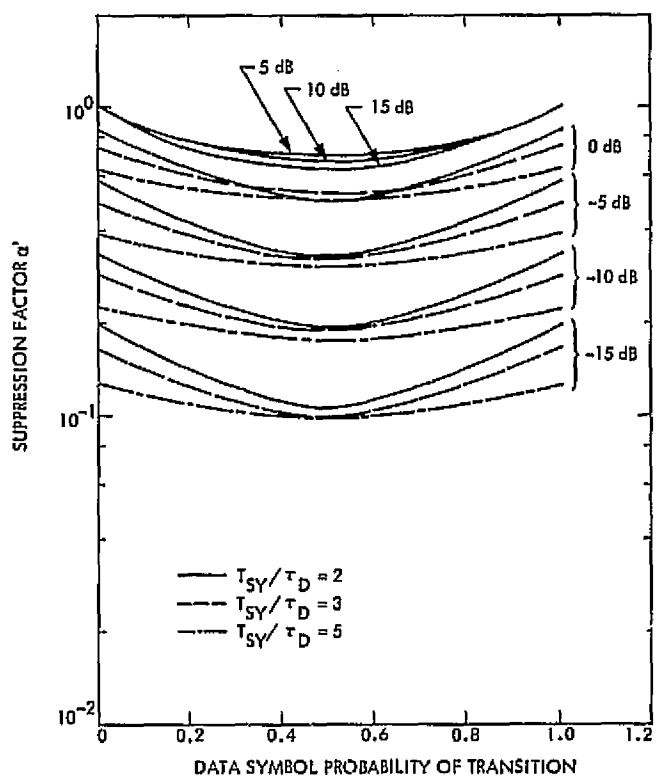

Fig. 5. Data suppression factor vs data symbol probability of transition

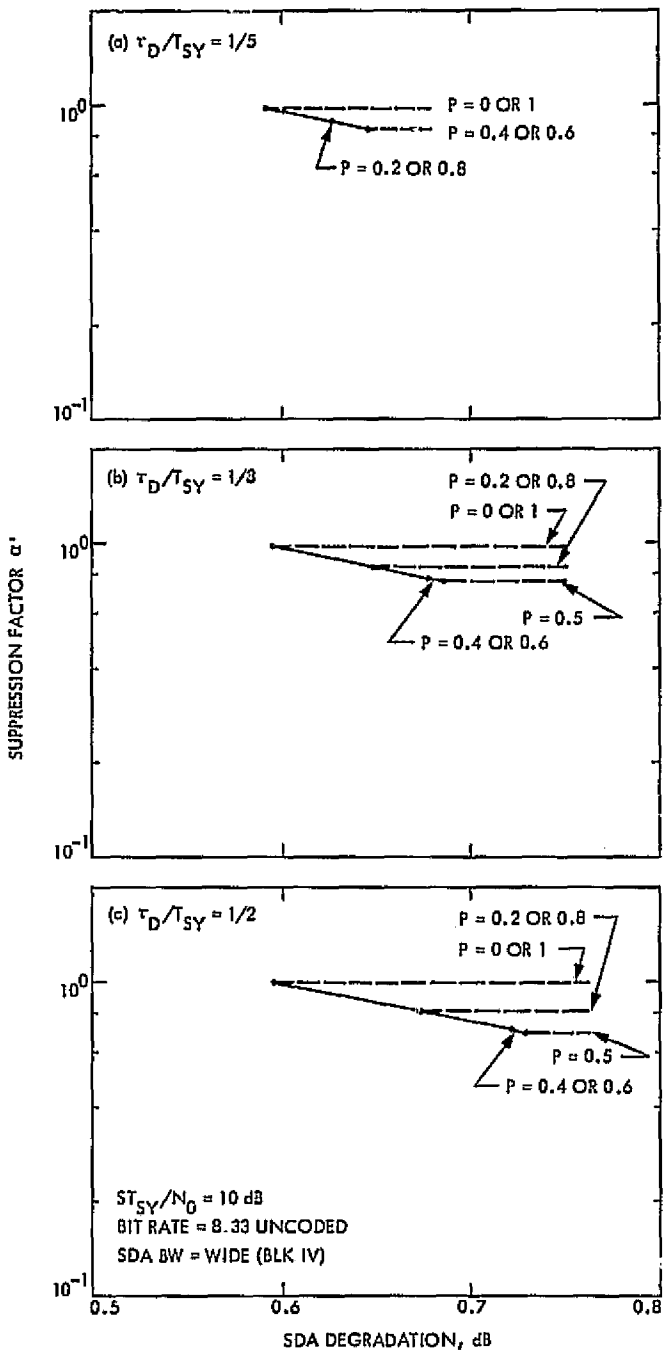

Fig. 6. BLK IV SDA model sensitivity to α' suppression factor and τ_D/T_{SY} variations

Appendix

The following analysis yields the data suppression factor α' for the special cases where the incoming signal is all 1 or all -1. Suppression factors thus obtained should agree with those of probability of transition equal to 0 or probability of transition equal to 1.

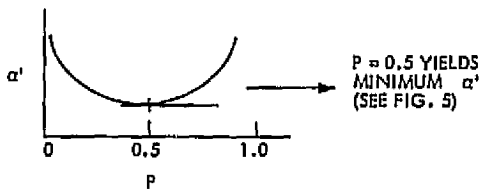

Assume incoming signal is all -1:

$$E(u(t)\,x(t)) = -VP\{u(t)=1\} + (-V)(-1)\,P\{u(t)=-1\}$$

$$= -VP\{u(t)=1\} + V[1 - P\{u(t)=1\}]$$

$$= -V[2P\{u(t)=1\} - 1]$$

$$P\{u(t)=1\} = P\{y(t)\geq 0\}$$

$$= P\left\{\int_0^\infty \frac{1}{\tau_D} e^{-\lambda/\tau_D}\,[x(t-\lambda) + n(t-\lambda)]\,d\lambda \geq 0\right\}$$

$$= P\left\{\int_0^\infty e^{-\lambda/\tau_D}\,n(t-\lambda)\,d\lambda \geq -\int_0^\infty e^{-\lambda/\tau_D}(-V)\,d\lambda\right\} \text{ (since } \tau_D \geq 0\text{, incoming signal is } -V)$$

$$= P\left\{\int_0^\infty e^{-\lambda/\tau_D}\,n(t-\lambda)\,d\lambda \geq V\tau_D\right\}$$

Since

$$n(t) = \int_0^\infty e^{-\lambda/\tau_D}\,n(t-\lambda)\,d\lambda \in n\left(0, \frac{N_0\tau_D}{4}\right)$$

so

$$P\{n(t)\geq V\tau_D\} = \int_{V\tau_D}^\infty \frac{e^{-x^2}\Big/\left(2\dfrac{N_0\tau_D}{4}\right)}{\sqrt{2\pi\dfrac{N_0\tau_D}{4}}}\,dx - (B)$$

Let

$$y^2 = \frac{X^2}{\dfrac{N_0\tau_D}{2}}$$

$$y = \sqrt{\frac{2}{N_0 \tau_D}}\, x$$

$$dy = \sqrt{\frac{2}{N_0 \tau_D}}\, dx$$

$$(B) = \int_{V\tau_D(2/N_0\tau_D)^{1/2}}^{\infty} \frac{e^{-y^2}\sqrt{2}}{\sqrt{\pi N_0 \tau_D}}\, dy \sqrt{\frac{N_0\tau_D}{2}}$$

$$= \frac{1}{\sqrt{\pi}} \int_{V(2\tau_D/N_0)^{1/2}}^{\infty} e^{-y^2}\, dy$$

$$= \frac{1}{2}\left(\frac{2}{\sqrt{\pi}} \int_0^{\infty} e^{-y^2}\, dy - \frac{2}{\sqrt{\pi}} \int_0^{V(2\tau_D/N_0)^{1/2}} e^{-y^2}\, dy\right)$$

$$= \frac{1}{2}\left[1 - \operatorname{erf}\left(V\sqrt{\frac{2\tau_D}{N_0}}\right)\right]$$

so

$$E(u(t)\,x(t)) = -V\left\{2 \cdot \frac{1}{2}\left[1 - \operatorname{erf}\left(V\sqrt{\frac{2\tau_D}{N_0}}\right)\right] - 1\right\}$$

$$= V \operatorname{erf}\left(V\sqrt{\frac{2\tau_D}{N_0}}\right)$$

$$= V \operatorname{erf}\left(V\sqrt{\frac{V^2 T}{N_0}} \cdot \frac{\sqrt{2\tau_D}}{V\sqrt{T}}\right); \qquad \text{let } \lambda = \frac{T}{\tau_D}$$

$$= V \operatorname{erf}\left(\sqrt{\frac{2R}{\lambda}}\right)$$

Network Control System Project Block III Software

S. E. Friesema, J. Blackstock, T. Gee, N. Hammerwold,
A. Irvine, N. Larson, and J. Williams
DSN Data Systems Development Section

The Network Control System (NCS) Project is responsible for the software implementation of the Network Operations Control Center (NOCC) Block III system. This involves the programming for a twenty-one computer distributed network (including on-line spares). This system is presently in a three-phase development plan. Phases I and II are currently designed and coding is in progress. Phase III requirements are being reviewed with respect to Phase I and II capabilities and NCS manpower availability. NOCC operational testing for Phases I and II will begin in September 1975, with final transfer to DSN operations Feb. 1, 1976. NOCC Phase III is tentatively scheduled for transfer to DSN operations on 1 July, 1976

I. Introduction

The Network Control System (NCS) software development is divided into three major implementations: Block I, Block II, and Block III. This report will summarily describe the software implementation elements and status for NCS Block III.

The NCS Block III is an 18-computer distributed system. There are additionally three controller and preprocessor computers utilized as part of larger computer subsystems. The NCS Block III System is being implemented to:

(1) Receive and provide accountability for high-speed data blocks (HSDBs) transmitted by Deep Space Stations (DSSs) to JPL.

(2) Transmit and display command data utilized in the configuration and control of DSSs.

(3) Generate, format, and transmit to selected DSSs:

  (a) Sequence of Events (SOE) files

  (b) Seven-day schedules

  (c) Radio-metric predict data

  (d) Telemetry predict data

  (e) Test data

  (f) Data recall control messages

(4) Provide printer dump of selected data being transmitted by the DSSs to JPL and from NCS to

the DSSs. This includes wideband data being received in either 1200- or 2400-bit block size.

(5) Provide sufficient HSDB analysis to assure meaningful displays for operational support in the areas of telemetry, tracking, command, and monitor.

(6) Provide operational status of the NCS to a level that will readily identify major system operational problems.

(7) Provide flight projects with an intermediate data record (IDR) tape. This tape should contain a merged file of the maximum number of useable HSD/wideband data (WBD) blocks recoverable by the DSN.

(8) Provide fast subsystem recovery by means of on-line spare processors.

The NCS Block III functional configuration is shown by the simplified block diagram in Fig. 1. The following paragraphs describe briefly the software for each of the major functional subsystems. The only exception to this is in the real-time monitor (RTM) area. Rather than presenting a summary of each monitoring application, the general software structure for the RTMs as a group is presented. For a more detailed description of the NCS hardware configuration see Ref. 1.

II. NCS Communication Log Processor and Network Control Processor

Control of the communication log processor (CLP)/network control processor (NCP) subsystems is accomplished through hardware-generated interrupts and operator control inputs (OCI) (Figs. 2, 3). At the completion of each data block transfer, either input or output, an interrupt is generated. This interrupt causes control to be transferred to the proper input/output (I/O) handler, either comm buffer handler, star switch controller (SSC) handler, terminet handler, magnetic tape (MT) label printer handler, MT handler, or disk handler. The I/O handler performs the proper processing, and if necessary, places the data block on queue to one of the internal subroutines or to another I/O handler. Input of an OCI by the operator may cause a change in the control of the program, such as a request to cease reading an input data line or cease outputting over a particular SSC path.

All input data blocks are received by the comm buffer handler or the SSC handler. They are then queued to the routing module. The routing module compares the information contained in the GCF header with the data contained in the proper routing table to obtain an output line number, or numbers. The data block, along with the output line numbers, is then queued to the proper handler, or handlers, for output. When an OCI is input by the operator it is queued to the OCI processor module, which takes the necessary action to complete the request.

The interface between the CLP and NCP subsystems is the HSD traffic, which has originated outside either subsystem and is routed by both to the proper destination. In only one case is a control message generated by one subsystem with the other subsystem as the destination. This is the case where the backup CLP has been changed to the prime CLP by operator input. In this case the CLP sends a control message, in HSDB format, to the NCP for it to become the prime NCP.

III. NCS Display Processor

The display subsystem operates in the Network Operations Control Area (NOCA) of Bldg. 230. Its purpose is to provide a centrally controlled facility for displaying data for the Network Operations Control Center (NOCC), and for receiving and processing operator control inputs to direct NOCC operation. Additionally, the display subsystem accepts bulk data, which it prints, or transmits to the Network Data Processing Area (NDPA) in Bldg. 202 (Fig. 4).

A. Displays

Up to 46 digital TV (DTV) display devices are driven at the NOCA. Of these, up to 31 are slave units, and up to 15 are master units with numeric keyboard for display channel selection. The DTV screen is logically divided into quadrants, each quadrant individually assignable to any defined display format. In addition to the DTVs, there are three CRT display devices, each with a display capability of two pages, where a CRT page equals a DTV quadrant in terms of display capacity. A subset of the display subsystem software resides in each other minicomputer subsystem of NOCC that has a local cathode-ray tube/keyboard (CRT/KB) display capability as backup.

B. Operator Control Inputs

OCI's are entered from the CRT/KB alphanumeric keyboard. The OCIs are validated at NOCA, and illegal entries are rejected with a response. OCI prompting is available to assist the operator. OCI's that pass NOCA validation are encoded for wideband data line (WBDL) transmission to Network Data Processing Area (NDPA). A subset of the OCI software resides in each other

minicomputer subsystem of the NCS that has a local CRT/KB display as backup.

C. Bulk Data

Prestored bulk data can be entered from the card reader, and acted upon as prestored OCIs, or as data for transmission to the NDPA. Additionally, bulk data received from the NDPA can be printed at the NOCA. The Network Operations Control Area also prints a log of system events, OCIs, responses, and system status on separate printers.

IV. NCS Real-Time Monitors

In order to support all of the software functions required of a real-time monitor (RTM) operating within the NOCC, we have identified the areas of commonality within each RTM and assigned the responsibility of interface/design and implementation to people who are not programming each RTM applications module. This approach frees the applications programmers of common supporting activities and eliminates multiple designs of the same logical function. The end result is a series of stand-alone products which have been modularly developed (Fig. 5).

All data arriving at an RTM consists of two types: (1) DSS originated or (2) Intra-NOCC data (a single exception to this is Ground Communication Facility (GCF) monitor-originated status which is sent to the monitor RTM for status processing). The GCF handler is responsible for bringing the data, in the form of 1200 or 2400 bit data blocks, into I/O buffers allocated by the application. Deep Space Station-originated data are queued directly for application processing while intra-NOCC data are queued for further analysis by the preprocessor routine. The preprocessor uses information contained in the GCF header to route the data to the proper routine by queueing the data onto one of several queues which have been defined by the application. The application module performs the required analysis of DSS-originated data, using the services of the high-speed data block (HSDB) reformatter to extract and realign the data as received for ease of processing. It then saves the extracted data in its subsystem control and data tables for further use and for subsequent display. Incoming data are also used to update the system performance record (SPR)/network performance record (NPR) (monitor RTM only), which is written to disk by the SPR control processor when full. Both the application and the HSDB validation and accountability routines add to the GAP list when block sequence anomalies occur. The GAP list is also maintained on disk by the SPR control processor. At operator request or when the SPR/NPR or GAP list on the disk is nearly full, the SPR despool processor will be advised to begin transferral of the data to the NC support subsystem. This is done by acquiring a 2400-bit I/O buffer and reading the accumulated SPR/NPR or GAP list data from the disk into the buffer and queueing the buffer for transmission, via the GCF handler, when it is full.

OCI's entered locally are validated and reformatted by the operator communications processor, and are queued for processing by the application. When the application has completed its processing, the response indicated by the application is returned to the CRT/KB terminal from which the OCI was issued to complete the processing.

Asynchronous to other processing, the display preparation processor can be preparing a new display in response to a request from the display processor or preparing an update to an active format which is being displayed locally or remotely in the NOCA. To do this, the routine draws upon the data contained in the display data table and the format control table employing the services of the applications display address resolution routine to access the data contained in the subsystem control and data tables. If the data is to be displayed remotely, the accumulated data is packed into 2400-bit I/O buffers and queued for transmission to the display computer via the GCF handler.

V. NCS Support Processor

The Network Control Support Subsystem (NCSS) is required to perform the non-real time functions of five subsystems as well as its own tasks. The non-real time programs common to those subsystems can be generally categorized as:

(1) File extraction and HSD output

(2) SPR/NPR data extraction and recording

(3) Standards and limits generation

(4) Predicts generation

(5) System analysis

The NCSS program shall operate in a multi-use environment in that it will have the capability to operate in several different modes as it services the needs of the different subsystems. (Fig. 6).

(1) Batch mode. In this mode the NCSS will operate in a non-real time computational manner. Such func-

tions as sequence of events and tracking predictions shall be performed in this mode.

(2) Demand-responsive mode. The NCSS shall be capable of a dialog with an end-user. Such functions as standards and limits (S&L) update shall be performed in this mode.

(3) Near-real time mode. The NCSS shall be capable of responding to specific stimuli and provide controller responses under clock impulse. Such functions as the transmittal of HSDBs shall be performed in this mode.

(4) Development mode. The NCSS shall provide resources to develop and test programs for the entire NCS in a limited mode.

(5) Test mode. The NCSS shall be able to operate in a limited test mode.

The NCSS program shall operate asynchronously with respect to the NCS except at those times when it is called upon to act in a near-real time or demand-responsive mode. This means that events represented by messages from all data paths, including peripherals, shall be scheduled. Action shall be deferred until such time as the proper resources can be applied to servicing such events. Events shall be acted upon at some time later than their time of entry into the environment of the NCSS.

VI. NCS Data Records Processor

The functions of the data records processor (DRP) (Fig. 7) are primarily the following:

(1) The recall of the data from a DSS based upon a gap list received either from operator entry at the DRP (manual mode) or from the Support Computer (automatic mode).

(2) The generation of either an intermediate data record (IDR) or a fill data tape by combining a network data log (NDL) and a recall data tape.

(3) The replay of an NDL to a real-time monitor (RTM).

The transmission of data between the DRP and the Deep Space Stations, Support processor or an RTM will utilize the star handler and the buffer queueing/dequeueing common software. Operator inputs (OCIs) to initialize and/or control the functions within the DRP will utilize the OCI handler common software package. Any status or alarm messages generated by the above functions will be output to the CRT/KB display and will interface with the display handler, also a common software module.

The three prime functions run independentally of each other. Function (1) is activated upon receipt of an OCI or a gap list message from the support processor. Its output is the recall data tape. Function (2) takes this tape along with the NDL from the communications log processor (CLP) and combines them to produce either an IDR or a fill data tape. The last function causes an NDL to be replayed to an RTM at a selectable rate.

VII. NCS Test and Training Processor

The test and training Subsystem (TTS) provides test support to all of the subsystems within the Network Control System (NCS) and to the Deep Space Station (Fig. 8).

High-speed data blocks (HSDBs) or wide-band data blocks (WBDBs) will be created from card input. These blocks will be output through the star switch controller (SSC) by the GCF handler at timed intervals. These blocks will also be saved on magnetic tape or disk if requested. The created test blocks may be modified at any time by OCI or card input.

HSD or WBD blocks destined for other systems may also be switched to the TTS by the SSC. These blocks will be put into the HSDB queue by the GCF handler. They will then be written onto magnetic tape for later test transmission.

HSD or WBD blocks may also be input from previously recorded magnetic tapes. These blocks will be interrogated and the ones specified (by OCI) will be output through the SSC by the GCF handler. The TTS will process up to six streams defined by one or all of the following parameters: source code, destination code, spacecraft number, user-dependent type code, and data-dependent type code.

VIII. NCS Block III Software Status

The NCS Block III software development is divided into three phases:

(1) Phase I Development, complete Sept. 1, 1975. This phase includes the basic capabilities to receive, log, recall, and merge DSS data blocks.

(2) Phase II Development, complete Dec. 1, 1975. This phase meets all the basic capabilities listed in the introduction.

(3) Phase III Development, complete approximately July 1, 1976. Refinements to allow more efficient control as well as increased status visibility will be

incorporated in this phase. Lower priority functions and approved operational change requests will be implemented as manpower and operations permit.

Presently a large portion of the systems software development is being consumed in the new interface (hardware and software) integration. Due to the relatively large number of newly developed interface assemblies as well as new vendor-developed handlers, the system integration has been delayed. It is anticipated that problems will be corrected and the scheduling will be met for NCS Block III.

Reference

1. Petrie, R. G., "NCS Minicomputer Systems Status Report," in *The Deep Space Network Progress Report 42-22*, pp. 152–159. Jet Propulsion Laboratory, Pasadena, Calif., Aug. 15, 1974.

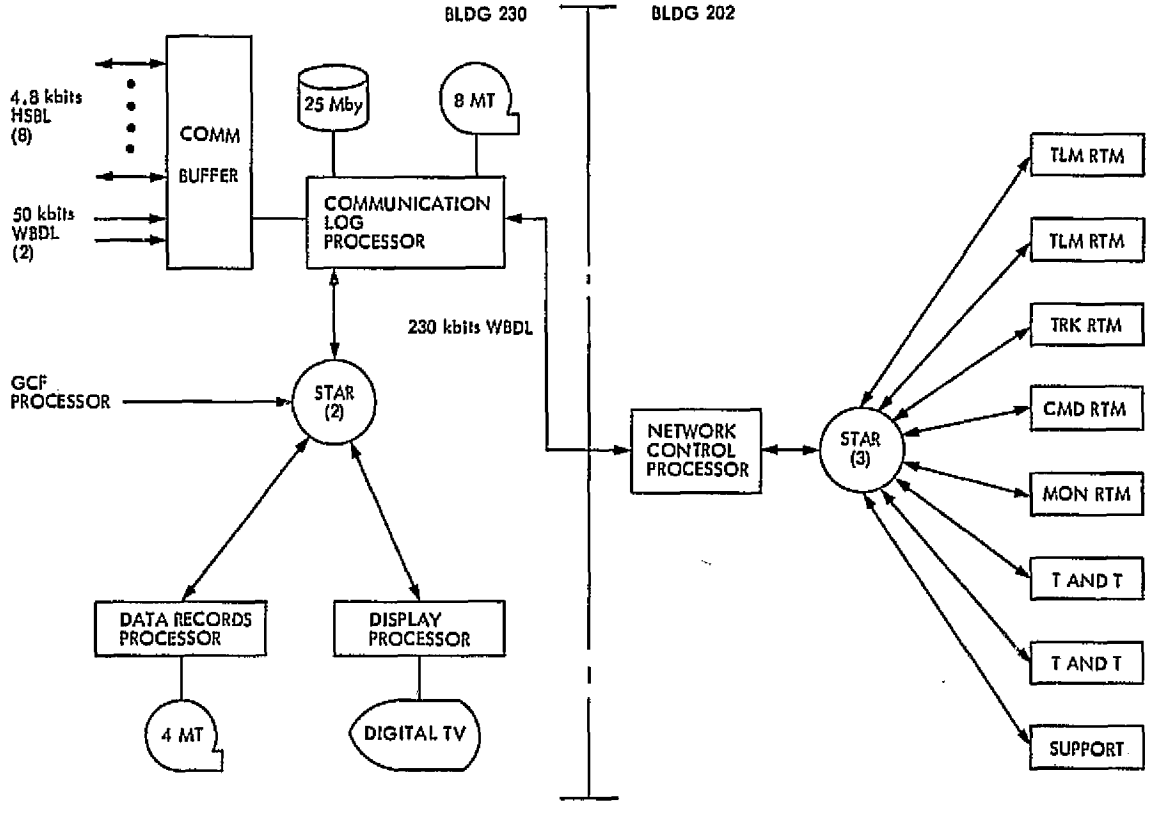

Fig. 1. Network Control System Block III configuration

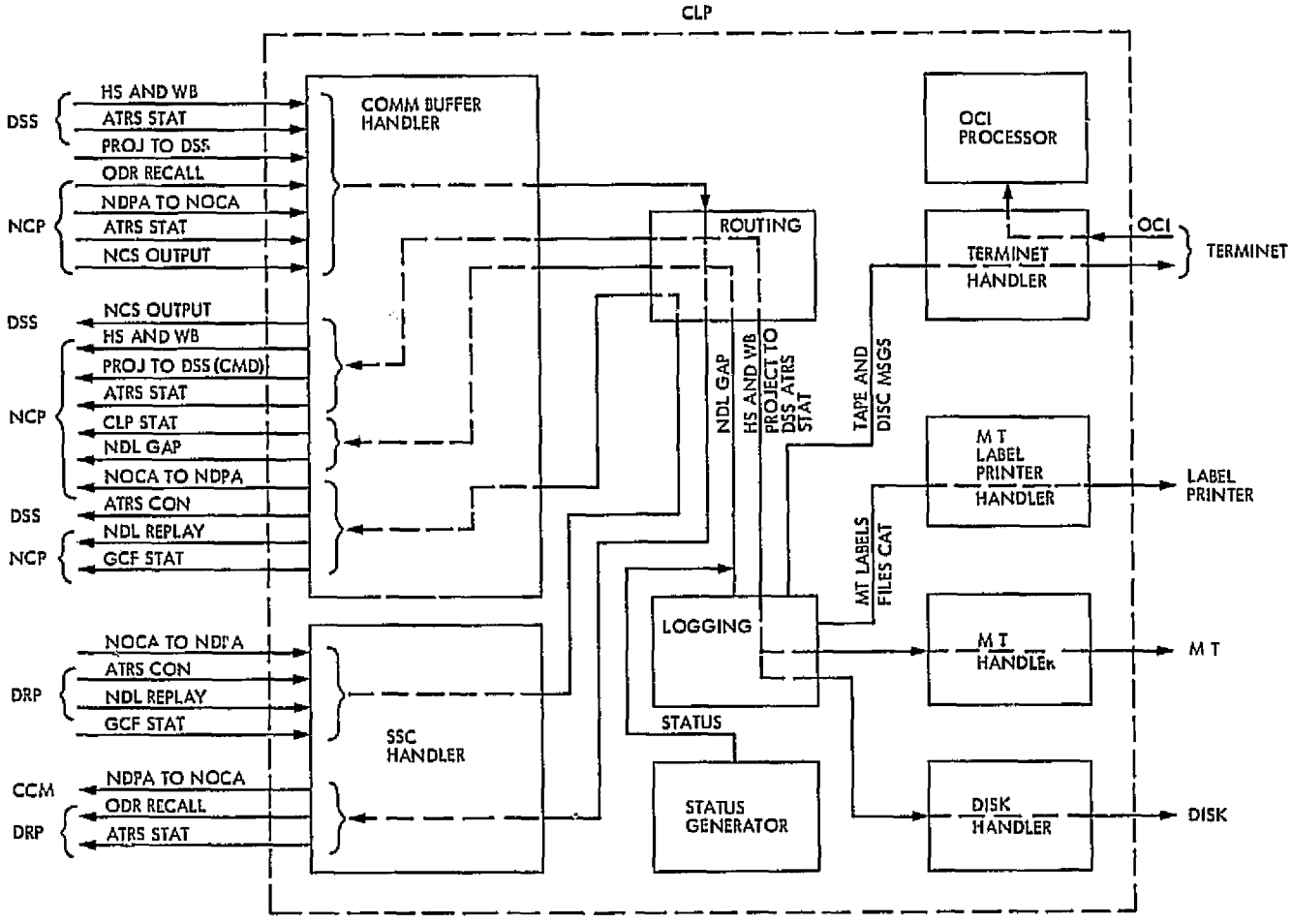

Fig. 2. Communication log processor software module diagram

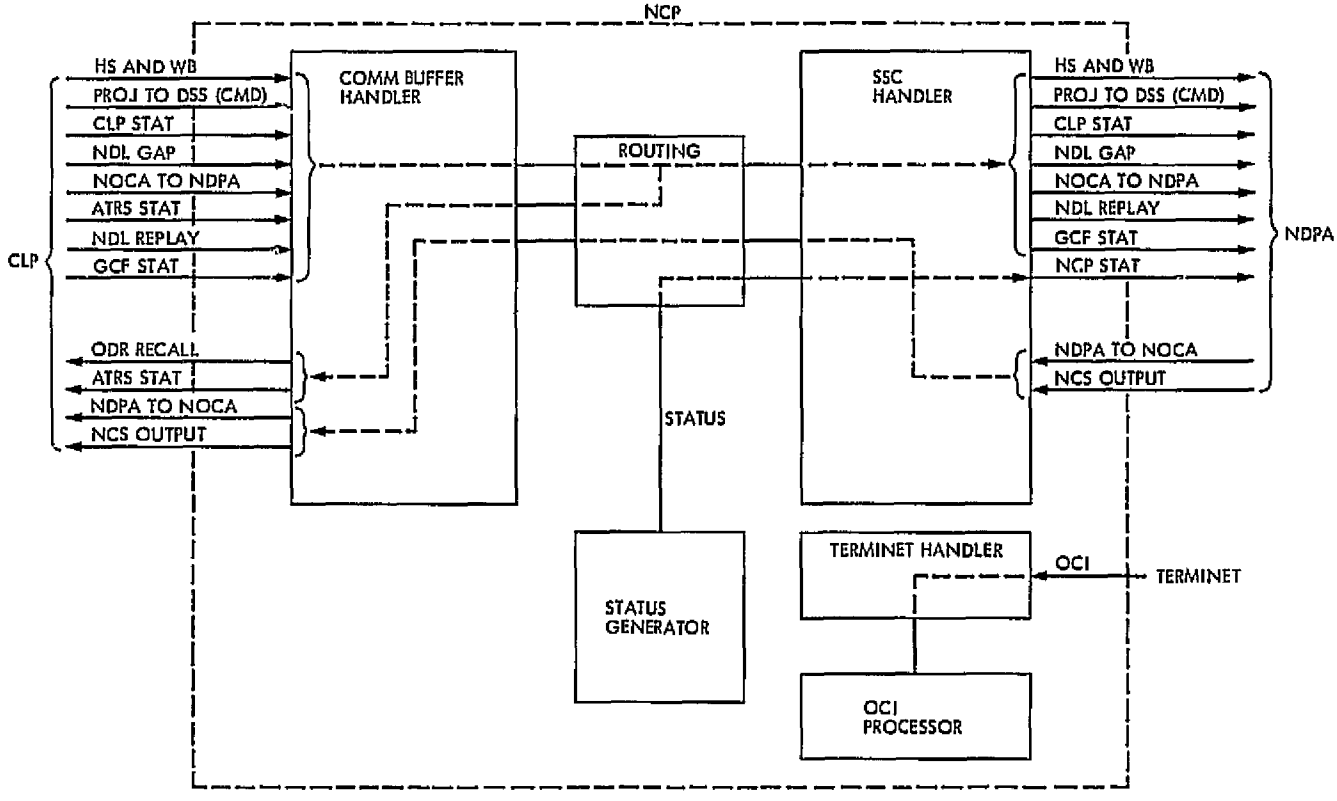

Fig. 3. Network Control Processor software diagram

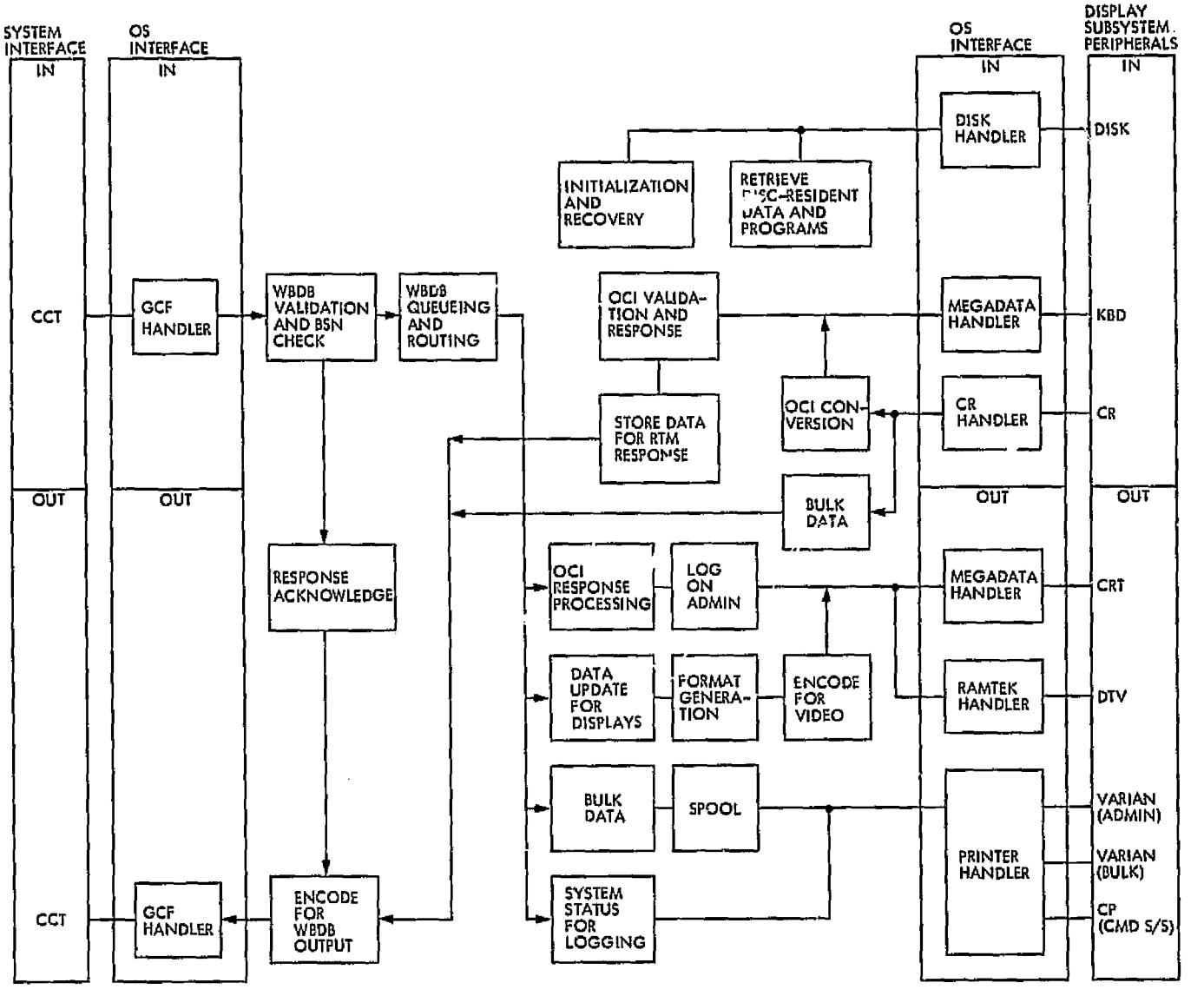

Fig. 4. Display subsystem software module diagram

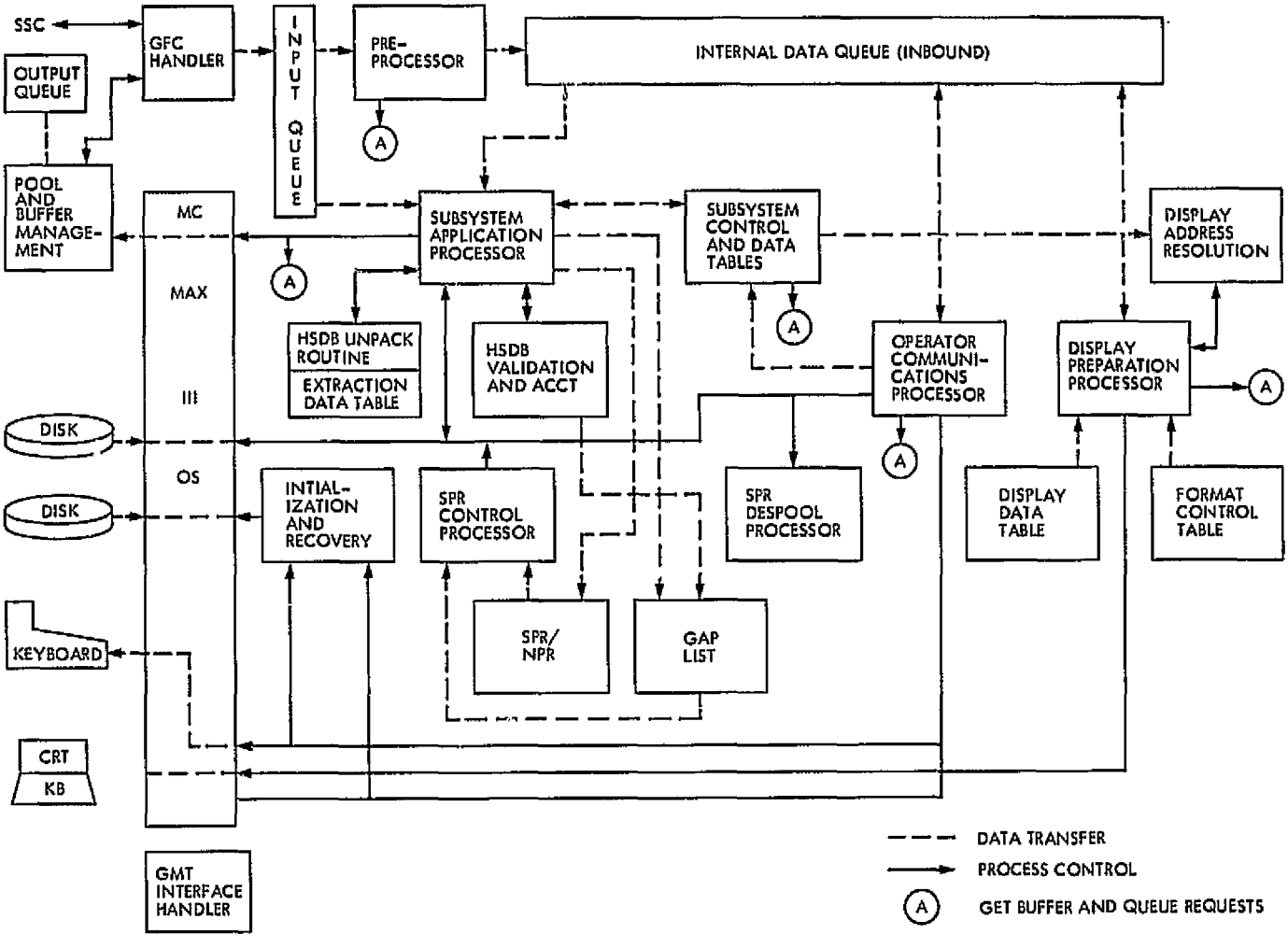

Fig. 5. Typical real-time monitor software module diagram

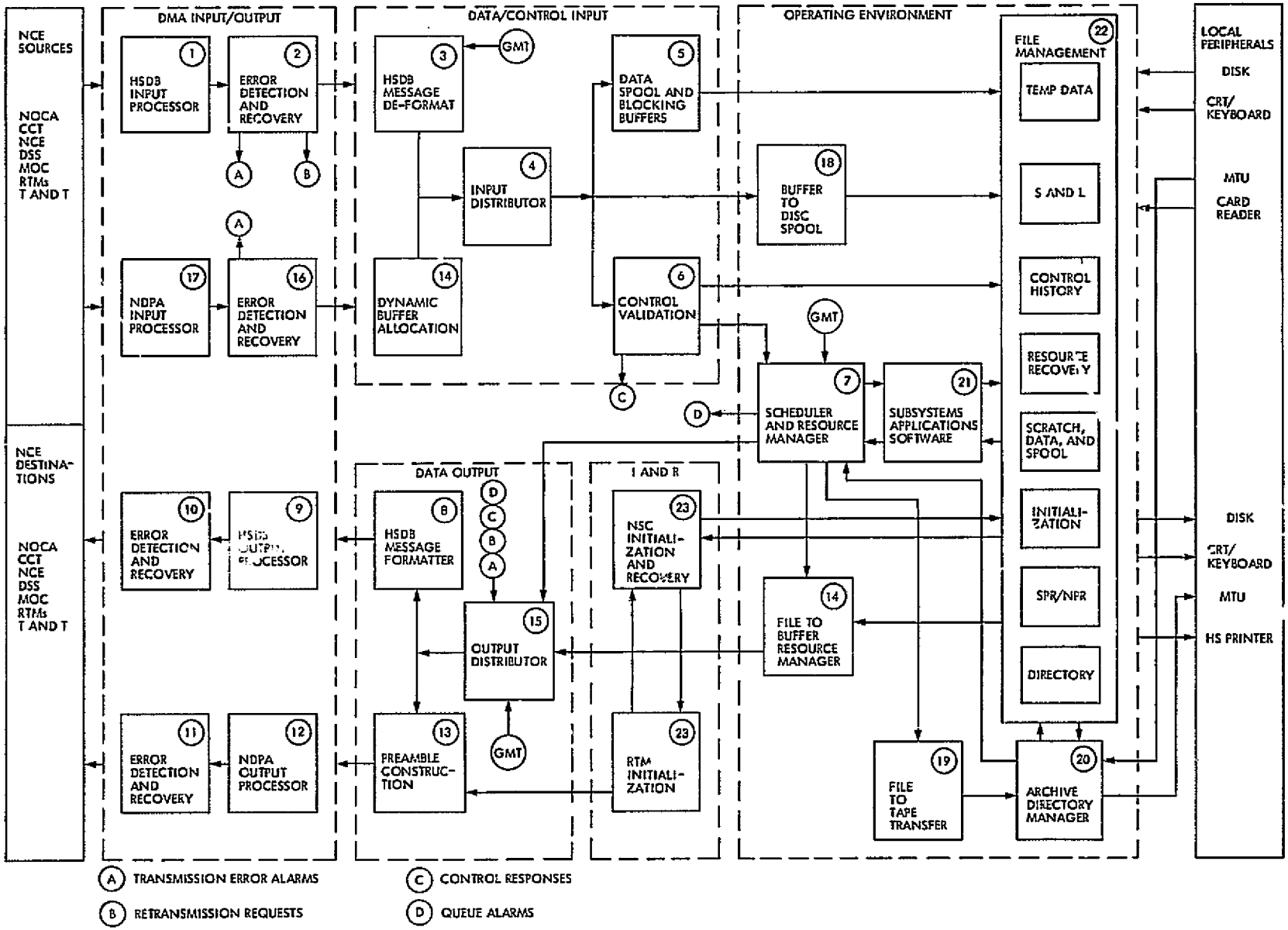

Fig. 6. Support subsystem software module diagram

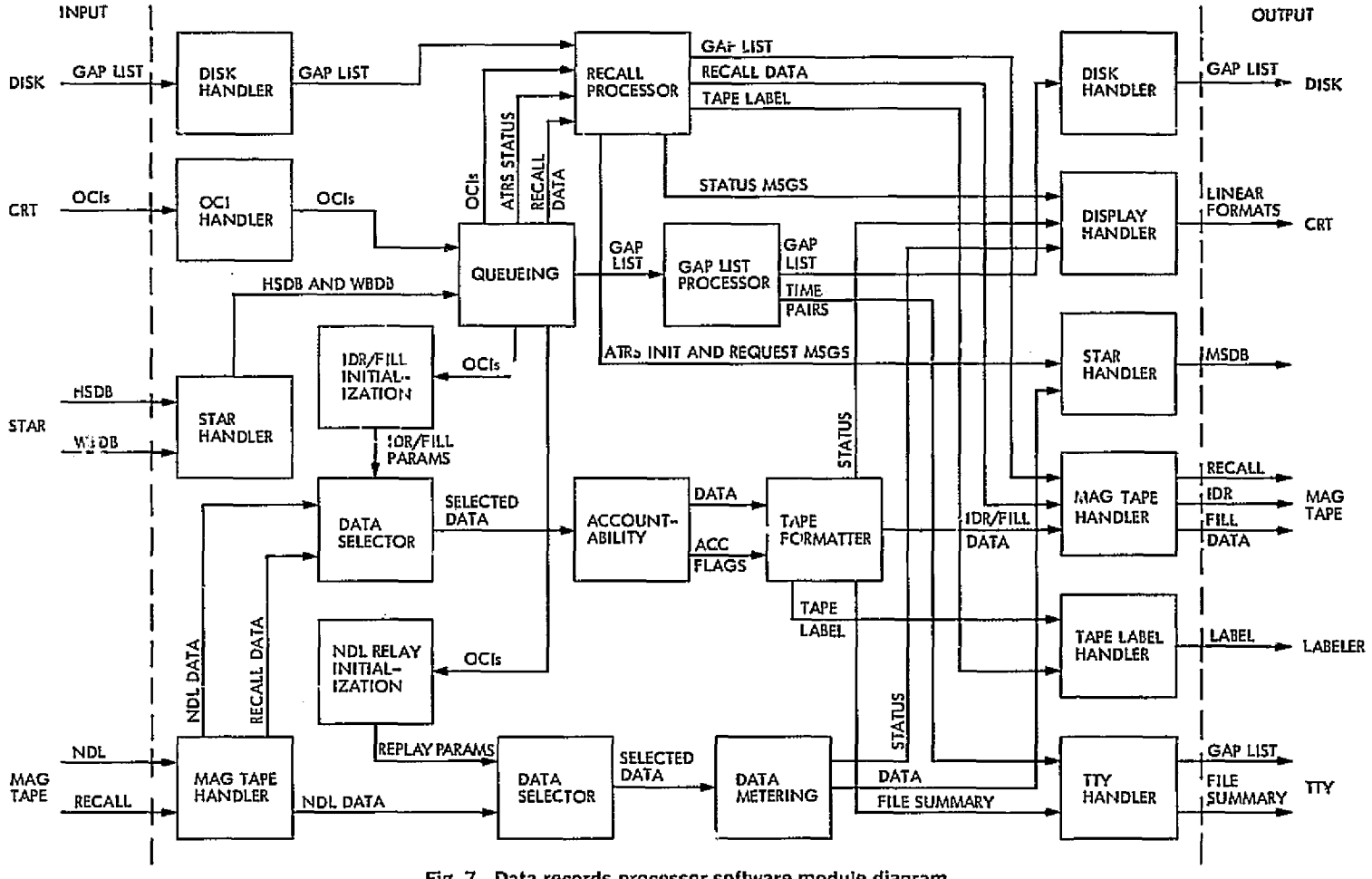

Fig. 7. Data records processor software module diagram

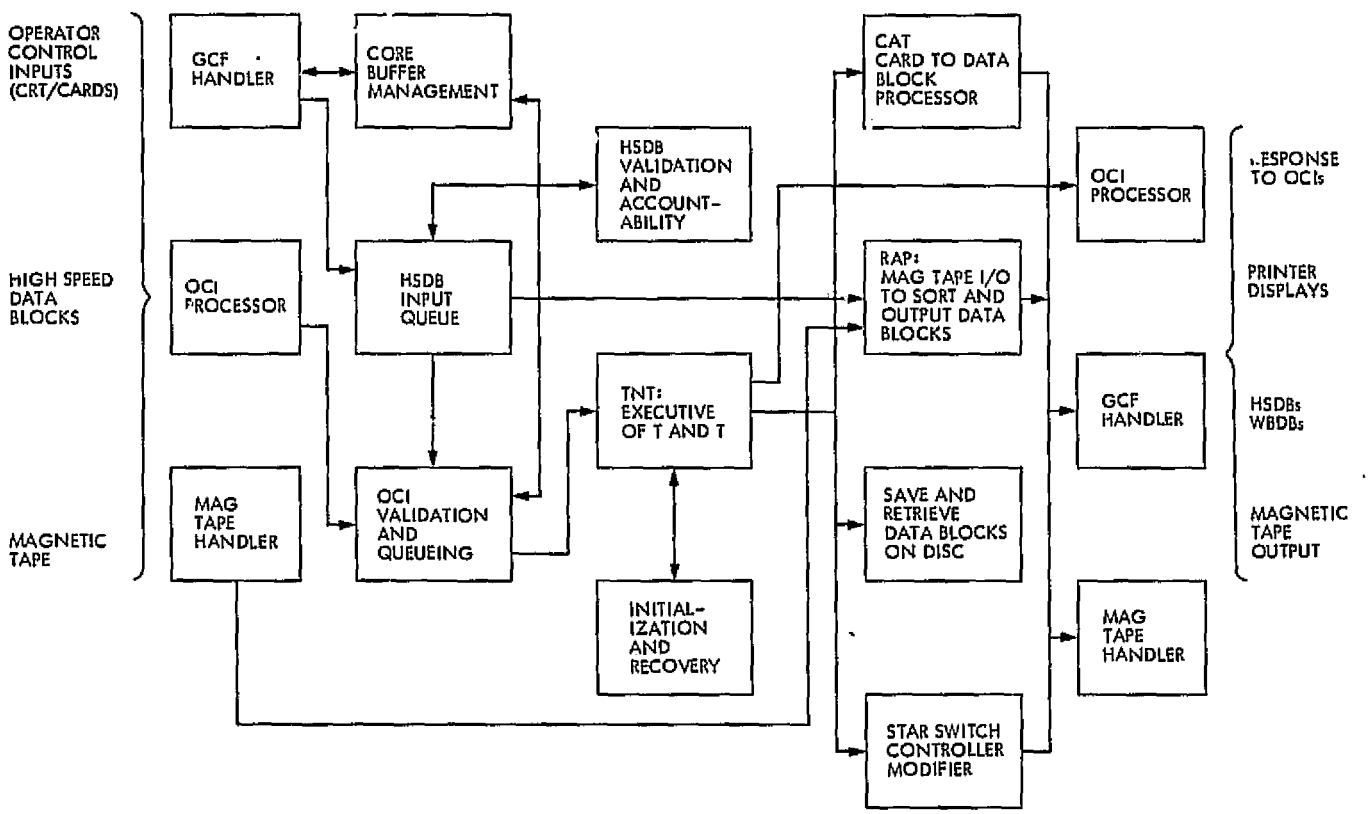

Fig. 8. Test and training subsystem software module diagram

Extension of Automatic Flow Charting Capabilities

R. J. Margolin and W. O. Paine
Quality Assurance DSN and Mechanical Hardware Section

A new macro generation facility within the AUTOFLOW II flow charting system was used to process assembly language programs for the MODCOMP II computer. This article describes the nature of this new facility and how it was used, as well as describing other capabilities for automatic flow charting.

In its search for tools to aid in auditing DSN software, the Software Quality Assurance Group has made use of graphic macro facilities within AUTOFLOW II[1] to enable automatic flow charting of assembly language source programs for the MODCOMP II[2] computer used in the Deep Space Network.

This facility in AUTOFLOW II is known as *macro definition*. It permits the representation of the individual instructions of a target computer (in this case, the MODCOMP II) in terms of flow chart symbols with accompanying text information. A group of macro definition statements is used to express an instruction and each time that instruction occurs:

(1) The type and number of flow chart symbols for that instruction are generated.

(2) The text associated with each symbol is generated, including literal expressions and indicated parts of the source instructions.

(3) In the case of decision, branch, and subroutine symbols, the location of the field which specifies the destination data is given.

(4) For decision symbols, the in-line and out-of-line path labels are supplied.

Over 500 lines of macro definition statements were used to form 236 macro definitions of assembler directives and instructions for the MODCOMP assembler with some of the macro assembler features added. Twenty-three of the macro definitions were for assembler directives. Twenty-seven of the remaining 213 macro definitions were for

[1] AUTOFLOW II is a program product of Applied Data Research, Inc., Princeton, New Jersey. There are many modules in AUTOFLOW II. One module, the chart/assembly module, accepts programs written in IBM 360/370 assembly language and automatically provides flow charts and analytical listings which make the structure of the program clearer. This system has been installed on the IBM 360/75 since early 1973.

[2] The MODCOMP II computer is a product of Modular Computer Systems, Fort Lauderdale, Florida.

separate definitions of those instructions (indicated in MODCOMP code by an asterisk as the last character of the operation) where the memory reference was indirect. In addition, a group of specific MODCOMP executive service macros was defined.

A simple and conventional approach to graphic macro definition would have been to select the appropriate boxes and merely repeat the source coding along with the comment. It was our desire to provide a type of documentation suitable even for one not reasonably familiar with MODCOMP coding. In an effort to do this, we have expressed the instructions in a combination of English, logical, and program language-related symbolic notation. This enables a new reader to understand the operations more easily without knowing the many details of addressing modes. A certain lack of flexibility in the macro definition feature may cause pairs of parentheses to appear with null contents. This serves to indicate non-use of indexing where potentially available.

Where an assembler itself offers macro capabilities, it is possible to provide parallel AUTOFLOW macro definitions, depending on the complexity of the assembler macros used. This was done by Quality Assurance in the case of the Communication Buffer and Quad Standard Interface Adaptor (SIA) Test Program, part of which is shown as a sample. Part of the macro definitions, source code, and chart output are illustrated in Figs. 1, 2, and 3. Normally, the parallel AUTOFLOW macro definitions would be prepared to the general standard used for the original assembler macros.

In addition to handling 360/370 assembly language programs, AUTOFLOW II also has additional capabilities. AUTOFLOW has a built-in facility known as chart code. It is unrelated to any programming language, but is a vehicle for indicating the structure of the program at a design level. AUTOFLOW can also handle assembly language programs for a number of other computers and a variety of languages, such as PL/1, COBOL, JCL. Some of these are options which may be delivered with the basic AUTOFLOW II, while others are preprocessors which dovetail with AUTOFLOW or produce output that may be input to AUTOFLOW.

The status of other AUTOFLOW activities is as follows:

(1) The current options in extensive use are FORTRAN and XDS Sigma Assembly Language.

(2) The installed preprocessors are SDS 920, UNIVAC 1108, and CDC 3100.

(3) Other preprocessors (which use the macro definition facility) are for the INTERDATA 4 and INTERDATA 70.

(4) Other uses have been examined and it is possible to automatically chart assembly code for the PDP-8, NOVA, MAC-16, and PDP-11.

Bibliography

AUTOFLOW II Assembly Series Reference Manual P402A, Applied Data Research, Inc., Princeton, N.J., 1974.

The New AUTOFLOW Sigma Series Reference Manual, Applied Data Research, Inc., Princeton, N.J., 1972.

AUTOFLOW Preprocessor System Maintenance and Technical Manual, Applied Data Research, Inc., Princeton, N.J., 1969 (prepared for NASA-GSFC under Contract No. NAS5-10587).

MODCOMP II Computer Reference Manual 210-102000, Modular Computer Systems, Fort Lauderdale, Fla., 1973.

MODCOMP Assembler/Macro Assembler Reference Manual 210-600101, Modular Computer Systems, Fort Lauderdale, Fla., 1971.

```
06/23/75        INPUT LISTING                    AUTOFLOW CHART SET - MODCOMP  TEST PROGS (SCO,HND,ERP,TIM)

 CARD NO        ****                              CONTENTS                                    ****

    222         * MDEF IF                                                                  *D IF   1
    223         * MDEF    INC                                                               *D INC
    224         * MDEF INS                                                                  *D INS
    225         * MDEF INT,EN,D1/OP(ALL)/                                                   *D INT  1
    226         * MDEF    ISA,I                                                             *D ISA  1
    227         * CON /'INPUT STATUS FROM DEVICE',Q(2),'TO REG.',Q(1),';',OP(ALL),C/        *DISA  2
    228         * MDEF    ISB,I                                                             *D ISB  1
    229         * CON /'INPUT STATUS FROM DEVICE',Q(2),'TO REG.',Q(1),';',OP(ALL),C/        *DISB  2
    230         * MDEF    ISC,I                                                             *D ISC  1
    231         * CON /'INPUT STATUS FROM DEVICE',Q(2),'TO REG.',Q(1),';',OP(ALL),C/        *DISC  2
    232         * MDEF    ISD,I                                                             *D ISD  1
    233         * CON /'INPUT STATUS FROM DEVICE',Q(2),'TO REG.',Q(1),';',OP(ALL),C/        *DISD  2
    234         * MDEF    LAD,P                                                             *D LAD  1
    235         * CON /'SHIFT LT ARITH DBL REG.',Q(1),Q(2),'BITS;',OP(ALL),C/               *D LAD  2
    236         * MDEF    LAS,P                                                             *D LAS  1
    237         * CON /'SHIFT  LT,AR,SNGL REG.',Q(1),Q(2),'BITS;',C/                        *D LAS  2
    238         * MDEF    LBR,P                                                             *D LBR  1
    239         * CON /'LOAD BIT',Q(2),'INTO REG.',Q(1),';',OP(ALL),C/                       *D LBR  2
    240         * MDEF    LBRB,P                                                            *D LBRB 1
    241         *         CON  /'LOAD BIT',Q(2),'INTO REG.',Q(1),';',C/                     *D LBRB 2
    242         * IBID B,D1/OP(1)/                                                          *D LBRB 3
    243         * CON /OP(1)/                                                               *D LBRB 4
    244         * MDEF LBX,P                                                                *D LBX  1
    245         * CON /'LOAD BYTE INTO REG.',Q(1),'PER REG.',Q(2),';',OP(ALL),C/            *D LBX  2
    246         * MDEF LDI,P                                                                *D LDI  1
    247         * CON /'LOAD',OP(1),'INTO REG.',Q(1),';',C/                                 *D LDI  2
    248         * MDEF LDM,P                                                                *D LDM  1
    249         * CON /'LOAD REG.',Q(1),'WITH (',OP(1),'+(REG.',Q(2),'));',C/               *D LDM  2
    250         * MDEF LDM*,P                                                               *D LDM* 1
    251         * CON /'LOAD REG.',Q(1),'WITH ((',OP(1),'+(REG.',Q(2),'))');',C/            *D LDM* 2
    252         * MDEF LDS,P                                                                *D LDS  1
    253         * CON /'LOAD REG.',Q(1),'WITH ((R1)+',Q(2),');',OP(ALL),C/                  *D LDS  2
    254         * MDEF LDX,P                                                                *D LDX  1
    255         * CON /'LOAD REG.',Q(1),'FROM ((REG.',Q(2),'));',OP(ALL),C/                 *D LDX  2
    256         * MDEF LFM,P                                                                *D LFM  1
    257         * CON /'LOAD FILE TO REG',Q(1),'ETC FROM',OP(1),'+(',Q(2),');',C/           *D LFM  2
    258         * MDEF LFM*,P                                                               *D LFM* 1
    259         * CON /'LOAD FILE TO REG',Q(1),'ETC FROM (',OP(1),'+(',Q(2),'))',C/         *DLFM* 2
    260         * MDEF LFS,P                                                                *D LFS  1
    261         * CON /'LOAD FILE TO REG',Q(1),'ETC FROM((R1)+',Q(2),');',OP(ALL),C/        *DLFS  2
    262         * MDEF LFX,P                                                                *D LFX  1
    263         * CON /'LOAD FILE TO RG.',Q(1),'ETC FRM ((RG.',Q(2),'));',OP(ALL),C/        *DLFX  2
    264         * MDEF    LLD,P                                                             *D LLD  1
    265         * CON /'SHIFT LEFT LOG DBL REG',Q(1),Q(2),'BITS;',OP(ALL),C/                *D LLD  2
    266         * MDEF    LLS,P                                                             *D LLS  1
    267         * CON /'SHIFT LEFT LOGIC REG',Q(1),Q(2),'BITS;',OP(ALL),C/                  *D LLS  2
    268         * MDEF    LRS,P                                                             *D LRS  1
    269         * CON /'LEFT ROTATE REG.',Q(2),'INTO REG.',Q(1),';',OP(ALL),C/              *D LRS  2
    270         * MDEF LST                                                                  *D LST
    271         * MDEF MAC                                                                  *D MAC
    272         * MDEF MBL,P                                                                *D MBL  1
    273         * CON /'MOVE BYTE LEFT FROM REG.',Q(2),'TO REG.',Q(1),';',OP(ALL),C/        *DMBL  2
    274         * MDEF MBR,P                                                                *D MBR  1
    275         * CON /'MOVE BYTE RIGT FROM REG.',Q(2),'TO REG.',Q(1),';',OP(ALL),C/        *DMBR  2
    276         * MDEF MLR,P                                                                *D MLR  1
```


Fig. 1. Part of macro definition statements for MODCOMP instructions

```
1397                LDI.R2      #4020                PICK UP OCX INSTRUCTION          HND04110
1398                ORS.R2,0                         ADD GROUP AND UNIT NUMBERS       HND04120
1399                STM.R2      M3COND               STORE CCX INSTR IN CONDITIONING  HND04130
1400                STM.R2      M3WRIT               AND WRITE MODE INSTRUCTIONS      HND04140
1401                LDS.R2,5                         PICK UP IOS AND FUNCTION CODE    HND04150
1402                MLR.R2,R2                        ZERO I/O STATE                   HND04160
1403                ORI.R2      #0100                SET I/O STATE TO 1  WRITING MODEHND04170
1404                STS.R2,5                                                          HND04180
1405                BLM.R14     SETIME               SET TIMER                        HND04190
1406                LDI.R2      #4000                PICK UP CONDITIONING COMMAND     HND04200
1407          M3COND OCB.R2,0                        OUTPUT CONDITIONING COMMAND      HND04210
1408                LDI.R2      #D000                PICK UP TI COMMAND               HND04220
1409          M3WRIT OCB.R2,0                        OUTPUT TI COMMAND                HND04230
1410                BRU         DQINT                DEQUEUE NEXT INTERRUPT           HND04240
1411                EJT                                                               HND04250
1412          M3TERM BLM.R14    CKSTAT               CHECK STATUS                     HND04260
1413                LDS.R2,5                         PICK UP I/O STATE                HND04270
1414                MBR.R2,R2                                                         HND04280
1415                CRMB.R2     ONE,M3CKSM,M3HLT     IF IOS = 1 GO CHECK SIMUL I/O    HND04290
1416                CRMB.R2     THREE,M3STRD,M3HLT   IF IOS = 3 GO SET MEMORY READ    HND04300
1417                CRMB.R2     FOUR,M3BEGN,M3HLT    IF IOS = 4 GO BEGIN AGAIN        HND04310
1418          M3HLT HLT                              INVALID I/O STATE                HND04320
1419          M3CKSM TBRB.R4,2  M3ST3                IF SIMUL I/O NOT SET GO READ MEMHND04330
1420                BRU         SIMUL                GO PROCESS SIMULTANEOUS I/O      HND04340
1421          M3ST3 LDI.R2      #FFF8                PICK UP LENGTH OF 8 WORDS        HND04350
1422                STM*.R2,R1  1                    STORE IN TC LOCATION             HND04360
1423                LDI.R2      16                   PICK UP LENGTH OF 16 BYTES       HND04370
1424                STS.R2,3                         STORE IN TABLE                   HND04380
1425                LDI.R2      M3BUF                PICK UP ADDR OF MEMORY BUFFER    HND04390
1426                STM*.R2,R1  2                    STORE IN TA LOCATION             HND04400
1427                STS.R2,4                         STORE IN TABLE                   HND04410
1428                LDI.R2      #4020                PICK UP OCX INSTRUCTION          HND04420
1429                ORS.R2,0                         ADD GROUP AND UNIT NUMBERS       HND04430
1430                STM.R2      M3READ               STORE OCX IN READ INSTRUCTION    HND04440
1431                LDS.R2,5                         PICK UP IOS AND FUNCTION CODE    HND04450
1432                MLR.R2,R2                        ZERO I/O STATE                   HND04460
1433                ORI.R2      #0300                SET I/O STATE TO 3  READING MEM HND04470
1434                STS.R2,5                                                          HND04480
1435                BLM.R14     SETIME               SET TIMER                        HND04490
1436                LDI.R2      #D800                PICK UP TI COMMAND               HND04500
1437          M3READ OCB.R2,0                        OUTPUT TI COMMAND                HND04510
1438                BRU         DQINT                DEQUEUE NEXT INTERRUPT           HND04520
1439          M3STRD LDS.R2,4                        SET INDICATOR FOR MEMORY PRINT   HND04530
1440                STS.R2,15                        STORE BUFFER ADDR IN TABLE       HND04540
1441                LDS.R2,5                         PICK UP IOS AND FUNCTION CODE    HND04550
1442                MLR.R2,R2                        ZERO I/O STATE                   HND04560
1443                ORI.R2      #0200                SET IOS TO 2 WAITING             HND04570
1444                STS.R2,5                                                          HND04580
1445                BLM.R14     DELAY                GO SET DELAY TIMER               HND04590
1446                BRU         DQINT                GO DEQUEUE NEXT INTERRUPT        HND04600
1447                EJT                                                               HND04610
1448          M3TIME LDS.R2,5                        PICK UP IOS AND FUNCTION CODE    HND04620
1449                MBR.R2,R2                        ZERO FUNCTION CODE               HND04630
1450                CRMB.R2     FOUR,M3TIMO,M3CHK3   IF IOS = 4 GO ABORT AND START    HND04640
1451          M3CHK3 CRMB.R2    THREE,M3TIMO,M3CK2   IF IOS = 3 GO ABORT & START      HND04650
1452          M3CK2 CRMB.R2     TWO,M3BEGN,M3CK1     IF IOS = 2 GO START AGAIN        HND04660
1453          M3CK1 CRMB.R2     ONE,M3TIMO,M3HLTT    IF IOS = 1 GO ABORT & START      HND04670
```


Fig. 2. Part of sample source program

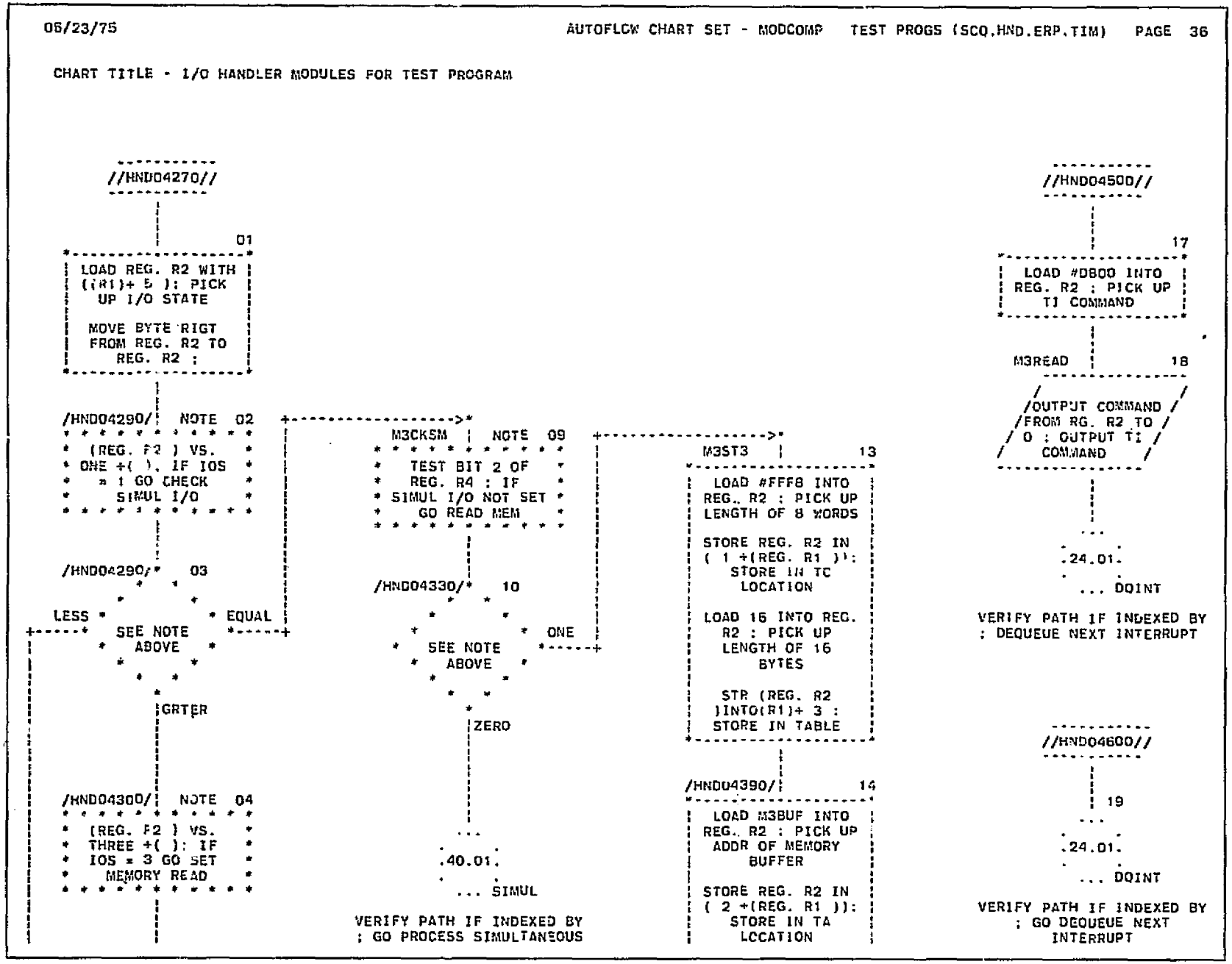

Fig. 3. Part of generated flow chart corresponding to sample in Fig. 2

Bibliography

Anderson, J. D., Null, G. W., and Thornton, C. T., *The Evaluation of Certain Astronomical Constants from the Radio Tracking of Mariner II*, Technical Report 32-476, Jet Propulsion Laboratory, Pasadena, Calif., reprinted from *Progr. Astronaut. Aeronaut.*, Vol. 14, 1964.

Anderson, J. D., *Determination of the Masses of the Moon and Venus and the Astronomical Unit from Radio Tracking Data of the Mariner II Spacecraft*, Technical Report 32-816, Jet Propulsion Laboratory, Pasadena, Calif., July 1, 1967.

Anderson, J. D., et al., "The Radius of Venus as Determined by Planetary Radar and Mariner V Radio Tracking Data," *J. Atmos. Sci.*, pp. 1171–1174, Sept. 25, 1968.

Anderson, J. D., and Hilt, D. E., "Improvement of Astronomical Constants and Ephemerides from Pioneer Radio Tracking Data," *AIAA J.*, Vol. 7, No. 6, pp. 1048–1054, June 1969.

Anderson, J. D., "Determination of Astrodynamic Constants and a Test of the General Relativistic Time Delay With S-Band Range and Doppler Data From Mariners 6 and 7," *Space Research*, Vol. XI, pp. 105–112, Akademie-Verlag, Berlin, 1971.

Barnum, P. W., et al., *Tracking and Data System Support for the Mariner Mars 1971 Mission: Orbit Insertion Through End of Primary Mission*, Technical Memorandum 33-523, Vol. III, Jet Propulsion Laboratory, Pasadena, Calif., May 15, 1973.

Barnum, P. W., and Renzetti, N. A., *Tracking and Data System Support for the Mariner Mars 1971 Mission: Extended Mission Operations*, Technical Memorandum 33-523, Vol. IV, Jet Propulsion Laboratory, Pasadena, Calif., Dec. 15, 1973.

Bathker, D. A., *Radio-Frequency Performance of an 85-ft Ground Antenna: X-Band*, Technical Report 32-1300, Jet Propulsion Laboratory, Pasadena, Calif., July 1, 1968.

Bathker, D. A., *Radio Frequency Performance of a 210-ft Ground Antenna: X-Band*, Technical Report 32-1417, Jet Propulsion Laboratory, Pasadena, Calif., Dec. 15, 1969.

Bathker, D. A., *Predicted and Measured Power Density Description of a Large Ground Microwave System*, Technical Memorandum 33-433, Jet Propulsion Laboratory, Pasadena, Calif., Apr. 15, 1971.

Baumert, L., et al., *Coding Theory and Its Applications to Communications Systems*, Technical Report 32-67, Jet Propulsion Laboratory, Pasadena, Calif., Mar. 31, 1961.

Baumgartner, W. S., *High-Power CW Radar Transmitter*, Technical Report 32-656, Jet Propulsion Laboratory, Pasadena, Calif., Sept. 1, 1964.

Berman, A. L., *Tracking System Data Analysis Report, Ranger VII Final Report*, Technical Report 32-719, Jet Propulsion Laboratory, Pasadena, Calif., June 1, 1965.

Biber, K. W., and Whittlesey, A. C., *Description and Analysis of 890-MHz Noise-Measuring Equipment*, Technical Report 32-898, Jet Propulsion Laboratory, Pasadena, Calif., Mar. 31, 1966.

Brockman, M. H., and Posner, E. C., *Power Requirements for Deep-Space Telecommunication Links*, Technical Report 32-1395, Jet Propulsion Laboratory, Pasadena, Calif., reprinted from *IEEE Spectrum*, Vol. 6, No. 3, pp. 95–99, Mar. 1969.

Bunce, R. C., *Unified S-Band Receiver-Exciter Subsystem*, Technical Report 32-809, Jet Propulsion Laboratory, Pasadena, Calif., Sept. 15, 1968.

Butman, S., "A General Formulation of Linear Feedback Communication Systems with Solutions," *IEEE Trans. Inform. Theor.*, Vol. IT-15, No. 3, pp. 392–400, May 1969.

Butman, S., "Rate Distortion Over Band-Limited Feedback Channels," *IEEE Trans. Inform. Theor.*, Vol. IT-17, No. 1, pp. 110–112, Jan. 1971.

Butman, S., and Timor. U., "Interplex—An Efficient Multichannel PSK/PM Telemetry System", *IEEE Trans. Commun.*, Vol. COM-20, No. 3, pp. 415–419, June 1972.

Cain, D. L., and Hamilton, T. W., *Determination of Tracking Station Locations by Doppler and Range Measurements to an Earth Satellite*, Technical Report 32-534, Jet Propulsion Laboratory, Pasadena, Calif., Feb. 1, 1964.

Carey, C. N., and Sjogren, W. L., *Gravitational Inconsistency in the Lunar Theory: Confirmation by Radio Tracking*, Technical Report 32-1290, Pt. II, Jet Propulsion Laboratory, Pasadena, Calif., reprinted from *Science*, Vol. 160, No. 3830, pp. 875–876, May 24, 1968.

Carpenter, R. L., *Study of Venus by CW Radar—1964 Results*, Technical Report 32-963, Jet Propulsion Laboratory, Pasadena, Calif., reprinted from *Astron. J.*, Vol. 71, No. 2, pp. 142–152, Mar. 1966.

Chadwick, H. D., and Springett, J. C., "The Design of a Low Data Rate MSFK Communication System," *IEEE Trans. Commun. Technol.*, Vol. COM-18, No. 6, pp. 740–750, Dec. 1970.

Chaney, W. D., *Final Mariner II Tracking System Data Analysis Report*, Technical Report 32-727, Jet Propulsion Laboratory, Pasadena, Calif., Sept. 1, 1965.

Charles, F. J., and Lindsey, W. C., *Some Analytical and Experimental Phase-Locked Loop Results for Low Signal-to-Noise Ratios*, Technical Report 32-1027, Jet Propulsion Laboratory, Pasadena, Calif., reprinted from *Proc. IEEE*, Vol. 54, No. 9, pp. 1152–1166, Sept. 1966.

Clark, B. G., et al., "High Resolution Observations of Compact Radio Sources at 13 cm," *Astrophys. J.*, Vol. 161, pp. 803–809, Sept. 1970.

Clauss, R. C., et al., *Total System Noise Temperature: 15°K*, Technical Report 32-691, Jet Propulsion Laboratory, Pasadena, Calif., Nov. 1964.

Clauss, R. C., *A 2388-Mc Two-Cavity Maser for Planetary Radar*, Technical Report 32-583, Jet Propulsion Laboratory, Pasadena, Calif., reprinted from *Microwave J.*, Vol. 8, pp. 74–77, May 1965.

Clauss, R. C., *A Traveling Wave Maser for Deep Space Communication at 2295 and 2388 MHz*, Technical Report 32-1072, Jet Propulsion Laboratory, Pasadena, Calif., Feb. 15, 1967.

Cohen, M. H., et al., "Compact Radio Source in the Nucleus of M87," *Astrophys. J.*, Vol. 158, No. 2, Pt. 2, pp. L83–L85, Nov. 1969.

Coyner, J. V., Jr., *Radial Rib Antenna Surface Deviation Analysis Program*, Technical Memorandum 33-518, Jet Propulsion Laboratory, Pasadena, Calif., Dec. 15, 1971.

Curkendall, D. W., and McReynolds, S. R., "A Simplified Approach for Determining the Information Content of Radio Tracking Data," *J. Spacecraft Rockets*, Vol. 6, No. 5, pp. 520–525, May 1969.

Curkendall, D. W., and Stephenson, R. R., "Earthbased Tracking and Orbit Determination—Backbone of the Planetary Navigation System," *Astronaut. Aeronaut.*, Vol. 7, No. 5, pp. 30–36, May 1970.

Curkendall, D. W., "Planetary Navigation: The New Challenges," *Astronaut. Aeronaut.*, Vol. 7, No. 5, pp. 26–29, May 1970.

"The Deep Space Network—An Instrument for Radio Navigation for the Mariner Mission to Mars—1969," *Proceedings of the Second International Conference of STM and AERA*, Reidel Publishing Company, Holland, May 1969.

Description of the Deep Space Network Operational Capabilities as of January 1, 1966, Technical Memorandum 33-255, Jet Propulsion Laboratory, Pasadena, Calif., July 1, 1966.

Didday, R. L., and Lindsey, W. C., *Subcarrier Tracking Methods and Communication System Design*, Technical Report 32-1317, Jet Propulsion Laboratory, Pasadena, Calif., reprinted from *IEEE Trans. Commun. Technol.*, Vol. COM-16, No. 4, pp. 541–550, Aug. 1968.

Downs, G. S., and Reichley, P. E., "Observations of Interstellar Scintillations of Pulsar Signals at 2388 MHz," *Astrophys. J.*, Vol. 163, No. 1, Pt. 2, pp. L11–L16, Jan. 1971.

Downs, G. S., et al., "Mars Radar Observation, A Preliminary Report," *Science*, Vol. 174, No. 4016, pp. 1324–1327, Dec. 24, 1971.

Downs, G. S., et al., "Martian Topography and Surface Properties as Seen by Radar: The 1971 Opposition," *Icarus*, Vol. 18, No. 1, pp. 8–21, Jan. 1973.

Downs, G. S., Reichley, P. E., and Morris, G. A., "Pulsar Detections at Frequencies of 8.4 and 15.1 GHz," *Astrophys. J.*, Vol. 181, No. 3, Part 2, pp. L143–L146, May 1, 1973.

Easterling, M., *A Long-Range Precision Ranging System*, Technical Report 32-80, Jet Propulsion Laboratory, Pasadena, Calif., July 10, 1961.

Easterling, M., *Methods for Obtaining Velocity and Range Information from CW Radars*, Technical Report 32-657, Jet Propulsion Laboratory, Pasadena, Calif., Sept. 1, 1964.

Easterling, M., and Goldstein, R., *The Effect of the Interplanetary Medium on S-Band Telecommunications*, Technical Report 32-825, Jet Propulsion Laboratory, Pasadena, Calif., Sept. 1, 1965.

Efron, L., and Solloway, C. B., *Proceedings of the Conference on Scientific Applications of Radio and Radar Tracking in the Space Program*, Technical Report 32-1475, Jet Propulsion Laboratory, Pasadena, Calif., July 1, 1970.

Esposito, P. B., and Wong, S. K., "Geocentric Gravitational Constant Determined from Mariner 9 Radio Tracking Data," paper presented at the International Symposium on Earth Gravity Models (American Geophysical Union, NASA), St. Louis, Aug. 1972.

Fearey, J. P., and Renzetti, N. A., "Navigation Results on the Mariner Mars Mission to Mars 1969," International Navigation Conference, Hamburg, Oct. 1969.

Fjeldbo, G., Kliore, A. J., and Seidel, B. L., "Bistatic Radar Measurements of the Surface of Mars with Mariner 1969," *Icarus*, Vol. 16, No. 3, pp. 502–508, June 1972.

Fjeldbo, G., and Eshleman, V. R., "Radio Occultation Measurements and Interpretations," in *The Atmospheres of Venus and Mars*, p. 225, Gordon and Breach, Science Publishers, Inc., New York, N.Y., 1968.

Fjeldbo, G., "Radio Occultation Experiments Planned for Pioneer and Mariner Missions to the Outer Planets," *Planet. Space Sci.*, Vol. 21, No. 9, pp. 1533–1547, Sept. 1973.

Flanagan, F. M., et al., *Deep Space Network Support of the Manned Space Flight Network for Apollo: 1962–1968*, Technical Memorandum 33-452, Vol. I, Jet Propulsion Laboratory, Pasadena, Calif., July 1970.

Flanagan, F. M., et al., *Deep Space Network Support of the Manned Space Flight Network for Apollo: 1969–1970*, Technical Memorandum 33-452, Vol. II, Jet Propulsion Laboratory, Pasadena, Calif., May 1, 1971.

Fredricksen, H., *Error Correction for Deep Space Network Teletype Circuits*, Technical Report 32-1275, Jet Propulsion Laboratory, Pasadena, Calif., June 1, 1968.

Gary, B., Olsen, E. T., and Rosenkranz, P. W., "Radio Observations of Cygnus X-3 and the Surrounding Region," *Nature Phys. Sci.*, Vol. 239, No. 95, pp. 128–130, Oct. 23, 1972.

Georgevic, R. M., *Mathematical Model of the Solar Radiation Force and Torques Acting on the Components of a Spacecraft*, Technical Memorandum 33-494, Jet Propulsion Laboratory, Pasadena, Calif., Oct. 1, 1971.

Goldstein, R., Stevens, R., and Victor, W. K., *Radar Exploration of Venus: Goldstone Observatory Report for October–December 1962*, Technical Report 32-396, Jet Propulsion Laboratory, Pasadena, Calif., Mar. 1, 1965.

Goldstein, R. M., *The Analysis of Uncooperative Radar Targets*, Technical Report 32-658, Jet Propulsion Laboratory, Pasadena, Calif., Sept. 1, 1964.

Goldstein, R. M., et al., *The Superior Conjunction of Mariner IV*, Technical Report 32-1092, Jet Propulsion Laboratory, Pasadena, Calif., Apr. 1, 1967.

Goldstein, R. M., "Radar Time-of-Flight Measurements to Venus," *Astron. J.*, Vol. 73, No. 9, Aug. 1968.

Goldstein, R. M., et al., "Preliminary Radar Results of Mars," *Radio Sci.*, Vol. 5, No. 2, pp. 475–478, Feb. 1970.

Goldstein, R. M., and Rumsey, H., "A Radar Snapshot of Venus," *Science*, Vol. 169, Sept. 1970.

Goldstein, R. M., "Radar Observations of Mercury," *Astron. J.*, Vol. 76, No. 10, pp. 1152–1154, Dec. 1971.

Goldstein, R. M., Holdridge, D. B., and Lieske, J. H., "Minor Planets and Related Objects: XII. Radar Observations of (1685) Toro," *Astron. J.*, Vol. 78, No. 6, pp. 508–509, Aug. 1973.

Golomb, S. W., "New Problems of Space Communications: Part I. Beware of the Tigers," *Astronautics*, Vol. 7, No. 6, p. 19, June 1962.

Golomb, S. W., "New Problems in Space Communications: Part 3," *Astronautics*, Vol. 7, No. 8, p. 26, Aug. 1962.

Golomb, S. W., "Ferreting Signals Out of Noise," *Int. Sci. Technol.*, No. 22, pp. 72–82 and 120, Oct. 1963.

Gordon, H. J., et al., *The Mariner 6 and 7 Flight Paths and Their Determination From Tracking Data*, Technical Memorandum 33-469, Jet Propulsion Laboratory, Pasadena, Calif., Dec. 1, 1970.

Gottlieb, P., et al., "Lunar Gravity over Large Craters from Apollo 12 Tracking Data," *Science*, Vol. 168, No. 3930, pp. 477–479, Apr. 1970.

Gray, R. M., and Tausworthe, R. C., "Frequency-Counted Measurements, and Phase Locking to Noise Oscillators," *IEEE Trans. Commun. Technol.*, Vol. COM-19, No. 1, pp. 21–30, Feb. 1971.

Gubbay, J., et al., "Variations of Small Quasar Components at 2,300 MHz," *Nature*, Vol. 224, No. 5224, pp. 1094–1095, Dec. 1969.

Gulkis, S., and Gary, B., "Circular Polarization and Total-Flux Measurements of Jupiter at 13.1 cm Wavelength," *Astron. J.*, Vol. 76, No. 1, pp. 12–16, Feb. 1971.

Gulkis, S., et al., "Observations of Jupiter at 13-cm Wavelength During 1969 and 1971," *Icarus*, Vol. 18, No. 2, pp. 181–191, Feb. 1973.

Hall, J. R., *Tracking and Data System Support for Lunar Orbiter*, Technical Memorandum 33-450, Jet Propulsion Laboratory, Pasadena, Calif., Apr. 1970.

Hamilton, T. W., et al., *The Ranger IV Flight Path and Its Determination From Tracking Data*, Technical Report 32-345, Jet Propulsion Laboratory, Pasadena, Calif., Sept. 15, 1962.

Hartop, R. W., *Power Loss Between Arbitrarily Polarized Antennas*, Technical Report 32-457, Jet Propulsion Laboratory, Pasadena, Calif., Sept. 1, 1964.

Havens, W. F., et al., *Scan Pointing Calibration for the Mariner Mars 1971 Spacecraft*, Technical Memorandum 33-556, Jet Propulsion Laboratory, Pasadena, Calif., Aug. 1, 1972.

Heftman, K., and Renzetti, N. A., "Data Return Capabilities of the Deep Space Network in the 1970's," AIAA Paper 67-648, *Proceedings of the AIAA Space Program Issues of the 70's Meeting*, Aug. 1967.

Higa, W. H., *Low-Level Microwave Mixing in Ruby*, Technical Report 32-1016, Jet Propulsion Laboratory, Pasadena, Calif., reprinted from *Proc. IEEE*, Vol. 54, No. 10, p. 1453, Oct. 1966.

Higa, W. H., "Time Synchronization via Lunar Radar," *Proc. IEEE*, Vol. 60, No. 5, pp. 552–557, May 1972.

Holmes, J. K., "On a Solution to the Second-Order Phase-Locked Loop," *IEEE Trans. Commun. Technol.*, Vol. COM-18, No. 2, pp. 119–126, Apr. 1970.

Holmes, J. K., "First Slip Times Versus Static Phase Error Offset for the First and Passive Second-Order Phase-Locked Loop," *IEEE Trans. Commun. Technol.*, Vol. COM-19, No. 2, pp. 234–235, Apr. 1971.

Holmes, J. K., and Tegnelia, C. R., *Digital Command System Second-Order Subcarrier Tracking Performance*, Technical Report 32-1540, Jet Propulsion Laboratory, Pasadena, Calif., Oct. 1, 1971.

Holmes, J. K., "Performance of a First Order Transition Sampling Digital Phase-Locked Loop Using Random-Walk Models," *IEEE Trans. Commun.*, Vol. COM-20, No. 2, pp. 119–131, Apr. 1972.

Hurd, W. J., and Anderson, T. O., *Digital Transition Tracking Symbol Synchronizer for Low SNR Coded Systems*, Technical Report 32-1488, Jet Propulsion Laboratory, Pasadena, Calif., reprinted from *IEEE Trans Commun. Technol.*, Vol. COM-18, No. 2, pp. 141–147, Apr. 1970.

Jaffe, R., and Rechtin, E., *Design and Performance of Phase-Lock Loops Capable of Near-Optimum Performance over a Wide Range of Input Signal and Noise Levels*, Progress Report 20-243, Jet Propulsion Laboratory, Pasadena, Calif., Dec. 1, 1954; also available in *IRE Trans. Inform. Theory*, No. 1, pp. 66–67, Mar. 1955.

Jordan, J. F., "Orbit Determination for Powered Flight Space Vehicles on Deep Space Missions," *J. Spacecraft Rockets*, Vol. 6, No. 5, pp. 545–550, May 1969.

Kellerman, K. I., et al., "High Resolution Observations of Compact Radio Sources at 13 Centimeters," *Astrophys. J.*, Vol. 161, No. 3, pp. 803–809, Sept. 1970.

Kelly, A. J., *Microwave Probe for Plasma Plumes*, Technical Report 32-625, Jet Propulsion Laboratory, Pasadena, Calif., Feb. 1965.

Kliore, A., Cain, D. L., and Hamilton, T. W., *Determination of Some Physical Properties of the Atmosphere of Mars from Changes in the Doppler Signal of a Spacecraft on an Earth-Occultation Trajectory*, Technical Report 32-674, Jet Propulsion Laboratory, Pasadena, Calif., Oct. 15, 1964.

Kliore, A., and Tito, D. A., *Radio Occultation Investigations of the Atmosphere of Mars*, Technical Report 32-1157, Jet Propulsion Laboratory, Pasadena, Calif., reprinted from *J. Spacecraft Rockets*, Vol. 4, No. 5, pp. 578–582, May 1967.

Kliore, A., "Radio Occultation Measurements of the Atmospheres of Mars and Venus," in *The Atmospheres of Venus and Mars*, edited by J. C. Brandt and M. B. McElrow, p. 205, Gordon and Breach Science Publishers, Inc., New York, N.Y., 1968.

Kliore, A. J., et al., "Summary of Mariner 6 and 7 Radio Occultation Results on the Atmosphere of Mars," *Space Research*, Vol. XI, pp. 165–175, Akademie-Verlag, Berlin, 1971.

Kliore, A. J., et al., "Mariner 9 S-Band Martian Occultation Experiment: Initial Results on the Atmosphere and Topography of Mars," *Science*, Vol. 175, No. 4019, pp. 313–317, Jan. 1972.

Kliore, A. J., et al., "The Atmosphere of Mars From Mariner 9 Radio Occultation Measurements," *Icarus*, Vol. 17, No. 2, pp. 484–516, Oct. 1972.

Kliore, A. J., et al., "S Band Radio Occultation Measurements of the Atmosphere and Topography of Mars with Mariner 9: Extended Mission Coverage of Polar and Intermediate Latitudes," *J. Geophys. Res.*, Vol. 78, No. 20, pp. 4331–4351, July 10, 1973.

Labrum, R. G., et al., *The Surveyor V, VI, and VII Flight Paths and Their Determination from Tracking Data*, Technical Report 32-1302, Jet Propulsion Laboratory, Pasadena, Calif., Dec. 1, 1968.

Laeser, R. P., et al., *Tracking and Data System Support for the Mariner Mars 1971 Mission: Prelaunch Phase Through First Trajectory Correction Maneuver*, Technical Memorandum 33-523, Vol. I, Jet Propulsion Laboratory, Pasadena, Calif., Mar. 15, 1972.

Layland, J. W., "On Optimal Signals for Phase-Locked Loops," *IEEE Trans. Commun. Technol.*, Vol. COM-17, No. 5, pp. 526–531, Oct. 1969.

Layland, J. W., and Lushbaugh, W. A., "A Flexible High-Speed Sequential Decoder for Deep Space Channels," *IEEE Trans. Commun. Technol.*, Vol. COM-19 No. 5, pp. 813–820, Oct. 1971.

Leavitt, R. K., *The Least-Squares Process of MEDIA for Computing DRVID Calibration Polynomials*, Technical Memorandum 33-542, Jet Propulsion Laboratory, Pasadena, Calif., May 15, 1972.

Lesh, J. R., *Signal-to-Noise Ratios in Coherent Soft Limiters*, Technical Report 32-1589, Jet Propulsion Laboratory, Pasadena, Calif., Sept. 15, 1973.

Levy, G. S., Otoshi, T. Y., and Seidel, B. L., *Ground Instrumentation for Mariner IV Occultation Experiment*, Technical Report 32-984, Jet Propulsion Laboratory, Pasadena, Calif., Sept. 15, 1966.

Levy, G. S., et al., *Lunar Range Radiation Patterns of a 210-Foot Antenna at S-Band*, Technical Report 32-1079, Jet Propulsion Laboratory, Pasadena, Calif., reprinted from *IEEE Trans. Antennas Propagation*, Vol. AP-15, No. 2, pp. 311–313, Mar. 1967.

Levy, G. S., et al., *The Ultra Cone: An Ultra-Low-Noise Space Communication Ground Radio-Frequency System*, Technical Report 32-1340, Jet Propulsion Laboratory, Pasadena, Calif., reprinted from *IEEE Trans. Microwave Theor. Tech.*, Vol. MTT-16, No. 9, pp. 596–602, Sept. 1968.

Levy, G. S., et al., "Pioneer 6: Measurement of Transient Faraday Rotation Phenomena Observed During Solar Occultation," *Science*, Vol. 166, No. 3905, pp. 596–598, Oct. 1969.

Lieske, J. H., and Null, G. W., "Icarus and the Determination of Astronomical Constants," *Astron. J.*, Vol. 74, No. 2, Mar. 1969.

Lieske, J. H., et al., "Simultaneous Solution for the Masses of the Principal Planets from Analysis of Optical Radar and Radio Tracking Data," *Celest. Mech.*, Vol. 4, No. 2, pp. 233–245, Oct. 1971.

Lindsey, W. C., *Optimum and Suboptimum Frequency Demodulation*, Technical Report 32-637, Jet Propulsion Laboratory, Pasadena, Calif., June 15, 1964.

Lindsey, W. C., *Improvements to be Realized Through the Use of Block-Coded Communication Systems*, Technical Report 32-947, Jet Propulsion Laboratory, Pasadena, Calif., reprinted from *IEEE Trans. Aerosp. Electron. Syst.*, Vol. AES-2, No. 3, pp. 364–366, May 1966.

Lindsey, W. C., *Phase-Shift-Keyed Signal Detection with Noisy Reference Signals*, Technical Report 32-968, Jet Propulsion Laboratory, Pasadena, Calif., reprinted from *IEEE Trans. Aerosp. Electron. Syst.*, Vol. AES-2, No. 4, pp. 393–401, July 1966.

Lindsey, W. C., *A Theory for the Design of One-Way and Two-Way Phase-Coherent Communication Systems: Phase-Coherent Tracking Systems*, Technical Report 32-986, Jet Propulsion Laboratory, Pasadena, Calif., July 15, 1969.

Lindsey, W. C., *Optimal Design of One-Way and Two-Way Coherent Communication Links*, Technical Report 32-988, Jet Propulsion Laboratory, Pasadena, Calif., reprinted from *IEEE Trans. Commun. Technol.*, Vol. COM-14, No. 4, pp. 418–431, Aug. 1966.

Lindsey, W. C., and Charles, F. J., *A Model Distribution for the Phase Error in Second-Order Phase-Locked Loops*, Technical Report 32-1017, Jet Propulsion Laboratory, Pasadena, Calif., reprinted from *IEEE Trans. Commun. Technol.*, Vol. COM-14, No. 10, pp. 662–664, Oct. 1966.

Lindsey, W. C., *Performance of Phase-Coherent Receivers Preceded by Bandpass Limiters*, Technical Report 32-1162, Jet Propulsion Laboratory, Pasadena, Calif., Sept. 15, 1967.

Lindsey, W. C., "Block Coding for Space Communications," *IEEE Trans. Commun. Technol.*, Vol. COM-17, No. 2, pp. 217–225, Apr. 1969.

Lindsey, W. C., *Block-Coded Communications*, Technical Report 32-1380, Jet Propulsion Laboratory, Pasadena, Calif., Aug. 15, 1969.

Lindsey, W. C., *Nonlinear Analysis of Generalized Tracking Systems*, Technical Report 32-1453, Jet Propulsion Laboratory, Pasadena, Calif., reprinted from *Proc. IEEE*, Vol. 57, No. 10, pp. 1705-1722, Oct. 1969.

Lindsey, W. C., and Simon, M. K., "The Effect of Loop Stress on the Performance of Phase-Coherent Communication Systems", *IEEE Trans. Commun. Technol.*, Vol. COM-18, No. 5, pp. 569–588, Oct. 1970.

Lindsey, W. C., and Simon, M. K., "Carrier Synchronization and Detection of Polyphase Signals," *IEEE Trans. Commun.*, Vol. COM-20, No. 3, pp. 441–454, June 1972.

Lindsey, W. C., and Simon, M. K., "L-Orthogonal Signal Transmission and Detection," *IEEE Trans. Commun.*, Vol. COM-20, No. 5, pp. 953–960, Oct. 1972.

Lindsey, W. C., and Simon, M. K., "On the Detection of Differentially Encoded Polyphase Signals, " *IEEE Trans. Commun.*, Vol. COM-20, No. 6, pp. 1121–1128, Dec. 1972.

Lindsey, W. C., *Synchronization Systems in Communication and Control*, Prentice-Hall, Inc., Englewood Cliffs, N. J., 1972.

Lindsey, W. C., and Tausworthe, R. C., *A Bibliography of the Theory and Application of the Phase-Lock Principle*, Technical Report 32-1581, Jet Propulsion Laboratory, Pasadena, Calif., Apr. 1, 1973.

Lindsey, W. C., and Simon, M. K., *Telecommunication Systems Engineering*, Prentice-Hall, Inc., Englewood Cliffs, N. J., 1973.

Lorell, J., Anderson, J. D., and Sjogren, W. L., *Characteristics and Format of the Tracking Data to Be Obtained by the NASA Deep Space Instrumentation Facility for Lunar Orbiter*, Technical Memorandum 33-230, Jet Propulsion Laboratory, Pasadena, Calif., June 15, 1965.

Lorell, J., Sjogren, W. L., and Boggs, D., *Compressed Tracking Data Used for First Iteration in Selenodesy Experiment, Lunar Orbiters I and II*, Technical Memorandum 33-343, Jet Propulsion Laboratory, Pasadena, Calif., May 1, 1967.

Lorell, J., and Sjogren, W. L., *Lunar Orbiter Data Analysis*, Technical Report 32-1220, Jet Propulsion Laboratory, Pasadena, Calif., Nov. 15, 1967.

Lorell, J., *Lunar Orbiter Gravity Analysis*, Technical Report 32-1387, Jet Propulsion Laboratory, Pasadena, Calif., June 15, 1969.

Lorell, J., et al., "Icarus: Celestial Mechanics Experiment for Mariner," *Int. J. Sol. Sys.*, Vol. 12, Jan. 1970.

Lorell, J., and Laing, P. A., *Compilation of Lunar Orbiter Tracking Data Used for Long-Term Selenodesy*, Technical Memorandum 33-419, Jet Propulsion Laboratory, Pasadena, Calif., Feb. 1, 1970.

Lorell, J., "Estimation of Gravity Field Harmonics in the Presence of Spin-Axis Direction Error Using Radio Tracking Data," *J. Astronaut. Sci.*, Vol. XX, No. 1, pp. 44–54, Aug. 1972.

Ludwig, A. C., et al., *Gain Calibration of a Horn Antenna Using Pattern Integration*, Technical Report 32-1572, Jet Propulsion Laboratory, Pasadena, Calif., Oct. 1, 1972.

Madrid, C. A., et al., *Tracking System Analytic Calibration Activities for the Mariner Mars 1971 Mission*, Technical Report 32-1587, Jet Propulsion Laboratory, Pasadena, Calif., Mar. 1, 1974.

Martin, D. P., *A Combined Radar–Radiometer With Variable Polarization*, Technical Memorandum 33-570, Jet Propulsion Laboratory, Pasadena, Calif., Oct. 15, 1972.

McEliece, R. J., *Optimal Communications Nets*, Technical Report 32-697, Jet Propulsion Laboratory, Pasadena, Calif., Apr. 15, 1965.

McNeal, C. E., *Ranger V Tracking Systems Data Analysis Final Report*, Technical Report 32-702, Jet Propulsion Laboratory, Pasadena, Calif., Apr. 15, 1965.

Melbourne, W. G., et al., *Constants and Related Information for Astrodynamical Calculations*, Technical Report 32-1306, Jet Propulsion Laboratory, Pasadena, Calif., July 15, 1968.

Melbourne, W. G., "Planetary Ephemerides," *Astronaut. Aeronaut.*, Vol. 7, No. 5, pp. 38–43, May 1970.

Merrick, W. D., et al., *Deep Space Communications*, Technical Release 34-10, Jet Propulsion Laboratory, Pasadena, Calif., Jan. 29, 1960; also available in *IRE Trans. Mil. Electron.*, Vol. MIL-4, No. 2-3, pp. 158–163, April–June 1960.

Miller, L., et al., *The Atlas-Centaur VI Flight Path and Its Determination from Tracking Data*, Technical Report 32-911, Jet Propulsion Laboratory, Pasadena, Calif., Apr. 15, 1966.

Moyer, T. D., *Mathematical Formulation of the Double-Precision Orbit Determination Program (DPODP)*, Technical Report 32-1527, Jet Propulsion Laboratory, Pasadena, Calif., May 17, 1971.

Muhleman, D. O., *Relationship Between the System of Astronomical Constants and the Radar Determinations of the Astronomical Unit*, Technical Report 32-477, Jet Propulsion Laboratory, Pasadena, Calif., Jan. 15, 1964.

Muhleman, D. O., Goldstein, R., and Carpenter, R., *A Review of Radar Astronomy—Parts I, II*, Technical Report 32-824, Jet Propulsion Laboratory, Pasadena, Calif., Jan. 30, 1966, reprinted from *IEEE Spectrum*, Oct. and Nov. 1965.

Muhleman, D. O., et al., *JPL Radar Range and Doppler Observations of Venus, 1961–1966*, Technical Report 32-1123, Jet Propulsion Laboratory, Pasadena, Calif., July 1, 1968.

Mulhall, B. D., et al., *Tracking System Analytic Calibration Activities for the Mariner Mars 1969 Mission*, Technical Report 32-1499, Jet Propulsion Laboratory, Pasadena, Calif., Nov. 15, 1970.

Mulholland, J. D., and Sjogren, W. L., *Lunar Orbiter Ranging Data*, Technical Report 32-1087, Jet Propulsion Laboratory, Pasadena, Calif., reprinted from *Science*, Vol. 155, No. 3758, pp. 74–76, Jan. 6, 1967.

Mulholland, J. D., *Proceedings of the Symposium on Observation, Analysis and Space Research Applications of the Lunar Motion*, Technical Report 32-1386, Jet Propulsion Laboratory, Pasadena, Calif., Apr. 1969.

Muller, P. M., and Sjogren, W. L., *Consistency of Lunar Orbiter Residuals With Trajectory and Local Gravity Effects*, Technical Report 32-1307, Jet Propulsion Laboratory, Pasadena, Calif., Sept. 1, 1968.

Muller, P. M., and Sjogren, W. L., *Mascons: Lunar Mass Concentrations*, Technical Report 32-1339, Jet Propulsion Laboratory, Pasadena, Calif., reprinted from *Science*, Vol. 161, No. 3842, pp. 680–684, Aug. 16, 1968.

Newburn, R. L., Jr., et al., *Earth-Based Research on the Outer Planets During the Period 1970–1985*, Technical Report 32-1456, Jet Propulsion Laboratory, Pasadena, Calif., Mar. 15, 1970.

Null, G. W., et al., *Mariner IV Flight Path and Its Determination From Tracking Data*, Technical Report 32-1108, Jet Propulsion Laboratory, Pasadena, Calif., Aug. 1, 1967.

O'Neil, W. J., et al., *The Surveyor III and Surveyor IV Flight Paths and Their Determination From Tracking Data*, Technical Report 32-1292, Jet Propulsion Laboratory, Pasadena, Calif., Aug. 15, 1968.

O'Neil, W. J., et al., *Mariner 9 Navigation*, Technical Report 32-1586, Jet Propulsion Laboratory, Pasadena, Calif., Nov. 13, 1973.

Otoshi, T. Y., *The Effect of Mismatched Components on Microwave Noise-Temperature Calibrations*, Technical Report 32-1345, Jet Propulsion Laboratory, Pasadena, Calif., reprinted from *IEEE Trans. Microwave Theor. Tech.*, Vol. MTT-16, No. 9, pp. 675–686, Sept. 1968.

Otoshi, T. Y., Stelzried, C. T., and Yates, B. C., "Comparisons of Waveguide Losses Calibrated by the DC Potentiometer, AC Ratio Transformer, and Reflectometer Techniques," *IEEE Trans. Microwave Theor. Tech.*, Vol. MTT-18, No. 7, pp. 406–409, July 1970.

Otoshi, T. Y., and Stelzried, C. T., "A Precision Compact Rotary Vane Attenuator," *IEEE Trans. Micro. Theor. Technique*, Vol. MTT-19, No. 11, pp. 843–854, Nov. 1971.

Otoshi, T. Y., "Precision Reflectivity Loss Measurements of Perforated-Plate Mesh Materials by a Waveguide Technique," *IEEE Trans. Instr. Meas.*, Vol. IM-21, No. 4, pp. 451–457, Nov. 1972.

Pease, G. E., et al., *The Mariner V Flight Path and Its Determination From Tracking Data*, Technical Report 32-1363, Jet Propulsion Laboratory, Pasadena, Calif., July 1, 1969.

Posner, E. C., *Properties of Error-Correcting Codes at Low Signal-to-Noise Ratios*. Technical Report 32-602, Jet Propulsion Laboratory, Pasadena, Calif., June 15, 1964.

Potter, P. D., *The Design of a Very High Power, Very Low Noise Cassegrain Feed System for a Planetary Radar*, Technical Report 32-653, Jet Propulsion Laboratory, Pasadena, Calif., Aug. 24, 1964.

Potter, P. D., Merrick, W. D., and Ludwig, A. C., *Large Antenna Apertures and Arrays for Deep Space Communications*, Technical Report 32-848, Jet Propulsion Laboratory, Pasadena, Calif., Nov. 1, 1965.

Potter, P. D., *A Computer Program for Machine Design of Cassegrain Feed Systems*, Technical Report 32-1202, Jet Propulsion Laboratory, Pasadena, Calif., Dec. 15, 1967.

Potter, P. D., et al., *A Study of Weather-Dependent Data Links for Deep Space Applications*, Technical Report 32-1392, Jet Propulsion Laboratory, Pasadena, Calif., Oct. 15, 1969.

Rechtin, E., "Communication Techniques for Space Exploration," *IRE Trans. Space Electron. Telem.*, Vol. SET-5, No. 3, pp. 95–98, Sept. 1959.

Rechtin, E., Stevens, R., and Victor, W. K., *Data Transmission and Communications*, Technical Release 34-55, Jet Propulsion Laboratory, Pasadena, Calif., Apr. 30, 1960.

Rechtin, E., *Space Communications*, Technical Release 34-68, Jet Propulsion Laboratory, Pasadena, Calif., May 1, 1960.

Rechtin, E., Rule, B., and Stevens, R., *Large Ground Antennas*, Technical Report 32-213, Jet Propulsion Laboratory, Pasadena, Calif., Mar. 20, 1962.

Rechtin, E., *Lunar Communications*, Technical Memorandum 33-133, Jet Propulsion Laboratory, Pasadena, Calif., June 28, 1963.

Rechtin, E., "Surprises on Venus," *Int. Sci. Technol.*, No. 20, pp. 13–14, Aug. 1963.

Renzetti, N. A., et al., "Radio Tracking Techniques and Performance of the U.S. Deep Space Instrumentation Facility," *Space Research II, Proceedings of the Second International Space Science Symposium*, Florence, Italy, April 1961, North Holland Publishing Company, Amsterdam.

Renzetti, N. A., and Ostermier, B. J., *Communications with Lunar Probes*, Technical Report 32-148, Jet Propulsion Laboratory, Pasadena, Calif., Aug. 23, 1961.

Renzetti, N. A., *Tracking and Data Acquisition for Ranger Missions I–V*, Technical Memorandum 33-174, Jet Propulsion Laboratory, Pasadena, Calif., July 1, 1964.

Renzetti, N. A., *Tracking and Data Acquisition for Ranger Missions VI–IX*, Technical Memorandum 33-275, Jet Propulsion Laboratory, Pasadena, Calif., Sept. 15, 1966.

Renzetti, N. A., *Tracking and Data Acquisition Support for the Mariner Venus 1962 Mission*, Technical Memorandum 33-212, Jet Propulsion Laboratory, Pasadena, Calif., July 1, 1965.

Renzetti, N. A., *Tracking and Data Acquisition Report, Mariner Mars 1964 Mission: Near-Earth Trajectory Phase*, Technical Memorandum 33-239, Vol. I, Jet Propulsion Laboratory, Pasadena, Calif., Jan. 1, 1965.

Renzetti, N. A., *Tracking and Data Acquisition Report, Mariner Mars 1964 Mission: Cruise to Post-Encounter Phase*, Technical Memorandum 33-239, Vol. II, Jet Propulsion Laboratory, Pasadena, Calif., Oct. 1, 1967.

Renzetti, N. A., *Deep Space Network Support, Atlas/Centaur Missions 1–9*, Technical Memorandum 33-347, Jet Propulsion Laboratory, Pasadena, Calif., Sept. 15, 1967.

Renzetti, N. A., "Tracking and Data Acquisition System for Mariner Missions," *Proceedings of the Seventh International Symposium on Space Technology and Science*, Tokyo, 1967.

Renzetti, N. A., *Tracking and Data Acquisition Report, Mariner Mars 1964 Mission: Extended Mission*, Technical Memorandum 33-239, Vol. III, Jet Propulsion Laboratory, Pasadena, Calif., Dec. 1, 1968.

Renzetti, N. A., and Fearey, J. P., "The Deep Space Network: An Instrument for the Radio Navigation for the Mariner Mission to Mars 1969," IInd International Conference on Space Engineering, Venice, Italy, D. Reidel Publishing Co., Dordrecht, Holland, May 1969.

Renzetti, N. A., *Tracking and Data System Support for Surveyor: Missions I and II*, Technical Memorandum 33-301, Vol. I, Jet Propulsion Laboratory, Pasadena, Calif., July 15, 1969.

Renzetti, N. A., *Tracking and Data System Support for Surveyor: Missions III and IV*, Technical Memorandum 33-301, Vol. II, Jet Propulsion Laboratory, Pasadena, Calif., Sept. 1, 1969.

Renzetti, N. A., *Tracking and Data System Support for Surveyor: Mission V*, Technical Memorandum 33-301, Vol. III, Jet Propulsion Laboratory, Pasadena, Calif., Dec. 1, 1969.

Renzetti, N. A., *Tracking and Data System Support for Surveyor: Mission VI*, Technical Memorandum 33-301, Vol. IV, Jet Propulsion Laboratory, Pasadena, Calif., Dec. 1, 1969.

Renzetti, N. A., *Tracking and Data System Support for Surveyor: Mission VII*, Technical Memorandum 33-301, Vol. V, Jet Propulsion Laboratory, Pasadena, Calif., Dec. 1, 1969.

Renzetti, N. A., *Tracking and Data System Support for the Mariner Venus 67 Mission: Planning Phase Through Midcourse Maneuver*, Technical Memorandum 33-385, Vol. I, Jet Propulsion Laboratory, Pasadena, Calif., Sept. 1, 1969.

Renzetti, N. A., *Tracking and Data System Support for the Mariner Venus 67 Mission: Midcourse Maneuver Through End of Mission*, Technical Memorandum 33-385, Vol. II, Jet Propulsion Laboratory, Pasadena, Calif., Sept. 1, 1969.

Renzetti, N. A., *Tracking and Data System Support for the Pioneer Project: Pioneer VI. Prelaunch to End of Nominal Mission*, Technical Memorandum 33-426, Vol. I, Jet Propulsion Laboratory, Pasadena, Calif., Feb. 1, 1970.

Renzetti, N. A., *Tracking and Data System Support for the Pioneer Project: Pioneer VII. Prelaunch to End of Nominal Mission*, Technical Memorandum 33-426, Vol. II, Jet Propulsion Laboratory, Pasadena, Calif., Apr. 15, 1970.

Renzetti, N. A., *Tracking and Data System Support for the Pioneer Project: Pioneer VIII. Prelaunch Through May 1968*, Technical Memorandum 33-426, Vol. III, Jet Propulsion Laboratory, Pasadena, Calif., July 15, 1970.

Renzetti, N. A., *Tracking and Data System Support for the Pioneer Project: Pioneer IX. Prelaunch Through June 1969*, Technical Memorandum 33-426, Vol. IV, Jet Propulsion Laboratory, Pasadena, Calif., Nov. 15, 1970.

Renzetti, N. A., *Tracking and Data System Support for the Pioneer Project: Pioneer VI. Extended Mission: July 1, 1966–July 1, 1969*, Technical Memorandum 33-426, Vol. V, Jet Propulsion Laboratory, Pasadena, Calif., Feb. 1, 1971.

Renzetti, N. A., *Tracking and Data System Support for the Pioneer Project: Pioneer VII. Extended Mission: February 24, 1967–July 1, 1968*, Technical Memorandum 33-426, Vol. VI, Jet Propulsion Laboratory, Pasadena, Calif., Apr. 15, 1971.

Renzetti, N. A., *Tracking and Data System Support for the Pioneer Project: Pioneer VII. Extended Mission: July 1, 1968–July 1, 1969*, Technical Memorandum 33-426, Vol. VII, Jet Propulsion Laboratory, Pasadena, Calif., Apr. 15, 1971.

Renzetti, N. A., *Tracking and Data System Support for the Pioneer Project: Pioneer VIII. Extended Mission: June 1, 1968–July 1, 1969*, Technical Memorandum 33-426, Vol. VIII, Jet Propulsion Laboratory, Pasadena, Calif., May 1, 1971.

Renzetti, N. A., *Tracking and Data System Support for the Pioneer Project: Pioneers VI–IX. Extended Missions: July 1, 1969–July 1, 1970*, Technical Memorandum 33-426, Vol. IX, Jet Propulsion Laboratory, Pasadena, Calif., Aug. 15, 1971.

Renzetti, N. A., and Siegmeth, A. J., *Tracking and Data System Support for the Pioneer Project: Pioneers 6–9. Extended Missions: July 1, 1971–July 1, 1972*, Technical Memorandum 33-426, Vol. XI, Jet Propulsion Laboratory, Pasadena, Calif., May 1, 1973.

Renzetti, N. A., et al., *Tracking and Data System Support for the Mariner Mars 1969 Mission: Planning Phase Through Midcourse Maneuver*, Technical Memorandum 33-474, Vol. I, Jet Propulsion Laboratory, Pasadena, Calif., May 15, 1971.

Renzetti, N. A., et al., *Tracking and Data System Support for the Mariner Mars 1969 Mission: Midcourse Maneuver Through End of Nominal Mission*, Technical Memorandum 33-474, Vol. II, Jet Propulsion Laboratory, Pasadena, Calif., Sept. 1, 1971.

Renzetti, N. A., Linnes, K. W., and Taylor, T. M., *Tracking and Data System Support for the Mariner Mars 1969 Mission: Extended Operations Mission*, Technical Memorandum 33-474, Vol. III, Jet Propulsion Laboratory, Pasadena, Calif., Sept. 15, 1971.

Renzetti, N. A., *A History of the Deep Space Network: From Inception to January 1, 1969*, Technical Report 32-1533, Vol. I, Jet Propulsion Laboratory, Pasadena, Calif., Sept. 1, 1971.

Renzetti, N. A., "Radio Communications at Planetary Distances," paper presented at the International Convention on Radio Communication, Rome and Bologna, Italy, Mar. 1974.

Richter, H. L., Rechtin, E., and Walter, W. K., *National Ground-Based Surveillance Complex (U)*, Publication 146, Jet Propulsion Laboratory, Pasadena, Calif., Feb. 16, 1959 (Confidential).

Rusch, W. V. T., *Phase Error and Associated Cross-Polarization Effects in Cassegrainian-Fed Microwave Antennas*, Technical Report 32-610, Jet Propulsion Laboratory, Pasadena, Calif., May 30, 1965.

Rusch, W. V. T., and Stelzried, C. T., *Observations of the Lunar Eclipse of December 19, 1964, at a Wavelength of 3.3 MM*, Technical Report 32-1097, Jet Propulsion Laboratory, Pasadena, Calif., reprinted from *Astrophys. J.*, Vol. 148, No. 1, pp. 255–259, Apr. 1967.

Rusch, W. V. T., *Applications of Two-Dimensional Integral-Equation Theory to Reflector-Antenna Analysis*, Technical Memorandum 33-478, Jet Propulsion Laboratory, Pasadena, Calif., May 1, 1971.

Sanger, D. K., *Digital Demodulation with Data Subcarrier Tracking*, Technical Report 32-1314, Jet Propulsion Laboratory, Pasadena, Calif., Aug. 1, 1968.

Siegmeth, A. J., Purdue, R. E., and Ryan, R. E., *Tracking and Data System Support for the Pioneer Project: Pioneers 6–9. Extended Missions: July 1, 1970–July 1, 1971*, Technical Memorandum 33-426, Vol. X, Jet Propulsion Laboratory, Pasadena, Calif., Aug. 15, 1972.

Siegmeth, A. J., et al., *Tracking and Data System Support for the Pioneer Project: Pioneer 10—Prelaunch Planning Through Second Trajectory Correction December 4, 1969 to April 1, 1972*, Technical Memorandum 33-584, Vol. I, Jet Propulsion Laboratory, Pasadena, Calif., Apr. 1, 1973.

Simon, M. K., "Nonlinear Analysis of an Absolute Value Type of an Early-Late Gate Bit Synchronizer," *IEEE Trans. Commun. Technol.*, Vol. COM-18, No. 5, pp. 589–596, Oct. 1970.

Simon, M. K., "Optimization of the Performance of a Digital-Data-Transition Tracking Loop," *IEEE Trans. Commun. Technol.*, Vol. COM-18, No. 5, pp. 686–689, Oct. 1970.

Simon, M. K., and Lindsey, W. C., "Data-Aided Carrier Tracking Loops," *IEEE Trans. Commun. Technol.*, Vol. COM-19, No. 2, pp. 157–168, Apr. 1971.

Simon, M. K., "On the Selection of an Optimum Design Point for Phase-Coherent Receivers Employing Bandpass Limiters," *IEEE Trans. Commun.*, Vol. COM-20, No. 2, pp. 210–214, Apr. 1972.

Simon, M. K., "On the Selection of a Sampling Filter Bandwidth for a Digital Data Detector," *IEEE Trans. Commun.*, Vol. COM-20, No. 3, pp. 438–441, June 1972.

Simon, M. K., and Springett, J. C., "The Performance of a Noncoherent FSK Receiver Preceded by a Bandpass Limiter," *IEEE Trans. Commun.*, Vol. COM-20, No. 6, pp. 1128–1136, Dec. 1972.

Simon, M. K., and Springett, J. C., *The Theory, Design, and Operation of the Suppressed Carrier Data-Aided Tracking Receiver*, Technical Report 32-1583, Jet Propulsion Laboratory, Pasadena, Calif., June 15, 1973.

Simon, M. K., and Smith, J. G., "Hexagonal Multiple Phase-and-Amplitude-Shift-Keyed Signal Sets," *IEEE Trans. Commun.*, Vol. COM-21, No. 10, pp. 1108–1115, Oct. 1973.

Sjogren, W. L., et al., *The Ranger V Flight Path and Its Determination From Tracking Data*, Technical Report 32-562, Jet Propulsion Laboratory, Pasadena, Calif., Dec. 6, 1963.

Sjogren, W. L., et al., *The Ranger VI Flight Path and Its Determination From Tracking Data*, Technical Report 32-605, Jet Propulsion Laboratory, Pasadena, Calif., Dec. 15, 1964.

Sjogren, W. L., *The Ranger III Flight Path and Its Determination From Tracking Data*, Technical Report 32-563, Jet Propulsion Laboratory, Pasadena, Calif., Sept. 15, 1965.

Sjogren, W. L., et al., *Physical Constants as Determined From Radio Tracking of the Ranger Lunar Probes*, Technical Report 32-1057, Jet Propulsion Laboratory, Pasadena, Calif., Dec. 30, 1966.

Sjogren, W. L., *Proceedings of the JPL Seminar on Uncertainties in the Lunar Ephemeris*, Technical Report 32-1247, Jet Propulsion Laboratory, Pasadena, Calif., May 1, 1968.

Sjogren, W. L., "Lunar Gravity Estimate: Independent Confirmation," *J. Geophys. Res.*, Vol. 76, No. 29, Oct. 10, 1971.

Sjogren, W. L., et al., "Lunar Gravity via Apollo 14 Doppler Radio Tracking," *Science*, Vol. 175, No. 4018, pp. 165–168, Jan. 14, 1972.

Slobin, S. D., "Beam Switching Cassegrain Feed System and Its Applications to Microwave and Millimeterwave Radioastronomical Observations," *Rev. Sci. Instr.*, Vol. 41, No. 3, pp. 439–443, Mar. 1970.

Spier, G. W., *Design and Implementation of Models for the Double Precision Trajectory Program (DPTRAJ)*, Technical Memorandum 33-451, Jet Propulsion Laboratory, Pasadena, Calif., Apr. 15, 1971.

Springett, J. C., and Simon, M. K., "An Analysis of the Phase Coherent-Incoherent Output of the Bandpass Limiter," *IEEE Trans. Commun. Technol.*, Vol. COM-19, No. 1, pp. 42–49, Feb. 1971.

Stelzried, C. T., *Post-Amplifier Noise Temperature Contribution in a Low-Noise Receiving System*, Technical Report 32-446, Jet Propulsion Laboratory, Pasadena, Calif., Jan. 1964.

Stelzried, C. T., Reid, M. S., and Petty, S. M., *A Precision DC-Potentiometer Microwave Insertion-Loss Test Set*, Technical Report 32-887, Jet Propulsion Laboratory, Pasadena, Calif., Mar. 15, 1966.

Stelzried, C. T., Reid, M. S., and Nixon, D., *Precision Power Measurements of Spacecraft CW Signal With Microwave Noise Standards*, Technical Report 32-1066, Jet Propulsion Laboratory, Pasadena, Calif., Feb. 15, 1968.

Stelzried, C. T., and Reid, M. S., *Precision Power Measurements of Spacecraft CW Signal Level With Microwave Noise Standards*, Technical Report 32-1070, Jet Propulsion Laboratory, Pasadena, Calif., reprinted from *IEEE Trans. Instrum. Measurement*, Vol. IM-15, No. 4, pp. 318–324, Dec. 1966.

Stelzried, C. T., and Rusch, W. V. T., *Improved Determination of Atmospheric Opacity From Radio Astronomy Measurements*, Technical Report 32-1115, Jet Propulsion Laboratory, Pasadena, Calif., reprinted from *J. Geophys. Res.*, Vol. 72, No. 9, pp. 2445–2447, May 1, 1967.

Stelzried, C. T., and Otoshi, T. Y., "Radiometric Evaluation of Antenna-Feed Component Losses," *IEEE Trans. Instrumen. Measurement*, Vol. IM-18, No. 3, pp. 172–183, Sept. 1969.

Stelzried, C. T., "Precision Microwave Waveguide Loss Calibrations," *IEEE Trans. Instrum. Measurement*, Vol. IM-19, No. 1, pp. 23–25, Feb. 1970.

Stelzried, C. T., *A Faraday Rotation Measurement of a 13-cm Signal in the Solar Corona*, Technical Report 32-1401, Jet Propulsion Laboratory, Pasadena, Calif., July 15, 1970.

Stelzried, C. T., et al., "The Quasi-Stationary Coronal Magnetic Field and Electron Density as Determined From a Faraday Rotation Experiment," *Sol. Phys.*, Vol. 14, No. 2, pp. 440–456, Oct. 1970.

Stelzried, C. T., "Operating Noise-Temperature Calibrations of Low-Noise Receiving Systems," *Microwave J.*, Vol. 14, No. 6, pp. 41–46, 48, June 1971.

Stelzried, C. T., et al., "Transformation of Received Signal Polarization Angle to the Plane of the Ecliptic," *J. Space. Rock.*, Vol. 9, No. 2, pp. 69–70, Feb. 1972.

System Capabilities and Development Schedule of the Deep Space Instrumentation Facility 1963–1967, Technical Memorandum 33-83, Jet Propulsion Laboratory, Pasadena, Calif., Mar. 2, 1962.

Tardani, P. A., *Madrid Site Selection Report*, Technical Memorandum 33-149, Jet Propulsion Laboratory, Pasadena, Calif., July 17, 1963.

Tausworthe, R. C., *A Precision Planetary Range-Tracking Radar*, Technical Report 32-779, Jet Propulsion Laboratory, Pasadena, Calif., reprinted from *IEEE Trans. Space Electron. Telem.*, Vol. SET-11, No. 2, pp. 78–85, June 1965.

Tausworthe, R. C., *Theory and Practical Design of Phase-Locked Receivers*, Technical Report 32-819, Vol. I, Jet Propulsion Laboratory, Pasadena, Calif., Feb. 15, 1966.

Tausworthe, R., *Cycle Slipping in Phase-Locked Loops*, Technical Report 32-1127, Jet Propulsion Laboratory, Pasadena, Calif., reprinted from *IEEE Trans. Commun. Technol.*, Vol. COM-15, No. 3, pp. 417–421, June 1967.

Tausworthe, R. C., Easterling, M. F., and Spear, A. J., *A High-Rate Telemetry System for the Mariner Mars 1969 Mission*, Technical Report 32-1354, Jet Propulsion Laboratory, Pasadena, Calif., Apr. 1, 1969.

Tausworthe, R. C., *DSS Subsystem Implementation by Time-Shared Computer*, Technical Memorandum 33-420, Jet Propulsion Laboratory, Pasadena, Calif., Oct. 1, 1969.

Tausworthe, R. C., "Convergence of Oscillator Spectral Estimators for Counted-Frequency Measurements," *IEEE Trans. Commun.*, Vol. COM-20, No. 2, pp. 213–217, Apr. 1972.

Tausworthe, R. C., "Simplified Formula for Mean-Slip Time of Phase-Locked Loops With Steady-State Phase Error," *IEEE Trans. Commun.*, Vol. COM-20, No. 3, pp. 331–337, June 1972.

Tausworthe, R. C., and Crow, R. B., "Improvements in Deep-Space Tracking by Use of Third-Order Loops," *Proceedings of the 1972 International Telemetering Conference, Los Angeles, California, October 10–12, 1972*, pp. 577–583.

Telecommunications Systems Design Techniques Handbook, Technical Memorandum 33-571, edited by R. E. Edelson, Jet Propulsion Laboratory, Pasadena, Calif., July 15, 1972.

Textor, G. P., Kelly, L. B., and Kelly, M., *Tracking and Data System Support for the Mariner Mars 1971 Mission: First Trajectory Correction Maneuver Through Orbit Insertion*, Technical Memorandum 33-523, Vol. II, Jet Propulsion Laboratory, Pasadena, Calif., June 15, 1972.

Thornton, J. H., Jr., *The Surveyor I and Surveyor II Flight Paths and Their Determination From Tracking Data*, Technical Report 32-1285, Jet Propulsion Laboratory, Pasadena, Calif., Aug. 1, 1968.

Timor, U., "Equivalence of Time-Multiplexed and Frequency-Multiplexed Signals in Digital Communications," *IEEE Trans. Commun.*, Vol. COM-20, No. 3, pp. 435–438, June 1972.

Titsworth, R. C., and Welch, L. R., *Power Spectra of Signals Modulated by Random and Pseudorandom Sequences*, Technical Report 32-140, Jet Propulsion Laboratory, Pasadena, Calif., Oct. 10, 1961.

Titsworth, R. C., *The Algebra of Periodic Sequences*, Technical Report 32-381, Jet Propulsion Laboratory, Pasadena, Calif., Jan. 7, 1963.

Titsworth, R. C., *Correlation Properties of Cyclic Sequences*, Technical Report 32-388, Jet Propulsion Laboratory, Pasadena, Calif., July 1, 1963.

Titsworth, R. C., *Optimal Ranging Codes*, Technical Report 32-411, Jet Propulsion Laboratory, Pasadena, Calif., Apr. 15, 1963.

Titsworth, R. C., *Equivalence Classes of Periodic Sequences*, Technical Report 32-568, Jet Propulsion Laboratory, Pasadena, Calif., June 15, 1964, reprinted from *Ill. J. Math.*, Vol. 8, No. 2, June 1964.

Titsworth, R. C., *The Role of Pseudorandom Codes in Communications*, Technical Memorandum 33-185, Jet Propulsion Laboratory, Pasadena, Calif., Aug. 3, 1964.

"Tracking and Data Acquisition System for Mariner Missions," *Proceedings of the Seventh International Symposium on Space Technology and Science*, Tokyo, May 1967.

Vegos, C. J., et al., *The Ranger IX Flight Path and Its Determination From Tracking Data*, Technical Report 32-767, Jet Propulsion Laboratory, Pasadena, Calif., Nov. 1, 1968.

Victor, W. K., Stevens, R., and Golomb, S. W., *Radar Exploration of Venus: Goldstone Observatory Report for March-May 1961*, Technical Report 32-132, Jet Propulsion Laboratory, Pasadena, Calif., Aug. 1, 1961.

Victor, W. K., Titsworth, R. C., and Rechtin, E., *Telecommunication Aspects of a Manned Mars Mission*, Technical Report 32-501, Jet Propulsion Laboratory, Pasadena, Calif., Aug. 20, 1963.

Viterbi, A. J., *Acquisition Range and Tracking Behavior of Phase-Locked Loops*, External Publication 673, Jet Propulsion Laboratory, Pasadena, Calif., July 14, 1959.

Viterbi, A. J., *On Coded Phase-Coherent Communications*, Technical Report 32-25, Jet Propulsion Laboratory, Pasadena, Calif., Aug. 15, 1960.

Viterbi, A. J., *Classification and Evaluation of Coherent Synchronous Sampled-Data Telemetry Systems*, Technical Report 32-123, Jet Propulsion Laboratory, Pasadena, Calif., June 15, 1961.

Viterbi, A. J., *Phase-Locked Loop Dynamics in the Presence of Noise by Fokker-Planck Techniques*, Technical Report 32-427, Jet Propulsion Laboratory, Pasadena, Calif., Mar. 29, 1963; also reprinted in *IEEE Proc.*, Vol. 51, No. 12, pp. 1737–1753, Dec. 1963.

Viterbi, A. J., *Orthogonal Tree Codes for Communication in the Presence of White Gaussian Noise*, Technical Report 32-1120, Jet Propulsion Laboratory, Pasadena, Calif., reprinted from *IEEE Trans. Commun. Technol.*, Vol. COM-15, No. 2, pp. 238–242, Apr. 1967.

Winn, F. B., "Selenographic Location of Surveyor VI," in *Surveyor VI Mission Report: Part II. Science Results*, Technical Report 32-1262, Jet Propulsion Laboratory, Pasadena, Calif., Jan. 10, 1968.

Winn, F. B., "Post Landing Tracking Data Analysis," in *Surveyor VII Mission Report: Part II. Science Results*, Technical Report 32-1264, Jet Propulsion Laboratory, Pasadena, Calif., Mar. 15, 1968.

Winn, F. B., "Surveyor Post-Touchdown Analysis of Tracking Data," in *Surveyor Project Final Report: Part II. Science Results*, Technical Report 32-1265, Jet Propulsion Laboratory, Pasadena, Calif., June 15, 1968.

Winn, F. B., *Surveyor Posttouchdown Analyses of Tracking Data*, NASA SP-184, National Aeronautics and Space Administration, Washington, D.C., p. 369.

Wollenhaupt, W. R., *Tracking System Data Analysis Report, Ranger 4 Final Report*, Technical Report 32-523, Jet Propulsion Laboratory, Pasadena, Calif., Mar. 1, 1964.

Wollenhaupt, W. R., et al., *The Ranger VII Flight Path and Its Determination From Tracking Data*, Technical Report 32-694, Jet Propulsion Laboratory, Pasadena, Calif., Dec. 15, 1964.

Wong, S. K., and Reinbold, S. J., "Earth–Moon Mass Ratio From Mariner 9 Radio Tracking Data," *Nature*, Vol. 241, No. 5385, pp. 111–112, Jan. 12, 1973.

Woo, R., and Ishimaru, A., "Remote Sensing of the Turbulence Characteristics of a Planetary Atmosphere by Radio Occultation of a Space Probe," *Radio Sci.*, Vol. 8, No. 2, pp. 103–108, Feb. 1973.

Woo, R., et al., *Effects of Turbulence in the Atmosphere of Venus on Pioneer Venus Radio—Phase I*, Technical Memorandum 33-644, Jet Propulsion Laboratory, Pasadena, Calif., June 30, 1973.

Yuen, J. H., "A Double-Loop Tracking System," *IEEE Trans. Commun.*, Vol. COM-20, No. 6, pp. 1142–1150, Dec. 1972.

NASA — JPL — Coml., L.A., Calif.